

PUBLISHER

On Behalf of Textile and Apparel Research
Application Center

Faruk BOZDOĞAN

EDITOR IN CHIEF

Arif Taner ÖZGÜNEY
arif.taner.ozguney@ege.edu.tr

ASSOCIATE EDITORS

Mehmet KÜÇÜK
mehmet.kucuk@ege.edu.tr

Pelin SEÇİM KARAKAYA
pelinsecim@mail.ege.edu.tr

EDITORIAL BOARD

Ahmet ÇAY

Aslı DEMİR

Gözde ERTEKİN

Hale KARAKAŞ

Hüseyin Aksel EREN

Pınar ÇELİK

ENGLISH EDITING SERVICE

Mengü Noyan ÇENGEL

SCIENTIFIC ADVISORY BOARD

Andrej DEMŠAR

Arzu MARMARALI

Bojana VONČINA

Bülent ÖZİPEK

E. Perrin AKÇAKOCA KUMBASAR

Ender BULGUN

Esen ÖZDOĞAN

Hüseyin KADOĞLU

Mirela BLAGA

Nilgün ÖZDİL

Oktay PAMUK

Ozan AVINÇ

Peter J. HAUSER

Recep EREN

Rıza ATAV

Savvas G. VASSILIADIS

Turan ATILGAN

ABSTRACTING / INDEXING

Science Citation Index Expanded (SCIE)

Scopus

WOS

EBSCO

Ulakbim

TYPESETTING AND PRINTING

AK-MAT Matbaacılık Yayıncılık Kır. Malz. San. Tic. Ltd. Şti
Barbaros Mah. Refik Tulga Cd. No: 13, Bornova – İzmir
akmatlimited@gmail.com Tel: 0 232 444 28 23

Printed Date: 29 September, 2022

**Investigation of the Effect of Raising and Finishing Process on the
Phycsical Performance of 3-Thread Fleece Fabric**
Çassan Asker, Onur Balcı 183

**Development of Temperature and pH Responsive Smart Cotton
Fabrics by P(NIPAM-co-MAM) Copolymer Finishing**
Sena Demirbağ Genç, Sennur Alay Aksoy 193

**CNN-Based Fabric Defect Detection System
on Loom Fabric Inspection**
Muhammed Fatih Talu, Kazım Hanbay, Mahdi Hatami Varjovi 208

**Investigation of Auxetic Performance and Various Physical
Properties of Fabrics Woven with Braid Yarns**
Mine Akgun, Fatih Suvvari, Recep Eren, Tugba Yurdakul 220

**Usage of UV-Curable Soybean Oil Based Coating
Formulations for Pretreated Cotton Fabrics**
Zehra Yildiz 232

An Investigation of Sensorial Comfort in Woven Women's Blouses
Ebru Akgün Esen Çoruh 243

Performance Investigation of Textile Triboelectric Generators
Aristeidis Repoulas, Sotiria F Galata, Argyro Kallivretaki,
Arzu Marmarali, Savvas Vassiliadis 252

**Application of Indigenous Plant-Based Vegetable Tanning Agent
Extracted from *Xylocarpus granatum* in Semi-Chrome and
Chrome Retanned Leather Production**
Raju Kumar Das, Al Mizan, Fatema-Tuj-Zohra, Bahri Basaran
Sobur Ahmed 258

**Characterization of high-pressure fuel hose with
braided reinforcement**
Mustafa Ertekin, Gözde Ertekin, Gökçe Bakiler,
İrem Seçkin İşcan, Seçkin Erden 265

**Effects of Needle Size and Sewing Thread on Seam Quality
of Traditional Fabrics**
Derya Tama Birkocak 277

**Maximization of Sewing Strength and Minimization of
Seam Pucker for Denim Fabrics Using Taguchi Method**
Gulsah Pamuk 288

CONTACT

Ege Üniversitesi Tekstil ve Konfeksiyon Araştırma-Uygulama Merkezi
35100 Bornova – İzmir, TÜRKİYE
Tel: +90 232 311 38 89-83

www.dergipark.gov.tr/tekstilvekonfeksiyon
E-mail: tekstilkonfeksiyon@mail.ege.edu.tr



Investigation of the Effect of Raising and Finishing Process on the Phycsical Performance of 3-Thread Fleece Fabric

Ğassan Asker  0000-0002-2019-0994

Onur Balcı  0000-0001-6885-7391

Kahramanmaraş Sütçü İmam University / Engineering and Architecture Faculty, Textile Engineering Department/Türkiye

Corresponding Author: ĞassanASKER, gassanasker@yahoo.com.tr

ABSTRACT

Within the scope of the study, pre-softening, raising and final softening processes were applied to 2 fleece fabrics under different conditions. The raising fastness, air permeability and bursting strength tests were performed on the samples obtained after the processes, and the effect of the process conditions on the researched performance values was examined. This paper is also detailed by statistical analysis. When the results were examined, it was seen that the best result in terms of raising fastness was the fabric with 50% waste + 50% PES back yarn. As a process, it was determined that the best result was obtained after a single passage with micro silicon pre-softening and raising at a speed of 15m / min, and then a low concentration softening process with a polyvinyl acetate-based binder and softener mixture.

1. INTRODUCTION

Knitted fabrics, which are called three threads, are fabrics that are knitted on special plain circular knitting machines equipped with different cam sets, special sinker structures and thread guides from three different ways. In 3 thread fleece fabrics, one of the two yarns that are mostly used in the same count or thickness is the face yarn that forms the ground, and the other is the binding yarn that acts as a filler. The third yarn is the back (fleece) yarn, which is thicker than these two yarns. The front of these structures looks like a plain knit. On the reverse, there are yarn floatings in the course direction [1].

The raising process plays an important role in obtaining thermal comfort in the production of three thread fleece fabrics. In this type of fabric, raising is applied to the back surface of the fabric that skin-contact. The raising process is a mechanical finishing process based on the physical pulling out of the fibers from the yarns of the fabric. As a result of this process, a fiber layer is formed on the surface of the fabric. The thickness and effect of this layer vary depending on the length of the fibers, how they pile and counter-pile, and the number of passages. Thanks to this

layer, the fabric turns into a bulkier structure and the existing air in the fabric pores is trapped, giving it a feature like an airbag. Thus, the heat retention ability of the fabric is also increased. In the raising process, rollers covered with pointed metallic wires are used to pull the fibers mechanically. While the hooks in one of the rollers pull the fiber from the fabric (pile roller), the hooks that mounted with reverse angel in the other roller comb the fibers (counter-pile roller) [3].

The softening process also has an important role in the production of three yarn fabrics. Softening application is used in two separate stages in the production processes of three thread fleece fabrics. The first of these is the pre-softening applied before raising and providing easy raising of the fabric, and the other is the 2nd softening applied after raising and improving the touch of the fabric. Silicone-based softeners are generally used in both processes. Silicone-based softeners are softeners that are mostly produced as oil-in-water emulsions (O/W), which are used to give textile products not only better softness, brightness, and lubricity, but also flexibility, bulkiness (fullness), easy sewing, and tear strength [4].

To cite this article: Asker Ğ, Balcı O. 2022. Investigation of the effect of raising and finishing process on the phycsical performance of 3-thread fleece fabric. *Tekstil ve Konfeksiyon*, 32(3), 183-192.

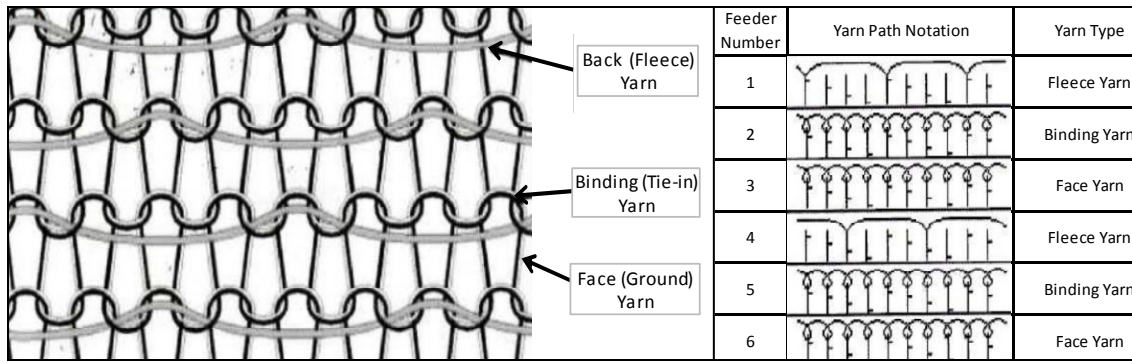


Figure 1. Structure of 3 thread fleece fabric and diagram of needle notation [2]

In this way, while the touch, bulkiness, and comfort features of knitted fabric exposed to raising and softening processes come to the fore in a positive sense, it has been determined that fiber loss occurs on the back of the fabric depending on the process and fabric conditions, and many important global brands, high amounts of customer complaints and negative returns were reflected on the manufacturer/seller. When garments made from these fabrics are used, fiber loss causes adhesion to the body or stains on other garments. Raising fastness is the resistance of the raising faces of three yarn futter fabrics to the adhesion of the fibers to the human body or to the garment they come into contact with when exposed to mechanical/chemical effects. The raising fastness test is an analysis designed by LC Waikiki to measure and rate this performance and applied with the "in house" method. Determining the root cause of this problem constitutes the main purpose of the study. Therefore, the research focused on the investigation of the relationship between raising fastness (fiber loss), bursting strength, air permeability performances of three thread fleece knitted fabrics, and the raising process and softening application.

When the literature is examined, the increase in the demands of knitted fabrics in recent years has also shown itself in studies related to these fabrics, and many studies have been carried out on the dimensional behavior of knitting especially in jersey, interlock, lacoste and futter fabrics. In all of these studies, knitted fabric properties are affected by all operating parameters, starting from the fiber properties used, to yarn, knitted surface properties, and finishing processes. It was stated that the desired properties of knitted fabrics at the place of use should be determined and the appropriate fiber, yarn, knitting surface and finishing processes should be selected [5-17]. It is seen that these studies are more limited in the 3 thread fleece fabrics, which are mostly referred to with the raising process. In studies conducted for this type of fabric, it has been observed that research on thermal comfort and thermal insulation have come to the fore. As a result of these studies, it was stated that the thickness of futter fabrics and especially the presence of the raising process increased the heat retention ability [18-19]. In another study, it was concluded that the front yarn should be knitted tightly, the rear yarn height should be kept short, and a separate study

should be done for raising fabric in order to have a lower combustion value of three yarns without raising [20]. Balci et al., In their studies, found that the quality of the back yarn of the two yarn futter fabric loses weight as a result of the cellulase enzyme application and raising process and therefore increases the waste rate so that the waste rate in the back yarn should not exceed 50% [21]. In a study on 3-yarn fabrics knitted with different front and back yarn combinations, water vapor and air permeability of knitted fabrics with tencel yarn gave the best results, while cotton fabrics remained worse [22]. As can be understood from all these previous studies, the relationship between three yarn knitted fabric, raising, and softening was examined experimentally and statistically within the scope of this research.

In this context, the knitted fabric with two different constructions which was determined according to the results of their experimental study before this study was presented, was selected to be used within the scope of this research by Asker and et al [23]. 192 finishing processes were applied to these two selected fabrics under various softening and raising process conditions within the ÖZEN MENSUCAT R&D Center. In this context, 7 different softeners were used in the study. The type of pre-softening and 2nd softening chemical (applied before and after raising), the number of raising passages, the speed of the raising machine, and the concentration of 2nd softener agent were selected as varied. In addition, 9 more trials were carried out to examine if the use of binder affected the performance of the second softening process. In the laboratories of LC Waikiki Stores, all samples were tested for raising fastness, bursting strength, and air permeability. One-way analysis of variance (ANOVA) was performed on the results, and evaluation of the effects of the selected input parameters on the outputs was presented.

2. MATERIAL AND METHOD

2.1 Material

Within the scope of this study, three thread fleece fabrics of two different constructions were used (Fabric 1 and Fabric 2). The variability in Fabric 1 and Fabric 2 being different is due to the back yarn blend. Open-end yarns defined as Type 1 (50% cotton-50% polyester) and Type 2 (50%

Waste cotton + 50% Polyester) were used for the back yarn. The cotton used in the back yarn defined as Type 1 and preferred for Fabric 1 is the original Turkmenistan blend, and the cotton defined as Type 2 and selected in Fabric 2 is the waste of the same blend.

In the previously published study of the researchers (Asker et al.) were applied 18 different finishing process combinations to three thread fleece knitted fabrics developed in 32 different constructions (as structural parameters, two different front yarns, four different back yarn fiber contents, two different back-yarn pile lengths pile and two different number of back-yarn floating were used), and as a result of this study, they determined that two constructions had the best results in terms of the raising fastness. Since the main subject of the study is fiber loss, it has been prioritized to make the first evaluation directly on the raising fastness. [23]. Accordingly, Ne 30/1 combed ring for face yarns, 70 denier filament polyester for binding yarns, and Ne 14/1 open-end yarns for back yarns were used in both fabrics. In these constructions, yarn lengths in 100 needles are 44/28/17 cm, and their weight is 295 g / m².

USTER and Tensorapid results of the back yarn (Type 1 and Type 2), which cause the differentiation of the two fabrics, are given in Table 1 and Table 2.

7 different softeners and 3 different binders were used within the scope of the study. 5 of these softeners were specially prepared for this research, and commercial samples were used for 2 of them. Information on softeners and binders is given below.

Softener 1: It is an amino-functional micro silicone emulsion. It is prepared to contain 15% silicone oil. 15%

oil, 9% tridecyl alcohol 6 ethoxylate based emulsifier is used in its recipe. The particle size of this developed product was determined as 80 nm.

Softener 2: It is an amino- functional macro silicone emulsion. It was provided from VESKIM as ready, with 15%. The particle size of this developed product was determined as 145 nm.

Softener 3: It is a hydrophilic macro silicone emulsion. It is prepared to contain 15% silicone oil. Quarterner ammonium modified silicone oil is prepared according to the oil in water emulsion principle. 15% oil, 1.5% tridecyl alcohol 6 ethoxylate-based emulsifier is used in its recipe. The particle size of this developed product was determined as 100 nm.

Softener 4: It is the mixed emulsion obtained by mixing the macro emulsions provided with the prepared micro silicones emulsions in equal proportions. The particle size of this developed product was determined as 80 nm.

Softener 5: It is a hydrophilic micro silicone emulsion prepared to contain 15% silicone oil. Quarterner ammonium modified silicone oil is prepared according to the oil in water emulsion principle. 15% oil, 3% tridecyl alcohol 6 ethoxylate-based emulsifier is used in its recipe. The particle size of this developed product was determined as 50 nm.

Softener 6: It was obtained from FOURKIM as commercial product. It is a mixed emulsion formed by hydrophilic macro and micro silicone emulsions in equal proportions. Hydrophilic macro emulsion produced by quarterner modified silicone oil while micro emulsion produced by amino-functional silicone oil.

Table 1. Uster values of back yarn type 1 and type 2

Fleece yarns type	Type 1			Type 2		
	Mean	CV	S	Mean	CV	S
U %	8,92	3,3	0,29	10,91	3	0,33
CVm %	11,28	3,3	0,37	13,84	3	0,41
Thin -40 % /km	14,00	81,9	12	103	27,7	28
Thick + 35% /km	101,00	23,7	24	510	19,7	100
Thick +50% /km	13,00	97,6	13	63	23,3	15
Neps +140% /km	397,00	29,1	116	3014	18,4	555
Neps +200% /km	31	52,7	16	555	22,7	126
Neps +280% /km	8	105	9	82	25,1	21
Neps +400% /km	2	202,4	4	11	33,5	4
H	5,94	2,8	0,17	6,01	2	0,12
S3u /100m	1582	16,6	263	1510	9	136

Table 2. Tensorapid test results of back yarn type 1 and type 2

Fleece yarns type		Time to break (s)	B-Force (cN)	Elongation (%)	Tenacity (cN/tex)	B-Work (N.cm)
Type 1	Mean	0,56	579,4	9,27	13,74	15,00
	S	0,05	35,76	0,75	0,85	1,88
	CV	8,09	6,17	8,07	6,17	12,55
Type 2	Mean	0,60	608,4	9,88	14,42	16,22
	S	0,04	81,39	0,69	1,93	2,50
	CV	6,95	13,38	7,03	13,38	15,42

Softener 7: Softener 6 was mixed with commercially available Binder (polyvinyl acrylate) and a special mixture was obtained. Binder was used in the softener at a concentration of 50 g / L.

In the experimental study, the effect of the chemical properties of the binder on the performance properties of futter fabrics was also investigated. In this context, 3 different commercial binders are used. These; Binder 1: Ferane NGU - Cationic Quaternary Amidation (A), Binder 2: Ruco-Plast EPG 18803 - Polyvinylacetate (B), Binder 3: Ruco-Plast PSM - Polyacrylate dispersion (C).

2.2. Method

According to the research published previously, it has been observed that the softener used in pre-softening and second softening processes is effective in fiber loss of fabrics. It has been seen that the 2nd softening has a negative effect on raising fastness whereas pre-softening reduces this negativity [23]. Based on these findings, within the scope of the research, the type of the softening chemical applied to facilitate the raising process (4 levels) before the raising process, the type and concentration of the softener used to improve the touch after the raising (4 levels), and the number of raising passages (2 levels) and the speed of the raising machine (2 levels) were selected as process parameters. The experiment plan created with these parameters was applied to Fabric 1 and Fabric 2, whose structural features were specified above, in a stenter machine under operating conditions.

In the second part of the study, three different binders were applied only to Fabric 2 in three different concentrations of 2nd softening chemicals. Experiment plans are given in Table 3 and Table 4.

In this study, all samples were prepared under the same conditions until the pre-softening stage. The machines and process conditions after this stage are given in Table 5.

The samples were subjected to raising fastness, bursting strength, and air permeability tests as per the test plans in Tables 3 and 4.

The process flow chart was carried out as Figure 2.

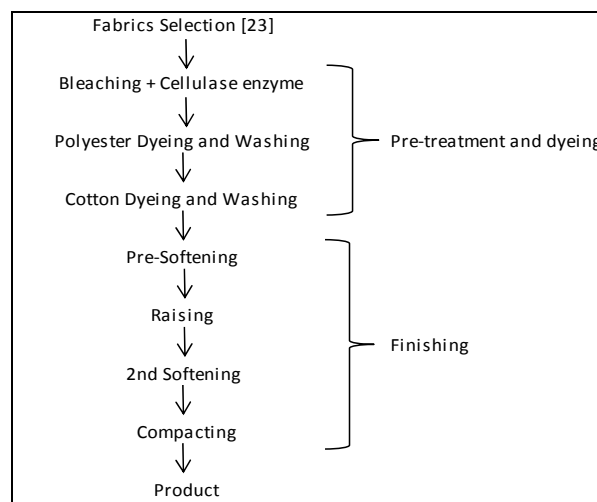


Figure 2. Experimental flow chart of the study

The raising fastness test was made to measure the fiber loss of the fabric, and LC Waikiki KMS05 standard was used for this test. According to this method, first of all, samples are cut from 4 different parts of the fabric to be tested. Optical white, carbon brush fabric (40/1-40/1 poplin 52/48, 100% cotton), is used as the top cloth in the test as reference. Then, the raised fabric to be tested and the reference fabric is tested in 5 rounds in the Martindale Pilling Tester. Finally, samples are evaluated by using scale. If the score is 3 or more over the 4-point scale, the test is considered as passed

The bursting strength test is carried out in James H. Heal brand Truburst2 device according to the Bursting Strength (ISO 13938-2) ISO 13938-2 standard. According to the standard 50 cm² (79.8 mm diameter) fabric is tested. The KPa value at the moment of explosion refers to the strength.

Table 3. Experiment plan 1

The type of fabric	The type of presoftening agent	The number of passages	The speed of raising	The type of 2nd softening agent	The concentration of 2nd softening agent
Fabric 1	Softener 1	Single Pass	S1-10 m/dk.	Softener 1	Low-5 g/l
Fabric 2	Softener 2	Double Pass	S2-15 m/dk.	Softener 5	Medium-15 g/l
—	Softener 3	—	—	Softener 6	Normal-30 g/l
—	Softener 4	—	—	Softener 7	—

Table 4. Experiment plan 2

Trial no	Binder type	Amount (g/l)	Trial no	Binder type	Amount (g/l)	Trial no	Binder type	Amount (g/l)
1	A	10	4	B	10	7	C	10
2	A	30	5	B	30	8	C	30
3	A	50	6	B	50	9	C	50
Original (Without Binder)								

Table 5. Processes parameters and working conditions

Parameters	Pre-softening	Raising	2 nd Softening	Compacting
Used Machines (Trademark)	8 Chambers Stenter (Effe)	2 Drums Raising Machine (Has Group)	8 Chambers Stenter (Effe)	Sanfor Machine (Ferraro)
Application Method	wet on wet impregnation. Pick-up % 20-30	-	impregnation Pick-up %80-100	-
Amount of Softener (g/L)	125	-	50	-
Application pH	4.5-5.5	-	4.5-5.5	-
Drying Temperature (°C)	130	-	130	-
Machine Speed (m/min)	15	10-15	15	20

The air permeability test was made according to the standard of GOST 12088-77 / ISO 9237. The test was carried out under the conditions of 100 Pa test pressure and 5 cm² surface area, and the air permeability value is shown in l / min unit.

The relationship between fabric type and selected process parameters, and tested performance values was statistically analyzed using variance analysis with 95 percent confidence limits on the results obtained from the trials and tests. Input parameters in all variance analysis; A- Fabric Type, B- Pre-softening Softener Type, C-Number of Passages, D-Raising Speed, E- The Type of 2nd Softening Agent, F- The Concentration of 2nd Softener Agent. F and p values were used in the evaluation. For an investigated main factor or interaction to be statistically significant, the p value must be less than 0.005. In addition, it can be said that the larger the F value, the greater the significance state of the parameter examined and its effect on the variability.

3. RESULTS AND DISCUSSION

3.1 Evaluation of Raising Fastness

The raising fastness test was performed on 384 samples collected in accordance with Table 3's experiment plan, and the results of the variance analysis are shown in Table 6. Figure 2 depicts the normal distribution curve used to assess the reliability of these test results. The distribution has a normal distribution character, as shown in Figure 3.

Table 6. Raising fastness variance analysis results

Parameters	F Value	p-value	Significance level
Model	55,39	< 0.0001	significant
A- Fabric Type	449,67	< 0.0001	significant
B- Pre-softening Softener Type	6,70	0.0002	significant
C- Number of Passages	30,76	< 0.0001	significant
D- Raising Speed	2,94	0.0873	insignificant
E- 2nd Softening Softener Type	33,58	< 0.0001	significant
F- 2nd Softening Softener Concentration	2,56	0.0785	insignificant

As seen in Table 6, it was determined that the model established was statistically significant. However, of the main parameters selected as an input, A parameter (fabric type), B parameter (Pre-softening softener type), C parameter (number of passages), and E parameter (The

Type of 2nd Softening Agent) are significant on the output. On the other hand, it was determined that D parameter (raising speed) and F parameter (The Concentration of 2nd Softener Agent) had no effect on raising fastness.

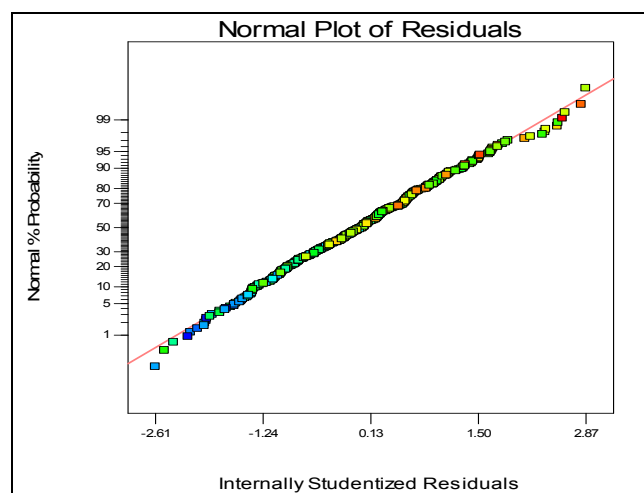


Figure 3. Normal distribution curve for raising fastness results

In Figure 4, raising fastness test results drawn depending on Parameters A and B are shown.

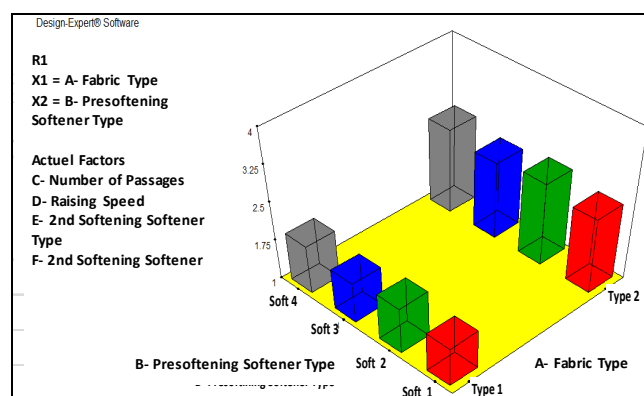


Figure 4. Model chart for raising fastness according to A and B parameters

It has been determined that the most important parameter affecting raising fastness is fabric type. The only difference between fabrics (Fabric 1-Fabric 2), which is the biggest cause of variability, is the cotton blend used in spinning the

back yarn. In Type 1 (Fabric 1) Cotton (50%) + Polyester (50%) was used in the back yarn blend, while in Type 2 Waste Cotton (50%) + Polyester (50%) was used. Therefore, the most important difference affecting raising fastness is the use of waste cotton instead of cotton at 50%. As seen in Figure 4, the results of raising fastness were higher in Type 2, that is, the fabric knitted from the back yarn with waste (Fabric 2). This result is thought to be due to the fact that the waste fibers in the back yarn are shed more during the raising process and are transferred with less waste to the finished product stage. Thus, there is little or no residual back yarn fiber to adhere to the reference fabric during the test. It is also thought that there is a relationship between the raising fastness performance and the USTER results of the yarns. It is thought that the type 1 yarn which has less thin / thick place amount and is smoother (see table 1), breaks more because it is raising harder and breaking harder, thus increasing the fiber loss and the raising fastness is lower.

In Figure 5, raising fastness test results drawn depending on C and E parameters are shown.

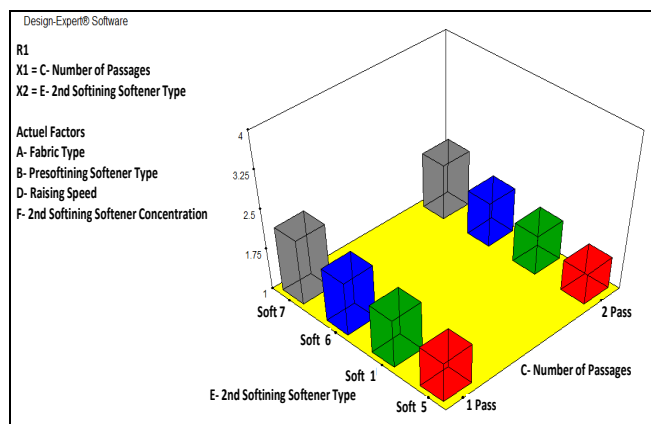


Figure 5. Model graph for raising fastness according to C and E parameters

As seen in Figure 5, The E parameter (The Type of 2nd Softening Agent) has the second greatest effect on raising fastness. The best result, namely the lowest fiber loss, has been obtained in applications where Softener 7 is used. On the other hand, the lowest result was found in applications where micro silicones (Softener 1 and Softener 5) are used. When the results are evaluated in terms of the number of passages, it is seen that fabrics applied with a single passage have better results than double passages. The reason for this is that the single passage raising application causes less damage to the fiber than the double passage and as a result, the fiber loss occurs less.

In Figure 6, raising fastness test results drawn depending on A and E parameters are shown. As can be seen from Figure 6, Softener 7 gave better raising fastness results, while Softener 5 gave the lowest values in the 2nd softening stage for both fabric types.

3.2. Evaluation of Bursting Strength Results

Variance analysis results on bursting strength test results are shown in Table 7. The normal distribution plotted to

analyze the reliability of these test results is provided in Figure 7. As seen in Figure 7, the curve shows a normal distribution character.

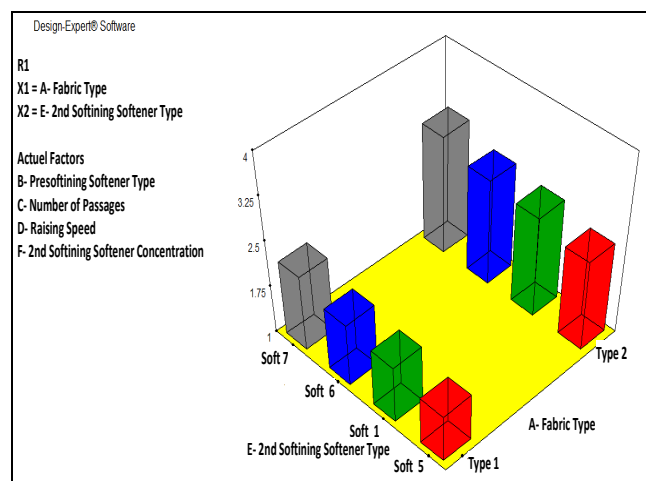


Figure 6. Model graph for raising fastness according to A and E parameters

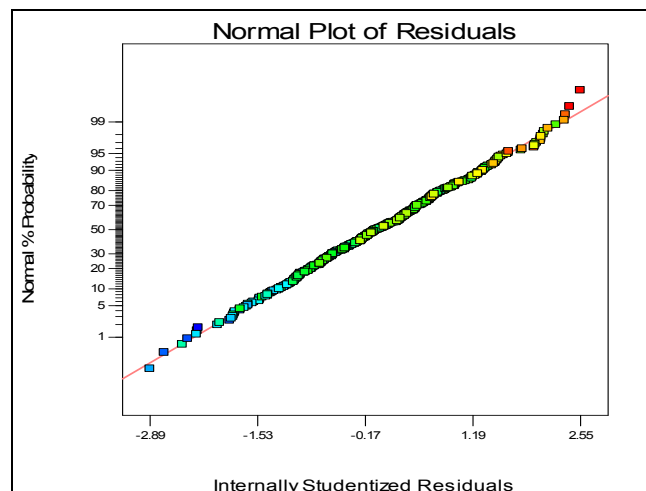


Figure 7. Normal distribution curve for bursting strength

When examined in Table 7, it was found that the model established was statistically significant. Besides this, it was determined that the parameters A (fabric type), C (passage number), and E (The Type of 2nd Softening Agent), which are among the main parameters selected as the input, are significant on the output. On the other hand, B (Pre-softening softener type), D (raising speed) and F (The Concentration of 2nd Softener Agent) parameters did not affect the change in bursting strength at a statistically significant level.

It has been determined that E (The Type of 2nd Softening Agent) applied after raising along with the A parameter (the fabric type) was the most important variable, among the significant parameters. The number of passages (C parameter) applied to the back of the fabric followed these 2 variables. The type of softener (A parameter) applied before the raising process did not affect the bursting strength. The fact that the 2nd softening material (E

parameter) increased the lubricity of the yarns while improving the handle, reduced the yarn-yarn friction, and this decrease caused the strength value to decrease. The different particle sizes and chemical structures of the selected softeners caused the change in bursting strength to differ depending on the type of softener. However, the amount of use of these softeners did not change the bursting strength performance.

Table 7. Burst strength variance analysis results

Parameters	F Value	p-value	Significance level
Model	26,70	< 0.0001	significant
A- Fabric Type	53,92	< 0.0001	significant
B- Pre-softening Softener Type	1,14	0.3321	insignificant
C- Number of Passages	14,98	0.0001	significant
D- Raising Speed	0,00	0.9492	insignificant
E- 2nd Softening Softener Type	73,24	< 0.0001	significant
F- 2nd Softening Softener Concentration	1,25	0.2866	insignificant

3D model graphs showing the interactions of these parameters (A-C, A-E and C-E) are shown in Figure 8, Figure 9 and Figure 10.

As seen in Figure 8-10, the strength values were higher in samples exposed to single passage raising process. In other words, the strength performances of the samples that were mechanically less exposed to the raising hooks over the raising machine were measured higher. This is a result of the direct break-off effect of the raising process on the fibers and the resulting fiber damage. Although there is no direct decrease after the first passage, the performance is lower after the second passage.

When examined in terms of softening at the end of raising, it shows that the fabrics to which Softener 7 is applied have higher strength performance and from here, the binder chemical in it has a positive contribution to the strength. When other softeners are examined, it has been determined that those with microparticle size show lower strength performance.

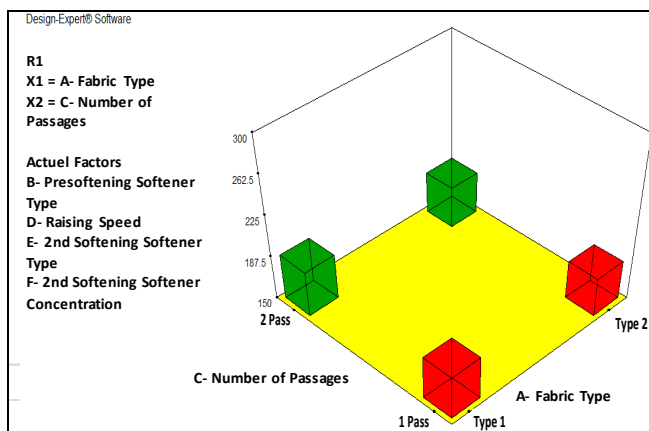


Figure 8. Model graph for bursting strength according to parameters A and C

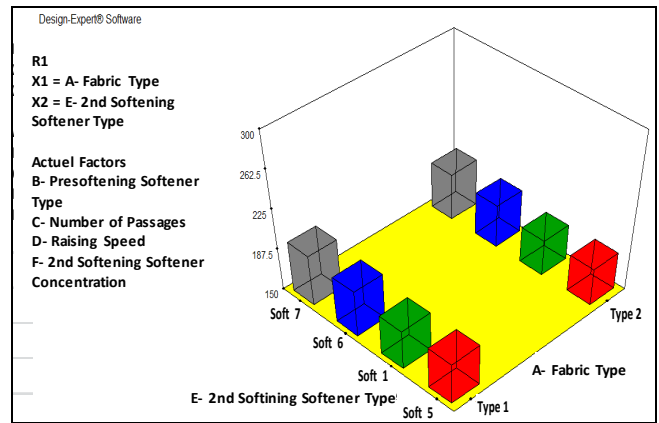


Figure 9. Model graph for bursting strength according to parameters A and E

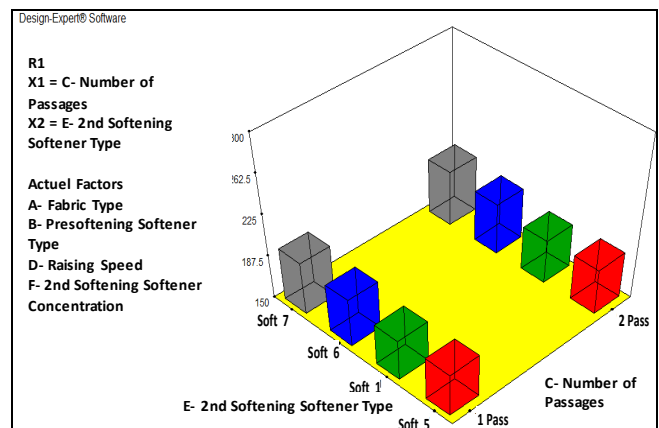


Figure 9. Model chart for bursting strength according to parameters C and E

3.3 Evaluation of the Air Permeability

One-way variance analysis results on air permeability test results are shown in Table 8. The normal distribution curve drawn to analyze the reliability of these test results is given in Figure 11. As seen in Figure 11, the curve shows a normal distribution character. When Table 8 is examined, it is seen that the model established is statistically significant. However, it was determined that C (passage number) and E parameters (The Type of 2nd Softening Agent), which are the main parameters selected as an input, are also significant on the output. However, it was determined that the parameters A (fabric type), B (Pre-softening softener type), D (raising speed) and F parameters (The Concentration of 2nd Softener Agent) had no effect on air permeability. It was determined that the most important factor on the change in air permeability performance is the number of raising passages. The difference in the air permeability value depending on the number of passages can be explained by the change in the surface hairiness after raising.

Table 8. The ANOVA results of Air Permeability Data

Parameters	F Value	p-value	Significance Level
Model	23,62	< 0.0001	significant
A- Fabric Type	0,22	0.6399	insignificant
B- Pre-softening Softener Type	0,52	0.6676	insignificant
C- Number of Passages	87,82	< 0.0001	significant
D- Raising Speed	7,62	0.0061	insignificant
E- 2nd Softening Softener Type	52,92	< 0.0001	significant
F- 2nd Softening Softener Concentration	1,15	0.3164	insignificant

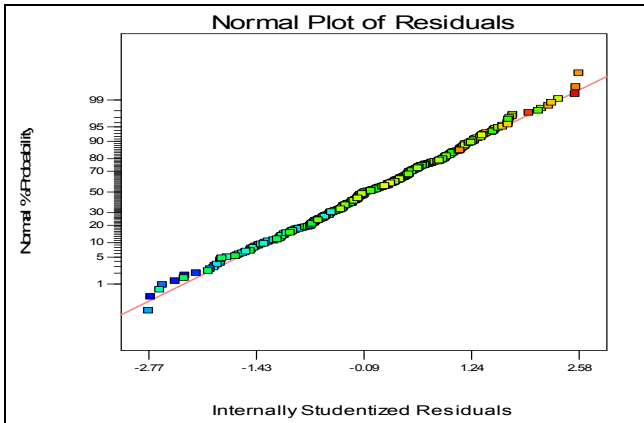


Figure 11. Air permeability normal distribution curve

The 3D model graph of parameter C (passage number) and parameter E (The Type of 2nd Softening Agent), among themselves is given in Figure 12.

As can be seen in Figure 12, the air permeability of the fabrics treated with softening agent 7 was higher. It can be concluded that, with the binder effect used in the recipe, the adhesion of the fibers in the fabric pores to each other and to the yarns on the surface creates a channel and increases the pore passage with the vacuum effect created by the channel. With the number of passages, one more combing was made. In this combing, fibers emerging in the first combing and physically weakly attached to the surface will fall off the surface. Thus, these fibers that reduce the permeability on the fabric surface will fall off and disappear. So that the fabric surface will be eliminated which reduces the permeability decreased in those fibers. The disappearance of these fibers was also proven in the test of raising fastness, in this respect there is a correlation

between the results. Air permeability has increased due to the falling of these fibers from the surface. In addition, with the second passage raising process, the smoothing of the fibers on the surface and the raising effect can be counted among the reasons that cause this situation.

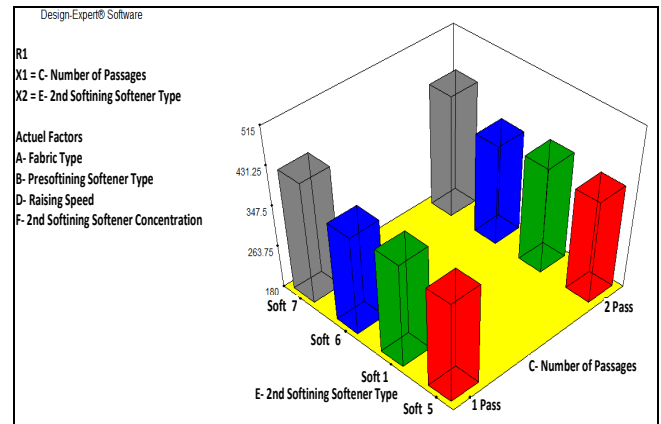


Figure 12. Model graph for air permeability according to C and E parameters

3.4 Test Results and Evaluation of Binder Applications

In the first part of the study, it has been seen that the use of binders (samples using Softener 7) improved raising fastness and other measured performance properties. Hereupon, it was decided to conduct a more detailed study on the use of binders and the study was deepened with 3 binders and 3 different concentrations. Accordingly, applications were made to Type 2 Fabric. In Table 9, the results of the tests (raising fastness, air permeability, and bursting strength) made on the samples obtained with the trial plan and planned trials using binder are given. Table 9 also shows the performance data of the reference fabric..

When the values in Table 10 are examined in terms of raising fastness, it has been determined that the reference sample with a performance of 3 showed an improvement of 0.5 - 1 points after binder applications. It was observed that the binder concentration was not an important variable, but the best results were measured after polyacrylate-derived binder application (Experiments 8 and 9). This situation led us to conclude that the active substance forming the chemical structure of the binder material adheres the raising fibers to the fabric surface better than the others.

Table 9. Test results for binder trials

Trial number	The type of binder	The concentration of binder (g/l)	Raising fastness	Air permability (l/min)	Bursting streng (kpa)
1	A	10	3/4	192	207
2	A	30	3	179	206
3	A	50	3/4	181	207
4	B	10	3	203	215
5	B	30	3	189	213
6	B	50	3	195	211
7	C	10	3	192	215
8	C	30	4	195	223
9	C	50	4	181	221
Original Sample (without binder)			3	218	218

When evaluated in terms of bursting strength, it was seen that the strength of the reference sample was 218 kPa, while all other trials were almost the same. It has been determined that these tests have no effect on bursting strength.

When the data shown in Table 10 are examined in terms of air permeability, it was determined after the measurements that all trials were at least 10% lower than the air permeability of the reference 218.78 l / min in the same table. Here, it has been determined that the layer formed by the polymeric binder chemical reduces the permeability and thus the comfort of use. However, it has been observed that there is no significant difference between polymer concentrations or types, they all cause a similar decrease.

4. CONCLUSION

3 thread futter knitted fabrics are fabrics known for raising the back side and napping the yarns on this side. This back surface napping is an application that improve the touch, bulk, and comfort properties of the fabric. However, when the back yarn is raising, the fibers in its structure cannot be attached to the fibers located in the yarn, its weak adhesion on the surface causes these fibers to form debris with mechanical effect. Then these rashes stick to their clothes or body in a way that disturbs the consumer. This negativity is recorded as the most important quality and reason for return by the consumer for the garments made of 3 thread fabrics. Within the context of the study, it is aimed to determine the changes over the physical performance properties of the fabric such as raising fast ness, air permeability, and bursting strength of some chemicals (silicone softeners, binders, etc.) which are used before and after the raising process and minimize the problem of raising fastness performance and therefore the problem of fiber shedding due to raising for 3-yarn fabrics. In order to make this evaluation, the results of the burst strength and air permeability tests, both of which are important for this type of knitted fabrics, were also examined in addition to the fiber loss performance, which is described as raising fastness.

In terms of raising fastness, performance, and product cost evaluation of all examined parameters for both fabrics (Fabric 1 and Fabric 2) was made. As a result, Type 2 fabric, which is single passage raising with Softener 7, gave the best performance. It can be emphasized that Pre-softening and raising speed do not affect the fastness of

raising in terms of performance, but considering the cost factor, it can be emphasized that working with speed 2 and Softener 1 will be more economical because fast working will directly contribute to production. While the end of raising softener type is very effective, it has been determined that the amount of use has no statistically significant effect. Accordingly, it can be said that using softener 7 at a low rate (5 g / L) would be more optimal. A comparison of parameters in terms of raising fastness can be seen in Table 10. According to table 10, the most suitable parameters in terms of raising fastness can be listed as follows; Type 2 fabric, Pre-softening softener 1, 15 m/min raising speed, single passage, and low concentration (5 g/l) with 2nd softening softener 7.

In terms of bursting strength, the strength values were higher in knitted samples with a single passage raising. Likewise, it was determined that the fabrics in which the softener 7 substance was applied in the softening at the end of the raising showed higher strength and from this, the binder in the Softener 7 made a positive contribution to the strength. It is thought that the other three parameters (Pre-softening Softener Type, Raising Speed and The Concentration of 2nd Softener Agent) do not have statistically significant effects and it will be sufficient to evaluate them only in terms of cost. As a result of the evaluations made in terms of performance and cost for bursting strength, suitable working conditions; It was determined that it is similar to the process sequence specified in raising fastness.

As a result of the performance evaluation for both fabrics in terms of air permeability, it was determined that all parameters were very close to each other, and fabrics treated with Softener 7 only after raising were more permeable.

The high performance demonstrated by the application of Softener 7 in 3 thread futter fabrics created the need for a more detailed study of the studies on the binder. As a result of the experiments conducted to examine the use of binder in raising fabrics, it was determined that the use of binder improves the fiber loss performance after raising regardless of the concentration but does not change the burst strength. However, it has been observed that it harms air permeability and touch. It has been determined that polyacrylate-based binders improve the fastness of raising, but together with it increase the hardness of the fabric.

Table 10. Comparison of parameters in terms of raising fastness

Parameters	The type of fabric	The type of pre-softening agent	The number of passages	The speed of raising	The type of 2nd softener agent	The concentration of 2nd softener agent
Level	Fabric 2 Type 2	Softener 1	Single Passage	S2-15 m/dk.	Softener 7	Low-5 g/l
Technical Results	Better performance	No matter	Better performance	Better performance	Better performance	No matter
Economical Results	More economical	No matter	More economical	More economical	No matter	More economical

It was seen that the best result in terms of raising fastness was the fabric with 50% waste + 50% Polyester back yarn. As a process, it was determined that the best result was obtained after a single passage with micro silicon pre-softening and raising at a speed of 15m / min, and then a low concentration 2nd softening process with a polyvinyl acetate-based binder and softener mixture. It has been observed that the binder additive also increases the bursting strength and air permeability.

REFERENCES

- Marmaralı A.B., (2004). *Atkı Örmeciliğine Giriş*. Ege University Publication of Research and Application Center of Textile and Apparel Manufacturing, İzmir.
- Sarker M., Rahman T., Rahman M., (2012). Study on Fleece Knit Fabric. Daffodil International University, Dhaka.
- Pailthorpe M., (2009). *Dry Finishing of Wool Fabrics*. The Australian Wool Education Trust Licensee for Educational Activities University of New England.
- Schindler W.D., Hauser P. J., (2004). *Chemical Finishing of Textile*. Woodhead Publishing Ltd. Cambridge, England.
- Candan C., Önal L., (2002). Dimensional, Pilling, and Abrasion Properties of Weft Knits Made from Open-End and Ring Spun Yarns. *Textile Research Journal*. 72(2), 164-169.
- Çoruh E.H., (2004). Investigation of Dimensional Stability of Knitted Fabric (Master's Thesis). Textile Engineering University of Gaziantep, Gaziantep.
- Gülsevin N., (2005). A Research About Comfort Properties of Sportswear (Master's Thesis). Department of Textile Engineering, Institute of Science and Technology, Aegean University, İzmir
- Meriç B., Demirhan F., (2005). The Searching Of Dimensional Changes On The Knitted Fabrics And Garments After Washing And Drying. *Pamukkale Üniversitesi Mühendislik Bilimleri Dergisi*, 3, 381-390.
- Güneşoğlu C., (2006) Developing Performance Properties of Sportswear Fabrics Using Nanotechnological Products and Investigation of Application Techniques (Doctoral Thesis). Department of Textile Engineering, Institute of Science and Technology, Uludag University, Bursa.
- Erkoç S., (2006). Yuvarlak Investigation of The Parameters Affecting The Properties of Knitting Fabric Manufactured by Circular Knitting Machine (Master's Thesis). Department of Textile Engineering, Institute of Science and Technology, Çukurova University, Adana.
- Emirhanova N., Kavuşturan Y., (2008). Effects of Knit Structure on the Dimensional and Physical Properties of Winter Outerwear Knitted Fabrics, *Fibres&Textiles in Eastern Europe*, (16)2, 69-74.
- Baçan V., (2010). Specification of Technologic Aspect of Industrial Knitted Clothing Products (Ph.D. Thesis). Home Economic (Handcrafts) Department, Institute of Science and Technology, Ankara University, Ankara.
- Mezarcıöz S., (2010). Investigation and Statistical Modelling of Selected Properties of Fabrics Knitted Using The Yarns Spun By Different Spinning Systems (Doctoral Thesis). Department of Textile Engineering, Institute of Science and Technology, Çukurova University, Adana.
- Özyazgan V., (2010). Final Processes Dependent Dimensional Changes of Double Knit Fabrics (Doctoral Thesis). Department of Textile Engineering, Institute of Science and Technology, Marmara University, İstanbul
- Ertekin G., Marmaralı A., (2011). Effects of Tuck and Miss Stitches on Thermal Comfort Properties of Plain Knitted Fabrics. *Tekstil ve Mühendis Dergisi*, (18) 83, 22-26.
- Taştan E.Ö., (2013). Investigation of Heat and Moisture Transfer Properties of Some Knitted Fabrics Used in Active Sportswear (Master's Thesis). Department of Textile Engineering, Institute of Science and Technology, Uludag University, Bursa.
- Yurdakul B., Özçelik E., Sakin S., (2014). Development of Water Repellant Sportswear by The Combination of Chemical Treatment and Membrane Structures. XIII th International İzmir Textile and Apparel Symposium, İzmir, Türkiye.
- Güneşoğlu S., Meriç B., Güneşoğlu C., (2005). Thermal Contact Properties of 2-Yarn Fleece Knitted Fabrics. *Fibres&Textiles in Eastern Europe*, 13, 2(50), 46-50.
- Güneşoğlu S., (2005). Investigation of Comfort Features of Sports Wear (Doctoral Thesis). Department of Textile Engineering, Institute of Science and Technology, Uludag University, Bursa.
- Tatlı N.Ö., (2007). Effects of Structure of Three Thread Fleece Fabrics and Applied Finishing Treatments on Flammability Characteristics of These Fabrics (Master's Thesis). Department of Textile Engineering, Institute of Science and Technology, İstanbul Technical University, İstanbul.
- Balcı O., Asker Ğ., Yolaçan G., Örtlek H.G., C., (2011). Determination of the Parameters Having Effect on the Production and Usage Performances of 2-Thread Fleece Knitted Fabrics. *Tekstil&Teknik Dergisi*, 27 (323), 86-92.
- Badr A.A., El-nahrawy A., (2016). Moisture Properties of Raised 3-Thread Fleece Fabric Knitted with Different Face and Fleecy Yarns. *Alexandria Engineering Journal* 55, 2881-2892
- Asker Ğ., Akkuş E., Arslan İ., Sevilmiş M., Pektaş K. and Balcı O., (2019). Investigation of The Fibre Loss Effect of Raised 3-Thread Fleecy Fabric. *Tekstil ve Mühendis*, 26(116), 346-352.

Acknowledgement

This study was supported by The Scientific and Technological Research Council of Turkey (TÜBİTAK) with Project No: 3161066.



Development of Temperature and pH Responsive Smart Cotton Fabrics by P(NIPAM-co-MAM) Copolymer Finishing

Sena Demirbağ Genç^{1,2}  0000-0003-1634-6391

Sennur Alay Aksoy^{3*}  0000-0002-5878-6726

¹Uşak University/Textile Engineering Department/Uşak 64200, Türkiye

²Uşak University/ Scientific Analysis and Technological Application and Research Center/Uşak 64200, Türkiye

³Süleyman Demirel University/ Textile Engineering Department/ Isparta 32260, Türkiye

Corresponding Author: Sennur Alay Aksoy sennuralay@sdu.edu.tr

ABSTRACT

In this study, fabrication of smart polymer and cotton fabrics with temperature- and pH-responsive as well as antibacterial activity was aimed. For this aim, random poly(N-isopropylacrylamide-co-methacrylamide) P(NIPAM-co-MAM) copolymers containing different ratio of NIPAM/MAM monomers were synthesized through free radical addition polymerization method via 2,2'-azobis (2 methylpropionamide) dihydrochloride as an initiator. Analysis results showed that the copolymers were synthesized successfully and their LCST values were in the range of 33°C to 41°C. A selected sample of the synthesized copolymers was applied to the cotton fabric via double-bath impregnation method and thermo-responsive wetting property of the fabric was examined via wetting time and water uptake tests, contact angle measurement. The test results indicated that hydrophilic character of the fabric changed to the hydrophobic character reversibly depending on change in temperature. Besides, the fabric exhibited pH-responsive water absorption ability. The fabric could manage water vapor permeability via changing its pore size as well as hydrophilic character depending on temperature. Besides, it was concluded that the fabric had strong antibacterial activity against *S.aureus* bacteria.

1. INTRODUCTION

Clothing textiles are objects with a large surface area used notably for the protection of the body from environmental conditions. Therefore, they can be used with great benefit for the wearer as a smart interface. For example, the fabrics used to fabricate clothing could develop better thermal exchange with the environment as active surface to manage temperature and moisture of the body. The conventional clothing fabrics save passive thermophysiological comfort to the clothing, which is inadequate to adapt to the changes in environmental conditions and activity levels of the wearer. However, the feature, known as active comfort regulation which means to manage the heat transfer between the body and environment in a dynamic environment and keep the body temperature constant in

sudden environment (temperature and humidity) change, can be achieved with the smart fabrics. The active comfort regulation function of the clothing can be provided by application of the various smart materials such as stimuli-responsive polymers, shape memory polymers and phase change materials to the clothing fabrics. [1,2] Nowadays, the textile industry shows an increasing interest in environmentally responsive or stimuli-responsive textiles containing stimuli-responsive polymer which is one of the kind of the smart polymers.[3]

Temperature-responsive polymer which is one of the type of the stimuli responsive polymers has a critical solution temperature (CST), which can be defined as a critical temperature. The solution of the polymer exhibits a phase separation at the CST, which moves from the isotropic state

To cite this article: Demirbağ Genç S, Alay Aksoy S. 2022. Development of temperature and pH responsive smart cotton fabrics by P(NIPAM-co-MAM) copolymer finishing. *Tekstil ve Konfeksiyon*, 32(3), 193-207.

ARTICLE HISTORY

Received: 05.08.2021

Accepted: 12.04.2022

KEYWORDS

Smart textile, thermo-responsive polymer, stimuli responsive, pH-responsive, cotton fabric

to the anisotropic state. The lower critical solution temperature (LCST) defined as a critical temperature at which the polymeric solution shows a phase separation. A polymer with lower critical solution temperature (LCST) shows the solution phase below LCST and becomes insoluble over LCST. [4] Thermo-responsive polymers with LCST change their hydrophilic-hydrophobic properties reversibly depending on change in temperature. At temperatures below LCST, polymer macromolecules are swollen state because of the formation of hydrogen bonds between hydrophilic groups in the polymer chain and the water molecules taken into the structure, and exhibit hydrophilic character. At temperatures above LCST, polymer macromolecules shrink due to increased interaction between hydrophobic groups in molecular structure, and display hydrophobic character. [5-8] The change in porosity caused by the swelling or shrinkage of the polymer molecules enables use of these polymers for smart filters [9,10] and smart textile materials. [11-14] Recently, these polymers have been used in drug release [15, 16] and tissue engineering. [17] Poly(N-isopropylacrylamide) (PNIPAM) consisting of amide and propyl moieties is the most known of thermo-responsive polymer and exhibits temperature-dependent hydrophilic/ hydrophobic switching at the critical solution temperature of 32 °C. [18] Below LCST, water molecules solve the hydrophilic amide groups of the PNIPAM and causes it to be water soluble and in a flexible, coiled form. Above LCST, PNIPAM becomes insoluble in water, the interactions between its hydrophobic propyl groups become stronger and the hydrogen bonds weaken, resulting existing of globular form of the molecules. The polymer chains collapse and water loss from the structure occurs. LCST of the PNIPAM polymer can be changed by copolymerization of the NIPAM monomer with various polymers such as poly (ethylene glycol), poly (acrylic acid) and cellulose, etc. [19-21] The copolymerization with hydrophobic polymers results a decrease in LCST of the PNIPAM. On the other hand, copolymerization with hydrophilic polymers leads to an increase in LCST due to the overall increase in hydrophilicity of the molecule and hence an increase in the hydrogen-bonding interactions between the polymer and water molecules. [22] Additionally, copolymerization of the PNIPAM with ionic molecules offers pH sensitivity to the polymer as well as thermo-sensitivity. The pH responsive polymers are smart polymers that can react to pH change as a variable condition. There are acidic or basic ionizable groups in their structures which take or give a proton depending on change in pH. The proton exchange results change in the polymer chain conformation, resulting in swelling or shrinkage of the polymer. [23, 24] The pH responsive polymers with acidic side groups ionize when the pH of the medium is higher than their value of pKa (the acid dissociation constant), which causes an increase in the hydrophilicity of the polymer network. In contrast, the hydrophilicity of the pH responsive polymers with basic side groups rise at the pH value lower than pKb (the basic dissociation constant). [25-27] A pH and thermo-responsive

copolymer attract or repel the water according to ambient pH and temperature. Hence, textiles functionalized with pH/thermo-responsive polymer are expected to exhibit controlled moisture/water management properties, depending on changes of their surrounding environment. Such functionalized textiles offer new opportunities for applicable to biomedical and protective clothing. [28]

According to the literature survey, copolymers of the PNIPAM with various co-monomers have been synthesized to tailor LCST for particular applications. Some researchers synthesized the PNIPAM copolymers be able to apply to the fabrics for usage in developing smart textiles. For example, Wang et al. (2016) were synthesized poly(N-isopropylacrylamide)/chitosan (PNIPAAm/Cs) hydrogels using redox initiator and applied to cotton fabric using glutaric dialdehyde (GA) as a crosslinker in order to increase the thermo-sensitive behavior and antibacterial activity. The LCST of the synthesized hydrogel was determined as 33 °C. Their results confirmed that the fabric exhibited hydrophobicity around the LCST and high antibacterial activity. [29] Štular et al. (2017) investigated the fabrication of stimuli responsive cotton fabric by applying temperature and pH responsive microgel and nanogel. They applied temperature responsive poly (N-isopropylacrylamide) and pH responsive chitosan hydrogels to the cotton fabric by pad-dry method. The results indicated that fabric having thermo-responsive air and moisture management ability was achieved regardless of hydrogel particle size. Besides, it was determined that their application at 4 times lower concentration, due to the decreasing size of the nanogels, gave lower stiffness as well as comparable responsiveness to the fabric. [30] Wang et al. (2017) synthesized a random poly(n-isopropylacrylamide-co-ethylene glycol methacrylate) P(NIPAM-co-EGMA) copolymer by atom transfer radical polymerization (ATRP) method and crosslinked it to cotton fabric via cross-linker citric acid. They concluded that increase in the molar ratio of ethylene glycol methacrylate (EGMA) increased the transition temperature of the copolymer due to the hydrophilic character of the EGMA. However, Tg of the copolymer significantly dropped with increase in EGMA molar ratio because of its hydrophobicity and low Tg. The cotton fabrics cross-linked with P(NIPAM-co-EGMA) exhibited a dual function. Above transition temperature, air and moisture permeability of the cotton fabrics crosslinked by copolymer dramatically increased due to porous structure formed on the fabrics. The cross-linked fabrics were able to nearly recover the values of the untreated fabric although they were polymer coated. Additionally, the fabrics had significantly higher inhibition of bacterial adhesion at room temperature compared to that of original cotton, reaching values of PEGMA coatings. [31] Huang et al. (2019) was synthesized a random poly (N-isopropylacrylamide-co-furfuryl methacrylate) copolymer through free radical polymerization method using 2,2'-azobis (2-methylpropionitrile) (AIBN) as an initiator. The researchers determined that LCST value of the copolymer decreased compared to the PNIPAm polymer because of

introduction of the hydrophobic comonomer. The nylon fabric treated with the synthesized copolymer could able to control its pore size by the shrinkage and swelling of the copolymer depending on change in temperature.[32] Chaudhuri and Wu synthesized a random poly[(N-isopropylacrylamide)-co-(2-hydroxyethylmethacrylate)-co-(N-methylolacrylamide)] copolymer using free radical polymerization method and coated it onto polyethylene terephthalate fabric. They revealed that thermo-responsive copolymer which LCST was tailored by changing the molar ratio of the comonomer was successfully synthesized. The fabrics treated with copolymers exhibited switchable wettability and moisture absorption/release properties as a function of the temperature. The moisture management feature of the fabric depending on temperature provided active thermophysiological clothing comfort by balancing the humidity of the microclimate with the surrounding air conditions. [33]

Cotton is a natural, breathable fiber and has a soft attitude, high moisture and sweat absorption capacities. These properties make the cotton clothing the popular in daily life. However, the cotton fabric absorbs sweat and metabolic products, which may provide nutrient sources for the growth of microorganisms such as bacteria and fungi. These microorganisms under atmosphere conditions grow rapidly and lead to unpleasant odor, stains, discoloration, reducing the fabric mechanical strength and increasing cross-contamination probability. [34] To overcome these type problems and develop the thermal clothing comfort there is a high requirement for cotton fabrics having antibacterial activity and dynamic temperature regulation function in various end use areas such as sport wearing and medical textiles. Considering this requirement, this study aimed to fabricate cotton fabric having active thermal comfort regulation and antibacterial activity by cross-linking of a dual function polymer.

For this aim, LCST type temperature- sensitive polymer, which could provide dynamic thermal regulation by change from a warming fabric to a cooling fabric above the LCST, was preferred. Among these polymers, PNIPAM polymer, whose LCST value was close to human body temperature, was chosen. In the study, it was focused on synthesis of a random PNIPAM copolymer containing components responsible for temperature/pH sensitivity and antibacterial activity. The authors in their previous work, a thermo-responsive PNIPAA homopolymer was synthesized and grafted onto the cotton fabric using free radical polymerization in order to fabricate thermo-responsive cotton fabric capable of smart moisture/water management. In the study, polymer synthesis and grafting to the cotton fabric were carried out simultaneously by a single process.[7] In this study, unlike their previous studies, the authors focused on synthesizing a new PNIPAM copolymer providing antibacterial activity and pH sensitive functions as well as smart moisture management and wettability depending on temperature to the cotton fabric. For this aim, P(NIPAM-co-MAM) copolymers were synthesized by free

radical addition polymerization method using different ratio of NIPAM/MAM monomers and then applied to the cotton fabric by a double bath impregnation process. In the study, the effect of the addition of methacrylamide to the poly(N-isopropylacrylamide) back bone on the LCST of the copolymer was also investigated. The chemical structures of the synthesized copolymers were examined using Fourier- Transform Infrared (FT-IR) spectroscopy and ¹H-Nuclear magnetic resonance (¹H NMR) analyses. Turbidity test was performed to investigate the thermo-responsive behavior of the copolymers. The cotton fabrics capable of pH and temperature responsive smart moisture/water management were fabricated by application of the synthesized P(NIPAM-co-MAM) copolymer. For this, the copolymer with the closest LCST value to body temperature was cross-linked to the cotton fabric accompanied by a carboxylic acid-based cross-linker (BTCA) via a double bath impregnation method. Scanning Electron Microscopy (SEM) analysis was carried out to study morphology of the copolymer-applied fabrics. To characterize thermo-responsive hydrophilic/hydrophobic behavior of the fabrics, the wetting time test, water uptake test, contact angle measurements and water vapor permeability test were performed at temperatures below and above the LCST. To study pH sensitivity of the fabrics, the alteration in their water absorption ability at acidic, neutral and basic pH values was determined at temperature of 20 °C. Antibacterial activity of copolymer containing fabric against *S. aureus* bacteria was tested by quantitative test method. The effect of polymer application on the mechanical properties of the fabrics was measured by tear strength and bending stiffness tests. Besides, durability of the thermo-responsive property of the copolymer-applied fabrics was investigated after repeated washings.

2. MATERIAL AND METHOD

2.1 Material

N-isopropylacrylamide (NIPAM) purchased from Sigma Aldrich company was used as monomer to synthesize temperature responsive polymer. Methacrylamide (Acros Organics) (MAM) and 2,2'-azobis (2 methylpropionamide) dihydrochloride (AMPA) (Acros Organics) were used as co-monomer and initiator, respectively. All chemicals used directly without purification. Polymer synthesis was carried out in distilled water.

A 100 % cotton plain weaved fabric, which was scoured and bleached, supplied from Söktaş Textile Company (Turkey) was used to produce temperature responsive fabric. The weight of the fabric was 151 g/m² and it had 61 threads per cm in the warp direction and 38 threads per cm in the weft direction. 1,2,3,4-Butanetetracarboxylic acid (BTCA) as cross-linker and sodium hypophosphite (SHP) as its catalyst were used in order to fix the copolymer to the cotton fabric. They were purchased from Sigma-Aldrich company.

2.2. Method

2.2.1. Synthesis of dual responsive copolymer

Synthesis of the P(NIPAM-co-MAM) copolymer, expected to exhibit both thermo-responsive and pH-responsive properties was carried out using free radical addition polymerization method. The schematic representation of the polymerization reaction was given in Figure 1. In the synthesis of copolymer, NIPAM/MAM monomer ratios were chosen as 9/1, 9.5/0.5 and 9.75/0.25. NIPAM and MAM monomers were dissolved separately in 15 mL and 5 mL distilled water, respectively, and then the solutions were mixed. AMPA (1 % mole) dissolved in distilled water was added dropwise to the mixture of NIPAM and MAM monomer solutions. The reaction solution poured into glass tube was purged with nitrogen gas for 1 minute and then synthesis of the copolymer was carried out in a water bath for 5 hours at 80 °C. The powder copolymer was obtained by removing water after the polymerization reaction was terminated. The copolymers synthesized with NIPAM/MAM monomer ratios of 9/1, 9.5 / 0.5 and 9.75/0.25 were named as P(NIPAM-co-MAM)-1, P(NIPAM-co-MAM)-2 and P(NIPAM-co-MAM)-3, respectively.

2.2.2. Application of the P(NIPAM-co-MAM)-2 polymer to the cotton fabric

The P(NIPAM-co-MAM)-2 copolymer was chosen as a sample polymer to apply fabric because of its closest LCST value to human body temperature. Before polymer application, fabric was washed in the bath containing 2 g/L of nonionic surfactant (Span 20) at 60 °C for 40 minutes in order to remove possible residues, rinsed and dried at room temperature. Polymer application was carried out via a double-bath impregnation method. In the first bath, fabric samples were impregnated with the first bath solution under a pressure of 2 bar and a speed of 2 m/min on laboratory type foulard machine and then dried at 80 °C for five minutes and cured at 160 °C for five minutes. The first bath contained 3.75 g BTCA cross-linker per 1 g polymer and ratio of the SHP catalyst to the cross-linker was 4/1. Fabric treated with the first bath was immersed in the aqueous polymer solution (the second bath at concentration of 30 g/L or 50 g/L) for 1 hour. At the end of 1 hour, the fabric was passed from foulard, dried at 80 °C and cured 160 °C for five minutes. The fabrics treated with polymer concentrations of 3% and 5% were termed as CF-P

(NIPAM-co-MAM)-3 and CF-P (NIPAM-co-MAM)-5, respectively. In the study, fabrics treated by BTCA at the same amounts used in the polymer application baths were tested to examine the effect of BTCA application on the properties of the fabric. The abbreviations for these control fabrics were defined as BTCA-3 and BTCA-5.

2.2.3. Characterization of the copolymer

¹H NMR and Fourier Transform Infrared (FT-IR) spectroscopy analyses were used to investigate chemical structure of the synthesized P(NIPAM-co-MAM) copolymers. The ¹H NMR analysis was carried out on a Bruker 400 MHz instrument and deuterated dimethyl sulfoxide (DMSO) was used as solvent in the analysis. FT-IR spectroscopy analysis was performed using Perkin Elmer Spectrum BX instrument, on KBr disks, between wavenumbers of 4000 cm⁻¹ and 400 cm⁻¹. The molecular weights of the synthesized copolymers were determined by cryoscopy method. The basis of this method is to determine the decrease in the freezing point of a solution in which organic matter is dissolved. Water was selected as solvent in the analysis and Equation (1) was used to calculate molecular weight of the polymer.

Where t_d is decrease in freezing point; M is molecular weight of the solute, W_1 is weight of the solvent (g), W_2 is weight of the solute (g) and K_d is freezing temperature drop constant)

$$\Delta T_d = \frac{1000 \times K_d \times W_2}{M \times W_1} \quad \text{Equation (1)}$$

Thermo-responsive properties of the synthesized P(NIPAM-co-MAM) copolymers were examined by turbidity test. In the test, 1 % aqueous polymer solutions were used. The solutions were heated in 1 °C increment from 30 °C to 40 °C and taken their photographs at each temperature increment to observe the temperatures at which they begin to be turbid. The temperature at which the polymer solution began to be turbid was accepted as its LCST value. Additionally, LCST value of a selected copolymer was measured by Differential Scanning Calorimeter (DSC) analysis (Netsch Polyma instrument). DSC analysis was performed range of the temperatures of -10°C and 60 °C at 5 °C/min heating rate under inert nitrogen gas atmosphere at a flow rate of 60 ml/min.

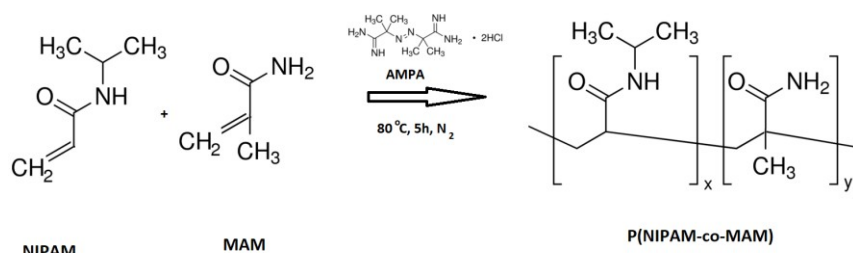


Figure 1. Schematic illustration for the synthesis of the P(NIPAM-co-MAM) copolymer

2.2.4. Characterization of the fabrics

Graft yield of the P(NIPAM-co-MAM)-2 copolymer onto the fabric was calculated using changes in the weights of fabrics before and after the grafting process. Morphology of the fabrics was investigated using Scanning Electron Microscopy (SEM, Phillips XL-30S FEG model). Their chemical structures were studied using FT-IR spectroscopy. The analyses were realized on KBr disk in the range of the wavenumbers of 4000 cm^{-1} to 400 cm^{-1} .

In the study, to investigate thermo-responsive wetting properties of the copolymer incorporated fabrics, the fabrics at different temperatures were tested by various tests such as immersion test [7, 35], drop test and water uptake test. Besides, contact angle measurement on the fabrics and surface energy calculation were carried out at temperatures above and below LCST of the copolymer. The wetting times of the fabrics owning 20 °C and 40 °C fabric surface temperatures were determined according to the AATCC 79 test standard. The surface contact angles of the fabric samples were measured by a sessile drop method using a goniometer (Dataphysics OCA 15 plus model instrument) and a CCD camera. Measurements were realized on the fabric surface, the temperature of which was gradually increased from 25 to 35 °C in an air environment with 10-25% relative humidity. The surface temperature of the fabric was checked with a Fluke Ti100 Thermal Imager during measurements. Water uptake of the fabrics was determined at temperatures changing between 25 °C and 35 °C with 2 °C increments using gravimetric method. [7] In order to determine pH responsive behavior of the fabric samples, their water absorption capacity at different pH values (pH 3, pH 7, pH 10) were investigated. The pH of the distilled water was adjusted to pH 3 adding acetic acid and pH 10 adding sodium carbonate (Na_2CO_3). Distilled water at room temperature was used in the test. The sample fabrics were thrown into the water with different pH values and kept in the water for 1 hour. At the end of the test, water uptake value was calculated using gravimetric method. [36,37] In the study, thermo-responsive water vapor permeability of the fabrics treated with copolymer was measured in a drying oven according to the modified BS 3424 control dish method. [7,38] To determine the significant differences ($p < 0.05$) of the test results statistically, a Duncan Multiple Dispersion Tests were applied using SPSS 20.0 software package.

To assess durability of the thermo-responsive features of the fabrics against to repeated washings, fabrics were washed at 30 °C for 30 minutes according to test standard of TS EN 20105-C06: 2001. The washings were repeated ten times. Water uptake capacities of the washed fabrics were measured.

Antibacterial activity of the copolymer incorporated fabrics against gram positive bacteria was determined using ASTM E2149-01 test method. This test method is designed to evaluate the resistance of specimens to the growth of

microbes under dynamic contact conditions. Antibacterial activity is determined by calculating the reduction rate in the number of microorganisms living in the solution. The same number of bacteria is inoculated to untreated (pure) and treated samples, and the decrease in the number of bacteria after 24 hours is calculated as a percentage. In the test, *S. aureus* (ATCC 29213) was used as test bacteria. In method, counting of bacterial colonies on the samples immediately after sowing (0 contact time) and after 1 hour, 3 hours and 24 hours' incubation was done using standard counting method and reduction rate in the number of bacteria was calculated using Equation (2). In the formula, A is the number of the bacteria obtained from test samples at contact time "0" and B is the number of the bacteria obtained from test samples incubated for a certain hour. [39]

$$\text{Bacteria reduction rate (\%)} = \frac{(A - B)}{A} \times 100 \quad \text{Equation (2)}$$

The effects of polymer application on mechanical properties of the fabrics were examined by tear strength and bending rigidity tests. Tear strength test was carried out according to TS EN ISO 13937-2 standard using a Lloyd LR5K Plus electronic tensile tester. Bending rigidity test was performed according to TS 1409 standard. Statistical analysis of the test results was carried out using the SPSS 20.0 statistical software, and Duncan Multiple Dispersion Tests was performed to determine significant differences ($p < 0.05$).

3. RESULTS AND DISCUSSION

3.1. Characterization of The P (NIPAM-co-MAM) Copolymer

3.1.1. FT-IR analysis results

The successful copolymerization of the NIPAM and MAM monomers were proved using FT-IR spectroscopy. As seen from FT-IR spectra given in Figure 2, the emerging C=C stretching peaks at 1620 cm^{-1} in the spectrum of NIPAM and at 1603 cm^{-1} in the spectrum of MAM disappeared in FT-IR spectrum of the P(NIPAM-co-MAM)-2. Disappeared C=C peak originated from addition reaction realized between NIPAM and MAM monomeric radicals, which were formed by opening of their double bonds by initiator. Moreover, the peaks at 1654 cm^{-1} and 1742 cm^{-1} in the spectrum of P(NIPAM-co-MAM)-2 were stretching vibrations of the C=O groups of the monomers. These two peaks showed the presence of the monomers in the copolymer molecule chain. The peaks at 1560 cm^{-1} and 1540 cm^{-1} in the P(NIPAM-co-MAM)-2 spectrum were characteristic bending vibrations of NH (amide II) group of the NIPAM monomer. The asymmetric and symmetric bending vibration of $-\text{CH}_3$ in isopropyl groups of the NIPAM monomer appeared at 1388 cm^{-1} and 1370 cm^{-1} in the spectrum of copolymer. The peaks at 2928 cm^{-1} and 2858 cm^{-1} in the spectrum of P(NIPAM-co-MAM)-2 were CH stretching peaks.

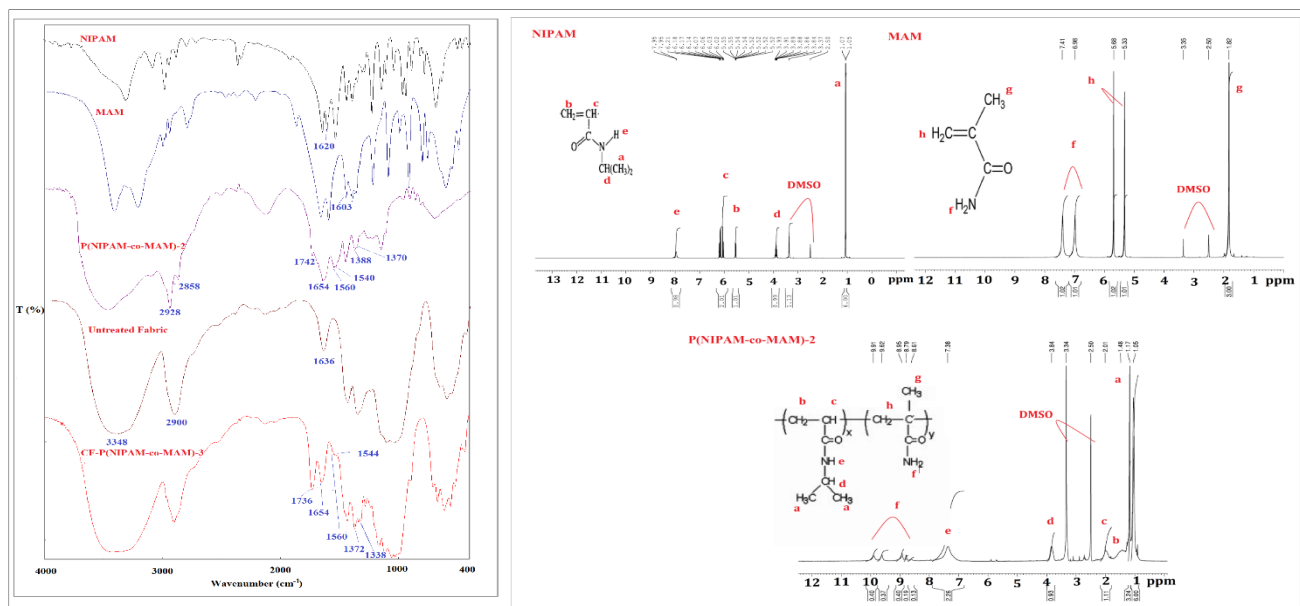


Figure 2. The FT-IR spectra (on the left) and ^1H -NMR spectra (on the right) of the NIPAM and PNIPAM

3.1.2. ^1H NMR analysis results

Figure 2 showed NMR spectra and molecular formulas of the monomers and copolymer. The protons displayed as "b" and "c" in the molecular formula of the NIPAM monomer appeared in the range of 5.52-5.55 ppm and 6.02-6.21 ppm in the spectrum, respectively. The methyl groups in the isopropyl group were in the range of 1.05-1.07 ppm in the spectrum of NIPAM monomer. The single proton in the isopropyl group, displayed as "d" in the spectrum, appeared at 3.9 ppm. Besides, NH group proton, displayed as "e", appeared at 7.95 ppm in the spectrum. According to the ^1H NMR spectrum of the MAM monomer given in Figure 2 methyl groups illustrated as "g" sharply appeared at 1.82 ppm. The peaks arose at 6.98 ppm and 7.5 ppm in the spectrum of the MAM comonomer were protons of the amine groups which displayed as "f" in the molecular formula. [40] In addition, vinylic hydrogen protons (=CH) illustrated with "h" in the molecular formula were observed at 5.33 ppm and 5.68 ppm. As seen from the spectrum of P(NIPAA-co-MAM)-2 copolymer, peaks of the monomer and comonomer were displaced in the spectrum of the copolymer and peaks of the vinyl groups disappeared. Methylene and methyl groups in the molecular structure of the MAM comonomer and methyl groups in the structure of the NIPAM monomer merged at 1.05 ppm and 1.17 ppm in the ^1H NMR spectrum of the copolymer. All these findings showed that the P (NIPAM-co-MAM) -2 copolymer has been successfully synthesized.

3.1.3. Determination of molecular weight

The number average molecular weight of the synthesized copolymers was determined by the cryoscopy method. The number average molecular weight was determined to be 4500 g/mole for P(NIPAM-co-MAM)-1 polymer, 4200 g/mole for P(NIPAM-co-MAM)-2 polymer, 4300 g/mole for P(NIPAM-co-MAM)-3 polymer. The synthesized

copolymers were concluded to have low and close to each other molecular weights.

3.1.4. Turbidity test results

To investigate thermo-responsive properties and determine LCST values of the synthesized copolymers, turbidity test was carried out. The aqueous solutions of the copolymers were transparent at a certain temperature range because of their water solubility (Figure 3). As known, a thermo-responsive polymer exhibits hydrophilic property and is water soluble at temperatures below its LCST value. However, polymer is insoluble in the water at temperatures above its LCST value because of increasing interaction between hydrophobic groups in its macromolecule chains. The interaction between hydrophobic groups of the polymer causes phase separation and its solution becomes to be turbid. [5] Temperature at which the polymer solution began to cloudy is accepted as LCST value of that polymer. As seen from Figure 3 a, turbidity of P(NIPAM-co-MAM)-1 copolymer solution started at 41 °C and its LCST value was determined as 41 °C. According to Figure 3 b-c, LCST values of P(NIPAM-co-MAM)-2 and P(NIPAM-co-MAM)-3 were detected as 34 °C and 33-34 °C, respectively. According to turbidity test results, LCST value of the P(NIPAM-co-MAM)-2 copolymer was found close to human body temperature. Therefore, its LCST value was verified by DSC analysis before application to fabric. According to the DSC analysis, LCST value of the P(NIPAM-co-MAM)-2 copolymer was measured as 34 °C (Figure 4). It was concluded that LCST value of the synthesized copolymer increased as the amount of hydrophilic copolymer added to the structure increased. This result was attributed to increasing interaction between the water molecules and hydrophilic and charged groups of the copolymers. Moreover, the P(NIPAM-co-MAM)-2 copolymer was chosen as proper thermo-responsive copolymer to be applied fabric because its LCST value was quite close to the human body temperature.



Figure 3. Images of the P(NIPAM-co-MAM)-1(a), P(NIPAM-co-MAM)-2 (b) and P(NIPAM-co-MAM)-3 (c) polymer solutions at different temperatures

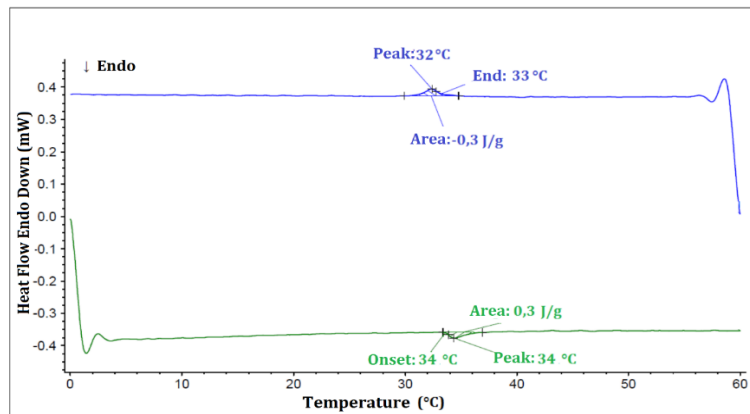


Figure 4. DSC thermogram of PNIPAM-co-MAM-2 copolymer

3.2. Characterization of Dual Responsive Fabric

3.2.1. Determination of grafting yield

Amount of the polymer added on the fabric structure was determined as grafting yield. The values were calculated as 19.24 % for the CF-P(NIPAM-co-MAM)-3 fabric and 20.6% for the CF-P(NIPAM-co-MAM)-5 fabric. According to the results, increase in the polymer concentration impregnated to the fabric slightly increased amount of the polymer transferred to the fabric.

3.2.2. SEM analysis results

Figure 5 indicated SEM micrographs of the untreated fabric and the fabrics treated with P(NIPAM-co-MAM)-2 copolymer. According to the images, fiber surfaces in the structure of the CF-P(NIPAM-co-MAM)-3 and CF-P(NIPAM-co-MAM)-5 fabrics were completely covered by polymer. Besides, the polymeric fractions forming the inter-fiber connections was observed on the CF-P(NIPAM-co-MAM)-3 fabric. However, a smoother and homogeneous coating was formed on the CF-P(NIPAM-co-MAM)-5 fabric surface because of increasing polymer concentration (Figure 5c) and this polymeric coating completely filled the spaces among the fibers.

3.2.3. Chemical analysis results by FT-IR spectroscopy

The chemical structure of the fabrics treated with copolymer was studied by FT-IR spectroscopy to confirm cross-linking of the P(NIPAM-co-MAM)-2 copolymer on the cotton fabric. In FT-IR spectrum of the untreated fabric, the peak at 3348 cm^{-1} corresponded to hydrogen-bonded OH stretching.

Besides, the C-H stretching peak at 2900 cm^{-1} and C-H wagging peaks at $1315\text{ -}1373\text{ cm}^{-1}$ were observed. The peak appeared at 1636 cm^{-1} was due to absorbed water molecules. [41,42] Compared to the FT-IR spectrum of the untreated fabric in Figure 2, the characteristic peaks of the P(NIPAM-co-MAM)-2 copolymer were observed in the FT-IR spectrum of the CF-P(NIPAM-co-MAM)-3 fabric. The typical amide I and II stretch vibrations of the copolymer were arisen at 1654 cm^{-1} , 1560 cm^{-1} and 1544 cm^{-1} . In addition, the characteristic peaks of the isopropyl groups of the copolymer were observed at 1372 cm^{-1} and 1338 cm^{-1} wavelengths. A peak appeared at 1736 cm^{-1} corresponding to the ester carbonyl group formed between BTCA and the hydroxyl groups (OH) of cotton fabric. [43,44]

3.2.4. Determination of the thermo-responsive wetting property

The change in hydrophilic property of the fabrics as a function of the temperature was examined by sinking behavior of the fabrics in the water and wetting time tests. Untreated fabric and copolymer-applied fabrics sank in the water at $20\text{ }^{\circ}\text{C}$ because of their hydrophilic character. When the temperature of the water increased to $40\text{ }^{\circ}\text{C}$, copolymer-applied fabrics moved to the water surfaces while the untreated fabric kept its position in the water (Figure 6). The upward movements of the copolymer-applied fabrics in hot water and their settling on the surface of the water were indicators of their hydrophobic character. The fabrics exhibited hydrophobic character at temperature above

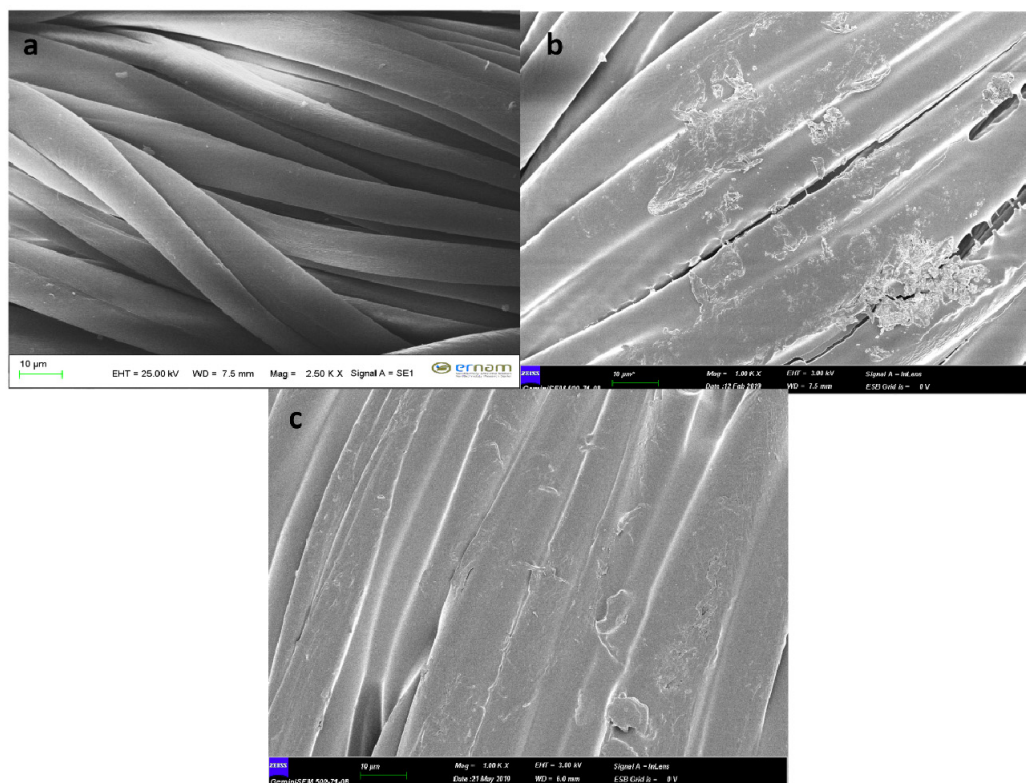


Figure 5. SEM micrographs of untreated cotton (a) [7], CF-P(NIPAM-co-MAM)-3 (b) and CF-P(NIPAM-co-MAM)-5 (c) fabrics.

LCST of the copolymer resulting with decreasing the adhesion force between the copolymer and the water molecules.^[7] The wetting time test confirmed these results. Wetting time of the untreated fabric at 20°C and 40°C was determined to be 0 s. Unlike, as the fabric surface temperature increased from 20°C to 40°C, the wetting time rose from 2.40s to 26.60s for the CF-P(NIPAM-co-MAM)-3 and from 3.9 s to 39 s for the CF-P(NIPAM-co-MAM)-5. This result showed that hydrophilic character of the CF-P(NIPAM-co-MAM)-3 and CF-P(NIPAM-co-MAM)-5 fabrics altered depending on change in temperature.

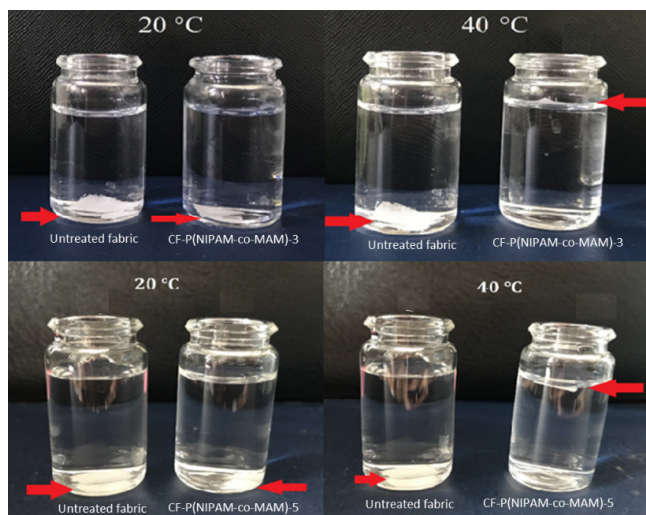


Figure 6. Sinking behavior of the untreated cotton fabric and treated fabrics in distilled water

In the study, thermo-responsive wettability behaviors of the fabrics were examined by measuring contact angle. Figure 7 a showed contact angles of the fabrics measured at different temperatures ranging from 25°C to 50°C. The contact angle of the untreated fabric was accepted to be 0° at each temperature due to the fact that the contact angle value cannot be measured as a result of instant absorption of the water drop. The contact angle of the copolymer-applied fabrics was measured almost 30° at temperature of 25°C. This showed unimportant decrease of the hydrophilic character of fabrics due to crosslinking of the cellulose molecules by BTCA. However, unlike untreated fabric, there was a sudden increase in contact angles of CF-P(NIPAM-co-MAM)-3 and CF-P(NIPAM-co-MAM)-5 fabrics in temperature range of 30 °C to 45 °C. LCST value (34°C) of the copolymer was in this temperature range. The maximum contact angle was determined to be 72.65° for CF-P(NIPAM-co-MAM)-3 and 63.98° for CF-P(NIPAM-co-MAM)-5. It was found the contact angle values measured for the CF-P(NIPAM-co-MAM)-5 fabric sample were lower than that of the CF-P(NIPAM-co-MAM)-3 because of decreasing surface roughness (Figure 7 a). The increment in the contact angle confirmed that the fabrics incorporated with copolymer transformed from the hydrophilic character to the hydrophobic character due to the temperature increase and had a thermo-responsive

wetting property. However, the contact angles of the CF-P(NIPAM-co-MAM)-3 and CF-P(NIPAM-co-MAM)-5 fabrics were not measured high enough to explain the hydrophobic character. As seen from SEM images given in Figure 5, application of the polymer caused to reduce the fabric surface roughness because of filling inter-fiber gaps by polymer molecules. This has prevented the contact angle value from reaching the desired angles ($\theta > 90^\circ$) at high temperatures.

3.2.5. Determination of the thermo-responsive water uptake property

In the study, water uptake values of the fabrics left in water with temperatures changing in the range of 25 °C to 40°C were measured to investigate thermo-responsive water uptake properties of the fabrics. The water uptake values of the pretreated fabrics and copolymer-applied fabrics were presented in Figure 7b. According to the results, water uptake behaviors of the untreated fabric, BTCA-3 fabric and BTCA-5 fabric were not significantly affected by change in temperature. However, crosslinking of cotton cellulose with BTCA caused to decrease in water uptake value compared to the untreated fabric. The cotton fabrics absorb water molecules by forming H bonds between hydroxyl (-OH) groups of the cellulose molecules and water molecules. In the esterification of cellulose molecules with BTCA, hydroxyl groups, which ensure the absorption of water molecules, react with the carboxylic acid groups of BTCA.^[44] Consequently, water uptake of the fabric is reduced because of the decreasing free -OH groups of cellulose. However, temperature rise affected water uptake values of the copolymer-applied fabrics. An important reduction in water absorption capacities started at 27 °C for the CF-P(NIPAM-co-MAM)-3 fabric and 29 °C for the CF-P(NIPAM-co-MAM)-5. The water absorption capacity diminished from 200% at 25 °C to 70% at 40 °C for the CF-P(NIPAM-co-MAM)-3 fabric. The value decreased from 90.75% to 65 % for the CF-P(NIPAM-co-MAM)-5 fabric. Decreasing water absorption capacity was more pronounced for the CF-P(NIPAM-co-MAM)-3 fabric. The high difference was due to the fact that P(NIPAM-co-MAM)-3 fabric had higher hydrophilicity at 25 °C. This decrease in water uptake was related to the predominance of hydrophobic groups in the P(NIPAM-co-MAM) macromolecule on the fabric surface with increasing temperature. As mentioned earlier, around their LCST value, the temperature sensitive polymers get hydrophobic character and their molecules shrinkage. The CF-P(NIPAM-co-MAM)-3 fabric had higher hydrophilic character at temperatures below LCST compared to CF-P(NIPAM-co-MAM)-5 fabric because of usage the less BTCA during polymer application. These results revealed that fabrics changed their hydrophilic character depending on increase in temperature and they exhibited temperature sensitive water absorption ability.

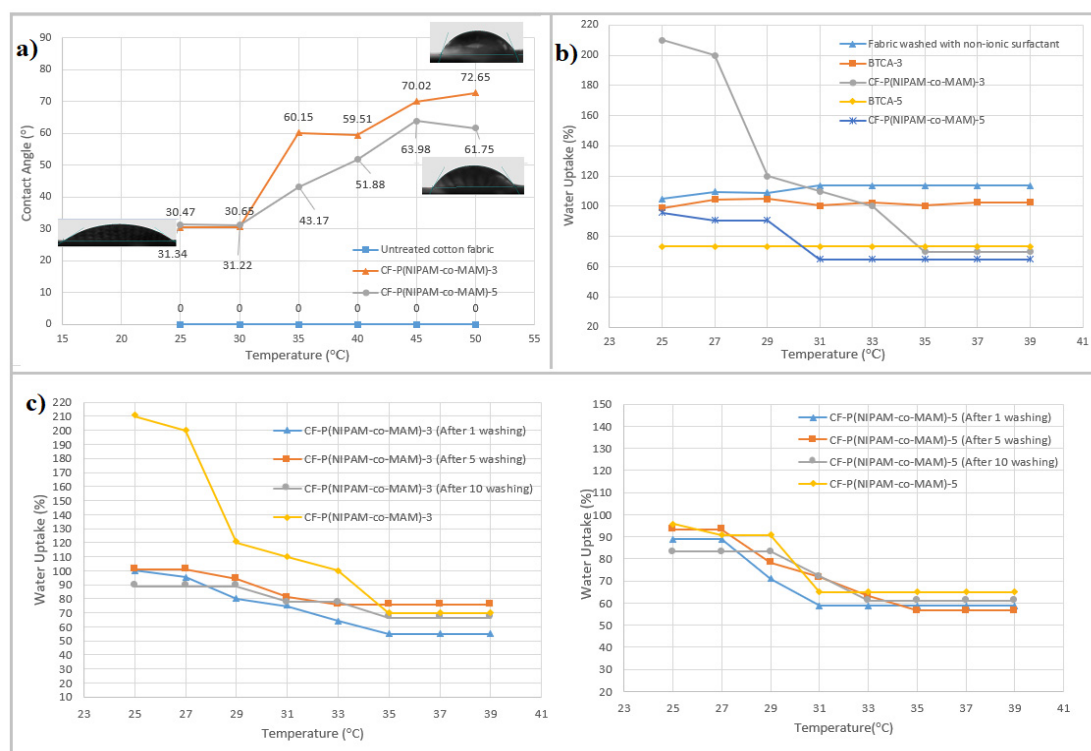


Figure 7. Test results of the fabrics (contact angle at different temperature (a), water uptake at different temperature (b), water uptake after repeated washings (c))

In the study, durability of the fabric thermo-responsive property against to repeated washings was examined by determining the changes in water uptake values of the washed fabrics. For this aim, water absorption capacities of the fabrics at temperature below and above LCST were measured after repeated washings. Water uptake values of the CF-P(NIPAM-co-MAM)-3 and CF-P(NIPAM-co-MAM)-5 fabrics after 1, 5 and 10-times washings were presented in Figure 7 c. According to the results, difference between the water absorption capacities measured above and below LCST started to decrease even if the first washing for the CF-P(NIPAM-co-MAM)-3 fabric and the CF-P(NIPAM-co-MAM)-5 fabric. After each wash cycle, the difference between water absorption capacity values measured above and below LCST value has closed. It was concluded that thermo-responsive property of the CF-P(NIPAM-co-MAM)-3 was weakened after especially first washing. However, the difference did not close completely even after 10 washes and was over 20% for the CF-P(NIPAM-co-MAM)-3 fabric. Based on this finding, it was concluded the fabrics kept their thermo-responsive properties even after 10 washes. However, it was concluded that increasing in the molecular weight of the synthesized polymer and developing the binding of the polymer to the fabric could positively change the permanence of the thermo-responsive property of the fabric.

3.2.6. Determining of the thermo-responsive water vapor permeability

To study temperature sensitive moisture management property of the copolymer-applied fabrics depending on

changes in the hydrophilicity and molecules conformation of the thermo-responsive polymer, water vapor permeability of the fabrics was measured at temperature below and above LCST of the copolymer. Water vapor permeability test results of the fabrics and statistical analysis results were shown in Figure 8 and Table 1, respectively. According to the results measured at 20°C, the fabrics treated with BTCA transferred less water vapor compared to untreated fabric. As described earlier, BTCA application reduces free OH groups in the cellulose molecule resulting decline in water vapor permeability by absorption. However, water vapor permeability increased after copolymer application to the fabrics pretreated by BTCA. Water vapor permeability of the CF-P(NIPAM-co-MAM)-3 and the CF-P(NIPAM-co-MAM)-5 fabrics was measured as higher compared to fabrics treated with BTCA because of increase in their hydrophilic character. Although the pores in the fabric structure were closed by polymer layer formed on the fabric surface after the copolymer application as seen from SEM images (Figure 5), the water vapor permeability increased. It was thought that increase was resulted from increasing hydrophilic feature of the copolymer grafted to the fabric surface at temperature below LCST. However, their water vapor permeability was lower compared to untreated fabric because the fabric pores were blocked by swollen hydrophilic copolymer molecules at temperatures below LCST (20°C). Increase in the amount of polymer transferred to the fabric significantly promoted this reduction in the water vapor permeability ($p < 0.05$). Regarding to the results measured at 40°C, evaporation of more water molecules at high temperature caused to rise in

water vapor permeability values of all fabrics. Application of the copolymer at concentration of 3% positively affected water vapor permeability. As expected, water vapor permeability of the CF-P(NIPAM-co-MAM)-3 fabric was statistically higher than other fabrics ($p < 0.05$) (Table 1). Shrinkage of the copolymer at 40°C (above the LCST) because of the increasing interaction between its hydrophobic groups resulted opening of the fabric pores and increasing water vapor permeability. However, unexpectedly, water vapor permeability of the CF-P(NIPAM-co-MAM)-5 was lower significantly compared to untreated fabric. This was due to limitation of opening of the pores resulted from shrinkage of polymer molecules because of high amount of the polymer transferred to the fabric. As known, the water vapor permeability is related to porosity and hydrophilicity [45] and the water vapor permeability of the fabrics can be controlled by a thermo-responsive smart polymer application which exhibits changeable porosity and hydrophilicity depending on change in temperature.

3.2.7. Determination of the pH responsive water uptake value

Presence of basic amino groups in the chemical structure of the MAM monomer of the synthesized copolymer provides

to copolymer pH sensitivity. The dissociation constant (pK_b) of the MAM co-monomer is pH 8. MAM molecule is found in ionic form at pHs less than pK_b . It exhibits hydrophobic property in alkaline environments ($pH > pK_b$). [25,46] It was expected that gaining hydrophobic character of the MAM molecules of the copolymer at pH 10 resulted reduction in the water absorption of the fabrics. In the study, to examine pH responsive properties of the copolymer-applied fabrics, water absorption ability of the fabrics at different pH values at temperature of 20 °C was measured. As seen from Figure 9, no significant difference in the water absorption ability of the untreated fabric was observed depending on change in pH. Although there was no significant difference between water uptake values of the fabrics measured at acidic pH and neutral pH, water uptake values of the copolymer-applied fabrics decreased prominently when the pH increased from 3 to 10. The water absorption capacity decreased from 105.53% at pH 3 to 80.14% at pH 10 for the CF-P(NIPAM-co-MAM)-3 fabric. The value decreased from 90.46% to 72.67% for the CF-P(NIPAM-co-MAM)-5 fabric. Consequently, the water uptake capacities of the copolymer-applied fabrics changed significantly depending on change in pH and the fabrics exhibited pH sensitive water uptake property as well as temperature sensitive water uptake property.

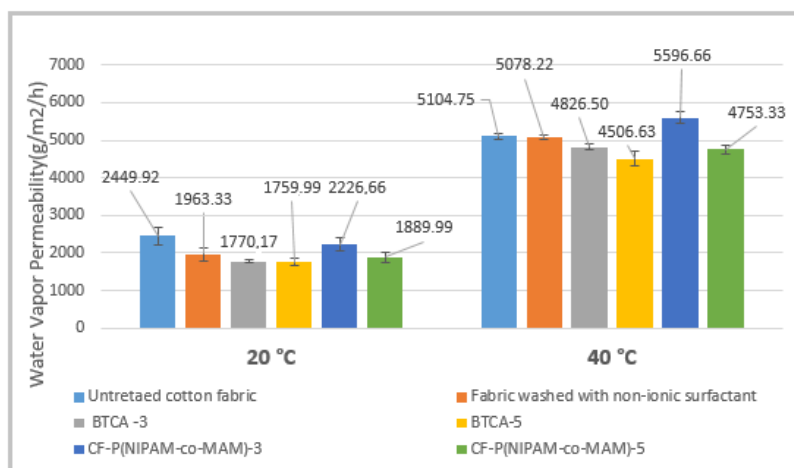


Figure 8. Water vapor permeability of the fabrics measured at 20 °C and 40 °C

Table 1. Statistical analysis results of the water vapor permeability, bending rigidity and warp tear strength test results

Sample	Water Vapour Permeability				Bending Rigidity				Warp tear strength					
	20 °C		40 °C		Subset for alpha = 0.05									
	1	2	1	2	3	4	1	2	3	4	5			
Untreated fabric		2449.92				5104.75		170.74						4.94
Fabric washed with non-ionic surfactant	1963.33					5078.22		-	-	-	-	-	-	-
BTCA-3	1770.17				4826.50		193.36	193.36						2.51
BTCA-5	1759.99				4506.63			209.43	209.43				1.98	
CF-P(NIPAM-co-MAM)-3		2226.66							225.97			1.36		
CF-P(NIPAM-co-MAM)-5										542.58		1.05		
Sig.	0.151	0.091	1.000	0.493	0.803	1.000	0.066	0.184	0.172	1.000	1.000	1.000	1.000	1.000

3.2.8. Determination of the antibacterial activity

Antibacterial activity of the CF-P(NIPAM-co-MAM)-3 fabric was investigated under dynamic conditions using *S.aureus* bacteria by a quantitative method (ASTM E2149-01 test method). In the Table 2, bacterial reduction rates (%) of the untreated fabric and CF-P(NIPAM-co-MAM)-3 fabric after 3-hours, 6-hours and 24-hours incubation were given. According to the test results, a gradual decrease in the number of bacterial colonies in the control group and untreated fabric was observed. After 24 hours, there was a 98.71% reduction for the control group and 99.87% for the untreated fabric in the number of bacteria colonies. The reason of decreasing was to die of the bacteria in the solution depending on time. On the other hand, 100% bacteria reduction was detected at the end of the 3-hours incubation for the CF-P(NIPAM-co-MAM)-3 fabric. It meant that all bacteria in the environment died during this period. This finding indicated that CF-P(NIPAM-co-MAM)-3 fabric had strong antibacterial activity against the *S.aureus* bacteria. Antibacterial activity of the synthesized copolymer, resulting in bacterial death might be due to the interactions between the positively charged groups on the polymer chains and negatively charged carboxylic acid groups of the macromolecules of the bacterial cell wall. The copolymerization of NIPAM with MAM increases cationic centers on the macromolecules, consequently, the net positive charge of the molecules is strengthened because of the protonated C=O and NH groups. [47,48]

3.2.9. Determining mechanical properties

Bending rigidity and warp tear strength tests were carried out in order to examine the effect of copolymer application on the mechanical properties of the fabrics and test results were presented in Table 3. Bending rigidity is associated with fabric stiffness and fabric stiffness rises as bending rigidity increases. [49] According to the test results, the bending rigidity increased after treatments with the BTCA and copolymer compared to untreated fabric. Moreover, increase in polymer concentration caused the bending stiffness to be significantly higher (CF-P(NIPAM-co-MAM)-5 fabric) ($p < 0.05$) (Table 1). Covering of the fiber surfaces and filling gaps between the fibers by the copolymer molecules as well as crosslinking of the fiber elements by BTCA cross-linker limited the movement of fibers and yarns and caused to increase of the bending resistance of the fabrics. [50] Besides, tear strength of the fabrics decreases as increasing bending rigidity because increased bending resistance causes the threads to break one by one. [51] Additionally, treatment by chemical finishes which restricts movement of the yarns in the fabric results in low tear strength. This decrease in tear strength may be attributed to acidic pH of the application bath as well as reduced yarn slippages. [52] The results of warp tear strength in Table 3 overlapped with this information. Each pretreatment and copolymer application caused to reduce in warp tear strength of the fabric significantly ($p < 0.05$) (Table 1).

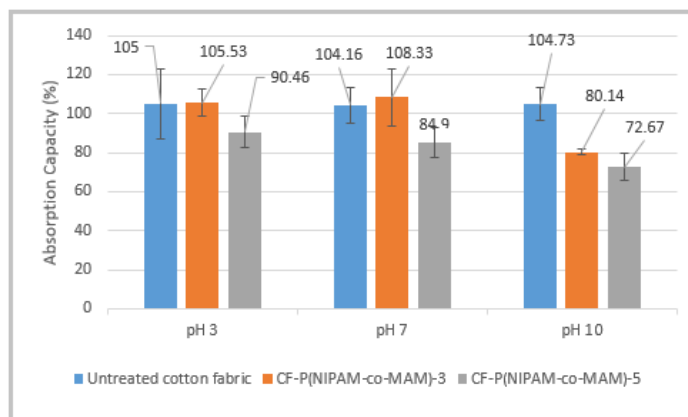


Figure 9. Water uptake test results at different pH values

Table 2. Antibacterial activity test results

Sample	Bacteria Reduction					
	3 hours		6 hours		24 hours	
	%	log	%	log	%	log
Control group	-7.69	-0.03	-42.31	-0.24	-98.71	-1.89
Untreated fabric	-19.23	-0.09	-79.62	-0.69	-99.87	-2.87
CF-P(NIPAM-co-MAM)-3	-100.00	-5.37	-100.00	-5.37	-100.00	-5.37

* The bacteria concentration transferred to each sample weighing 1 gram was calculated as 2.36×10^5 (log 5.37) cfu * / ml.

** (cfu: Colony forming unit).

*** Bacteria values given as (+) indicate an increase in the number of bacteria, and bacteria values given as (-) indicate a decrease in the number of bacteria. The value of (-) 100% indicates that all bacteria on the surface have been killed.

Table 3. The bending rigidity and warp tear strength test results

Sample	Bending rigidity test results (mg.cm) [SD]	Tear strength test results (N) [SD]
Untreated fabric	170.74 [21.81]	4.94 [0.01]
BTCA-3	193.36 [11.39]	2.51 [0.00]
BTCA-5	209.43 [7.00]	1.98 [0.06]
CF-P(NIPAM-co-MAM)-3	225.97 [8.83]	1.36 [0.15]
CF-P(NIPAM-co-MAM)-5	542.58 [36.61]	1.05 [0.01]

4. CONCLUSION

In this study, synthesis of a random PNIPAM copolymer containing components responsible for temperature/pH sensitivity and antibacterial activity and fabrication of cotton fabric having active comfort regulation and antibacterial activity were aimed. For this aim, a random copolymer of N-isopropylacrylamide with methacrylamide (P(NIPAM-co-MAM)) was synthesized via free radical addition copolymerization method and applied to the cotton fabric. The copolymer exhibited temperature sensitivity because of the presence of the NIPAM monomer and pH sensitivity because of the presence of the MAM monomer. The chemical structure of the copolymer was described by FT-IR spectroscopy and ¹H NMR analyses. Its thermo-responsive property was proved by turbidity test and DSC analysis. LCST values of the copolymers were detected in the range of the 34 °C and 41 °C depending on the change in MAM co-monomer ratio. The addition of hydrophilic MAM monomer to the polymer backbone increased LCST value of the synthesized copolymer compared to PNIPAM homopolymer because of increasing interaction between the water molecules and hydrophilic and charged groups of the copolymers. Thus, it was possible LCST value of the thermo-responsive PNIPAM polymer closer to the body temperature. In the study, synthesized copolymer (P(NIPAM-co-MAM)-2) with NIPAM/MAM monomer ratio of 9.5/0.5 had LCST of 34 °C and was chosen as polymer to be applied to fabric.

P(NIPAM-co-MAM)-2 copolymer was applied to the cotton fabric using a double-bath impregnation method. SEM analysis showed that copolymer covered fiber surfaces and filled gaps between the fibers. The smoother and uninterrupted coating on the fabric surface which completely filled spaces among the fibers was formed as the copolymer concentration increased in the bath. According to the fabric wetting and water absorption test results, copolymer-applied fabrics exhibited hydrophobic character at temperatures above LCST and their water absorption capacities decreased as a result of decreasing the adhesion forces between the molecules of the copolymer

and water molecules. However, the fabrics at temperatures below LCST exhibited hydrophilic character and their water absorption capacities increased. Additionally, it was concluded that fabrics kept their thermo-responsive properties even after 10 washes. However, it is thought increasing in the molecular weight of the synthesized polymer and developing the binding of the polymer to the fabric can positively change the permanence of the thermo-responsive property of the fabric. The fabrics treated with the thermo-responsive copolymer could manage their water vapor permeability by means of altering their porosity and hydrophilicity depending on change in temperature. The water vapor permeability of the copolymer-applied fabrics was lower compared to untreated fabric because the fabric pores were blocked by swollen hydrophilic copolymer molecules at temperatures below LCST. The decreasing in the water vapor permeability was insignificant for the lower polymer concentration (CF-P(NIPAM-co-MAM)-3 fabric) ($p > 0.05$). However, increase in the concentration of the copolymer caused to significant decrease in the water vapor permeability compared to untreated fabric. Shrinkage of the copolymer on the fabric surface at 40°C (above LCST) resulted the opening of the fabric pores and increasing water vapor permeability. Although the presence of the polymer coating on the surface of the fabric, their water vapor permeability at high temperatures was found to be higher significantly than the untreated fabric ($p < 0.05$). However, this effect was limited by the high amount of the polymer transferred to the fabric. Consequently, the CF-P(NIPAM-co-MAM)-3 fabric was found as a suitable thermo-responsive fabric capable of smart water vapor management. The copolymer-applied fabrics exhibited pH sensitive water uptake property. Their water uptake values decreased at basic pH, which was above the value of p_{kb} (pH 8) of the MAM co-monomer, compared to acidic and neutral pH values because decreasing hydrophilicity of the copolymer molecules.

In conclusion, in the study, dual stimulus sensitive cotton fabrics were produced successfully. It was concluded that fabrics produced in this study could be used to design smart thermo-responsive and pH sensitive textile products. Besides, fabric treated with copolymer had strong antibacterial activity against *S.aureus* bacteria. It is concluded this feature of the fabrics will be beneficial in terms of protecting both the cotton fabric and the user from the harmful effects of the bacteria in question. In addition, it is thought that developed fabric structures will be promising in the production of medical textile structures where antibacterial activity and thermophysiological comfort are important.

Acknowledgement

This work was financially supported by the Suleyman Demirel University (Project No. 4486-D2-16).

REFERENCES

- Dragan J. 2016. Polymer-Based Smart Coatings for Comfort in Clothing. *Tekstilec*. 59(2), 107-114.
- Korkmaz Memiş, N., S. Kaplan. 2020. "Dual Responsive Wool Fabric by Cellulose Nanowhisker Reinforced Shape Memory Polyurethane". *Journal of Applied Polymer Science* 137(19):48674.
- Crespy D., Rossi RM. 2007. Temperature-responsive polymers with LCST in the physiological range and their applications in textiles. *Polymer International* 56(12), 1461-1468.
- Chatterjee S., Hui CL. 2019. Review of stimuli-responsive polymers in drug delivery and textile application. *Molecules* 24(14), 2547.
- Xiao M., González E., Monterroza AM., Freya M. 2017. Fabrication of thermo-responsive cotton fabrics using poly(vinylcaprolactam-co-hydroxyethyl acrylamide) copolymer. *Carbohydrate Polymers* 174, 626-632.
- Zhang Q., Weber C., Schubert US., Hoogenboom R. 2017. Thermo-responsive polymers with lower critical solution temperature: from fundamental aspects and measuring techniques to recommended turbidimetry conditions. *Materials Horizons* 4, 109.
- Demirbag S., Alay Aksoy S. 2019. Fabrication of thermoresponsive cotton graft PNIPAM fabric. *Journal of Textile Institute* 110, 171-178.
- Ter Schiphorst J., Van den Broek M., T. de Koning, Murphy JN., Schenning APHJ., Esteves ACC. 2016. Dual light and temperature responsive cotton fabric functionalized with a surface-grafted spiropyran-NIPAAm-hydrogel. *Journal of Materials Chemistry* 4, 8676-8681.
- Zhao Y., Wen J., Sun H., Pan D., Huang Y., Bai Y., Shao L. 2020. Thermo-responsive separation membrane with smart anti-fouling and self-cleaning properties. *Chemical Engineering Research and Design* 156, 333-342.
- Liu H., Zhu J., Hao L., Jiang Y., Van der Bruggen B., Sotto A., Shen J. 2019. Thermo- and pH-responsive graphene oxide membranes with tunable nanochannels for water gating and permeability of small molecules. *Journal of Membrane Science* 587, 117163.
- Lübben JF., Keck A., Kemajou CT., Bräuning M., Frick JE., Melnikov J. 2017. Functionalization of textiles with thermoresponsive polymers. *Journal of Fashion Technology & Textile Engineering* S4, 016.
- Zhang Q., Chen YY., Guan SL., Fang Q. 2015. Smart cleaning cotton fabrics cross-linked with thermo-responsive and flexible poly(2-(2-methoxyethoxy)ethoxyethyl methacrylate-co-ethylene glycol methacrylate). *RSC Advances* 5, 38382-38390.
- Chen T., Fang Q., Zhong Q., Chen Y., Wang J. 2015. Synthesis and thermosensitive behavior of polyacrylamide copolymers and their applications in smart textiles. *Polymers* 7, 909-920.
- Tourrette A., Geyter ND., Jovic D., Morent R., Warmoeskerken MMCG, Leys C. 2009. Incorporation of poly (n-isopropylacrylamide)/chitosan microgel onto plasma functionalized cotton fibre surface. *Colloids and Surfaces A: Physicochemical and Engineering Aspects* 352, 126-135.
- Sahle FF., Giubudagian M., Bergueiro J., Lademann J., Calderón M. 2017. Dendritic polyglycerol and N-isopropylacrylamide based thermoresponsive nanogels as smart carriers for controlled delivery of drugs through the hair follicle. *Nanoscale* 9, 172-182.
- Zhao C., Zhuang X., He P., Xiao C., He C., Sun J., Jing X. 2009. Synthesis of biodegradable thermo- and pH-responsive hydrogels for controlled drug release. *Polymer* 50(18), 4308-4316.
- Ohya S., Nakayama Y., Matsuda T. 2001. Thermoresponsive Artificial Extracellular Matrix for Tissue Engineering: Hyaluronic Acid Bioconjugated with Poly(N-isopropylacrylamide) Grafts. *Biomacromolecules* 2(3), 856-863.
- Nagase K., Okano T., Kanazawa H. 2018. Poly (N-isopropylacrylamide) based thermoresponsive polymer brushes for bioseparation, cellular tissue fabrication, and nano actuators. *Nano-Structures & Nano-Objects* 16, 9-23.
- Farooqi ZH., Khan HU., Shah SM., Siddiq M. 2017. Stability of poly (N-isopropylacrylamide-co-acrylic acid) polymer microgels under various conditions of temperature, pH and salt concentration. *Arabian Journal of Chemistry* 10(3), 329-335.
- Haddow P., McAuley WJ., Kirton SB., Cook MT. 2020. Poly(N-isopropyl acrylamide) – poly(ethylene glycol) – poly(N-isopropyl acrylamide) as a thermoreversible gelator for topical administration. *Materials. Advances* 1(3), 371.
- Yang L., Zhang J., He J., Zhang J., Gan Z. 2015. Synthesis and characterization of temperature-sensitive cellulose-graft-poly(N-isopropylacrylamide) copolymer. *Chinese Journal of Polymer Science* 33, 1640-1649.
- Sarwan, T., Kumar, P., Choonara, Y. E., & Pillay, V. 2020. Hybrid thermo-responsive polymer systems and their biomedical applications. *Frontiers in Materials* 7, 73.
- Reyes-Ortega F. 2014. pH-responsive polymers: properties, synthesis and applications. Maria Rosa Aguilar (Ed.), *Smart Polymers and Their Application*. Spain: Woodhead Publishing.
- Özkahraman B. 2014. Usage of Polymeric Hydrogels and Microgels in Drug Release Applications, PhD Thesis, University of Istanbul, Istanbul.
- Grainger SJ., El-Sayed MEH. 2010. Stimuli-Sensitive Particles for Drug Delivery. In E. Jabbari and A. Khademhosseini (Ed). *Biologically-Responsive Hybrid Biomaterials*. Singapore: World Scientific.
- Şimşek, C., 2016. Investigation of The In Vitro Drug Release Kinetics of PNIPAAm Hydrogels, M.Sc Thesis, University of Istanbul, Istanbul.
- Bashari A., Hemmatinejad N., Pourjavadi A. 2013. Surface Modification of Cotton Fabric with Dual-Responsive PNIPAM/Chitosan Nano Hydrogel. *Polymers for Advanced Technologies*. 24, 797-806.
- Glampedaki P., Calvimontes A., Dutschk, V. Warmoeskerken, MM. 2012. Polyester textile functionalization through incorporation of pH/thermo-responsive microgels. Part II: polyester functionalization and characterization. *Journal of materials science*. 47(5), 2078-2087.
- Wang B., Wu X., Li J., Hao X., Lin J., Cheng D., Lu Y. (2016). Thermosensitive behavior and antibacterial activity of cotton fabric modified with a chitosan-poly (N-isopropylacrylamide) interpenetrating polymer network hydrogel. *Polymers*, 8(4), 110.
- Štular D, Tomšič B, Simončič B, Jerman I, Mihelčič M, Čolović M. 2017. Modification of cotton fabric with temperature/pH responsive hydrogel: influence of particles size. *IOP Conf. Series: Materials Science and Engineering*. 254, 072024.
- Wang J., Chen Y., An J., Xu K., Chen T., Müller-Buschbaum P., Zhong Q. 2017. Intelligent textiles with comfort regulation and inhibition of bacterial adhesion realized by cross-linking poly (n-isopropylacrylamide-co-ethylene glycol methacrylate) to cotton fabrics. *ACS Applied Materials & Interfaces*. 9(15), 13647-13656.
- Huang ZS, Shiu JW, Way TF, Rwei SP. 2019. A thermo-responsive random copolymer of poly (NIPAm-co-FMA) for smart textile applications. *Polymer*. 184, 121917.
- Chaudhuri S, Wu CM. 2020. Switchable Wettability of Poly(NIPAAm-co-HEMA-co-NMA) Coated PET Fabric for Moisture Management. *Polymers*. 12,100.
- Chen S., Yuan L., Li Q., Li J., Zhu X., Jiang Y., Sha Q., Yang X., Xin JH., Wang J., Stadler FJ., Huang P. 2016. Durable antibacterial and nonfouling cotton textiles with enhanced comfort via zwitterionic sulfopropylbetaine coating. *Small*, 12(26), 3516.
- Hengrui Y. 2012. A Smart Temperature Responsive Polymeric System For Textile Materials, Phd Thesis The Hong Kong Polytechnic University.

-
36. Lavric PK, Warmoeskerken MMCG, Jocic D.2012. Functionalization of cotton with poly-nipamm/chitosan microgel: Part I. stimuli-responsive moisture management properties. *Cellulose*, 19, 257-271.
 37. Jocic D, Tourrette A, Glampedaki P, Warmoeskerken MMCG. 2009. Application of temperature and pH responsive microhydrogels for functional finishing of cotton fabric. *Materials Technology* 24, 14-23.
 38. Demirbağ Genç, S. 2019. Development of thermo-responsive and pH-sensitive smart textiles. Phd Thesis, Suleyman Demirel University.
 39. Besen B, Balcı O, Orhan M, Gunesoglu C., Tatli II. 2015. An Investigation on antibacterial activities of nonwovens treated with ozonated oils, *Journal of Textiles and Engineer* 22(100), 25-31.
 40. Derkaoui S, Belbachir M, Haoue S, Zeggai FZ., Rahmouni A., Ayat M. 2019. Homopolymerization of methacrylamide by anionic process under effect of maghnite-nağ (algerian MMT). *Journal of Organometallic Chemistry* 893, 52-60.
 41. Chung C, Lee M., Choe EK. 2004. Characterization of cotton fabric scouring by FT-IR ATR spectroscopy. *Carbohydrate Polymer* 58, 417-420.
 42. Yang H., Esteves ACC., Zhu H., Wang D., Xin JH. 2012. In-situ study of the structure and dynamics of thermo-responsive PNIPAMm grafted on a cotton fabric. *Polymer* 53, 3577-3586.
 43. Soleimani-Gorgani A, Karami Z. 2016. The effect of biodegradable organic acids on the improvement of cotton ink-jet printing and antibacterial activity. *Fibers and Polymer* 17, 512-520.
 44. Alay-Aksoy S., Genç E. 2015. Functionalization of cotton fabrics by esterification cross-linking with 1,2,3,4-butanetetracarboxylic acid (BTCA). *Cellulose Chemistry Technology*, 49, 405-413.
 45. Save NS., Jassal M. Agrawal AK. 2005. Smart breathable fabric. *Journal of Industrial Textiles* 34, 139-155.
 46. Madhavan V, Lichtin NN. Hayon E. 1975. Protonation reactions of electron adducts of acrylamide derivatives. a pulse radiolytic-kinetic spectrophotometric study. *Journal of the American Chemical Society* 97(11), 2989-2995.
 47. Badwaik HR., Alexander A., Sakure K. 2019. Understanding the significance of microwave radiation for the graft copolymerization of acrylamide on carboxymethyl xanthan gum. *Current Microwave Chemistry*. 6(1), 13-22.
 48. Zhao N., Yuan W. 2022. Highly adhesive and dual-crosslinking hydrogel via one-pot self-initiated polymerization for efficient antibacterial, antifouling and full-thickness wound healing. *Composites Part B: Engineering*, 230 (109525), 1-14.
 49. Qi K., Wang X., Xin JH. 2011. Photocatalytic self-cleaning textiles based on nanocrystalline titanium dioxide. *Textile Research Journal* 81, 101-110.
 50. Tozum MS.2014. Determination of thermo-regulating and comfort properties of the fabrics treated with heat storing microcapsule. Master's Thesis, Suleyman Demirel University.
 51. Bulut Y., Sular V. 2015. General properties and performance tests of fabrics produced by coating and lamination techniques. *Journal of Textiles and Engineer*, 70, 5-16.
 52. Hussain T., Ali S., Qaiser F. 2010. Predicting the crease recovery performance and tear strength of cotton fabric treated with modified N-methylol dihydroxyethylene urea and polyethylene softener. *Coloration Technology* 126(5), 256-260.



CNN-Based Fabric Defect Detection System on Loom Fabric Inspection

Muhammed Fatih Talu¹  0000-0003-1166-8404

Kazım Hanbay²  0000-0003-1374-1417

Mahdi Hatami Varjovi¹  0000-0001-6442-7175

¹ İnönü University / Department of Computer Engineering / Malatya, Türkiye

² İnönü University / Department of Software Engineering / Malatya, Türkiye

Corresponding Author: Mahdi Hatami Varjovi, mahdi.hatami.v@gmail.com

ABSTRACT

Fabric defect detection is generally performed based on human visual inspection. This method is not effective and it has various difficulties such as eye delusion and labor cost. To deal with these problems, machine learning and computer vision-based intelligent systems have been developed. In this paper, a novel real-time fabric defect detection system is proposed. The proposed industrial vision system has been operated in real-time on a loom. Firstly, two fabric databases are constructed using real fabric images and new defective patch capture (DPC) algorithm. One of the main objectives in this study is to develop a CNN architecture that focuses only on fabric defect detection. One of the most unique aspects of the study is to detect defective pixel regions of fabric images with Fourier analysis on a patch-based and integrate it with deep learning. Thanks to the novel developed fast Fourier transform-based DPC algorithm, defective texture areas become visible and defect-free areas are suppressed, even on complex denim fabric textures. Secondly, an appropriate convolution neural networks (CNN) model is developed. Thus the new dataset dataset is refined using negative mining method and CNN model. However, traditional feature extraction and classification approaches are also used to compare classification performances of deep models and traditional models. Experimental results show that our proposed CNN model integrated with negative mining can classify the defected images with high accuracy. Also, the proposed CNN model has been tested in real-time on a loom, and it achieves 96.5% detection accuracy. The proposed model obtains better accuracy and speed performance in terms of detection accuracy with a much smaller model size.

ARTICLE HISTORY

Received: 05.12.2021

Accepted: 17.04.2022

KEYWORDS

Computer vision, fabric defect detection, CNN, feature extraction

1. INTRODUCTION

It is a very important issue in the fabric industry to detect and classify defects during production. Traditionally, human-oriented defect detection is an approach that takes a lot of time and causes labor costs. In this approach, serious losses can occur in fabric production in cases such as operator distraction, eye fatigue, and distraction. For this reason, image processing and artificial intelligence-based automatic fabric control approaches are inevitable.

Automatic defect detection systems include two important stages: Obtaining clear images during fabric production and

detecting whether there are errors in the images. Capturing non-blur and noise images clear fabric images is quite a challenge. This is because fabric looms produce high levels of noise, there is lint constantly floating around, the dimensions of looms exceeding 2m and they produce high vibrations. In addition, the small size of defect size of 1mm and the constant movement of the fabric are other factors that make the image acquisition process difficult. The aforementioned difficulties significantly prevent the spread of some error detection systems based on image processing and artificial intelligence, which have high error detection accuracy. From this point of view, the disadvantages of

To cite this article: Talu MF, Hanbay K, Varjovi MH. 2022. CNN-based fabric defect detection system on loom fabric inspection. *Tekstil ve Konfeksiyon* 32(3), 208-219.

existing systems can be eliminated by examining the powerful feature extraction and machine learning methods in the literature.

Defect detection methods in the literature could be classified [1] as structural [2], [3], statistical [4], spectral [5,6]-[7], model-based [8], learning-based [9] and hybrid methods [10]. In this study, a CNN-based defect detection architecture is proposed in contrast to the current approaches. However, the process of building a large fabric data-set containing different fabric defects is costly and challenging.

Defects in fabric images disrupt regular fabric texture and pattern. Therefore, the problem addressed while analyzing images can be defined as texture-based image analysis and classification. Thus, the problem can be moved to the field of image processing and machine learning, and texture features can be extracted with well-known texture analysis methods. Defective fabric production can be prevented by detecting the location and type of defect with the meaningful features obtained. [11]. Starting from this point, using statistical measurements and histogram information, defects are defined in images containing regular texture patterns. [12]. By using the Gabor wavelet network and morphological filters, fabric background and fabric defect regions were distinguished and common fabric defects were detected. [4]. In another study, fabric defects were detected with adaptive wavelet transform. [13]. Histogram thresholding was performed by successfully separating the background and error regions with specially designed low and high pass filters. In a study that classifies fabric defects such as horizontal and vertical missing thread defect, colored thread, spot, and gap, statistical properties of the images were calculated. [13]. The features obtained using the Bayesian classifier were classified and a 99.85% classification success was achieved. In a recent study, defect detection was performed on 247 different fabric images containing repetitive textures. [14]. Considering the regular layout rule in the fabric images, the existing template and the regions in the fabric image were compared. The metric results were obtained and the existing template was analyzed for similarity. 5 different fabric defects that are common in fabrics containing 3 different texture types have been successfully detected. In addition, a comprehensive comparison with different feature methods was made and the error detection capacity of the method was highlighted. By analyzing the isotropic lattice structures in the fabric images, it can be understood whether the regular texture pattern is disrupted due to the error. For this process, fabric images are divided into non-overlapping sub-images and analyzed in a micro-level pattern. Jia and Liang [15] in their study, the image was divided into hundreds of lattice structures and focused on the error region without dealing with unrelated pixel regions. 5 different fabric defects were detected by pixel-based area calculation and histogram analysis of defective pixels in lattice regions. In a study examining the pattern regularity in fabric images with the autocorrelation function in polar coordinates, the changes in the pattern were also examined angularly and errors were detected [15]. With this method, both linear and blob-like defects were detected.

Hole, oil stains, warp-lacking, and weft-lacking errors in plain white fabric images of 512×512 size obtained from the field scanning camera were detected and classified. [16]. Filtering and thresholding pre-processes are applied to the obtained images and given as input to the artificial neural network. Over 90% classification success was achieved in all defect types. Rotation-independent analysis methods are used to detect defects in fabric images containing regular and rotational states. With the versatile and multi-scale feature of the Gabor transform, the features of the images are extracted and the defect regions are segmented. [17]. Segmentation results are improved by filtering the obtained segmented image with a Gaussian low-pass filter. Fractal geometry has been used frequently in recent years to describe the natural irregularity of self-similar natural objects. Due to its success in detecting regularity, it has been used to detect errors that disrupt regularity in fabric images. [18]. By characterizing the roughness and complexity of fabric textures with fractal calculations, images were classified with support vector machines. In a study that can detect knit fabric defects in real-time, shearlet transform and artificial neural networks are used. [19]. The shearlet coefficients of the images obtained from the line scan camera in different scales and directions were calculated. The weights of the trained artificial neural network were recorded and real-time error control was performed on the knitting machine. Multi-scale local texture analysis was performed by calculating the singular value decomposition information of the fabric images converted to the CIE color channel. [20]. In addition, defected regions were determined by measuring the cosine similarity between the defected fabric modeling and the images analyzed with different scales. Yildiz et al. [21] detected different fabric defect using thermal camera. To extract important textural features, they used gray level co-occurrence matrix. To classify fleece fabric images, local binary patterns were used [22]. Firstly, local texture features were calculated. Then Naive Bayes and K-nearest neighbor classifier were used to classify fabric images. Yildiz et al. [23] developed thermal defect detection system to eliminate fabric defects. They benefit from thermal differences between defective and defect-free fabric regions. These differences are helpful in characterizing the defective region. In another hybrid method, wavelet transform and principal component analysis were used together to classify cashmere and denim fabric images [24]. 95% success was achieved in the fabric images obtained with the thermal camera.

Although traditional methods of fabric defect detection give the desired results in most cases, most of these methods use hand-designed features such as filters, texture, and color. Although traditional methods can perform multi-scale and versatile feature calculations, they can perform limited analysis and calculations on the data. With the development of deep learning methods in recent years, the mentioned limitations have been removed. High-level inferences and decision-making processes are produced with deep learning algorithms. The main advantage of deep learning is to

obtain high-level feature analysis of data with a well-designed convolutional neural network (CNN). Such a designed network has been built and accepted as a powerful feature calculator and has become a decision-making system that gives better results than traditional methods. Jing et al. [25] used the improved AlexNet architecture for CNN fabric defect classification. Network layers and convolution filters are optimized to detect yarn dye defects. Wang and Jing [26] on the other hand, classified fabric defects with a deep learning architecture, which they proposed a pyramid-based pooling layer, without using labeled training data. In a study with the Faster R-CNN model, the region of fabric defect was determined by using Region Proposal Networks (RPN) and Fast R-CNN models together [27]. The success and speed of the method have been increased with the constructed multi-scale feature pyramid and defected region boxes. Zhou et al. On the other hand, they updated the architecture of the Faster R-CNN model in the deep learning model they called FabricNet [28]. Especially by replacing the last part of the mesh with the Deformable Convolution (DC) block structure, the classification success for fabric defects has been increased. In another study, effective results were obtained on two different fabric datasets by using principal component analysis and deep feature extraction strategy together [29]. First of all, the features of the images were extracted with the VGG16 deep learning model. Then, by calculating the saliency maps of the images with principal component analysis, the final results in which the defects are segmented are obtained. In another CNN-based study with a visual long-short-term memory module integrated, a deep network modeling close to human visual perception was carried out [9]. Although this network model has more complex modules, it is designed as an architecture that can detect fabric defects between 95% and 97%. Mei et al. [30] proposed a multi-scale convolutional denoising autoencoder (MSCDAE) architecture to detect fabric defects of different sizes. In this model, which includes multiple convolutional denoising autoencoder layers, images are processed with the Gaussian pyramid method and image patches are produced. In the encoder and decoder layers of the network, these patches are extracted with convolution layers. During the test phase, residual maps were produced that clearly show the defected areas in the images. A variational automatic encoder was used in a study that detected 9 different fabric defects by real-time fabric defect detection [31]. Using the Structural similarity index measurement (SSIM) parameter, the similarity between 3 different parameters between the constructed image at the input and output of the autoencoder was measured. With the built layer architecture, the desired SSIM residual map is built, making it easier to distinguish defected regions. The high success rate in fabric defect detection studies based on deep learning is remarkable. Especially their classification success against many different fabric defect types is remarkable. With these aspects, deep learning methods have an edge over traditional feature extraction and machine learning methods.

Fabric defect detection studies have been carried out both with traditional methods and with deep learning methods, although a small number of them. The number of studies that can work in real-time, especially on knitting and weaving machines, is very limited. The methods cannot produce the desired results due to reasons such as noise, light change, and vibration from the knitting/weaving machine, especially in the industrial working environment. From this point of view, in this study, a new method that makes real-time fabric defect detection with deep learning methods on the weaving machine has been developed.

The main contributions are summarized as follows:

- (1) To better classify the fabric textures, a novel CNN model with negative mining is proposed. This model improves the effectiveness and distinctiveness of the CNN model.
- (2) Thanks to the novel developed fast Fourier transform-based DPC algorithm, defective texture areas become visible and defect-free areas are suppressed, even on complex denim fabric textures.
- (3) The proposed model can meet the real-time requirements of defect detection on a loom.

The rest of this paper is arranged as follows. Section 2 briefly introduces the conventional defect detection systems and related feature extraction methods. Section 2 introduces our novel CNN-based defect detection method and gives details about the training, experimental setup of our defect detection system and fabric database. In Section 3, the classification results of the conventional feature extraction methods and our CNN model are provided to validate our method on a real fabric database. Section 4 presents real-time defect detection results on a loom. Finally, we conclude our study in Section 5.

2. MATERIAL AND METHOD

2.1 Material

2.1.1 Current Defect Detection Systems

Systems that can detect real-time defects in weaving looms can be divided into two according to the imaging approach: Still and systems using more than one camera, systems using mobile, and single camera. Figure 1.left shows an example defect detection system developed by Uster Technologies Vision [32] and includes 4 still cameras side by side. The most important advantage of using still cameras is the minimization of image degradation caused by vibration, resulting in a clear image. However, since a limited fabric area is seen with a single camera, it is necessary to use more than one camera side by side to view the entire fabric. More than one camera data is collected by the frame holder card. However, the increase in the number of cameras increases the cost of the system and makes defect detection management difficult.

To eliminate the high cost of still camera systems, some systems use a single mobile camera. The product named

Cyclops [33] from BMSvision company (see Figure 1.right) is relatively easy to manage. This German-origin product uses a rail mechanism that provides linear movement on the loom. This mechanism enables the display of the fabric surface produced by moving the camera on the horizontal axis. Cyclops transfer images to the server over the network and detect defects with the software on the server. Using blue-colored and flash lighting components, Cyclops can detect ten predefined fabric defects. The disadvantages of Cyclops are the server requirement and the ability to detect defects only on sparse fabrics. The embedded defect detection system suggested in this article eliminates the need for a server. In addition, thanks to the developed defect detection software, shallow fabric defects can be detected.

Both modern defect detection systems (Uster and Cyclops) mentioned having high costs. This negative situation significantly prevents the spread of these products with high defect detection accuracy in the market.

2.1.2 Defect detection algorithms

Existing defect detection algorithms transform fabric images into feature vectors and map these vectors to known classes with specific classification techniques (Nearest Neighbours (NN), Support Vector Machine (SVM), and K-Nearest Neighbours (KNN)). The difference between algorithms is based on the difference in feature extraction approaches. In this study, a total of six different feature extraction approaches, three of which are in the spatial domain (Histogram of Oriented Gradient (HoG), Co-

occurrence HOG (CoHoG) and Statistical), and three in the frequency domain (Fast Fourier Transform (FFT), Wavelet, and Shearlet), which are frequently used in the fabric defect detection literature, will be expressed.

2.1.2.1 HOG features

In the HOG method, the horizontal and vertical gradients of the image are calculated first. Then the pixel orientation matrix is obtained. Finally, the histogram of the orientation matrix is taken and the information obtained is used as attribute values [34]. Gradients and orientation matrix are calculated as follows:

2.1.2.2 CoHOG features

Gray Level Co-occurrence Matrix (GLCM) is frequently used in texture extraction studies. GLCM refers to the number of repetitions of pixel pairs in a particular direction [35]. Accordingly, the GLCM matrix of a gray level I image is calculated as follows:

Pixel values i and j ; spatial coordinates x and y in the image; $I(x, y)$ represent the brightness value in the image. The CoHOG method [36] calculates the density changes between pixels by scanning the image matrix according to different angle values. Unlike HoG, the image is analyzed by dividing the $M \times N$ region. GLCM is obtained by using the angle values (offsets) determined from each image region. A single feature vector is produced by combining the GLCMs obtained for all regions in the image (see Figure 2).

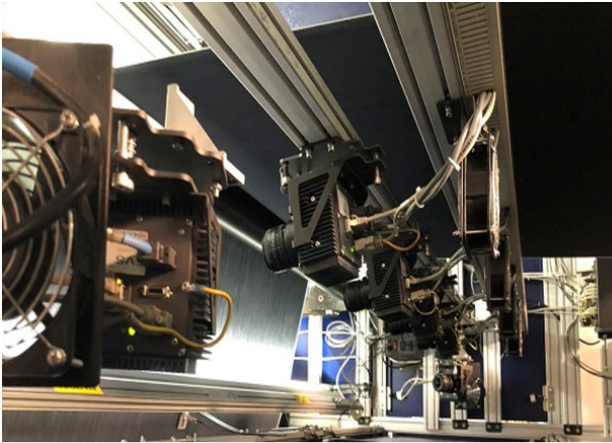


Figure 1. Current defect detection systems. (Left) Uster, (Right) Cyclops

$$f_x(x, y) = I(x+1, y) - I(x-1, y) \quad (1)$$

$$f_y(x, y) = I(x, y+1) - I(x, y-1) \quad (2)$$

$$\theta(x, y) = \tan^{-1} \left(\frac{f_y(x, y)}{f_x(x, y)} \right) \quad (3)$$

Where f_x and f_y , respectively are the horizontal and vertical gradients of the I image. θ express the orientation matrix.

$$C_{x,y}(i,j) = \sum_{p=1}^n \sum_{q=1}^m \begin{cases} 1, & \text{if } I(p,q) = i \quad \text{and} \quad I(p+x,q+y) = j \\ 0, & \text{otherwise} \end{cases} \quad (4)$$

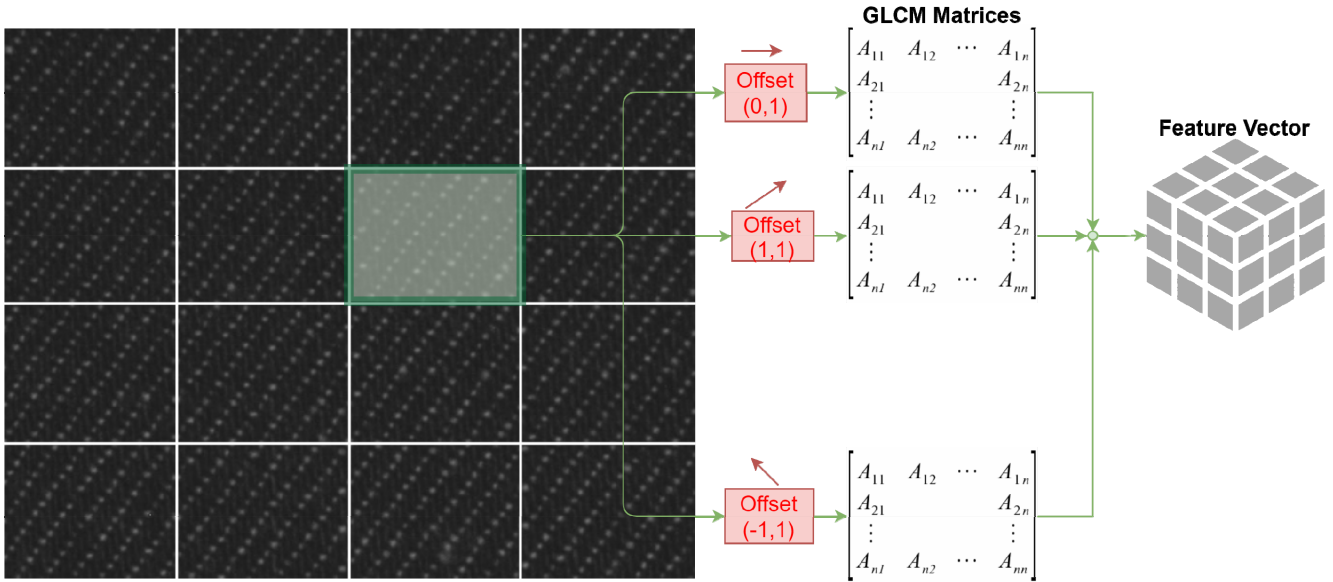


Figure 2. CoHog feature extraction

2.1.2.3 Statistical features

In the study [35], it is seen that four different statistical attributes (energy, contrast, correlation and homogeneity) of the gray co-formation matrix are obtained. These attributes are expressed as follows:

$$Energy = \sum_i \sum_j p(i,j)^2 \quad (5)$$

$$Contrast = \sum_i \sum_j |i-j|^2 p(i,j) \quad (6)$$

$$Correlation = \sum_i \sum_j \frac{(i-\mu_i)(j-\mu_j)p(i,j)}{\sigma_i \sigma_j} \quad (7)$$

$$Homogeneity = \sum_i \sum_j \frac{p(i,j)}{1+|i-j|} \quad (8)$$

2.1.2.4 Fourier features

It is known that frequency domain techniques are used to detect texture/pattern differences in the image [6], [37]. In the study conducted in the article with reference no [37], the Central Spatial Frequency Spectrum of the image is obtained by using FFT, and 7 different statistical attributes are extracted from the spectrum visual.

$$P_1 = |F(0,0)| \quad (9)$$

$$P_2 = 100 \times \frac{F(f_{x1}, 0)}{F(0,0)} \quad (10)$$

$$P_3 = f_{x1} \quad (11)$$

$$P_4 = 100 \times \left(\sum_{f_{x1}=0}^{f_{x1}} \frac{F(f_{x1}, 0)}{F(0,0)} \right) \quad (12)$$

$$P_5 = 100 \times \frac{F(0, f_{y1})}{F(0,0)} \quad (13)$$

$$P_6 = f_{y1} \quad (14)$$

$$P_7 = 100 \times \left(\sum_{f_{y1}=0}^{f_{y1}} \frac{F(0, f_{y1})}{F(0,0)} \right) \quad (15)$$

where P_1 expressing the mean spectral response, P_2 , P_3 and P_4 represent the spectral changes in the horizontal axis. Spectral changes on the vertical axis are also represented with P_5 , P_6 , and P_7 variables.

2.1.2.5 Wavelet features

In this section, it is expressed how the feature vector is obtained from fabric images using the wavelet transform technique. Three-level wavelet transform is used in this study. Figure 3 shows the sub-band images obtained after the three-level transformation. Accordingly, a total of nine band images are obtained, including three sub-bands at each level.

In the study [38], it is shown that the luminance histograms in the lower band images show a symmetrical distribution, so they can be modeled with Normal Distribution. Thus, each sub-band image can be represented by the parameters

of the Normal distribution (μ and σ). Since a total of 10 sub-band images are obtained after three-level transformation, the feature vector has 1×20 dimension.

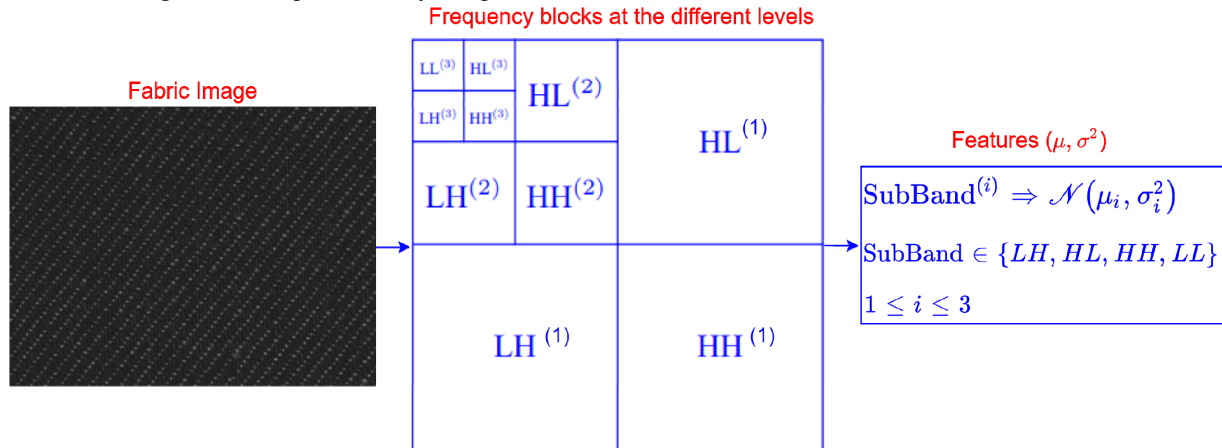


Figure 3. Wavelet feature extraction

2.1.2.6 Shearlet features

An important disadvantage of wavelet transform is that it can only obtain spectral responses of the image in horizontal and vertical directions. This limitation may cause pattern or texture features at different angles to be undetectable. The Shearlet transform has been developed to overcome this disadvantage of wavelet transform [39]. Accordingly, it enables multi-scale and multi-directional spectral analysis of the image. In this study, scale level 4 was determined, spectral responses of 10 degrees were calculated and features were obtained.

2.2 Method

In this study, a new product has been developed to be included in the mobile camera systems group. This product is very similar to Cyclops with its camera and linear motion system components. Its difference from Cyclops is that it can detect defects in shallow or sparsely woven fabrics and has embedded image processing capability. With this capability, it can instantly process images without transferring them to an additional server and reduces the system cost. With these features, it is thought that the proposed system will have a wide range of uses.

The prominent technical features of the proposed system when compared to its current counterparts are listed below:

- 1) Low cost (camera and loom machine synchronization is done through software and has no depended on multiple cameras to covering the whole fabric for data acquisition part.
- 2) An original and economical LED light apparatus was designed, produced and used.
- 3) A frequency-based approach specific to fabric types produced on looms is presented.
- 4) High accuracy values have been achieved because deep convolutional networks are used.

- 5) The proposed approach can work in real time.

2.2.1. Imaging hardware

In classical systems, the synchronization between the camera and the weaving loom is provided by hardware. Accordingly, a camera with a trigger output and a weaving loom with encoder connection are used. High-cost trigger cameras and encoder hardware increase the overall system cost. In the proposed system, the synchronization between the camera and the machine is software. For this, the production speed of the machine is determined by using the images obtained from the production before the recording process is made, and the camera movement speed and shooting speed parameters are updated accordingly. In this way, hardware requirements have been eliminated and an economical defect detection system has been produced.

The image recording module of the proposed system is shown in Figure 4. Accordingly, the image recording setup consists of the camera (FLIR Blackfly), lighting component, lens (Sony F-12mm), and linear system components. To obtain clear fabric images, attention has been paid to the fact that the camera has a "global shutter" feature and that the pixel size on the imaging sensor is high (5.86nm). The linear system has a length of 2m and allows the camera to move left and right on the loom. The camera table speed is fixed at approximately 18.8 cm/sec. Thus, a tour on the bench is completed at 11sec and the entire fabric surface produced can be viewed. Two different illumination apparatuses were designed and produced as samples to prevent the movement of the camera and fabric from blurring. In the first, 9 LEDs and lenses with a 50-degree angle were used. The lenses are used to prevent the light from spreading to the environment at a wide angle and provide focusing in a narrow area. In the other apparatus, 30 LEDs that can emit 4000K and 70 lumens light are used. Considering the quantum efficiency value of the imaging sensor, it has been ensured that the LEDs are at 525nm

wavelength. Thus, the efficiency of the imaging sensor to convert light into electricity is maximized. The fabric images recorded with both illumination apparatuses were examined and high-quality fabric images were obtained

with the second illumination apparatus. Thus, the second lighting apparatus was selected and the works started to create a fabric database.

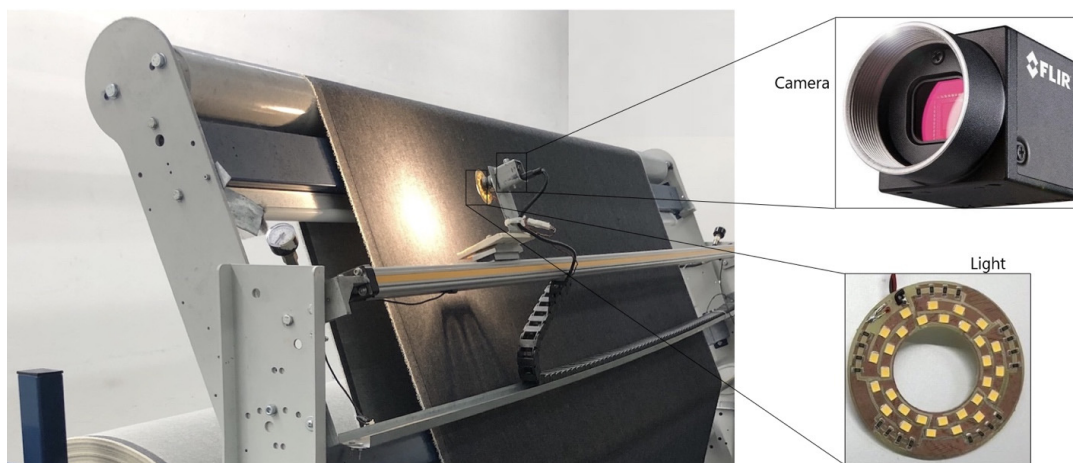


Figure 4. The proposed defect detection setup

2.2.2 Produced fabric databases

It should be emphasized that it is difficult to produce a sufficient number of different fabric defects due to the low probability of occurrence of defective fabrics in the fabric industry. This situation also leads to loss of production and labor in database construction. Therefore, this study focuses on detecting two different fabric defects. The first is the warp defect (H1), the second is the horizontal deformation defect (H2). Both types of defects were produced specially by the fabric operator and the defective fabric images were recorded. Accordingly, fabric images belonging to three classes without defect (14099 pieces), H1 (8936 pieces), and H2 (17289 pieces) were recorded in the DB1 database (see Figure 5). Produced dataset is available via this link <https://github.com/MahdiHatami/denim-fabric-dataset>.

The high size of the images in DB1 makes it difficult to detect small defect regions and causes memory insufficiency problems. Therefore, 1200×1920 DB1 images were saved in a new data set (DB2) in the form of 300×320 patches. The fabric images were divided into 6 equal parts and transferred to DB2. However, a patch must be taken from the defective parts of the H1 and H2 images. For this, the Defected Patch Capture (DPC) algorithm, whose stages are shown in Figure 6, is used.

The DPC algorithm developed within the scope of this study takes high-resolution defective images as input and only determines the center of the defective area (See Figure 7). Accordingly, the image in the spatial domain is transformed into a spectral image using the FFT transformation in the first step. Later, a special mask was designed to filter the main frequencies of weft and warp patterns in the fabric images. The two-level mask image contains five parallel ellipses. After the original spectral image is masked, reverse FFT conversion is made and a filtered fabric image is obtained. By filtering, defective areas became visible and defect-free areas were suppressed. A second process to make the defective areas more prominent is the power-law transformation. Finally, using a certain threshold (0.2), the image was reduced to a binary level. The two types of defects to be detected have a linear structure. For this reason, the longest striped region in the binary image was determined using Hough transform. The center of the detected line was set to be the center of the patch and 300×320 sized patches were taken from the defective area and recorded in DB2. As a result, a total of 31110 images (8265 H1, 5975 H2, and 16870 without defects) were recorded in the DB2 dataset.

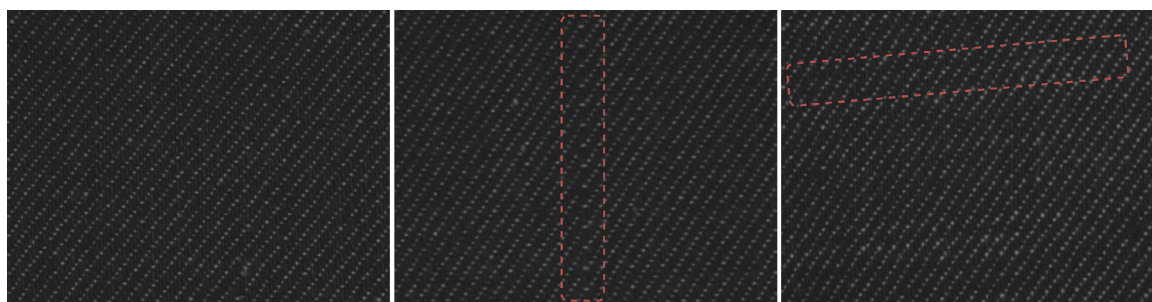


Figure 5. Fabric images. (left) without defect, (middle) warp defect-H1, (right) horizontal deformation defect-H2

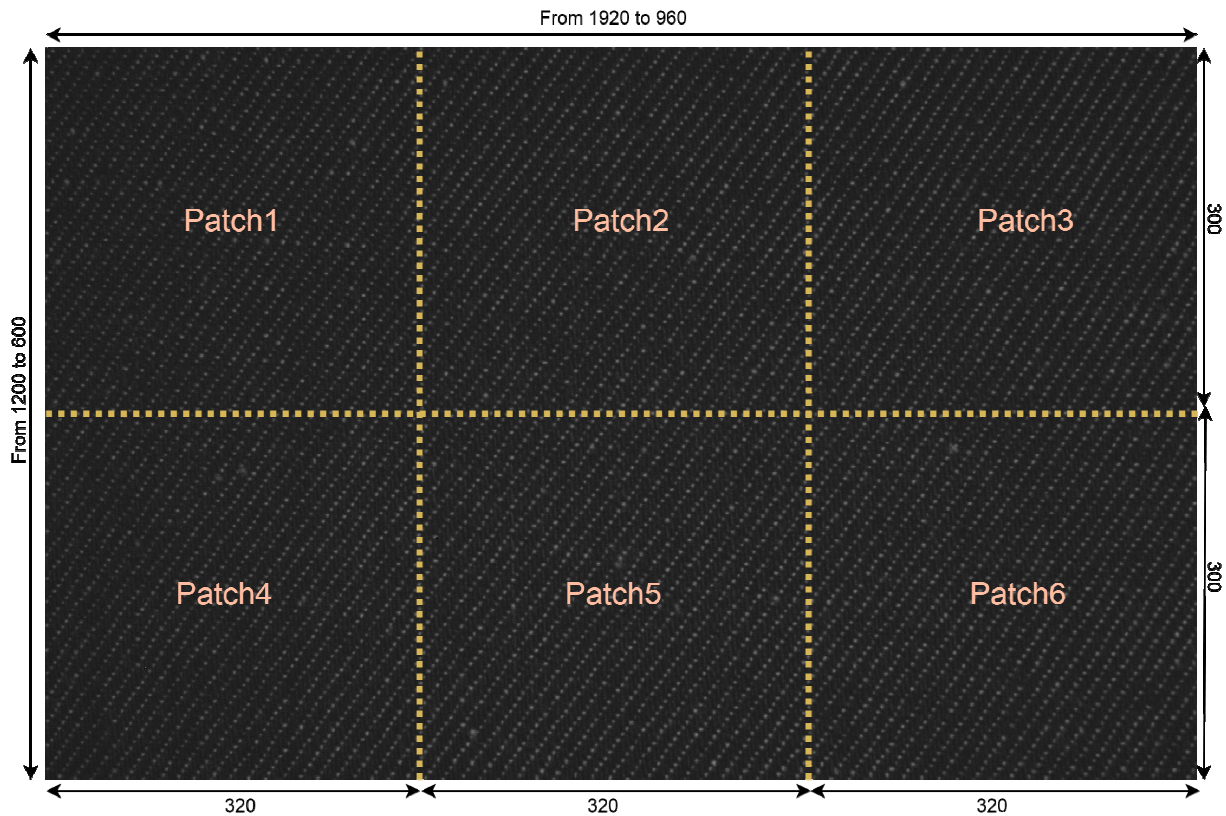


Figure 6. Splitting input image to patches

It should be emphasized that defected fabric production is approximately 1-2% of the normal production. Therefore, the number of fabric defect images is very low compared to the none-defected fabric image. There is an imbalance in obtained high resolution raw fabric images. However, this imbalance was resolved by producing patches from defect fabric images. For this, firstly, the defect region was made clear in the frequency domain, then the patches that would include the relevant region were saved. In this way, the number of defect images has been brought closer to the number of none-defected images. Training and testing activities were carried out on an improved training set.

2.2.3 Determining the appropriate CNN architecture

In this section, the structure of the CNN architecture that provides the highest classification accuracy is investigated. For this purpose, four different CNN architectures with

different layer depth, convolution mask number, and mask sizes were designed (see Table 1). Thus, the classification performances of a deeply structured architecture and a shallow architecture were evaluated. The parameters of the architectures used were set as epoch "10", optimizer "sgdm", package size "128", weight-decay "0.0005" and learning coefficient "0.001" and training/testing activities were carried out. For this, a server computer with 8GB GDDR5 GPU memory and Nvidia Quadro M4000 graphics card was used. 75% (~23322) of 31110 images in DB2 were used for training and 25% (~7778) for testing. As a result of the comparison, it was seen that the CNN network, whose architecture is clearly shown in Figure 8, provides the highest classification accuracy in training and test sets. This architecture number 4 which performs best amount other architectures structure given in Table 2.

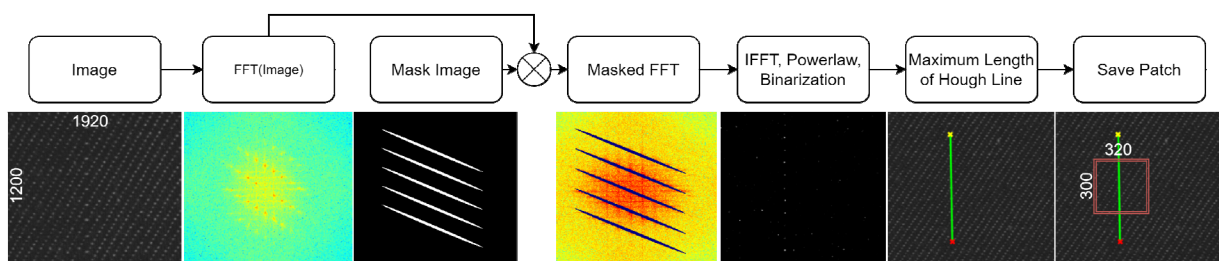


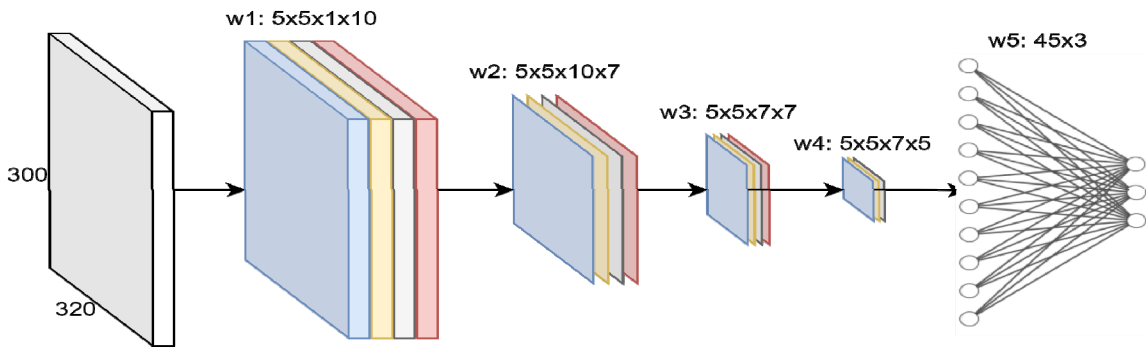
Figure 7. Stages of defected patch capture algorithm

Table 1. The CNN architectures

	Layer Number	Total parameters	Train Accuracy (%)	Test Accuracy (%)
CNN Architecture 1	11	75.243	93.44	93.28
CNN Architecture 2	16	7.773	93.44	93.64
CNN Architecture 3	11	160.173	91.09	90.28
CNN Architecture 4	19	4.325	97,6	97,3

Table 2. The CNN architectures 4 structures

	Layer	Output Size
Conv1	$5 \times 5, 10, \text{stride}(1,1)$	$300 \times 320 \times 10$
Pool1	$5 \times 5, 10, \text{stride}(2,2)$	$150 \times 160 \times 10$
Conv2	$5 \times 5, 7, \text{stride}(1,1)$	$150 \times 160 \times 7$
Pool2	$5 \times 5, 7, \text{stride}(2,2)$	$75 \times 80 \times 7$
Conv3	$5 \times 5, 7, \text{stride}(1,1)$	$75 \times 80 \times 7$
Pool3	$5 \times 5, 7, \text{stride}(2,2)$	$37 \times 40 \times 7$
Fully connected	10360	3

**Figure 8.** The proposed CNN architecture 4

3. RESULTS AND DISCUSSION

3.1 Comparison of Defect Detection Methods

In this section, the performance of defect detection methods is evaluated by considering the classification accuracy and working time. Before proceeding with the classification processes, the incorrectly classified images in the automatically generated DB2 data set were transferred to the correct classes. For this, the proposed CNN architecture

has not been classified correctly and the images in the 5% incorrect portion have been examined by the fabric operator and transferred to the correct classes. The approach known as "negative mining" in the literature has been repeated three times and the data set has been updated. The results obtained by running the classical defect detection methods and the proposed CNN architecture on the updated DB2 dataset are presented in Table 3 also the validation accuracy and cross entropy loss presented in Figure 9 respectively.

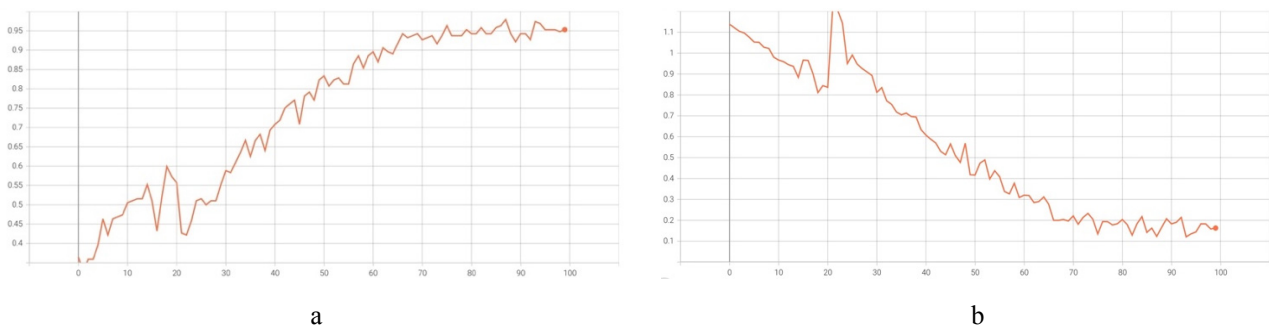
**Figure 9.** a) Classification accuracy b) Cross entropy loss

Table 3. Classification results of defect detection methods. (M: Million)

Methods	Feature Numbers	Accuracy (%)		Time (sec)
		Train	Test	For one image
Statistical	259	96.00	88.23	0.011
HOG	128	96.90	91.93	0.047
CoHOG	1536	95.31	87.52	0.312
Fourier	7	83.10	80.70	0.003
Wavelet	18	85.00	72.70	0.066
Shearlet	59	59.20	33.40	0.302
InceptionV3	6M	78.8	78.3	0.7
MobileNetV2	4.2M	65.5	63.5	0.65
Xception	22.8M	81.3	80.5	1.34
Self-Supervised	0.8M	94	94.2	0.88
Proposed model (Architecture 4)	4325	97.6	97.3	0.0061

When the results in Table 3 are examined, it is seen that the proposed CNN-based architecture has the highest classification accuracy. The reason for this is that CNN can extract low, medium, and high-level features from images thanks to its layered structure and can classify these features with high accuracy with the help of a fully connected layer. Also, the times of the methods to render a fabric image are given in the last column of the table. These time values were calculated by taking the arithmetic average of 100 image processing times. Accordingly, it is seen that the proposed CNN architecture works quite fast, so it is the most suitable method to use in real-time systems.

HOG and CoHOG methods calculate local and global features of fabric images based on gradient calculations. The light change in the fabric images and some non-defect noise information negatively affected the durability of the method. However, they have reached a better result than classical feature extraction methods in detecting fabric defects. Energy, contrast, correlation, and regularity used as statistical attributes seem to be successful in distinguishing fabric defects from the background. However, the success achieved in the training of the classifier is not at the desired level in the testing process of the classifier. Although the fabric images in the database have a regular pattern, this order is disrupted in the defect areas. The regularity parameter used is effective in capturing this situation. However, energy, correlation and contrast calculations were not sufficient to detect the defect with spatial pixel information. The reason for this is the insufficient local analysis of the fabric regions. Because the statistical calculations deal with the image as a whole, and therefore it is not possible to notice regional changes and reflect them on statistics. In other words, the statistical distribution in the pixel regions where the fabric defect occurs is lost among the pixel statistics of the whole image.

Fourier, shearlet, and wavelet transform methods that extract attributes by converting the image from the spatial domain to frequency domain failed to achieve the desired success in both the training and testing processes of the classifier. In particular, the Shearlet transformation method gave unsuccessful results in the type of woven fabric and its defects. In the Shearlet transformation applied in a multi-

scale and angular direction, textural features of the fabric images in different levels and directions were obtained. However, defects expressing the distortion of regular fabric patterns could not be distinguished from the background and regular patterns. The most important reason for this is that the method is not resistant to situations such as noise and light changes. In addition, since the types of defects examined are similar to the regular structure in the fabric, the shearlet method together with the wavelet transform and Fourier transform methods did not reflect the defective regions strongly in the frequency spectrum. The sub-band images obtained in the wavelet transform method were modeled with the Gauss function. However, there is no special study to express the defective regions of the image with the parameters of the Gaussian function. In the method based on wavelet transform and Gaussian distribution, the frequency components of the defective regions are ignored and a spectrum or sub-band analysis to express the defect is not performed. In these methods, updates should be made to analyze and examine the defective area at the local level. In Fourier transform, defective regions are visibly apparent in the spectrum. However, this information was lost during the calculation of statistical 7 different feature information from this spectrum with a classical method. Therefore, it has been understood that the frequency spectrum needs to be analyzed with different methods. On the other hand, state-of-the-art methods that achieve better classification rate on much larger datasets. We have seen that it has worse results than the cnn architecture we designed for denim fabric dataset. In the proposed CNN-based fabric defect detection method, exactly this point was taken into consideration and the spectrum information of the Fourier transform was analyzed in a very different way. The frequencies of weft and warp patterns are filtered and the defective areas are made clear. In addition, the regions that do not contain defects are suppressed and the defect is brought to the fore.

3.2 Real-Time Defect Detection Application

Fabric defects are less likely to occur, making it difficult to perform a systematic comparison of the algorithm. Furthermore, it takes extra time and cost to change a loom's warp beam, which limits the ability to quickly alter fabric

materials for online evaluation. These reasons lead us to evaluate the accuracy of the system. To perform real-time defect detection, we used our trained CNN 4 deep network architecture, which is described in Section 3. The proposed embedded vision-based defect detection has mounted on the Picanol OptiMax loom (see Figure 10). Hardware and image acquisition strategies have been described in Section 3. NVIDIA's Nano card is chosen as the embedded platform. This low-cost card has a suitable hardware infrastructure to run CNN architectures. Software in Python programming language has been developed so that the images provided by the BlackFly camera can be stored and classified in Nano. This software transfers 5 images of 1920×1200 per second to Nano's RAM using the API of the camera.

The transferred images are first subjected to size reduction and then to patching. Finally, each patch is given as an input to the deep model which is loaded into the Nano and used the trained model to classify defects. The proposed framework has analyzed the denim fabric for about 24 hours and with images of over 30000. The majority of 98% of the captured frames are defect-free fabric images (i.e., approx. 600 images contain defects). After completing the real-time defect detection process, we compared the results of our detection system and quality control reports. Examining the results of the quality control unit gives us an overall overview of the two separate defect detection methods. Thus, an objective comparison has been conducted between our real-time system and quality control unit. Our proposed method can detect all of the defects labeled by the quality control unit which is 550 defects. In addition to this, our system can capture extra 29 defects which overlooked by the quality control unit. In case a defective image is detected, the defect type and information about the number of meters of the fabric roll are recorded in a separate database and defect reports are produced. The generated defect reports have been matched with the defect reports produced in the quality control unit and the detected defects have been verified. Classification results are given in Table (4).

4. CONCLUSION

In this paper, a real-time fabric defect detection system is proposed and implemented. The proposed defect detection

system includes three main modules: vision system, CNN model, an embedded module. Firstly, a novel fabric database has been constructed by using an industrial vision system on a loom. Then, an effective CNN model with negative mining is proposed for fabric defect detection. In the proposed methodology, a novel defective patch capture algorithm based on fast Fourier transform is developed to suppress the background and highlight defect regions. This algorithm improves the effectiveness and distinctiveness of the CNN model. CNN model is trained using defective patch capture algorithm.

Real-time defect detection has been performed by moving the trained architecture to the embedded platform. The proposed model has some advantages such as the low computational cost and high detection rates. These advantages are the significant reasons for a detection system. Thus, real-time defect detection is performed, and high defect detection results have been obtained on a loom. However due to the environmental noise and loom machine vibration our test classification results dropped by $\sim 0.7\%$.

As noticed in the experiments, there are different defect types in fabric production. The constraints of camera and light source reduced the distinctiveness between foreground defects and fabric background texture in the obtained images. Therefore, in future work, we have planned to solve these problems. We will expand the fabric defect database in terms of the kinds of defects. Moreover, we also apply various learning algorithms to the fabric defect detection. To further real time defect detection, the design of learning algorithms will be investigated.

Acknowledgement

The implementation activities of this research study were carried out in the fabric production section of the CALIK DENIM [40] factory. The authors would like to thank CALIK DENIM employees. Funding was also provided by the Scientific and Technological Research Council of Turkey (TÜBİTAK, Teydep-5180054).

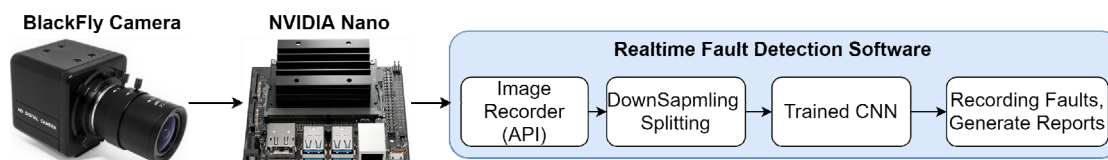


Figure 10. Real-time defect detection system.

Table 4. Real-time defect detection results

	Ground truth	Quality control unit	Our proposed method
Total images	30000	30000	30000
Defect-free	29400	27165	28371
Defected	600	550	579
	Classification results	$\sim 92.40\%$	$\sim 96.5\%$

REFERENCES

1. Hanbay K, Talu MF, Özgüven ÖF. 2016. Fabric defect detection systems and methods, A systematic literature review. *Optik* 127(24), 11960-11973.
2. Zuo H, Wang Y, Yang X, Wang X. 2012. Fabric defect detection based on texture enhancement. 5th International Congress on Image and Signal Processing. Chongqing, China, 876-880.
3. Duchesne C, Liu J. J, MacGregor J. F. 2012. Multivariate image analysis in the process industries: A review. *Chemometrics and Intelligent Laboratory Systems* 117, 116-128.
4. Mak K-L, Peng P, Yiu KFC. 2009. Fabric defect detection using morphological filters. *Image and Vision Computing* 27(10), 1585-1592.
5. Tong L, Wong WK, Kwong CK. 2016. Differential evolution-based optimal Gabor filter model for fabric inspection. *Neurocomputing* 173, 1386-1401.
6. Hanbay K, Talu MF, Özgüven ÖF. 2017. Real time fabric defect detection by using fourier transform. *Journal of the Faculty of Engineering and Architecture of Gazi University* 32, 151-158.
7. Anandan P, Sabeenian RS. 2018. Fabric defect detection using discrete curvelet transform. *Procedia computer science* 133, 1056-1065.
8. Monaco JP, Madabhushi A. 2012. Class-specific weighting for Markov random field estimation: Application to medical image segmentation. *Medical Image Analysis* 16(8), 1477-1489.
9. Zhao Y, Hao K, He H, Tang X, Wei B. 2020. A visual long-short-term memory based integrated CNN model for fabric defect image classification. *Neurocomputing* 380, 259-270.
10. Jing J, Zhang H, Wang J, Li P, Jia J. 2013. Fabric defect detection using Gabor filters and defect classification based on LBP and Tamura method. *Journal of the Textile Institute* 104(1), 18-27.
11. Hanbay K. 2016. Fabric Defect Detection System Based on Image Processing for Circular Knitting Machines (Doctoral dissertation). University of Inonu, Malatya.
12. Chen J, Jain AK. 1988. A structural approach to identify defects in textured images, in Proceedings of the IEEE International Conference on Systems, Man, and Cybernetics, Beijing, China, 1, 29-32.
13. Wen Z, Cao J, Liu X, Ying S. 2014. Fabric defects detection using adaptive wavelets. *International Journal of Clothing Science and Technology* 26(3), 202-211.
14. Jia L, Chen C, Xu S, Shen J. 2020. Fabric defect inspection based on lattice segmentation and template statistics. *Information Sciences* 512, 964-984.
15. Jia L, Liang J. 2017. Fabric defect inspection based on isotropic lattice segmentation. *Journal of the Franklin Institute* 354(13), 5694-5738.
16. Kuo CFJ, Lee CJ. 2003. A back-propagation neural network for recognizing fabric defects. *Textile Research Journal* 73(2), 147-151.
17. Mak KL, Peng P. 2008. An automated inspection system for textile fabrics based on Gabor filters. *Robotics and Computer-Integrated Manufacturing* 24(3), 359-369.
18. Bu H, Wang J, Huang X. 2009. Fabric defect detection based on multiple fractal features and support vector data description. *Engineering Applications of Artificial Intelligence* 22(2), 224-235.
19. Hanbay K, Talu MF, Özgüven ÖF, Öztürk D. 2019. Real-time detection of knitting fabric defects using shearlet transform. *Tekstil ve Konfeksiyon* 29(1), 3-10.
20. Zhang K, Yan Y, Li P, Jing J, Wang Z, Xiong Z. 2020. Fabric defect detection using saliency of multi-scale local steering kernel. *IET Image Processing* 14(7), 1265-1272.
21. Yıldız K, Buldu A, Demetgul M. 2016. A thermal-based defect classification method in textile fabrics with K-nearest neighbor algorithm. *Journal of Industrial Textiles* 45(5), 780-795.
22. Yildiz K. 2017. Dimensionality reduction-based feature extraction and classification on fleece fabric images. *Signal, Image and Video Processing* 11(2), 317-323.
23. Yildiz K, Buldu A, Demetgul M, Yildiz Z. 2015. A novel thermal-based fabric defect detection technique. *The Journal of The Textile Institute* 106(3), 275-283.
24. Yıldız K, Buldu A. 2017. Wavelet transform and principal component analysis in fabric defect detection and classification. *Pamukkale University Journal of Engineering Sciences* 23(5), 622-627.
25. Jing J, Dong A, Li P, Zhang K. 2017. Yarn-dyed fabric defect classification based on convolutional neural network. *Optical Engineering* 56(9), 93104.
26. Wang Z, Jing J. 2020. Pixel-wise fabric defect detection by CNNs without labeled training data. *IEEE Access* 8, 161317-161325.
27. An M, Wang S, Zheng L, Liu X. 2020. Fabric defect detection using deep learning: An improved faster R-approach. International Conference on Computer Vision, Image and Deep Learning (CVIDL). Chongqing, China, 319-324.
28. Zhou H, Jang B, Chen Y, Troendle D. 2020. Exploring faster RCNN for fabric defect detection. Third International Conference on Artificial Intelligence for Industries (AI4I). Irvine, CA, USA, 52-55.
29. Dong Y, Wang J, Li C, Liu Z, Xi J, Zhang A. 2020. Fusing multilevel deep features for fabric defect detection based NTV-RPCA. *IEEE Access* 8, 61872-161883.
30. Mei S, Wang Y, Wen G. 2018. Automatic fabric defect detection with a multi-scale convolutional denoising autoencoder network model. *Sensors* 18(4), 1064.
31. Wei W, Deng D, Zeng L, Zhang C. 2020. Real-time implementation of fabric defect detection based on variational automatic encoder with structure similarity. *Journal of Real-Time Image Processing* 1-17.
32. Uster Technologies AG. Fabric inspection. Retrieved from <https://www.uster.com/en/instruments/fabric-inspection/> (accessed Jul. 15, 2021).
33. BMSvision, Camera Inspection. 2019.
34. Dalal N, Triggs B. 2005. Histograms of oriented gradients for human detection. IEEE Computer Society Conference on Computer Vision and Pattern Recognition (CVPR'05). San Diego, CA, USA, 1, 886-893.
35. Haralick RM, Shanmugam K, Dinstein I. 1973. Textural features for image classification. *IEEE Transactions on Systems, Man, and Cybernetics* SMC-3(6), 610-621.
36. Watanabe T, Ito S, Yokoi K. 2009. Co-occurrence histograms of oriented gradients for pedestrian detection. in Wada T, Huang F, Lin S. (Eds.), *Advances in Image and Video Technology*. Germany:Springer-Verlag, 37-47.
37. Chan CH, Pang GKH. 2000. Fabric defect detection by Fourier analysis. *IEEE Transactions on Industry Applications* 36(5), 1267-1276.
38. Do MN, Vetterli M. 2002. Wavelet-based texture retrieval using generalized Gaussian density and Kullback-Leibler distance. *IEEE transactions on image processing* 11(2), 146-158.
39. Easley G, Labate D, Lim WQ. 2008. Sparse directional image representations using the discrete shearlet transform. *Applied and Computational Harmonic Analysis* 25(1), 25-46.
40. CALIK DENIM. <https://www.calikdenim.com> (accessed Jul. 20, 2020).



Investigation of Auxetic Performance and Various Physical Properties of Fabrics Woven with Braid Yarns

Mine Akgun¹ 0000-0002-6415-7782

Fatih Suvani¹ 0000-0001-5708-7993

Recep Eren¹ 0000-0001-9389-0281

Tugba Yurdakul² 0000-0003-0369-3757

¹Bursa Uludag University / Faculty of Engineering / Textile Engineering Department, Bursa, Türkiye

²Bursa Uludag University / Graduate School of Natural and Applied Sciences / Textile Engineering Department, Bursa, Türkiye

Corresponding Author: Mine Akgun, akgunm@uludag.edu.tr

ABSTRACT

In this study, the auxetic performance and various physical properties of fabrics woven with braid yarn were examined. Fabrics were woven in plain weave with conventional warp and braid weft yarn. Experimental results showed that fabrics woven with braid weft yarn exhibited an auxetic behavior by giving Negative Poisson's Ratio (NPR) up to a certain elongation value under tension in the warp direction. In addition, it was observed that the NPR of fabric was affected by the thickness of the braid yarn and the tightness (compactness) of the fabric. It was found that the use of braid yarn in woven fabric improved various physical properties such as tensile strength, thermal resistivity and abrasion resistance. Use of braid yarns increased the tensile strength in the weft direction where braid yarns were used, increased thermal resistivity values at the fabric woven with thick and bulky braid yarns and also increased abrasion resistance.

1. INTRODUCTION

The design of multifunctional woven fabrics by developing basic performance properties of conventional woven fabric structures has become necessary to obtain composite textile structures mostly used in technical textiles where high performance is required. Since auxetic structures could show many improved performance features, it would be possible to bring many functional properties to the structure in one step by developing auxetic woven fabric structures.

Poisson's ratio is one of the essential properties used in many engineering fields to determine the material structure [1]. Poisson's ratio (ν) is defined as the negative ratio of the transverse strain occurring perpendicular to the force applied to a material to the longitudinal strain in the direction that the force is applied. Auxetic materials are the type of materials with a Negative Poisson's Ratio (NPR). As opposed to materials with a positive Poisson's ratio, auxetic materials expand laterally when stretched and contract laterally when compressed [1-6]. Increased mechanical properties (breaking strength, abrasion resistance, indentation resistance, fracture toughness, shear resistance, etc.), variable permeability, improved acoustic absorption, and high energy absorption properties make auxetic materials superior to conventional materials [1,3,7-12].

To cite this article: Akgun M, Suvani F, Eren R, Yurdakul T. 2022. Investigation of auxetic performance and various physical properties of fabrics woven with braid yarns. *Tekstil ve Konfeksiyon*, 32(3), 220-231.

ARTICLE HISTORY

Received: 07.12.2021

Accepted: 28.04.2022

KEYWORDS

Auxetic effect, negative Poisson's ratio, braid yarn, woven fabric, fabric's physical parameters

In literature studies, it is explained that conventional fabric structures show positive Poisson's Ratio (PR) values due to contracting laterally when stretched [13,14]. A study on the worsted fabrics states that fabrics with higher weft yarn density have a higher Poisson's ratio value. And also, it is stated that this ratio is related to the structural stiffness of the fabric [13]. In a study investigating the effects of various mechanical properties of yarns and structural parameters of fabrics on the Poisson's ratio of a woven fabric, it was pointed out that, in general, the yarn spacing (i.e., the distance between two adjacent yarns in a fabric) ratio and the yarn diameter ratio between warp and weft yarns have more significant effects on the Poisson's ratio of a woven fabric than the yarn Young's modulus ratio [14]. Warp and weft yarns that intersect in the woven fabric structures are crimped due to the paths that they have to follow around each other as a result of this intersection. When the fabric is stretched in one direction, due to the stretching of the yarn in the loading direction, the yarn crimps decrease until they reach zero. Axially stretched yarns cause the yarns perpendicular to the loading direction to be more crimped. As a result, the fabric contracts in the lateral direction, and a positive PR is obtained [15,16].

In the literature, there are two approaches for auxetic fabric production. The first is creating an NPR effect through

knitting or weaving in a special geometric configuration using conventional fibers and yarns [17-20]. The second is to use directly auxetic fibers and yarns so that the NPR effect can be created using simple woven or knitted structures [21-23].

In studies on yarn development with auxetic properties, a yarn structure with auxetic properties is presented with multifilament yarn construction consisting from components that do not have auxetic properties. The helical auxetic yarn (HAY) structure was first presented by Hook [24,25]. This yarn structure was obtained by helically winding a high stiff filament around a thick and low stiff filament. Under longitudinal stretching, the high stiff filament straightens and displaces the lower stiffness filament into a curved shape. As a result of this, the yarn structure is expanded in the lateral direction [24,25]. It was stated that the starting wrap angle of HAY had the greatest effect on the auxetic behavior and the other parameters which influence auxetic performance were found to be the diameter ratio of wrap to core fibers and the fibers' inherent Poisson's ratio. In the literature, it is stated that the auxetic structures can be obtained by combining two or more multifilament structures appropriately [3,26].

The term braid refers to the placement of the sheath yarns, which are made of one or more filaments. They are released from the reels placed on the carriers in the braiding machine, and they cross the axis of the yarn diagonally without making a full rotation around each other. A basic braid structure is circular, with half of the yarn bundles moving clockwise at a certain angle to the braid yarn axis and the other half moving counterclockwise by alternately passing over and under the first group bundles [27-28].

In the literature, a novel type of braided yarn structure exhibiting auxetic behavior was proposed. In this study, it was found that parameters such as the initial wrap angle, the initial braiding angle and the braiding yarn diameter were all important on the auxetic effect of tubular braided structure. It was stated in this research that the negative Poisson's ratio could be achieved in a structure with the use of a wrap yarn having higher modulus than that of the braiding yarns and core yarn. Also, it was stated that braided yarn structure with a lower initial wrap angle, a higher initial braiding angle and a larger braiding yarn diameter had a better auxetic performance [29].

In this study, the changes in Poisson's ratio of the fabrics woven with braid weft yarns of different thicknesses are investigated. With the use of braid yarns in the formation of woven fabric, the deformation state of the braid weft yarns that intersect with the conventional warp yarns in the fabric under tension and the possible auxetic behavior are evaluated. In addition, various physical and thermal comfort tests were carried out to examine the effects of the use of braid yarn in woven fabric structures on the physical performances.

2. MATERIAL AND METHOD

2.1 Material

In the experimental study, braid polyester yarns consisting of 12 sheath yarns were used as weft yarn. Braid yarns were

supplied from Yayteks İplik Mak. Ltd. Şti. (Bursa) company. Microscopic images (30 times magnification) of braid yarns used as weft are presented in Figure 1.

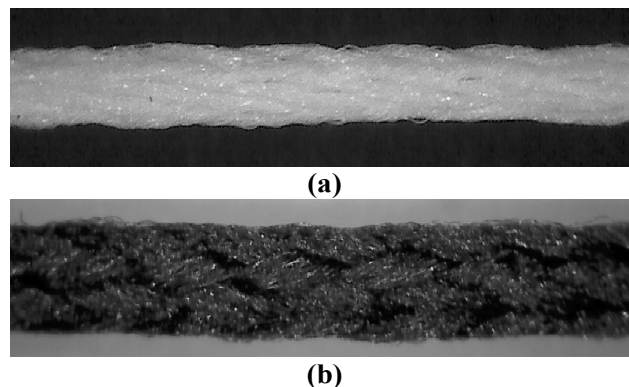


Figure 1. Microscopic images of braid yarn (Mag: 30X)
a) F1 fabric's weft yarn b) F2 fabric's weft yarn

Fabrics in plain weave structure were woven using polyester braid yarn in the weft and conventional textured polyester yarn in the warp on the hand weaving loom (Gülas Makina), as presented in Figure 2.



Figure 2. Weaving loom

Structural parameters and microscopic images of fabrics with 20 times magnification are presented in Table 1 and Figure 3, respectively.

In addition, the positioning of the braid weft yarns in the fabric structure is presented in Figure 4 for the F2 fabric.

In addition, a conventional sample fabric structure was investigated to compare the Poisson's ratio change tendencies of fabric woven with braid yarn and fabric woven with conventional yarn. For this reason, it was preferred to use a plain weave conventional fabric sample with the same yarn type (100% textured polyester) and yarn counts (300 denier) in warp and weft. In this way, the tendency of Poisson's ratio change of a conventional plain woven fabric sample was presented.

2.2 Method

2.2.1 Performed tests on fabrics

Various physical and thermal comfort tests were carried out to examine the effects of the use of braid yarn in woven fabric structures on the physical performances. For this purpose, fabrics' maximum strength, elongation, air permeability, thermal resistivity, abrasion resistance, and fabric thickness changes under different compression pressures were investigated. Fabric samples were conditioned at $65\pm 2\%$ relative humidity and $20\pm 2^\circ\text{C}$ for 24 hours by the ASTM D 1776-08 [30] standards before all the mentioned tests.

Tensile tests

Tensile measurements of fabrics at warp and weft directions were conducted using Shimadzu AG-X plus tensile testing machine by ISO 13934-1 (2013) standard test method [31]. Fabric sample strip dimensions were kept at $100\text{ mm}\times 50\text{ mm}$, and the tensile speed were set at 10 mm/min . Fabrics were photographed by a digital microscope (INSIZE ISM-PRO) with a time interval of 5 seconds until a total elongation of 10 mm (60 seconds) is reached during the tensile test. The setup of the testing system is presented in Figure 5.

Table 1. Structural parameters of fabrics

Fabric code	Yarn properties		Yarn count [denier]		Yarn density [thread/cm]		Fabric mass per unit area [g/m^2]
	Warp	Weft	Warp	Weft	Warp	Weft	
F1	Textured Polyester	Circular braided yarn with 12 sheath yarn (sheath yarn count: 150 denier)	600	1962	10	8	404
F2	Textured Polyester	Circular braided yarn with 12 sheath yarn (sheath yarn count: 510 denier)	600	6210	10	6	575

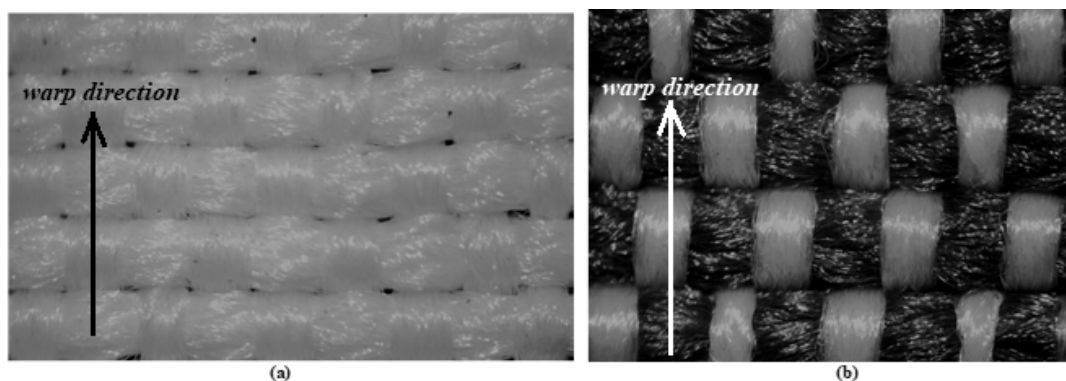


Figure 3. Microscopic images of fabrics (Mag: 20X) a) F1 fabric b) F2 fabric

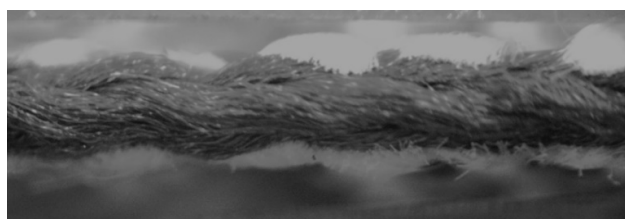


Figure 4. Cross-section view of F2 fabric (Mag: 30X) (transverse section of the warp yarns - longitudinal section of weft yarn)

With the help of markers placed on the fabric (Figure 6), the changes in the width (average of x values) and length (average of y values) of the fabric were calculated with the help of the software developed in MATLAB over the images taken every 5 seconds.

The distances between markers placed on the fabric were measured with the help of a method [32] developed using MATLAB for both the free state and stretched state to calculate the strains in both transverse and longitudinal fabric directions. Poisson's ratio (ν) was calculated [1] using Equation (1) as follows;



Figure 5. Measurement setup

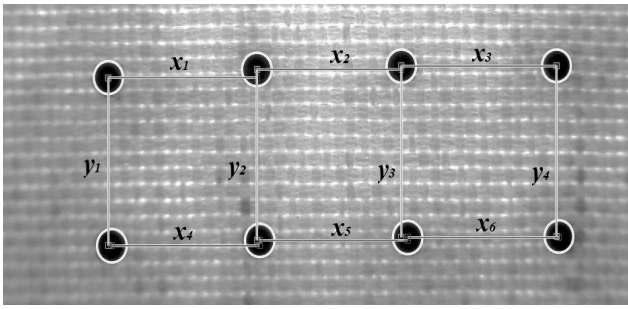


Figure 6. Placement of markers on fabric

$$\nu = - (\text{transverse strain} / \text{longitudinal strain}) \quad (1)$$

Changes of the F1 and F2 fabrics in the transverse direction under different elongation values up to 10 mm in warp direction are presented in Figures 7 and 8, respectively. In Figures 7 and 8, the distance between the first and last markers placed on the fabric was indicated in order to visually demonstrate the transverse expansion effect of the fabric. In the calculation of Poisson's ratios, the distance between each marker was measured with the help of MATLAB, as shown in Figure 6, and average values were taken.

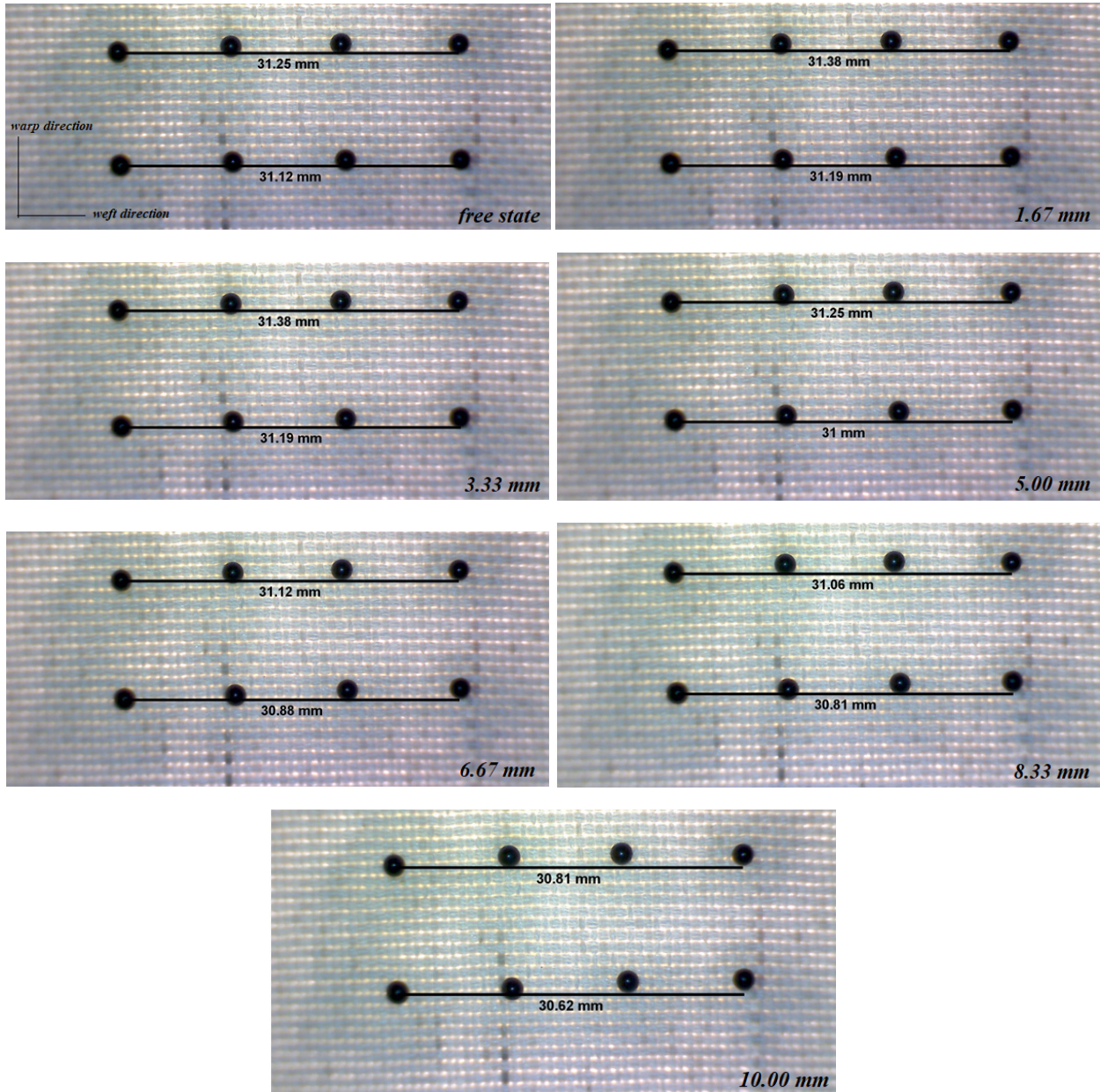


Figure 7. Changes of the F1 fabric in the transverse direction under different elongation values in warp direction

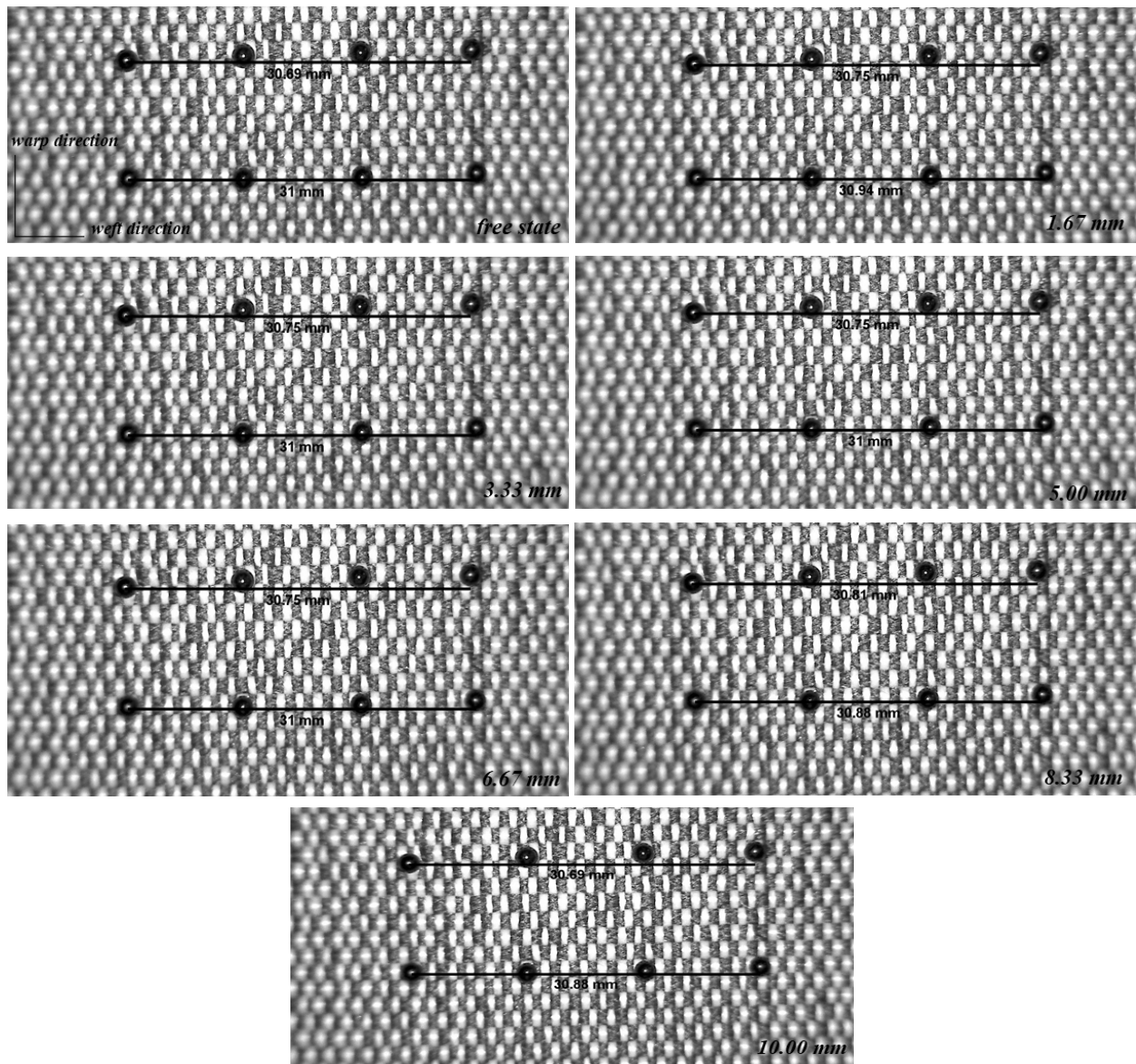


Figure 8. Changes of the F2 fabric in the transverse direction under different elongation values in warp direction

Mass per unit area and thickness of fabric

Mass per unit area of fabrics were measured according to ASTM D3776 [33]. The thickness of fabrics was measured according to ASTM D1777-96 [34] standard with James Heal's R&B Cloth thickness tester.

Measurement of yarn crimp

Yarn crimps in fabric samples were measured according to ASTM D3883-04 [35]. Percentage crimp values and crimp amplitude values were calculated using Equations (2) – (4), respectively [35,36];

$$\text{Yarn crimp (\%)} = \frac{\text{Straightened yarn distance} - \text{Distance in the fabric}}{\text{Distance in the fabric}} \times 100 \quad (2)$$

$$\frac{h_1}{P_2} = \frac{4}{8} \sqrt{C_1} \quad (3)$$

$$\frac{h_2}{P_1} = \frac{4}{8} \sqrt{C_2} \quad (4)$$

where, h_1 and h_2 are the warp and weft yarn crimp amplitudes; c_1 and c_2 are the warp and weft yarn crimps; and P_1 and P_2 are the thread spacing of individual warp and weft yarns (Figure 9), respectively.

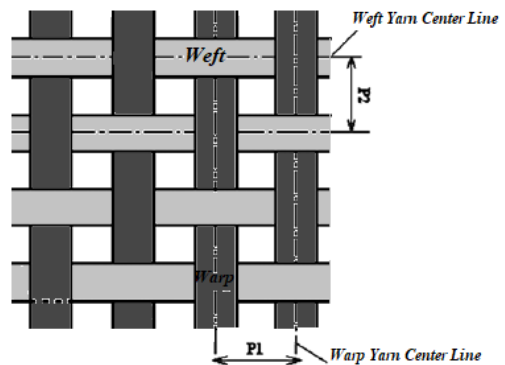


Figure 9. Schematic presentation of the thread spacing of individual warp (P_1) and weft (P_2) yarns

The crimp values of the yarns in the fabric were measured (Equation (2)), and the crimp amplitude values were calculated according to Equations (3) and (4). It was found that the braid weft yarns in the fabric structure did not take measurable yarn crimp in contrast to warp yarns, and the crimp and crimp amplitude values of the warp yarns are presented in Table 2.

Air permeability

Air permeability of fabrics was measured based on EN ISO 9237 [37] standard using an SDL Atlas Digital Air Permeability Tester Model M021A. Measurements were performed by applying 100 Pa air pressure per 5 cm² fabric surface.

Thermal Resistivity

Thermal resistivity (r) is defined as the material's resistance against heat flow. Thermal resistance of fabrics was measured by using the Alambda instrument. The thermal resistance is connected with fabric thickness and thermal conductivity coefficient by Equation (5) [38].

$$r = \frac{h}{\lambda} \quad (m^2KW^{-1}) \quad (5)$$

where,

r : thermal resistance,

h : fabric thickness (m),

λ : thermal conductivity coefficient (W/mK)

Abrasion test

The abrasion tests of the fabrics were carried out under the load of 9 kPa, in the Nu-Martindale abrasion test device by the standard of ASTM D 4966 [39]. The fabrics were abraded in 30000 abrasion cycles.

Microscopic Analysis

Microscopic images of the fabrics were taken under a microscope (Mshot Digital Microscope Camera MS60) coupled to a digital camera.

3. RESULTS AND DISCUSSION

3.1 Analysis of the Poisson's ratios

The Poisson's ratio – elongation curves of the fabrics are presented in Figures 10 and 11. F1 fabric was woven with thin braid weft yarn and F2 fabric with thick braid weft yarn. In Figures 10 and 11, it was seen that the fabrics woven with braid weft yarn demonstrated NPR value under tension in the warp direction. It was observed that NPR was obtained up to an elongation value of 3.33 mm in the fabric woven with thin braid weft yarn and up to 6.67 mm in the fabric woven with thick braid weft yarn.

Table 2. Warp yarn crimp amplitude values

Fabric Code	Warp yarn crimp [%]	Thread spacing of individual yarns [cm]		Warp yarn crimp amplitude [cm]
		Warp (P_1)	Weft (P_2)	
F1	10	0.1	0.125	0.053
F2	10	0.1	0.167	0.070

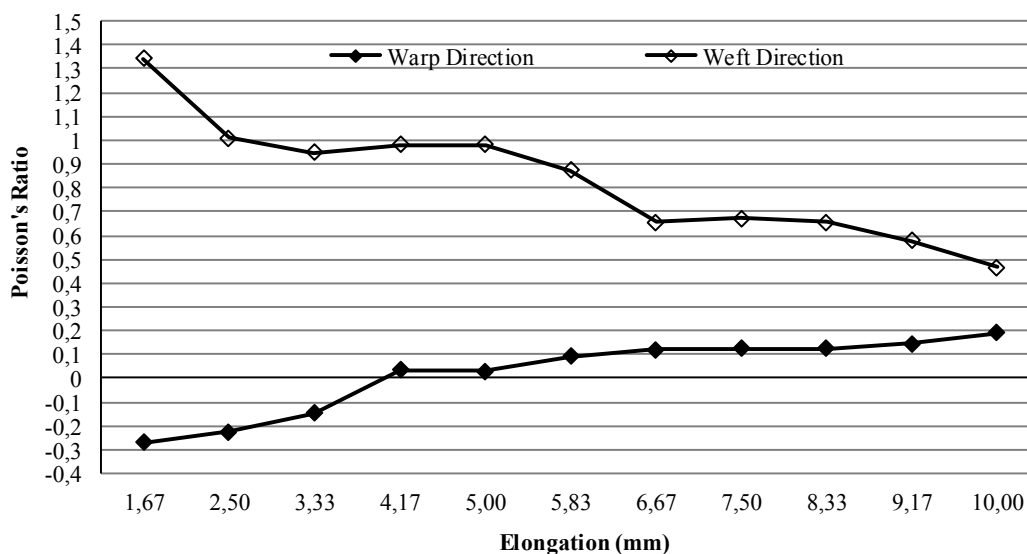


Figure 10. Poisson's ratio – elongation curve of F1 fabric

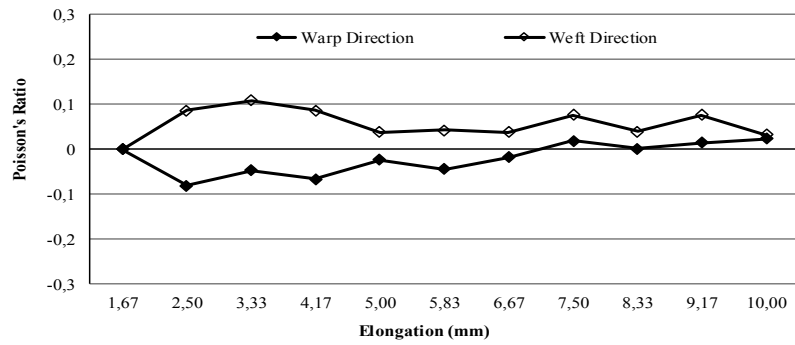


Figure 11. Poisson's ratio – elongation curve of F2 fabric

The warp yarns of the fabrics were of conventional structure. It was observed that braid weft yarns had a transverse expansion effect in the fabric, and NPR could be obtained in fabrics subjected to tension in the warp direction. It was considered that this was because the braid weft yarns in a structure with an entrant form that intersect diagonally with each other showed a widening effect in the transverse direction due to the effect of warp yarn compression under the tensile tension in the warp direction. It was observed that this transverse widening effect continued up to higher elongation values in fabric structure with the thick braid yarn.

However, when Figures 10 and 11 were examined, it was seen that while the maximum Poisson's ratio was obtained as ≈ -0.3 values for the F1 fabric (woven with thin braid weft yarn), the maximum Poisson's ratio was obtained as ≈ -0.1 for the F2 fabric (woven with thick braid weft yarn). As could be seen from Figure 3, this result might be because the F1 fabric was in a less tight (in a more open) form and the F2 fabric was in a tighter form due to its thick weft yarn structure. In the F1 fabric with a more open structure, it was considered that the braid weft yarns' transverse expansion behavior could occur more easily under the tensile tension in the warp direction. In the F2 fabric, it was assessed that the weft yarns could not expand easily in the transverse direction because the thick braid yarns created a tighter fabric structure. Due to this situation, it was observed that a higher negative Poisson's ratio could be obtained in the F1 fabric with thin braid weft yarn compared to the F2 fabric.

In Figures 10 and 11, when the changes in the weft direction Poisson's ratios of the fabrics were examined, it was seen that the Poisson's ratios showed a positive change. However, it was observed that the Poisson's ratio values of the F2 fabric with thick braid weft yarn under tension in the weft direction remained in the range of close to zero values such as 0.0 - 0.1 during the 10 mm elongation. Whereas, it was seen that F1 fabric with thin braid weft yarn demonstrated higher positive Poisson's ratio values under weft directional tension. This result showed that the transverse contraction behavior of the fabric was lower when thick braid weft yarn was used in fabric structure, under weft-directional tension (ie, when the tension applied to the fabric was applied in the direction of braid weft yarns) compared to the use of thin braid weft yarn in the fabric structure.

To examined the Poisson's ratio change of a fabric woven with conventional yarns, the Poisson's ratio–elongation tendency of a conventional fabric sample under tension is presented in Figure 12. It was seen that this conventional fabric had a positive Poisson's ratio under elongation. Considering the effects of factors, such as the warp and weft yarn counts were the same, and the fabric was woven in a plain weave structure, it was observed that the change of the Poisson's ratio–elongation curve was obtained with a similar tendency in the warp and weft directions. It was observed that the Poisson's ratios of a conventional fabric sample have a positive increasing tendency as the increased elongation value in the warp and weft direction.

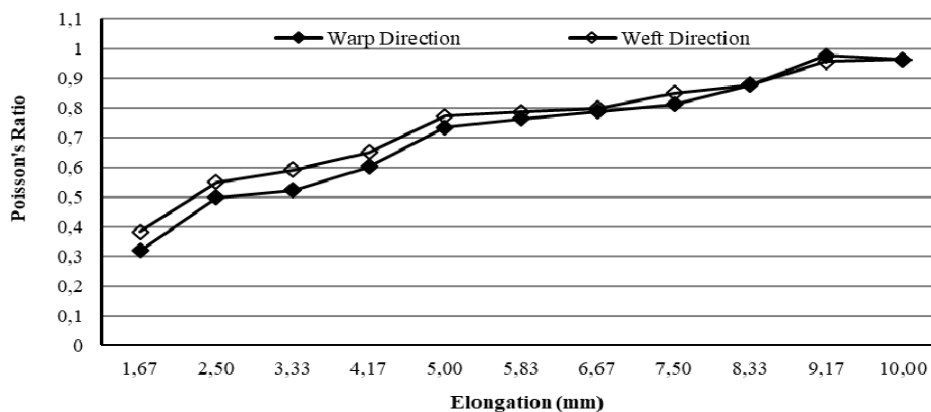


Figure 12. Poisson's ratio–elongation curve of a conventional fabric sample

3.2 Analysis of the tensile strength and elongation

The tensile strength and elongation values of fabrics are presented in Figure 13 and 14, respectively. In Figure 13, it was seen that the maximum fabric strength values in the weft direction, in which braid yarns were used as weft, were significantly higher than those in the warp direction. Although the weft yarn forming the F2 fabric was thicker than the weft yarn forming the F1 fabric, it was observed that the weft directional fabric strength of the F1 fabric was higher. It was thought that this might be due to the higher weft yarn density value per unit area of the F1 fabric (8 thread/cm) than F2 fabric (6 thread/cm). It was also observed that the use of braid yarn as weft yarn significantly increased the maximum strength values in the weft direction.

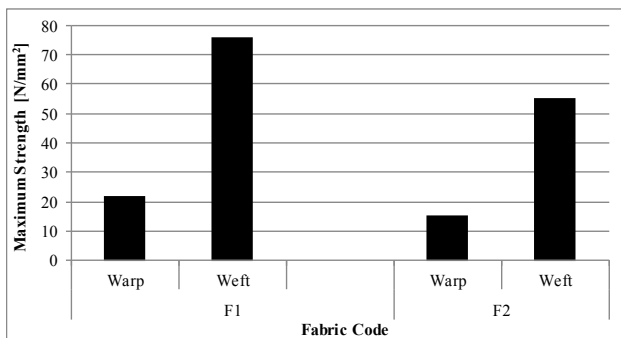


Figure 13. Tensile strength values of fabrics

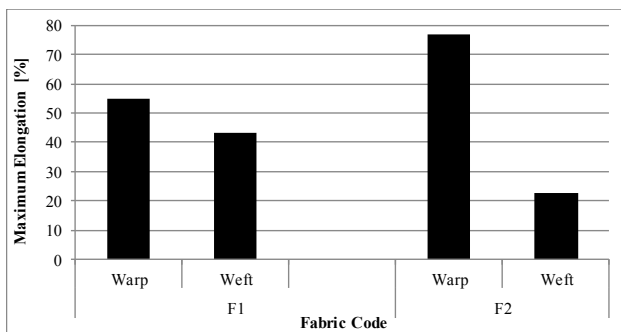


Figure 14. Maximum elongation (%) values of fabrics

In a study on the auxetic performance properties of woven fabrics [40], it was stated that a significant difference was observed between the warp and weft directional elongation values of the fabrics in which the NPR effect was obtained. In addition, it was stated that the warp directional elongation values were significantly higher than the weft directional elongation values in these fabric structures, and it was stated that the NPR effect observed in the warp direction of these fabrics was affected by this result [40].

In Figure 14, it could be seen that a similar result was obtained as stated in this literature. In Figures 10 and 11, it was seen that the NPR effect in F1 and F2 fabric was obtained in the warp direction. In Figure 14, it was observed that there was a difference between the warp and weft directional elongation values of fabrics. It was considered that greater elongation of the yarns in the warp

direction could cause the fabric to expand more in the transverse direction under elongation. In particular, due to the use of conventional yarns as warp in this study, the elongation of conventional warp yarns intersecting with braid weft yarns showed a significant widening effect in the transverse direction.

Also, it was seen that the difference between warp and weft directional elongation values was significantly higher in the F2 fabric compared to the F1 fabric. This result suggested that it might be related to the fact that the NPR effect continued under the longer elongation values in the F2 fabric structure, as seen in Figure 11, compared to the F1 fabric.

In Figure 14, it was observed that there was a difference between the warp directional elongation values of F1 and F2 fabrics. The reason for this was thought to be as explained below. The property and yarn density of the warp yarns were kept constant (Table 1). It was seen from Table 2 that the warp yarns had the same crimp value in both fabric structures. However, depending on the braid weft yarn thickness used in the fabrics, the weft yarn density value differed. As shown in Table 1, the weft yarn density of F1 fabric woven using thin braid weft yarn is 8 thread/cm, while the weft yarn density of F2 fabric woven using thick braid weft yarn is 6 thread/cm. The crimp amplitude values of the fabrics are presented in Table 2. It was seen that the crimp amplitude values of the warp yarns in the F2 fabric were higher than the crimp amplitude values of the warp yarns of the F1 fabric. Although there was less weft yarn per unit area, it was seen that the crimp amplitude values of the warp yarns in the F2 fabric, which were crimped around the braid weft yarns which have a very high thickness value (6210 denier), were higher. In this case, as seen in Figure 14, it was considered that the elongation values of the warp yarns in the F2 fabric were higher than the warp yarns in the F1 fabric.

From the results obtained, it was observed that there was a difference between the warp and weft directional elongation values in both fabric structures where the NPR effect was obtained. And it was seen that a longer-lasting NPR effect (Fig. 11) was obtained in the F2 fabric, in which this difference was higher. Also, it was observed that the warp directional elongation values were higher in these fabrics where the NPR effect was obtained in the warp direction. As a result, it was thought that more elongation of the yarns in the warp direction might cause the fabric to expand more in the transverse direction under elongation, causing the NPR effect.

3.3 Analysis of the fabric thickness

Auxetic materials expand under elongation and contract under compression. A local contraction is observed when compression occurs in an isotropic auxetic material. There is a material flow that condenses under the applied load, creating a denser material area with higher resistance to compression [1-3, 5,6].

For this reason, besides the behavior of woven fabric structures using braid yarns under tension, the changes in fabric thickness under different compression pressure values were also investigated. The thickness values of the fabrics under three different compression pressures (5, 10 ve 20 g/cm²) are presented in Figure 15.

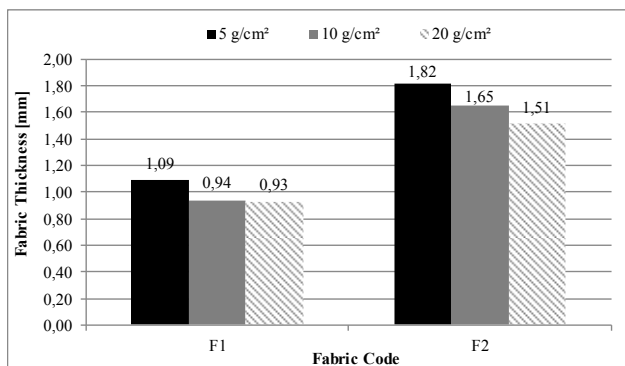


Figure 15. Fabric thickness

In Figure 15, when the pressure was increased from 5 g/cm² to 10 and 20 g/cm², it was observed that the F1 fabric thickness values decreased by 13.76% and 14.67%, respectively. However, it was observed that there was no significant change in fabric thickness values under compression pressures of 10 and 20 g/cm². This result was thought to be due to the condensation of the material towards the inner region under compression due to the entrant geometry of the braid weft yarn.

It was observed that the F2 fabric thickness decreased by 9.34% and 17.03% when the pressure was increased from 5 g/cm² to 10 and 20 g/cm². There was observed a decrease of 8.48% between the fabric thickness values under compression pressures of 10 and 20 g/cm². It was considered that the reason why the fabric thickness values were approximately constant under the compression pressures of 10 and 20 g/cm² in the F1 fabric, and the decrease in the F2 fabric was due to the fact that the braid weft yarn structure used in the F2 fabric was thicker and bulkier than the braid weft yarn in the F1 fabric.

In addition, when the pressure values were increased from 5 g/cm² to 10 g/cm², it was observed that the F1 and F2 fabric thickness values decreased by approximately 13.76% and 9.34%, respectively. In other words, it was observed that the decrease in thickness value was lower in the F2 fabric woven with thick braid weft yarn. It was thought that this situation might be due to the fact that the effect of condensing the material towards the inner region in the thick braid yarn structure under the compression effect might be more compared to the thin braid yarn structure.

3.4 Analysis of the air permeability

The air permeability values of fabrics are presented in Figure 16. It was seen that the air permeability value of F2 fabric with thick braid weft yarn was approximately 2.08 times lower than those of F1 fabric with thin braid weft

yarn. Also, considering the fabric thickness values in Figure 15 (for 5 g/cm² compression pressure), it was seen that the thickness value of the F2 fabric was 1.67 times higher than the thickness value of the F1 fabric.

In Figure 3, it was observed that the F1 fabric had a more open (a more porous) structure than the F2 fabric. It should be noted that this porous structure also increased the air permeability value. It was seen that the F2 fabric, which was woven using thick and bulky braid weft yarn, had a more compact structure. Considering the parameters such as the use of weft yarn with thick and bulky braid, and therefore the high fabric thickness and its more compact structure compared to the F1 fabric, it was observed that the air permeability value of F2 fabric had decreased significantly.

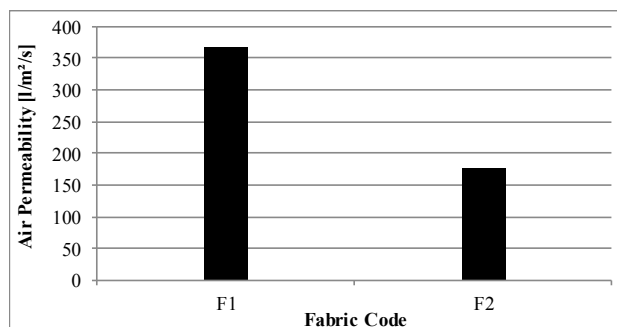


Figure 16. Air permeability values of fabrics

3.5 Analysis of the thermal resistivity

The thermal resistivity values of fabrics are presented in Figure 17. It was observed that the thermal resistivity value of the F2 fabric was 3.02 times higher than that of the F1 fabric. This result was affected by the yarn thickness and, therefore, the fabric thickness. In addition, it was considered that the effect of braid yarn structure should be taken into account. The braid yarns used in fabrics consist of 12 sheath yarns in tube form. This tubular structure was an essential parameter to consider that the stagnant air protection in the structure might be higher. In this case, the thermal resistivity value of the fabric might increase.

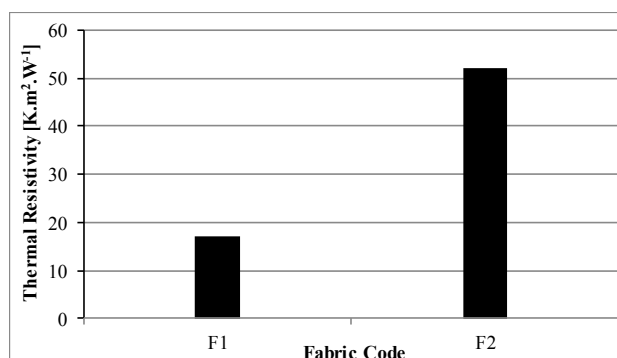


Figure 17. Thermal resistivity values of fabrics

The thermal conductivity of the fabric structure depends on the number of air gaps in the fabric. The ideal insulating material is the stagnant air, and the thermal conductivity of

stagnant air is much lower than that of all fibers. A high amount of air should be present in a textile material's inner structure with high thermal insulation. Bulky materials can hold excess air in them due to their structure [41,42].

The results obtained showed that very high thermal resistivity values could be obtained from compact fabrics woven by using braid yarn structures and appropriate yarn density values. One of the reasons why the thermal resistivity value of the F1 fabric was lower than that of F2 was thought to be due to the fact that the F1 fabric has a more open structure than the F2 fabric, as seen in Figure 3. From the experimental results, it was predicted that the thermal resistivity values of the fabrics could be improved further by creating a more compact fabric structure by weaving at higher weft density values in the fabric structures where thin braid yarns were used.

3.6 Analysis of the abrasion resistance

Evaluation of abrasion resistance of fabrics woven with braid weft yarn was made. Microscopic images of original

(non-abraded) and 30000 times abraded fabric samples (10 times magnified), were presented in Figures 18 and 19. When the fabric surfaces were examined, it was seen that the conventional warp yarns break at 30000 abrasion cycles. No breakage was observed in weft yarns with a braid structure. It could be foreseen that the fabric structures to be woven by using braid yarn structures in both warp and weft could form fabric structures with high abrasion and wear resistance.

4. CONCLUSION

This study evaluated the changes in Poisson's ratio of the fabrics woven with braid weft yarn and the possible auxetic performance properties. Fabrics were woven in plain weave with conventional warp and braid weft yarn. As a result of the experimental study, it was observed that fabrics woven with braid weft yarns exhibited an auxetic behavior by giving Negative Poisson's Ratio (NPR) under warp directional tension. In addition, it was observed that NPR of fabric was affected by the thickness of the braid yarn and the tightness (compactness) of the fabric.

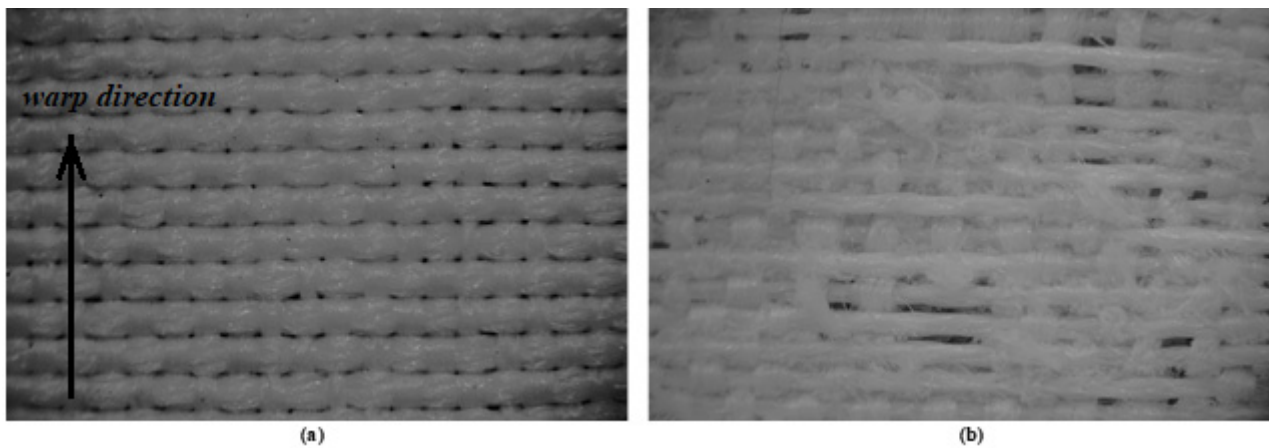


Figure 18. Microscopic images of F1 fabric a) non-abraded b) 30000 abrasion cycles (Mag: 10X)

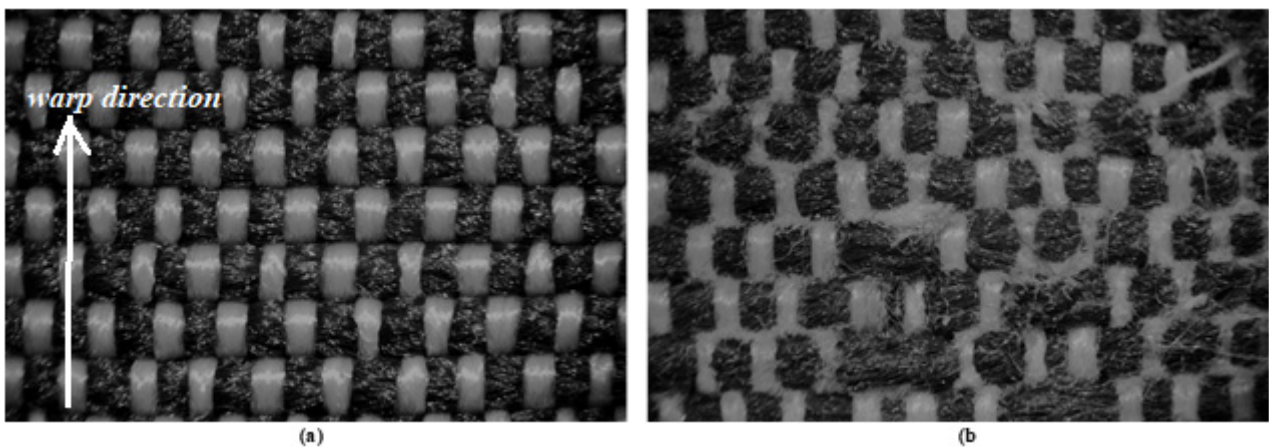


Figure 19. Microscopic images of F2 fabric a) non-abraded b) 30000 abrasion cycles (Mag: 10X)

Braid yarn structure consists of yarn components that make diagonal entrant intersections with each other. Using braid yarns in the formation of woven fabric as a weft, the deformation state of the braid weft yarns that intersect with the conventional warp yarns in the fabric under tension was evaluated. Under the warp-directed tension applied to the fabric, the compression effect of the warp yarns on the braid weft yarns which have an entrant form could cause a transverse expansion effect in the braid weft yarns in the fabric. As a result, it was observed that fabrics with braid weft yarn exhibited an auxetic behavior by giving NPR under warp directional tension.

In addition, it was observed that the fabrics gave higher NPR values because the braid yarn structures, which showed transverse expansion with the effect of compression by the warp yarns, could move more easily in the fabric with a less tight (in a more open) structure. It was observed that a lower NPR could be obtained in a tight fabric structure due to the restriction of the transverse expansion effect of the braid yarns in the fabric structure. It was found that the thickness of braid weft yarn affected the auxetic performance of the fabrics. Also, it was seen that the auxetic performance continued under higher elongation values in the fabric woven with thick braid weft yarn compared to the fabric woven with thin braid weft yarn.

In addition, it was found that the use of braid yarn in woven fabric structures provided an NPR effect to the structure and improved various physical performance properties. It was observed that in fabrics woven with braid weft yarns, the weft directional tensile strength values of the fabrics significantly increased compared to the warp directional

tensile strength values in which conventional warp yarns were used. It was observed that very high thermal resistivity values could be obtained in compact fabric structures woven with thick and bulky braid yarns. When the effect on abrasion resistance was examined, it was seen that there was no break in braid yarns in the abrasion cycles where the breakage occurred in conventional yarns. It could be predicted that the fabrics to be woven by using braid yarns in both warp and weft directions could create fabric structures with high abrasion and wear resistance.

As a result of the experimental study, it could be concluded that braid yarns could be used in the formation of auxetic woven fabric designs and improved various physical performance properties of fabrics.

Acknowledgement

This research has been supported by The Scientific and Technological Research Council of Türkiye (TÜBİTAK): Project No.119M358.

The authors would like to thank Yayteks İplik Mak. Ltd. Şti. (Bursa) for their contribution to the supply of braid yarns.

Note: This paper is an expanded version of a symposium abstract entitled 'Auxetic Performance Analysis of Fabrics Woven with Braid Yarn' presented at 9th International Fiber and Polymer Research Symposium (9th ULPAS), Uşak, Turkey, 19–20 November, 2021.

REFERENCES

1. Uzun M. 2010. Negative Poisson ratio (auxetic) materials and their applications. *The Journal of Textiles and Engineers* 17(77), 13-18.
2. Carneiro VH, Meireles J, Puga H. 2013. Auxetic materials – A Review. *Materials Science-Poland* 31, 561-571.
3. Darja R, Tatjana R, Alenka PC. 2013. Auxetic textiles. *Acta Chim Slov* 60, 715–723.
4. Evans KE, Nkansah MA, Hutchinson IJ, Rogers SC. 1991. Molecular network design. *Nature* 353, 124.
5. Evans KE, Alderson KL. 2000. Auxetic materials: the positive side of being negative. *Engineering Science and Education Journal* 9(4), 148–154.
6. Choi JB, Lakes RS. 1991. Design of a fastener based on negative Poisson's ratio foam. *Cellular Polymers* 10, 205-212.
7. Grima JN, Attard D, Gatt R, Cassar RN. 2009. A Novel process for the manufacture of auxetic foams and for their reconversion to conventional form. *Advanced Engineering Materials* 11(7), 533-535.
8. Evans KE, Alderson A. 2000. Auxetic materials: Functional materials and structures from lateral thinking. *Advanced Materials* 12(9), 617–628.
9. Yang W, Li ZM, Shi W, Xie BH, Yang MB. 2004. Review on auxetic materials. *Journal of Materials Science* 39, 3269–3279.
10. Uzun M. 2012. Mechanical properties of auxetic and conventional polypropylene random short fibre reinforced composites. *Fibres & Textiles in Eastern Europe* 20, 5(94), 70-74.
11. Choi JB, Lakes RS. 1992. Non-linear properties of polymer cellular materials with a negative Poisson's ratio. *Journal of Materials Science* 27, 4678–4684.
12. Liu Y, Hu H, Lam JKC, Liu S. 2010. Negative Poisson's ratio weft-knitted fabrics. *Textile Research Journal* 80(9), 856–863.
13. Shahabi NE, Saharkhiz S, Varkiyani SMH. 2013. Effect of fabric structure and weft density on the Poisson's ratio of worsted fabric. *Journal of Engineered Fibers and Fabrics* 8(2), 63–71.
14. Sun H, Pan N, Postle R. 2005. On the Poisson's ratios of a woven fabric. *Composite Structures* 68(4), 505–510.
15. Shahabi NE, Mousazadegan F, Varkiyani SMH, Saharkhiz S. 2014. Crimp analysis of worsted fabrics in the terms of fabric extension behaviour. *Fibers and Polymers* 15(6), 1211–1220.
16. Ng WS, Hu H. 2018. Woven fabrics made of auxetic plied yarns. *Polymers* 10(2):226, 1-19.
17. Hu H, Wang Z, Liu S. 2011. Development of auxetic fabrics using flat knitting technology. *Textile Research Journal* 81(14), 1493–1502.
18. Uğbolue SC, Kim YK, Warner SB, Fan Q, Yang C, Kyzymchuk O, Feng Y. 2010. The formation and performance of auxetic textiles. Part I: theoretical and technical considerations. *The Journal of The Textile Institute* 101(7), 660–667.
19. Uğbolue SC, Kim YK, Warner SB, Fan Q, Yang C, Kyzymchuk O, Feng Y, Lord J. 2011. The formation and performance of auxetic textiles. Part II: geometry and structural properties. *The Journal of The Textile Institute* 102(5), 424–433.

-
20. Wright JR, Burns MK, James E, Sloan MR, Evans KE. 2012. On the design and characterisation of low-stiffness auxetic yarns and fabrics. *Textile Research Journal* 82(7), 645–654.
 21. Vysanskav M, Vintrova P. 2013. Auxetic woven fabrics - Pores' parameters observation. *Journal of Donghua University* 30(5), 416–420.
 22. Hook PB. 2003. Auxetic mechanisms, structures & materials. Ph.D. Thesis, School of Engineering and Computer Science, University of Exeter, Exeter, UK.
 23. Douglas WA. 1964. *Braiding and braiding machinery*. Eindhoven: Centrex Publishing Company.
 24. Ge Z, Hu H, Liu S. 2016. A novel plied yarn structure with negative Poisson's ratio. *The Journal of The Textile Institute* 107(5), 578-588.
 25. Jiang N, Hu H. 2019. Auxetic Yarn Made with Circular Braiding Technology. *Phys Status Solidi B*, 256, 1-12.
 26. Sloan MR, Wright JR, Evans KE. 2011. The helical auxetic yarn - A novel structure for composites and textiles; Geometry, manufacture and mechanical properties. *Mechanics of Materials*, 43, 476–486.
 27. Ko FK, Pastore CM, Head AA. 1989. *Handbook of industrial braiding*, Covington, KY: Atkins & Pearce.
 28. Karaca Bayraktar, E. 1999. Investigation of effects of monofilament and braid structures of silk, polyamid 6, polyester, polypropylene sutures on some of the mechanical properties. PhD Thesis, Uludag University, Bursa.
 29. Jiang N, Hu H. 2018. A study of tubular braided structure with negative Poisson's ratio behaviour. *Textile Research Journal* 88(24), 2810–2824.
 30. ASTM D1776. 2009. Standard Practice for Conditioning and Testing Textiles.
 31. ISO 13934-1. 2013. Textiles – Tensile properties of fabrics – Part 1: Determination of maximum force and elongation at maximum force using the strip method.
 32. Suvvari F, Akgun M, Eren R, Yurdakul T. 2021. Determination of deformation behavior of woven fabrics under stress using image processing method. *Uludağ University Journal of the Faculty of Engineering* 26(2), 661-678.
 33. ASTM D3776. 2011. Standard Test Methods for Mass per Unit Area (Weight) of Fabric.
 34. ASTM D1777-96. 2007. Test method for thickness of textile materials.
 35. ASTM D3883-04. 2008. Standard test method for yarn crimp and yarn take-up in woven fabrics.
 36. Peirce FT. 1937. The geometry of cloth structure. *The Journal of The Textile Institute*, 28, 45–60.
 37. EN ISO 9237. 1995. Textiles, determination of the permeability of fabrics to air, International Organization for Standardization, Geneva.
 38. Frydrych I, Dziworska G, Bilska J. 2002. Comparative analysis of the thermal insulation properties of fabrics made of natural and man-made cellulose fibres. *Fibres & Textiles in Eastern Europe* October/December, 40-44.
 39. ASTM D 4966-12. 2012. Standard test method for abrasion resistance of textile fabrics.
 40. Akgun M, Eren R, Suvvari F, Yurdakul T. 2021. Investigation of the effect of pique weave on auxetic performance and related fabric properties. *The Journal of The Textile Institute* DOI: 10.1080/00405000.2021.1983978.
 41. Havenith G. 2002. Interaction of clothing and thermoregulation. *Exogenous Dermatology* 1(5), 221-230.
 42. Özdil N, Marmaralı A, Kretschmar S. 2007. Effect of yarn properties on thermal comfort of knitted fabrics. *International Journal of Thermal Sciences* 46(12),1318-1322.



Usage of UV-Curable Soybean Oil Based Coating Formulations for Pretreated Cotton Fabrics

Zehra Yıldız¹  0000-0002-1573-2074

Marmara University, Faculty of Technology, Department of Textile Engineering, RTE Campus, Maltepe/Istanbul/Türkiye

Corresponding Author: Zehra Yıldız, zehra.yildiz@marmara.edu.tr

ABSTRACT

This study aims to design an alternative way for the laminated fabric manufacturing with a cleaner production method, by using a bio-based coating formulation and time/cost saving, environmentally friendly UV-curing technology, compared to the conventional petroleum based, heat and solvent requiring laminating process. For this purpose, acrylated epoxidized soybean oil oligomer was synthesized and included in coating formulations for the application on cotton fabrics via UV-curing. The obtained oligomer was characterized by FTIR and ¹H NMR spectroscopies. In order to enhance the bonding between the fabric and coating layer, fabrics were pretreated by sodium hydroxide, pectinase enzyme, and a commercial washing agent prior to the coating process. The effects of pretreatment methods on the wettability, tensile and peel strength, and abrasion resistance of the fabrics were all examined before/after coating process. Enzyme pretreatment revealed promising results by increasing the surface roughness, fibrillation, and hydrophilicity of the cotton fabrics. After coating and UV-curing process, the highest increment in tensile strength, the highest peel strength, and the least weight loss value against abrasion were all recorded in enzyme pretreated fabric.

ARTICLE HISTORY

Received: 21.05.2021

Accepted: 09.05.2022

KEYWORDS

Soybean oil; cotton fabric; uv-curing; pectinase enzyme; peel test

1. INTRODUCTION

Nowadays the utilization of environmentally friendly, biodegradable, renewable materials in polymer manufacturing systems instead of conventional, petroleum based chemicals, is an important issue for both academicians and industry workers. Among all biodegradable resources, vegetable oils are important due to being universally available, non-volatile, non-toxic, non-depletable, cheap, and abundant. Vegetable oils consist of fatty acids/triglyceride molecules with different chain lengths, and number of double bonds. Fatty acids are the fundamental component of a vegetable oil that determine the chemical and physical properties of the oil. The unsaturation sites of the vegetable oil allow the chemical modification in order to be used as starting material in polymer synthesis. For instance, the major fatty acids of soybean oil are α -linolenic acid and linoleic acid have three and two double bonds on their backbone, enabling synthesis

of different types of polymers, respectively.

Soybean oils are favored due to the being abundant, inherently biodegradable, having low toxicity, and presenting five different unsaturated sites. Epoxidation is the most preferred functionalization reaction of vegetable oils. The oxirane ring of the epoxidized soybean oil (ESBO) allows to the modification of oil with different chemical species, generally by acids, in further reactions. In literature, a number of researches have been made about the chemical modification of ESBO. Acrylated and methacrylated ESBOs have been used for various purposes such as oil-absorbing materials, alkyd modifiers, flame retardant coatings, 3D printing materials, printing inks etc. For instance, ESBO has been modified by methacrylic acid and vinyl phosphonic acid to obtain an organic-inorganic hybrid coating with flame resist property [1]. In another study, ESBO has been used to improve the wettability, biodegradation, and thermal properties of poly(vinyl

To cite this article: Yıldız Z. 2022. Usage of UV-curable soybean oil based coating formulations for pretreated cotton fabrics. *Tekstil ve Konfeksiyon*, 32(3), 232-242.

alcohol) via the ring-opening reaction [2]. Soybean oil based methacrylates have been synthesized from ESBO as an alternative to the fossil-based resins and additives for the usage in stereolithography [3]. In another research, ESBO has been grafted on cellulose aerogels in order to enhance the absorbency and recyclability properties of aerogels for oil-absorbing materials [4]. In order to use the ESBO based oligomers in UV-curable formulations, the epoxide group of ESBO should be reacted by some chemical species containing acrylate/vinyl functional groups such as acrylic acid, methacrylic acid, vinyl phosphonic acid etc.

Among all coating techniques, UV-curing technology is favored due to the formation of the crosslinked structure in just a few seconds resulting a time saving property, and requiring none or less solvent resulting an environmentally friendly manufacturing technique. Additionally, the crosslinking reaction of the coating formulation is performed at low temperatures resulting a cost saving property. The other advantages of UV-curing are high optical clarity, good adherence on various surfaces, high curing rates, high stability at storage, controlled elasticity, and high scratch resistance [5-14]. UV-curable soybean oil based oligomers have been searched for various purposes. For instance, ESBO has been reacted with hydroxyethyl methacrylated maleate in order to obtain UV-curable coating formulations with higher biomaterial content [15]. In order to obtain polymeric films with better thermal stabilities, UV-curable soybean oil based coating formulations have been reported with the reaction of ESBO and acrylic acid (AA), by the inclusion of a trifunctional acrylate monomer (trimethylolpropane trimethacrylate) as crosslinking agent [16]. UV-curable formulations with better coating performances have also been reported by the synthesis of acrylated ESBO and acrylated sucrose oligomers with high biorenewable contents [17]. Due to the excellent pigment wetting property, UV-curable acrylated epoxidized soybean oil (AESBO) formulations have been also used in lithographic printing inks [18]. The usage of UV-curable AESBO oligomers have also been accomplished in phase change materials for thermal energy storage [19], and in crack repair patch system for chemical reservoirs [20]. Whereas according to the literature review, no research has been found about their usage in the manufacturing of laminated cotton fabrics.

Laminated cotton fabrics are defined as multipurpose textile composites that are used as tent fabrics, truck covers, tarpaulin, tablecloths, raincoats, bibs, mats, bags etc. and must be durable against some specific usage conditions such as UV-light, flame, chemicals, water, heat, mold etc. In laminated fabrics, the reinforcing layer is generally a cotton fabric, whereas the matrix layer is made by non-degradable polymers such as polyvinyl chloride (PVC), polyurethane (PU), acrylic, high density polyethylene (HDPE), and ethylene vinyl acetate (EVA) [21, 22]. In a conventional lamination related previous study, acrylic based adhesive formulations have been employed in the lamination of cotton and polypropylene fabrics via knife

coating method. The peel strength of these fabrics have been recorded in the range of 2.1-5.2 N [23]. In another study, polypropylene nonwoven fabrics have been laminated via knife coating method. The peel strength values have been found as 1.12-2.18 N for acrylic based and 4.2-12 N for polyurethane based adhesive formulations, respectively [24]. In order to enhance the performance of finishing and coating processes in textile industry, the hydrophobic impurities on fiber surface such as waxes, pectin, grease, hemicellulose, protein etc., should all be dissipated from the fiber. Therefore, textile surfaces need to be scoured by pretreatment methods in order to enhance the hydrophilicity and dyestuff uptake, to increase the bonding between the fiber/coating layer, and to improve the compatibility between fiber/finishing agent. In this study, an enzymatic washing process with pectinase enzyme, an alkali treatment with concentrated sodium hydroxide (NaOH) solution, and a commercial washing process with standard ECE washing agent were all employed as pretreatment methods. In textile industry, enzymes are used in various purposes such as scouring, bleaching, desizing, polishing, and denim abrading etc. Comparing to the other pretreatment methods, enzymatic washing steps present some superior properties such as being sustainable and eco-friendly, requiring less energy, and giving less deformation to the fiber surface. The alkali treatment on textile materials is used to improve the dye uptake, luster, appearance, dimensional stability, and drape. During the alkali treatment, the concentrated NaOH solution helps to dissolve the impurities such as lignin, hemicellulose, grease, and waxes on the fiber surface, resulting enhancement on absorbency due to the fibrillation. The ECE washing agent is a non-ionic, phosphated, without any optical brightening agent that is used in textile fastness tests by removing the water/detergent soluble impurities from the surface [25-29].

In this study, a light weight, bio-based laminated fabric was designed with a cleaner production method by using cotton fabric as reinforcing layer, AESBO as matrix layer, and UV-curing technology as coating method. For this purpose, ESBO was acrylated by AA then the obtained AESBO oligomers were included in coating formulations. AESBO oligomer was characterized by FTIR and ¹H NMR spectroscopies. In order to enhance the wettability of fabrics and to enhance the bonding mechanism between fabric and resin, cotton fabrics were pretreated by pectinase enzyme, NaOH, and ECE washing agent prior to the coating process. Coating formulations were applied on pretreated cotton fabrics and then cured by UV-light. SEM was employed to observe the effect of pretreatment methods on the fabric surface. Spray and absorbency tests were used to evaluate the wettability character of the fabrics after pretreatment methods. The abrasion and tensile properties of pretreated and coated UV-cured fabrics were investigated. Furthermore, the adhesion strength between the coated UV-cured fabric layers were also examined by means of peel test.

2. MATERIAL AND METHOD

2.1 Material

ESBO (MW=952 g/mole, EEW=232 g/equiv.), acrylic acid (AA), 1,6-hexanediol diacrylate (HDDA, reactive diluent), sodium hydroxide (NaOH), triphenyl phosphine (TPP, catalyst), hydroquinone (HQ, inhibitor) were all purchased from Merck and used as received. 1-hydroxycyclohexyl phenyl ketone (Irgacure® 184, photo initiator) was obtained from Ciba Specialty Chemicals. Non-ionic wetting agent (Uniwett HGA) and pectinase enzyme (Scourzyme L Novozymes) were purchased from Alfa Chemistry. ECE phosphated washing powder without optical brightening agent was purchased from SDL Atlas Co. Cotton fabrics (135 g/m², 42 warp/cm, 30 weft/cm, plain weaved) desized, bleached, ready to dye were supplied from a local manufacturer.

2.2 Oligomer Synthesis

Synthesis of the AESBO was performed in a round-bottom flask, equipped with a nitrogen gas inlet, a condenser, and a magnetic stirrer. Considering the epoxy equivalent weight (EEW) of ESBO (232 g/equiv.), the ESBO:AA molar ratio was set as 1:5. The synthesis of the oligomer can be seen in Scheme 1. First, ESBO and HDDA (30% out of the total ESBO and AA amount) were loaded into the flask. 300 ppm HQ and 1000 ppm TPP were dissolved in AA in a beaker by using an ultrasonic bath. Then the AA solution was added dropwise to the main flask. The reaction was proceeded for 3 h at 100 °C, and for another 3 h at 120 °C until a constant acid value (AV) of 65.12 mg KOH/g was recorded. The epoxide ring opening reaction between the epoxide group of soybean oil and AA was initiated by the nucleophilic attack of the catalyst (TPP) resulting with the formation of phosphonium betaine. A proton of AA was attached to the betaine then an ester bonding was formed by the effect of carboxylate anion on the electrophilic carbon of the phosphorus [30].

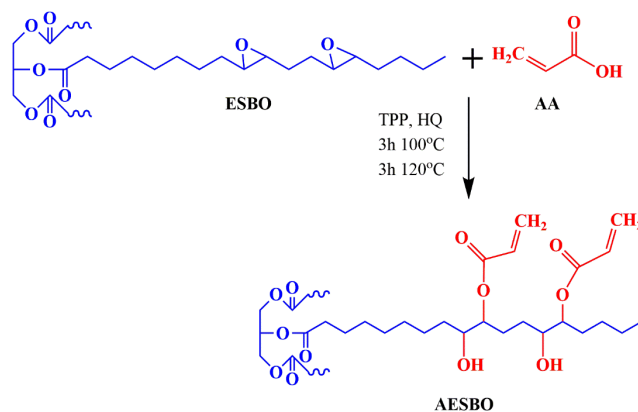
2.3 Surface Pretreatments of Cotton Fabrics

In order to enhance the wettability property of fabrics, and the adhesion between the fabric/coating layer, cotton fabrics were treated by ECE standard washing powder,

concentrated NaOH solution, and pectinase enzyme prior to the UV-coating process. The fabric pre-treatment parameters are set according to our previous study [31] and given in Figure 1. Pectinase enzyme was chosen to decompose the pectinic impurities on cotton fabric. The parameters of ECE and enzymatic washing processes were set according to the manufacturer's commercial formula. Whereas the alkali treatment parameters were adjusted according to the previous studies about giving cotton more hydrophilic property by NaOH [25, 32, 33]. Wetting agent was included to the washing process in order to reduce the surface tension of water and to help spreading of drops on the fiber surface. Distilled water was used for each washing/rinsing processes. Cotton fabrics were cut in 15x20 cm dimensions allowing to perform various testing/analysis. Then fabrics were immersed into the washing bath on a Pyrex glass in 25 cm diameter, equipped with a magnetic stirrer. The pH in pectinase washing media was checked with care as the pH is very effective on the working mechanism of enzymes.

2.4 Application of the Coating Formulation

The conventional laminated fabric manufacturing requires the usage of excessive heat, water, and solvent whereas the coating process in this proposed method is performed at room temperature without the usage of water/excessive solvent. The schematic representation of the coating process can be seen in Figure 2. First, the pre-treated cotton fabrics were dipped into the bath containing the AESBO oligomer and 3 % wt. photo initiator. After 3 min dipping time, the excess resin was dissipated by placing the fabric between two PE films and pressing it with a squeezing roller in 500 g weight by hand. In order to prevent the oxygen inhibition during the UV-curing process, fabrics were put between two glass plates and were exposed to UV-light for 3 min from both sides of the fabric at room temperature. During the UV-curing stage of double layered fabrics, the glass plates also helps to keep the fabric layers tightly together to prevent any slippage. These dip-coating steps were applied on both single and double layered fabrics to perform the targeted tests and analysis. The weight of the cotton fabrics was recorded as around 170 g/m² that means a 25 % weight increment was observed after coating and UV-curing process.



Scheme 1. Synthesis of AESBO oligomer.

ECE Washing	Alkali Washing	Enzymatic Washing
<ul style="list-style-type: none"> • 4 g/L ECE detergent (phosphated, without optical brightening agent) • At 40 °C • For ½ h • Rinsing with water at room temperature. 	<ul style="list-style-type: none"> • 0.2 mL/L wetting agent • 10 g/L NaOH • At 95 °C • For 1 h • At pH 11 • Rinsing with boiling temperature, at 70 °C, and at room temperature. 	<ul style="list-style-type: none"> • 0.2 mL/L wetting agent • 1.8 % wt. pectinase enzyme • At 55 °C • For ½ h • At pH 8.2-8.5 • Rinsing with water at 80 °C

Figure 1. Surface treatment parameters for each pre-treatment method.

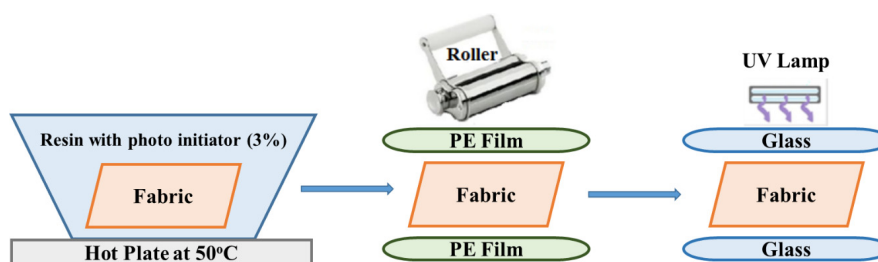


Figure 2. Schematic representation of the fabric coating and UV-curing steps.

2.5 Characterization

During the oligomer synthesis, the depletion of AA and epoxide groups were followed periodically with the help of titration methods according to the ASTM standards by means of AV [34] and EEW [35] measurements. The Fourier transform infrared (FTIR) spectra was recorded with a Perkin Elmer Spectrum-100 ATR FTIR spectrophotometer. The proton nuclear magnetic resonance (^1H NMR) spectra of the oligomer was obtained on Bruker AMX 500 MHz NMR instrument, in the solvent of dimethyl sulfoxide (DMSO) by using the internal reference of the tetramethylsilane (TMS). Physicochemical properties of the UV-cured free films were investigated in terms of degree of swelling (DS), gel fraction (GF), and weight loss against chemical reagents, respectively. All these tests were performed by dipping the free film particle into the solvent/solution at room temperature for one week. Toluene, ethanol, distilled water, and THF were all used as solvents for the DS and GF tests, respectively [36]. In order to measure the weight loss with chemical exposure, 10% hydrochloric acid (HCl), and 10% sodium hydroxide (NaOH) solutions were employed [37]. The morphological properties of fabrics after each surface treatments were investigated by using scanning electron microscopy (SEM, ZEISS® EVO MA 10 model). The wettability property of the pretreated cotton fabrics before and after coating process were evaluated by the absorbency test [36] based on the disappearance time of a water droplet on the surface that is recorded by a chronometer according to the AATCC-79 standard and the spray test [39] using a spray testing instrument with 45° slope according to the AATCC-22 standard. Tensile testing and peel test were both performed by using Instron 4411 tensile testing machine. In tensile test, the tensile strength and elongation values of pretreated

fabrics with and without coating layer were measured [40]. The peel test [41] was used to investigate the adhesion property between the fabric and coating layer from the double-layered coated fabrics. The abrasion test was applied on pretreated fabrics with [42] and without [43] coating layer by using a Martindale pilling and abrasion instrument.

3. RESULTS AND DISCUSSION

3.1 Characterization of the Oligomer

The aim of this study was to design a bio-based laminated fabric by using UV-curable coating formulations with an enhanced adhesion strength between the matrix and reinforcing layers. For this purpose, ESBO was modified with AA in order to obtain UV-sensitive functional groups in the oligomer structure. During the oligomer synthesis, the depletion of AA and epoxide groups was followed by titration methods, and given as AV and EEW. The obtained AESBO oligomer was also characterized by FTIR and ^1H NMR spectroscopies. EEW gives the weight of resin in grams which contains a 1 g equivalent of an epoxy group, whereas the AV illustrates the potassium hydroxide amount in milligram requiring to neutralize a 1 g of the oligomer [44]. The changes in AV and EEW during the reaction can be observed in Figure 3. Accordingly, the AV was gradually decreased due to the esterification reaction whereas the epoxide groups of soybean oil were depleted by the AA via epoxide ring opening mechanism. The reaction was ended after 6 h when a constant AV and EEW results were observed. As the epoxide concentration decreases EEW value increases. Thus, the highest EEW value and the least AV were recorded as 1,055 g/equiv. and 65 mg KOH/g, respectively.

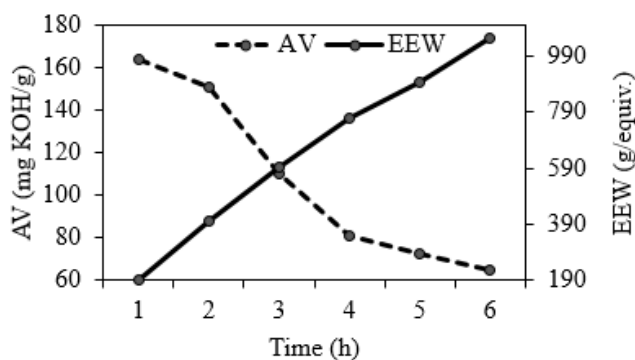


Figure 3. Changes in AV and EEW during the reaction.

The FTIR spectra of ESBO and AESBO oligomers were shown in Figure 4. The peak at 1744 cm^{-1} belongs to the carbonyl group of soybean oil. The C-H asymmetric stretching vibration peaks in $-\text{CH}_2-$ and $-\text{CH}_3$ groups were observed at 2924 cm^{-1} and 2854 cm^{-1} , respectively. In the spectra of ESBO, the C-O-C asymmetric stretching vibration peaks at 823 cm^{-1} and 1155 cm^{-1} were attributed to the existence of epoxide group. These peaks were both disappeared after the reaction with AA. The newly formed

peaks at 1619 cm^{-1} and 1636 cm^{-1} in AESBO spectra confirmed the existence of acrylate functionality with C=C double bond stretching vibration and C=O vibration. Additionally, the hydroxyl peak at 3474 cm^{-1} and C-H bending vibration peak at 809 cm^{-1} also support the epoxide ring opening reaction [45].

The reaction between the AA and epoxide groups of soybean oil can be confirmed by the ^1H NMR spectra. Figure 5 illustrates the ^1H NMR spectra of the AESBO oligomer with the assignation of the proton peaks. Accordingly, the peaks at 5.6-6.5 ppm region belong to the C=C structure of the acrylate functionality. The peaks at 1.1-1.4 ppm region are the protons of saturated triglyceryl backbone. The methylene protons of adjacent epoxy groups were observed at 1.4-1.7 ppm region. The characteristic methane and methylene proton peaks of the triglyceride backbone were appeared at 4.1-4.4 ppm and 5.1-5.3 ppm regions, respectively. The peak at 2.4 ppm is due to the protons in allylic positions. The methylene protons of the epoxide peaks at 3.6-3.8 ppm and the hydroxyl group proton peaks at 4.9-5.0 ppm regions confirm the epoxide ring opening reaction [15, 46].

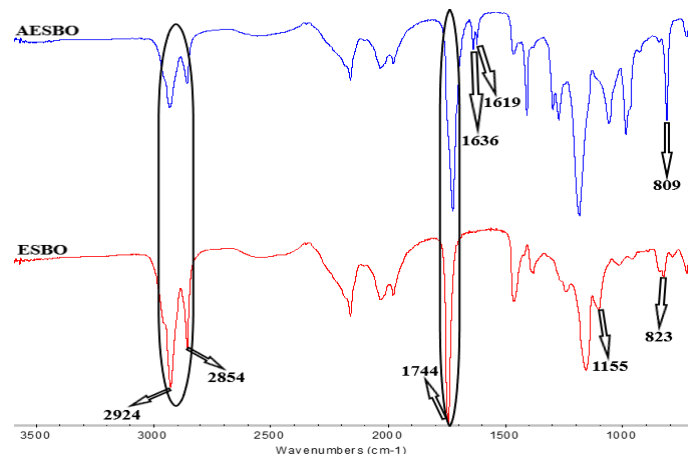


Figure 4. FTIR spectra of ESBO and AESBO oligomers.

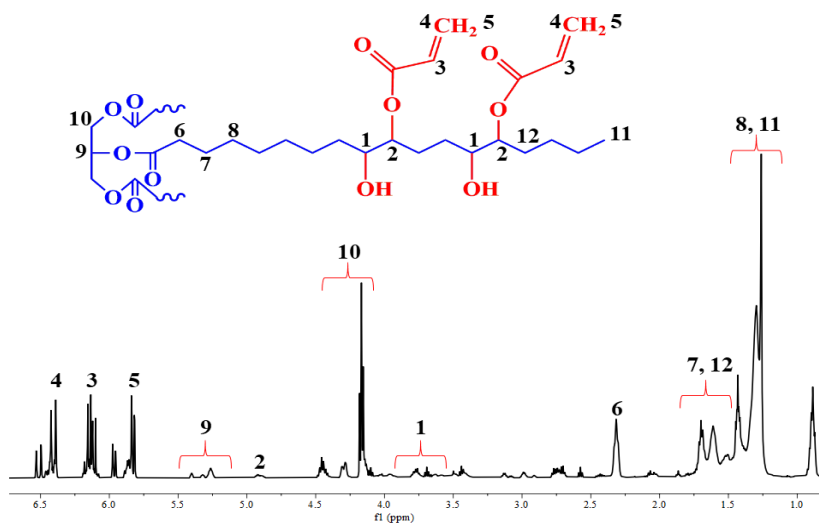


Figure 5. ^1H NMR spectra of AESBO oligomer.

3.2 Physicochemical Properties

The DS (%), GF (%), and weight loss (%) with chemical exposure values of the UV-cured free films and laminated fabrics in terms of each pretreatment method were all given in Table 1. The crosslinking density of polymeric structures is the key factor determining the physicochemical properties. The DS (%) and chemical resistance weight loss (%) values decrease with increasing crosslinking density. Whereas higher crosslinking densities are attributed to the higher GF (%) values. Accordingly, the GF values of raw fabric and fabrics with each treatment method were recorded as 100. This result can be explained by the lack of any extractable impurity on cotton fabric surfaces. Due to the highly cross-linked structure the highest GF value of 98.88% was recorded in UV-cured free film. The GF value of the UV-cured oligomer was slightly decreased after the application on fabric surfaces. Considering the treatment methods, the GF values were found in the following order: enzyme > ECE > NaOH. A remarkable decrease in GF value of coated raw fabric was observed. That may be incompatibility between the raw fabric and coating layer. After the surface treatment methods, a better cross-linked oligomer structure can be occurred between the fabric and coating layer thus the GF values were increased.

In order to observe the swelling properties of the samples ethanol, water, and toluene were chosen as solvents since they are not reactive at room temperature and may have only weak physical interactions with the sample. The swelling property is mainly related to the affinity between the sample and solvent, and the polarity of the solvent. Water and ethanol are strongly polar solvents whereas toluene shows slightly polarity [47]. Accordingly, due to the affinity between the hydroxyl groups of cotton fabric and polar solvents, the DS values were found as follows: water > ethanol > toluene in fabrics without coating layer. After the application of the coating layer, the DS values for each solvent by means of the treatment method were found in the following order: NaOH > ECE > enzyme. Considering the coated fabrics, the highest swelling values were observed in coated raw fabric due to the existence of impurities on fiber surface that inhibit a complete adherence of coating layer to the fiber surface.

The weight loss values of the UV-cured free film and coated fabrics in NaOH (10%) solution is greater than in HCl (10%) solution. This result can be expressed by the basic hydrolysis of the ester groups in the oligomer which is initiated by the attack of the hydroxyl ion on the carbonyl carbon resulting the formation of tetrahedral intermediate that collapses immediately and gives the sodium carboxylate salt in NaOH solution. Whereas the ester groups are more stable in HCl solution and only partially protonated because the acidic hydrolysis is reversible like esterification reaction and does not go to completion. Considering the fabrics without coating layer, the weight loss value in HCl solution is greater than in NaOH solution. This result can be supported by the durability of glycoside bonds of cellulose in alkaline environment. The hydrolysis of cellulose is occurred via the cleavage of glycoside bonds in the presence of acids. After the application of coating layer, the weight loss values for both chemical solution were recorded as follows: NaOH > ECE > enzyme [48-50]. Considering the overall physicochemical results, due to the highest fibrillation and scouring performance of enzyme treated fabric, the coating layer was adhered best to this sample. Thus the least DS and chemical resistance weight loss values with the highest GF value were all obtained in that sample.

3.3 SEM Images

The surface morphology of the pre-treated fabric samples without coating layer was observed by means of SEM. Figure 6 shows the SEM images of raw fabric and fabrics with each pre-treatment methods in various magnifications. Accordingly, a smooth and uniform fibrillar orientation was observed in the SEM images of raw fabric. The uniformity of the fibrillar orientation was partially destroyed by the pre-treatment methods. The fibrillation can be best observed in the SEM image of enzyme treated fabric in 600 magnification. Fibrils became apart from each other that means much more surface area was created allowing to the more resin penetration. Besides the fibrillation phenomenon, fibers gained a rougher look after pre-treatment methods due to the dissipation of the impurities via the abrasive/cleaning effects of NaOH solution, ECE detergent, and pectinase enzyme.

Table 1. Physicochemical properties of UV-cured free film and fabrics with each treatment method with/without coating layer.

Samples	DS (%)			GF (%)	Chemical resistance weight loss (%)	
	Toluene	Ethanol	Water		NaOH (10%)	HCl (10%)
UV-cured free film	6.47	11.93	16.21	98.88	14.42	4.92
Raw fabric	0	1.79	15.28	100	3.02	5.93
Coated raw fabric	3.92	4.03	4.39	89.91	12.28	1.92
NaOH treated fabric	0	2.13	19.35	100	1.79	4.18
Coated, NaOH treated fabric	2.16	2.54	3.78	94.59	11.06	1.21
ECE treated fabric	0	2.86	27.27	100	1.65	4.24
Coated, ECE treated fabric	1.43	2.01	3.01	98.27	10.52	0.46
Enzyme treated fabric	0	4.17	30.77	100	0.33	2.49
Coated, enzyme treated fabric	1.16	1.32	2.74	98.32	8.73	0.31

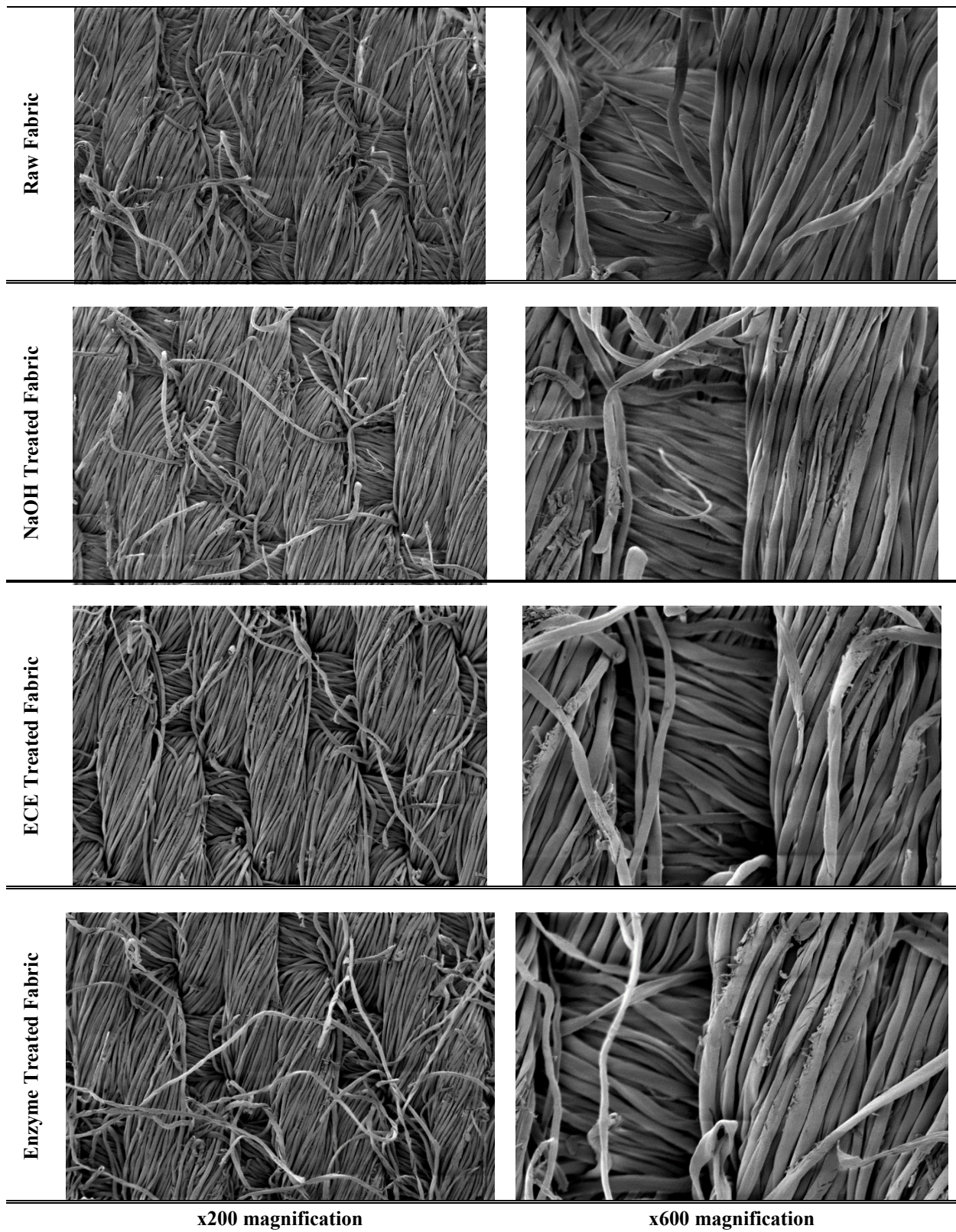


Figure 6. SEM images of raw fabric and fabrics after pre-treatment methods.

3.4 Wettability Properties

The wettability properties of fabrics for each pretreatment method before and after coating process were investigated by means of absorbency test and spray test according to the AATCC-79 [38] and AATCC-22 [39] standards,

respectively. The absorbency test value illustrates the disappearance time of a water droplet on the fabric surface that is measured by a chronometer. In the spray test, the specimen was placed with a 45o slope on a spray testing instrument and was wetted by a certain amount of distilled

water in a certain time period. The evaluation is made by comparing the wetted surface with the standard images. Results are given in the range of 0-100. Zero refers to a highly hydrophilic behavior whereas 100 means no wetting observed on the surface. Figure 7 shows the spray and absorbency test results of raw fabric and fabrics after the application of pretreatment methods without the coating layer. The spray test result of raw fabric was recorded as 50 that means the specimen was only wetted through the spray points. After pre-treatment processes, the spray test results were recorded as 40 (NaOH treated), 20 (ECE treated), and 0 (enzyme treated), respectively. This result proves the enhancement in wettability character of fabrics via pre-treatment methods. The enhancement in hydrophilicity was mainly based on the increased fibrillation with a more surface area for the connection of water molecules with fiber surface. The spray test results of fabrics after coating and UV-curing process were recorded as 100 for each sample due to the highly hydrophobic nature of the surface. Considering the absorbency test, the disappearance time of water droplet on the fabric surface decreased after the application of pre-treatment methods due to the fibrillation. The absorbency test results were found as 28 s (raw fabric), 7 s (NaOH treated), 5 s (ECE treated), and 3 s (enzyme treated). The spray and absorbency tests showed both consistent results supporting that the best hydrophilic nature was found in the enzyme treated fabric sample. The absorbency test was also applied on fabrics after coating and UV-curing process. The water droplet stayed more than 24 hours on the surface for each sample indicating that a hydrophobic character was observed due to the presence of the coating layer on the fabric surface.

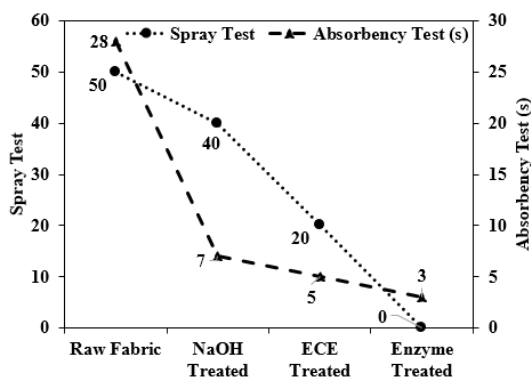


Figure 7. Wettability test results of raw fabric and fabrics after pre-treatment methods.

3.5 Tensile and Peel Test

The tensile and peel strength values of fabrics before and after coating process with each pre-treatment method were

Table 2. The tensile and peel strength values of fabrics before coating and after single/double-layered coating processes.

	Raw fabric	NaOH treated	ECE treated	Enzyme treated	
Tensile strength (N)	827	514	756	790	Uncoated
	862	617	988	1102	Single-layered coated
Peel strength (N)	17.6	18.3	19.9	23.6	Double-layered coated

all shown in Table 2, and the image of enzyme treated double-layered coated UV-cured fabric sample after peel test was illustrated in Figure 8. The tensile strength values of fabrics without coating layer were all decreased for each pre-treatment method due to the dissipation of the impurities with the cleaning and etching effects of the detergent, NaOH solution, and pectinase enzyme [51]. The highest tensile strength loss was observed in alkali pre-treated fabric. This result is stemming from the abrasive effect of alkaline media via the removal of the hemicelluloses and other non-cellulosic impurities [52]. In order to see the effect of coating layer to the tensile strength raw fabric and pre-treated fabrics were coated as single-layered. Accordingly, the coating layer helped to increase the tensile strength for each sample. The increment in tensile strength was recorded in the following order: enzyme>ECE>NaOH. Due to the best fibrillation performance of enzyme treatment, the coating layer was well penetrated on the fiber surface thus the highest tensile strength value of 1102 N was recorded in the enzyme treated fabric. For some specific applications, laminated fabrics were manufactured as double-layered for the enhanced tensile properties and durability. In order to investigate the adhesion property in double-layered laminated samples, peel test was employed. The peel strength values were all increased after the application of pre-treatment methods due to the fibrillation and increment in surface roughness that strengthens the adhesion forces between the fiber and the coating layer. The highest peel strength value of 23.6 N was recorded in the enzyme treated double-layered coated UV-cured fabric due to the highest fibrillation performance of enzyme treatment resulting a better coating formulation absorbance by the fibers. As can be seen in Figure 8, the peeling was observed between the fabric layers without any deterioration on the fabric surface/shape. The schematic representation of the bonding mechanism between the fabric and the coating layer can be observed in Figure 9.



Figure 8. Image of the enzyme treated double-layered coated UV-cured fabric sample after peel test.

3.6 Abrasion Test

The abrasion resistance values of raw fabric and fabrics with each pre-treatment methods, with and without coating layer were all given in Table 3. The used abrasive surface changes with regard to the fabric surface property, that means if there is no polymeric coating layer on the fabric surface the abrasive material should be a 100% wool fabric. Whereas if the fabric was coated by a polymeric material the abrasive surface should be a sandpaper. In order to perform the abrasion resistance test, fabrics were cut in 5 cm diameter and allowed to be abraded by a standard wool fabric for fabrics without coating layer [43], and by a sandpaper for fabrics with coating layer [42]. In the abrasion resistance test of fabrics without coating layer, the test was ended when a yarn break is observed in both warp and weft directions and results were given in terms of "cycle". Whereas the weight loss after 100 cycle abrasion was recorded in abrasion resistance test of fabrics with coating layer and results were given as weight loss percentage. Accordingly, the abrasion resistance of raw fabric was recorded as 49,000 cycle. After the application of pre-treatments, the abrasion resistance values were all decreased and recorded as 45,000 cycle (NaOH treated), 43,000 cycle (ECE treated), and 38,000 cycle (enzyme treated), respectively. This result can be explained by the

increment in fibrillation and surface roughness on the fabric surface. The abrasion resistivity of smooth surfaces is greater than the rough surfaces [53]. After coating process, the raw fabric showed a 6.05 % weight loss against abrasion. When the fabrics were pre-treated prior to the coating process, the weight loss percentages against abrasion were all decreased. Due to the increment in surface area via fibrillation and enhancement in surface roughness, a better penetration and adherence of the coating layer were all accomplished [54]. Thus a better bonding occurred between the fiber and the coating layer. The least weight loss value against abrasion was recorded as 2.81 % in enzyme treated fabric sample.

The possible bonding mechanism of double layered cotton fabric can be observed in Figure 9. The hydroxyl groups are responsible for the bonding mechanism which exist inherently on cotton fabric and occur in AESBO oligomer via ring opening reaction. Besides, the hydroxyl groups in AESBO oligomer give polarity to the coating layer resulting a better wettability character which helps to adhere cotton fabric [54, 55]. Accordingly, strong hydrogen bonding is formed between the hydroxyl groups of cotton fabric; carbonyl groups of acrylate, carbonyl groups of triglycerides, and hydroxyl groups of AESBO oligomer.

Table 3. Abrasion resistance results of the fabrics before/after coating process.

Abrasion resistance	Raw fabric	NaOH treated	ECE treated	Enzyme treated	
Cycle	49,000	45,000	43,000	38,000	Uncoated
Weight loss (%)	6.05	5.54	3.77	2.81	Coated

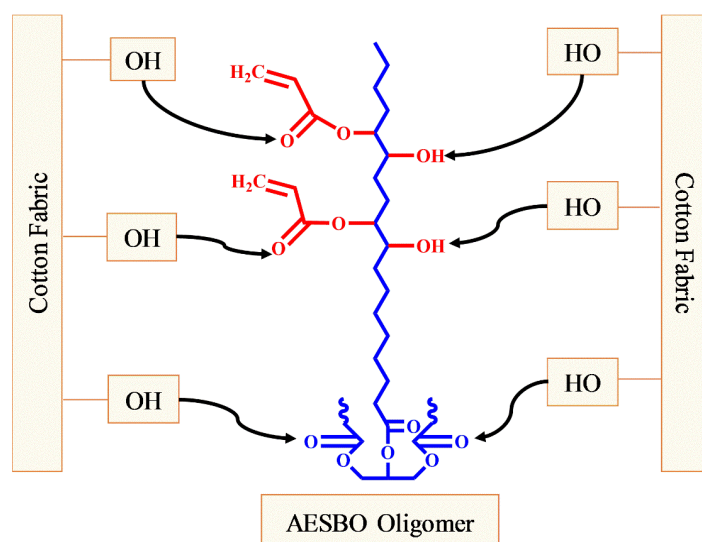


Figure 9. The bonding mechanism between the cotton fabric and the coating layer.

4. CONCLUSION

The manufacturing of a bio-based laminated fabric via environmentally friendly UV-curing technology was aimed by using cotton fabric and soybean oil based oligomer. ESBO was reacted with AA in order to obtain the UV-curable AESBO oligomer. FTIR and ¹H NMR spectroscopies prove the existence of acrylate groups on soybean oil structure and the newly formed hydroxyl groups via ring opening reaction. Cotton fabrics were pretreated by NaOH solution, ECE detergent, and pectinase enzyme prior to the coating process to obtain a better bonding between the fabric and the coating layer by supplying roughness, fibrillation, and hydrophilic character to the fabric.

Among all pretreatment methods, enzyme pretreatment showed the best performance by increasing the surface roughness, fibrillation, and hydrophilicity of the cotton fabrics. This result was supported by the spray, absorbency, swelling, gel fraction tests, weight loss measurement against chemical exposure, and SEM images. The spray and absorbency test results of coated UV-cured fabrics were found as 100 and >24 hours, respectively. These results

indicate a hydrophobic character was obtained after the application of the coating layer. The coated UV-cured fabrics were also examined in terms of tensile, peel, and abrasion properties. According to the overall results, the highest increment in tensile strength, the highest peel strength, and the least weight loss value against abrasion were all recorded in enzyme pretreated fabric. As mentioned in Introduction section, in conventional acrylic based lamination related studies, the peel strength values have been found in the ranges of 1.12-12 N. In the present study, a remarkable enhancement was achieved in enzyme treated double layered fabric sample with a peel strength value of 23.6 N. In summary, bio-based, hydrophobic, laminated UV-cured cotton fabrics with enhanced tensile properties were designed with a cleaner manufacturing route compared to the conventional laminating industry. Future studies are in the way of coloration, and giving flame resistance and thermal insulating properties to the proposed laminated fabrics.

Acknowledgement

This research received no specific grant from any funding agency in the public, commercial, or not-for-profit sectors.

REFERENCES

1. Baştürk, E., İnan, T. and Güngör, A. 2013. Flame retardant UV-curable acrylated epoxidized soybean oil based organic-inorganic hybrid coating *Progress in Organic Coatings*, vol. 76, no. 6, pp. 985-992.
2. Acik, G. 2019. Soybean oil modified bio-based poly (vinyl alcohol) s via ring-opening polymerization *Journal of Polymers and the Environment*, vol. 27, no. 11, pp. 2618-2623.
3. Guit, J. et al. 2020. Photopolymer resins with biobased methacrylates based on soybean oil for stereolithography *ACS Applied Polymer Materials*, vol. 2, no. 2, pp. 949-957.
4. Xu, X. et al. 2019. Preparation and characterization of cellulose grafted with epoxidized soybean oil aerogels for oil-absorbing materials *Journal of agricultural and food chemistry*, vol. 67, no. 2, pp. 637-643.
5. Moon, J., Shul, Y. G., Han, H., Hong, S., Choi, Y. and Kim, H. 2005. A study on UV-curable adhesives for optical pick-up: I. Photo-initiator effects *International journal of adhesion and adhesives*, vol. 25, no. 4, pp. 301-312.
6. Hwang, J. S., Kim, M. H., Seo, D. S., Won, J. W. and Moon, D. K. 2009. Effects of soft segment mixtures with different molecular weight on the properties and reliability of UV curable adhesives for electrodes protection of plasma display panel (PDP) *Microelectronics Reliability*, vol. 49, no. 5, pp. 517-522.
7. Giessmann, A. 2012. *Coating substrates and textiles: a practical guide to coating and laminating technologies*. Dormagen, Germany: Springer Science & Business Media.
8. Schnabel, W. 2007. *Polymers and light: fundamentals and technical applications*. Berlin, Germany: John Wiley & Sons.
9. Bajpai, M., Shukla, V. and Kumar, A. 2002. Film performance and UV curing of epoxy acrylate resins *Progress in Organic Coatings*, vol. 44, no. 4, pp. 271-278.
10. Sung, S. and Kim, D. S. 2013. UV - curing and mechanical properties of polyester-acrylate nanocomposites films with silane - modified antimony doped tin oxide nanoparticles *Journal of applied polymer science*, vol. 129, no. 3, pp. 1340-1344.
11. Habib, F. and Bajpai, M. 2010. UV Curable heat resistance Epoxy Acrylate Coatings *Journal of Chemistry & Chemical Technology*, vol. 4, no. 3, pp. 205-216.
12. Eksik, O., Tasdelen, M. A., Erciyes, A. T. and Yagci, Y. 2010. In situ synthesis of oil-based polymer/silver nanocomposites by photoinduced electron transfer and free radical polymerization processes *Composite Interfaces*, vol. 17, no. 4, pp. 357-369.
13. Xie, J., Zhang, N., Guers, M. and Varadan, V. K. 2002. Ultraviolet-curable polymers with chemically bonded carbon nanotubes for microelectromechanical system applications *Smart materials and structures*, vol. 11, no. 4, p. 575.
14. Bayramoğlu, G., Kahraman, M. V., Kayaman-Apohan, N. and Güngör, A. 2006. Synthesis and characterization of UV-curable dual hybrid oligomers based on epoxy acrylate containing pendant alkoxy silane groups *Progress in Organic Coatings*, vol. 57, no. 1, pp. 50-55.
15. Wu, Q. et al. 2018. High-performance soybean-oil-based epoxy acrylate resins: "green" synthesis and application in uv-curable coatings *ACS Sustainable Chemistry & Engineering*, vol. 6, no. 7, pp. 8340-8349.
16. Habib, F. and Bajpai, M. 2011. Synthesis and characterization of acrylated epoxidized soybean oil for UV cured coatings *Chemistry & Chemical Technology*, vol. 5, no. 3, pp. 317-326.
17. Chen, Z., Wu, J. F., Fernando, S. and Jagodzinski, K. 2011. Soy-based, high biorenewable content UV curable coatings *Progress in Organic Coatings*, vol. 71, no. 1, pp. 98-109.
18. Bajpai, M., Shukla, V., Singh, D., Singh, M. and Shukla, R. 2004. A study of the film properties of pigmented UV - curable epoxidised soybean oil *Pigment & resin technology*, vol. 33, no. 3, pp. 160-164.
19. Baştürk, E. and Kahraman, M. V. 2016. Photocrosslinked biobased phase change material for thermal energy storage *Journal of Applied Polymer Science*, vol. 133, no. 32, pp.1-8.
20. Lee, T. H., Park, Y. I., Lee, S. H., Shin, J., Noh, S. M. and Kim, J. C. 2019. A crack repair patch based on acrylated epoxidized soybean oil *Applied Surface Science*, vol. 476, pp. 276-282.

21. Salim, T. A. et al. 2018. Investigation on the Influence of Non-Degradable Polyvinyl Tarpaulin in Concrete Mixture *Sustainable Construction and Building Technology*, pp. 71-82.
22. Aliverdipour, N., Ezazshahabi, N. and Mousazadegan, F. 2020. Characterization of the effect of fabric's tensile behavior and sharp object properties on the resistance against penetration *Forensic science international*, vol. 306, p. 110097.
23. Armağan, O. G., Karagüzel Kayaoğlu, B., & Canbaz Karakaş, H. 2013. Plasma-induced adhesion improvement of cotton/polypropylene-laminated fabrics *Journal of adhesion science and technology*, vol. 27, no. 21, pp. 2326-2339.
24. Armağan, O. G., Kayaoglu, B. K., Karakas, H. C., & Guner, F. S. 2014. Adhesion strength behaviour of plasma pre-treated and laminated polypropylene nonwoven fabrics using acrylic and polyurethane-based adhesives *Journal of Industrial Textiles*, vol. 43 no.3, pp. 396-414.
25. Ozgen, H. 2018. Enzymatic Hydrophilization of Cotton Knitted Fabrics with Various Methods (Master's Thesis). Available from National Thesis Centre. (516567 Accession number)
26. Stanescu, M. D., Dochia, M., Radu, D. and Sirghie, C. 2010. Green solution for cotton scouring *Fibres & Textiles in Eastern Europe*, vol. 18, no. 3, p. 80.
27. Silverstein, R. A., Chen, Y., Sharma-Shivappa, R. R., Boyette, M. D. and Osborne, J. 2007. A comparison of chemical pretreatment methods for improving saccharification of cotton stalks *Bioresource technology*, vol. 98, no. 16, pp. 3000-3011.
28. Öztürk, H. B. and Bechtold, T. 2007. Effect of NaOH treatment on the interfibrillar swelling and dyeing properties of lyocell (TENCEL) fibres *Fibres & Textiles in Eastern Europe*, vol. 15, no. 5-6, pp. 64-65.
29. Öztürk, H. B. et al. 2009. Changes in the intra-and inter-fibrillar structure of lyocell (TENCEL®) fibers caused by NaOH treatment *Cellulose*, vol. 16, no. 1, p. 37.
30. Su, Y. C., Cheng, L. P., Cheng, K. C. and Don, T. M. 2012. Synthesis and characterization of UV-and thermo-curable difunctional epoxyacrylates *Materials Chemistry and Physics*, vol. 132, no. 2-3, pp. 540-549.
31. Yıldız, Z., Onen, H. A., Dehmen, O. G. and Gungor, A. 2021. Usage of Cellulose Acetate Butyrate Based Oligomeric Structures on Cotton Fabric Coatings *JOTCSA*, vol. 8, no. 1, pp. 305-312.
32. Li, L., Fan, T., Hu, R., Liu, Y. and Lu, M. 2017. Surface micro-dissolution process for embedding carbon nanotubes on cotton fabric as a conductive textile *Cellulose*, vol. 24, no. 2, pp. 1121-1128.
33. Yazdanshenas, M. E. and Shateri-Khalilabad, M. 2013. In situ synthesis of silver nanoparticles on alkali-treated cotton fabrics *Journal of industrial textiles*, vol. 42, no. 4, pp. 459-474.
34. ASTM D974-14e2, Standard Test Method for Acid and Base Number by Color-Indicator Titration, ASTM International, West Conshohocken, PA, 2014, www.astm.org.
35. ASTM D1652-11(2019), Standard Test Method for Epoxy Content of Epoxy Resins, ASTM International, West Conshohocken, PA, 2019, www.astm.org.
36. Bhusari, G. S., Umare, S. S. and Chandure, A. S. 2015. Effects of NCO: OH ratio and HEMA on the physicochemical properties of photocurable poly (ester-urethane) methacrylates *Journal of Coatings Technology and Research*, vol. 12, no. 3, pp. 571-585.
37. ASTM D543-20, Standard Practices for Evaluating the Resistance of Plastics to Chemical Reagents, ASTM International, West Conshohocken, PA, 2020, www.astm.org.
38. AATCC Test Method 79-2018: Absorbency of Bleached Textiles," ed, 2018.
39. AATCC Test Method 22-2005: Water Repellency: Spray Test," ed, 2005.
40. ISO 13934-1:2013 Textiles — Tensile properties of fabrics — Part 1: Determination of maximum force and elongation at maximum force using the strip method.
41. ASTM D1876-08(2015)e1, Standard Test Method for Peel Resistance of Adhesives (T-Peel Test), ASTM International, West Conshohocken, PA, 2015, www.astm.org.
42. ISO 5470-2:2003 Rubber- or plastics-coated fabrics — Determination of abrasion resistance — Part 2: Martindale abrader.
43. ISO 12947-2:2016 Textiles — Determination of the abrasion resistance of fabrics by the Martindale method — Part 2: Determination of specimen breakdown.
44. Sandler, S. R., Karo, W., Bonesteel, J. and Pearce, E. M. 1998. *Polymer synthesis and characterization: A laboratory manual*. Pennsylvania, USA: Elsevier.
45. Li, C., Xiao, H., Wang, X. and Zhao, T. 2018. Development of green waterborne UV-curable vegetable oil-based urethane acrylate pigment prints adhesive: Preparation and application *Journal of Cleaner Production*, vol. 180, pp. 272-279.
46. Uysal, N., Acik, G. and Tasdelen, M. A. 2017. Soybean oil based thermoset networks via photoinduced CuAAC click chemistry *Polymer International*, vol. 66, no. 7, pp. 999-1004.
47. Rianjanu, A., Hidayat, S., Julian, T., Suyono, E., Kusumaatmaja, A. and Triyana, K. 2020. Swelling behavior in solvent vapor sensing based on Quartz Crystal Microbalance (QCM) Coated Polyacrylonitrile (PAN) nanofiber in *IOP Conf. Ser. Mater. Sci. Eng*, 2018, vol. 367, p. 01.
48. Al-Shamary, M. N., Al-Lohedan, H. A., Rafiquee, M., El-Ablack, F. and Issa, Z. A. 2017. Micellar effect upon the rate of alkaline hydrolysis of carboxylic and carbonate esters *Journal of Saudi Chemical Society*, vol. 21, pp. S193-S201.
49. Yıldız, Z., Onen, H. A., Gungor, A., Wang, Y. and Jacob, K. 2018. Effects of NCO/OH ratio and reactive diluent type on the adhesion strength of polyurethane methacrylates for cord/rubber composites *Polymer-Plastics Technology and Engineering*, vol. 57, no. 10, pp. 935-944.
50. Maciel, M. M. A. D., Carvalho Benini, K. C. C., Voorwald, H. J. C. and Cioffi, M. O. H. 2019. Obtainment and characterization of nanocellulose from an unwoven industrial textile cotton waste: Effect of acid hydrolysis conditions *International journal of biological macromolecules*, vol. 126, pp. 496-506.
51. Cheng, Y. et al. 2019. A novel strategy for fabricating robust superhydrophobic fabrics by environmentally-friendly enzyme etching *Chemical Engineering Journal*, vol. 355, pp. 290-298.
52. Ivanovska, A., Cerovic, D., Maletic, S., Castvan, I. J., Asanovic, K. and Kostic, M. 2019. Influence of the alkali treatment on the sorption and dielectric properties of woven jute fabric *Cellulose*, vol. 26, no. 8, pp. 5133-5146.
53. Akgun, M., Becerir, B. and Alpay, H. R. 2018. Investigation of the relation between surface roughness and friction properties of polyester fabrics after abrasion *The Journal of the Textile Institute*, vol. 109, no. 3, pp. 322-337.
54. Tan, C., Chan, Y., Chan, H., Leung, N. and So, C. 2004. Investigation on bondability and reliability of UV-curable adhesive joints for stable mechanical properties in photonic device packaging *Microelectronics Reliability*, vol. 44, no. 5, pp. 823-831.
55. Park, Y. J., Lim, D. H., Kim, H. J., Park, D. S. and Sung, I. K. 2009. UV-and thermal-curing behaviors of dual-curable adhesives based on epoxy acrylate oligomers *International Journal of Adhesion and Adhesives*, vol. 29, no. 7, pp. 710-717.



An Investigation of Sensorial Comfort in Woven Women's Blouses

Ebru Akgün¹  0000-0003-4910-8373

Esen Çoruh²  0000-0002-6249-374X

¹Garment Technologist/ İstanbul/ Türkiye

²Ankara Hacı Bayram Veli University/ Faculty of Art and Design/ Department of Fashion Design/ Ankara/ Türkiye

Corresponding Author: Esen Çoruh, esen.coruh@hbv.edu.tr

ABSTRACT

The aim of this research was to investigate woven women's blouses in terms of sensorial comfort. In the research, a "Sensorial Comfort Assessment Model" including objective measurements and subjective evaluations was created. The objective measurement results showed that the silk fabric was the lightest and thinnest, the polyester fabric was the tightest, softest, loosest, driest and most resistant to wrinkle and the lyocell fabric was the heaviest one with the lowest air permeability. The subjective evaluation results showed that the fabrics were categorized into three groups as silk-polyester-viscose, cotton-lyocell and linen according to their similarities. In summary, the similarity coefficients between the objective measurement results and the subjective evaluation results obtained by touching the fabrics were at a low level; however, the level of similarities between the subjective evaluation results obtained by touching the fabrics and wearing the blouses were higher.

1. INTRODUCTION

Clothing is expected to give an ease of movement physiologically, to look aesthetic and to make people feel happy psychologically, to adapt the surrounding temperature thermophysiology and to make a pleasant feeling on the skin sensorially. All these functions of clothing are described as "clothing comfort". In addition, clothing, which is an indispensable part of human beings, is in constant contact with the body and wraps the body like a second skin. Such integration of clothing with human body increases the significance of the clothing comfort.

According to Milenkovic et al. (1999), clothing comfort is defined as "a person's satisfaction while wearing a clothing or feeling comfortable in this clothing" [1]. Clothing comfort may also differ from person to person depending on perceptions of people [2]. For example, the same clothing can be evaluated as comfortable or uncomfortable by different people [3].

Expanding the consumers' awareness about the clothing

comfort enables consumers to prefer clothes that make them feeling good inside as well as looking good [4]. Moreover, modern consumers have the clothing comfort down as one of the most important features in purchasing ready-to-wear products [5].

Clothing comfort has been identified as one of the key attributes in consumers' perception of the desirability of apparel products in all markets. In order to succeed in a highly competitive apparel market, manufacturers have to meet or even exceed consumers' needs and expectations [6]. For this reason, ready-to-wear manufacturers tend to focus on the comfort of their apparel products [5].

The most important textile material constituting clothing is fabric. Not only having a good painting, colorful solution and durability is enough for clothing fabrics, but also the fabrics should have good comfort properties [7]. The sensorial comfort might be one of the most important comfort properties of fabric and clothing, since the perceived sensorial comfort of wearers of garments depends

ARTICLE HISTORY

Received: 14.06.2021

Accepted: 10.05.2022

KEYWORDS

Woven fabric, clothing comfort, sensorial comfort, objective measurement and subjective evaluation

To cite this article: Akgün E, Çoruh E. 2022. An investigation of sensorial comfort in woven women's blouses. *Tekstil ve Konfeksiyon*, 32(3), 243-251.

to a great extent on the tactile properties of the fabrics [8].

According to Umbach (1988), the sensorial comfort is mainly determined by fabric surface properties. It is associated with skin contact sensations and is often expressed as feelings of softness, smoothness, clamminess, clinginess, prickliness and liking. These descriptors can be related to specific, measurable fabric mechanical and surface properties that are mainly determined by fiber, yarn and fabric construction [9].

The fabric properties are very important in terms of the sensorial clothing comfort. For example, the fabric properties such as blending, weight, texture type, thread density, strength, abrasion, pilling, shrinkage etc. significantly affect on the wearing performance of clothing [10].

Several marketing studies have pointed out that modern consumers consider the sensory evaluation as one of the most important attributes in their purchase of clothing. The sensorial comfort, many times just simply identified by “hand”, is essentially a result of how much stress is generated by the fabric and how it is distributed over the skin [8].

The sensorial clothing comfort is expected to continue to attract the attention of both apparel manufacturers and market researchers. Meanwhile, an objective comfort measurement coupled with a subjective comfort evaluation regarded as the appropriate approach for the sensorial comfort [6]. Briefly, the objective measurements are considered together with the subjective evaluations in the sensorial clothing comfort researches [11].

The objective measurement and the subjective evaluation in terms of the sensorial comfort express two different concepts [3]. It is crucial to convert the subjective evaluations to the numerical values to find a relationship with the objective measurements to analyze statistical evaluation [12]. Therefore, the objective measurements and the subjective evaluations of fabrics and garments are considered together in the sensorial comfort researches. While tests are performed to determine the fabric properties in the objective measurements, the feelings experienced by touching the fabrics are figured out in the subjective evaluations.

In Mäkinen et al. (2005) study, in order to find a method for the sensational evaluation of textiles, the concept of “fabric hand” is commonly used. According to Pan et al. (1988) study, since fabric hand is based on subjective preferences of people, obviously it can mean different things to people.

In another study performed by Kawabata (1980), each consumer examines the property of the fabric by his/her “hand” to select a good clothing material according to his/her feeling during purchasing [12].

Because the feelings experienced on the skin when touched by the clothing products are one of the determinants for the consumers' clothing purchasing behavior in fashion, textile and ready-to-wear clothing manufacturers’ concern to focus on the sensorial clothing comfort in order to satisfy consumers and to produce their products with this point of view is important.

In this research, which was carried out to investigate woven women's blouses in terms of the sensorial comfort, (1) the objective measurements of the fabrics and (2) the subjective evaluations of the fabrics and the blouses were made and then (3) the obtained results were compared. The objective measurements were performed with laboratory tests. Additionally, the subjective evaluations were made by touching the fabrics and wearing the blouses made from these fabrics. At the same time, this research was considered important in terms of revealing the implications of the objective measurements and the subjective evaluations and also comparing the results with similarity coefficients.

In this research, which was carried out to investigate woven women's blouses in terms of the sensorial comfort, (1) the objective measurements of the fabrics and (2) the subjective evaluations of the fabrics and the blouses were made and then (3) the obtained results were compared. The objective measurements were performed with laboratory tests. Additionally, the subjective evaluations were made by touching the fabrics and wearing the blouses made from these fabrics. Finally, the similarity coefficients were found for the relationship between the objective measurement and the subjective evaluation results. At the same time, this research was considered important in terms of revealing the implications of the objective measurements and the subjective evaluations and also comparing the results with similarity coefficients.

2. MATERIAL AND METHOD

The research material was consisted of six different fabrics and six different blouses which were produced from these fabrics. In the research, "Sensorial Comfort Assessment Model" was created in order to examine woven women's blouses in terms of the sensorial comfort. This model was divided into two as the objective measurements and the subjective evaluations.

Sensorial comfort assessment model		
Objective measurements	Subjective evaluations	
-Fabric Tests	-By Touching Fabrics	-By Wearing Blouses

As seen in the research model, fabric tests were made for the objective measurements, and also the subjective evaluations were made by touching fabrics and wearing blouses. In accordance with the research model, "Sensorial Comfort Descriptors" were determined, which include both the objective measurements and the subjective evaluations. These descriptors were determined based on the study of Bernard (2009) [13]. Meanwhile, the researches of Sular and Okur (2005), Gürcüm (2010) and Özçelik Kayseri et al. (2012) were also used to define the mentioned descriptors [12, 14, 15]. In Table 1, the descriptors of the sensorial comfort are given in relation to the objective measurements and the subjective evaluations.

Table 1 shows nine descriptors used for the objective measurements, 14 descriptors used subjectively by touching the fabrics and 15 descriptors by wearing the blouses, which could be evaluated in terms of the sensorial comfort.

2.1. Objective Measurements

In the research, the objective measurements of six different fabric types used in the production of women's blouses were made. These fabrics were woven 1x1 plain weaves and were made of silk (SE), lyocell (CLY), polyester (PL), cotton (CO), linen (LI) and viscose (VI) materials. Fiber analysis tests were performed on these fabrics selected within the scope of the research. Thus, it was proven that

each fabric was 100% from the same fiber group and was not contain a different fiber mixture. In the mean time, nine descriptors were selected appropriate for the objective measurements and supported by laboratory tests.

It is important to determine the test methods and standards of the fabrics correctly [16]. In this research, the nine different fabric tests were applied in accredited laboratories for the objective measurements. Table 2 contains information about the tests performed on the fabrics and their standards.

In this research, before the test on the fabrics were performed, they were washed in a home automatic washing machine without using detergent and softener as in the research of Masteikaitė et al. (2013) [17]. Cotton, linen, polyester, lyocell and viscose fabrics were washed at 30 °C in a short program, whereas silk fabric was washed at 30 °C in a delicate program. The washed fabrics were dried by the laying method in a laboratory environment. The fabrics were not ironed before the tests.

2.2. Subjective Evaluations

In the subjective evaluation phase of the research, evaluations were made by touching six different washed fabrics and wearing blouses made of these washed fabrics in order to determine the effects on the skin of the participants.

Table 1. The relationship between objective measurements and subjective evaluations

Sensorial comfort descriptors	Objective measurements		Subjective evaluations	
	fabrics tests		By touching fabrics	By wearing blouses
1. Heavy/Light	Fabric weight		√	√
2. Thick/Thin	Yarn count		√	√
3. Loose/Tight	Fabric density		√	√
4. Non-durable/Durable	Tear strength		√	√
5. Non-air permeable/Air permeable	Air permeability		-	√
6. Rigid/Soft	Fabric stiffness		√	√
7. Non-flowy/Flowy	Fabric stiffness		√	√
8. Wet/Dry	Moisture regain		√	√
9. Wrinkled/Non-wrinkled	Crease recover angle		√	√
10. Stretched/Non-stretched	-		√	√
11. Rough/Smooth	-		√	√
12. Non-slippery/Slippery	-		√	√
13. Cold/Hot	-		√	√
14. Prickly/Non-prickly	-		√	√
15. Itchy/ Non-itchy	-		√	√

Table 2. Tests and standards applied to fabrics

Fabric tests	Standards
Fiber analysis	AATCC 20-2013
Fabric weight	ISO 3801: 1977
Yarn count	ISO 7211-5: 1984
Fabric density	BS EN 1049-2: 1994
Tear strength	ISO 13937-1: 2000
Air permeability	GOST 12088-77/ISO 9237
Fabric stiffness	TS 1409: 1973
Moisture regain	TS 467: 1985
Crease recover angle	BS EN 22313: 1992

In the research, 30x30cm fabric samples were prepared to touch the fabrics. The blouses were selected to have long sleeves and round collars in order to increase the contact of the fabrics with the body. The chest width of the blouses was 54cm and the centre back length was 58cm. As seen in Figure 1, the subjective evaluations were obtained according to the scores given by the participants by touching the fabrics and wearing the blouses.

In the research, 30 female participants living in Istanbul, aged 18-45, sized 38-40 were randomly selected. The participants made the subjective evaluations over 14 sensorial comfort descriptors by touching the fabrics and 15 sensorial comfort descriptors by wearing the blouses. The descriptor of non-air permeable/air permeable was considered not to be able to feel by touching the fabric, therefore not evaluated.

The participants graded the sensorial comfort descriptors from “absolutely negative (1)” to “absolutely positive (5)” when making the subjective evaluations by touching the fabrics and wearing the blouses.

According to the grading given by the participants, arithmetic means were calculated. In addition to this, "Multidimensional Scaling Analysis (MDSA)" was performed on the data obtained in the research. When analysing the data, “Normalized Raw Stress” value to prove validity and “Tucker's Coefficient of Congruence” value to prove reliability was used.

According to Kalaycı (2005), if the stress value is in the range of $0.00 < 0.025$, it is considered as full compliance [18]. In the research, Normalized Raw Stress values were 0.005 by touching the fabrics and 0.004 by wearing the blouses for the subjective evaluations. Being less than 0.025 of these stress values shows that the analysis model adequately fits in two dimensions. Additionally, a result of 0.997 for Tucker's Coefficient of Congruence values reveals that the reliability of the multidimensional scaling analysis has a very high correlation between the subjective evaluations by touching the fabrics and by wearing the blouses.



Subjective evaluation by touching the fabric



Subjective evaluation by wearing the blouse

Figure 1. Subjective evaluation samples of fabrics and blouses**Table 3.** Stress values and correlation coefficients

Stress values	By touching the fabrics	By wearing the blouses
Normalized Raw Stress	<u>.005</u>	<u>.004</u>
Stress-I	.071a	.064 a
Stress-II	.177a	.158 a
S-Stress	.008b	.009b
Dispersion Accounted For (DAF)	.994	.995
Tucker's Coefficient of Congruence	<u>.997</u>	<u>.997</u>
a. Optimal scaling factor	1.06	1.06
b. Optimal scaling factor	.92	.92

2.3. Comparison of Objective Measurements and Subjective Evaluations

The results from the objective measurements and the subjective evaluations were compared in order to make a clear conclusion from the research. Sülar and Okur (2005) stated that the differences between fabrics in subjective evaluations can be ordered according to their values in order to compare each fabric one by one. In this research, in addition to the subjective evaluations, it was considered that the objective measurements could be put in order.

In this research, the objective measurement and the subjective evaluation results were ordered and then the similarity coefficients (r) were calculated. The similarity coefficients were compared in two different ways: the objective measurement (OM) with the subjective evaluation-touching (SE-T) and the subjective evaluation-touching (SE-T) with the subjective evaluation-wearing (SE-W). In these paired comparisons; $r=0.17$ one fabric or blouse, $r=0.33$ two fabrics or blouses, $r=0.50$ three fabrics or blouses, $r=0.67$ four fabrics or blouses, $r=0.83$ five fabrics or blouses and $r=1.00$ six fabrics or blouses were ordered in the same way.

To explain with an example; according to the description of heavy and light sensorial comfort, the objective measurements of the fabrics were ordered as CLY-LI-VI-CO-PL-SE and the subjective evaluation by touching the fabrics were ordered as LI-CLY-CO-VI-PL-SE. In this

example, the similarity in the order of polyester and silk fabrics (PL-SE) in both cases were evaluated as $r=0.33$. Likewise, according to the description of heavy and light sensorial comfort, the order of the subjective evaluations by touching the fabrics were LI-CLY-CO-VI-PL-SE and by wearing the blouses were LI-CLY-CO-VI-SE-PL. In this case, the four fabrics (LI-CLY-CO-VI) were ordered the same in both sequences; thus, the similarity coefficient was 0.67 and they were 67% similar.

3. RESULTS AND DISCUSSION

3.1. Objective Measurement Results

The results of the laboratory tests performed for the objective measurements of six different blouse fabrics used in the research are shared in Table 4.

As seen above, the objective measurements were limited with the fabrics properties as fabric weight, yarn count, fabric density, tear strength, air permeability, fabric stiffness, moisture regain and crease recover angle. At the same time, the objective measurement results were found differently, because of the different fabrics. For example, while silk fabric weight was calculated 52.7 g/m², lyocell fabric weight was found 202.5 g/m². Consequently, it was aimed both to reveal the objective measurement results and to order the fabrics by using these results.

Table 4. Objective measurement results

Fabric tests		Silk	Lyocell	Polyester	Cotton	Linen	Viscose		
1.	Fabric weight (g/m ²)	52.7	202.5	90.0	122.5	192.3	136.2		
2.	Yarn count removed from fabric (Ne)	Weft	109.4/1	20.1/1	71.8/1	41.8/1	10.0/1	29.3/1	
		Warp	107.4/1	20.0/1	97.7/1	41.5/1	11.4/1	27.8/1	
3.	Fabric density (pick/ends per cm)	Weft	41.0	24.0	38.4	24.0	15.0	24.0	
		Warp	49.4	36.4	64.4	55.0	19.0	33.4	
4.	Tear strength (gf)	Weft	710.1	2656.0	1152.0	909.8	6524.0	1244.0	
		Warp	813.6	3490.0	1740.0	1400.0	6524.0	1487.0	
5.	Air permeability (dm ³ /m ² /s)	597.0	208.0	330.0	215.0	808.0	564.0		
6.-7.	Fabric stiffness (mg.cm)	Bending length (cm)	Weft	1.5	1.8	1.2	4.5	2.6	1.3
		Warp	1.5	1.6	1.3	2.0	2.7	1.4	
		Bending strength (mg.cm)	Weft	18.1	116.0	15.6	54.3	330.9	29.6
		Warp	18.0	81.9	19.8	96.6	370.4	36.4	
8.	Moisture regain (%)	General bending strength	18.1	97.5	17.6	71.8	350.0	32.8	
		Weft-Front	5.9	8.7	0.1	5.3	5.4	9.0	
		Weft-Back	110.0	96.0	159.0	86.0	65.0	109.0	
9.	Crease recover angle (°)	Weft-Back	117.0	96.0	149.0	90.0	63.0	109.0	
		Warp-Front	110.0	95.0	159.0	80.0	65.0	110.0	
		Warp-Back	117.0	95.0	147.0	80.0	63.0	110.0	

Results regarding the laboratory tests performed for the objective evaluation of the fabrics used in the research were presented below. The orders of the fabrics were as follows:

1.	According to the weight from the heaviest to the lightest, the fabrics were ranked as lyocell, linen, viscose, cotton, polyester and silk.
2.	The fabrics from the thickest to the thinnest were lined up as linen, lyocell, viscose, cotton, polyester and silk, respectively.
3.	The fabrics were listed from loose to tight as linen, viscose, lyocell, cotton, silk and polyester.
4.	When the tear strength of the fabrics were evaluated from the lowest strength to the highest strength, they were lined up silk, cotton, viscose, polyester, lyocell and linen.
5.	According to the air permeability of the fabrics from lowest to highest, they were respectively listed as lyocell, cotton, polyester, viscose, silk and linen fabrics.
6.-7.	The fabric stiffnesses from the hardest to the softest were lined up as linen, lyocell, cotton, viscose, silk and polyester fabrics. Polyester fabric was the softest and the flowiest fabric.
8.	According to the moisture regains of the fabrics from the highest to the lowest, they were ordered as viscose, lyocell, silk, linen, cotton and polyester fabrics. Based on this result, the polyester was the fabric having the least moisture on it.
9.	According to crease recovers from the easiest to the hardest wrinkle, they were ranked as linen, cotton, lyocell, viscose, silk and polyester.

3.2. Subjective Evaluation Results

The results of the subjective evaluations of the women participating in the research by touching six different fabrics (T) and wearing six different blouses (W) are shared in Table 5.

When the general means for the subjective evaluation of the fabrics given in Table 5 are considered, it was found that the means obtained by touching the fabrics and wearing all blouses were close to each other. For example, while the mean of silk fabric was 3.82 by touching, it was calculated to be 3.80 by wearing. This result revealed that the sensorial comfort was perceived as similar between touching the fabric and wearing the blouse. In other words, close arithmetic means show that the fabrics and the

blouses were perceived as similar in terms of sensorial comfort descriptors.

In the research, Multidimensional Scaling Analysis (MDSA) was performed for the subjective evaluations by touching the fabrics and wearing the blouses. Dimensions on the two-dimensional spatial map should be named while interpreting MDSA. After the analysis, the subjective evaluation dimensions were named as "Sensory and Physical Perception" and the comments were made according to these dimensions. Sensory perception dimension expressed as the sensory effect created by fabrics on individuals. Physical perception dimension defined as the effect of physical structure of fabrics on individuals. Analysis results are showed in Figure 2.

Table 5. Subjective evaluation results

Sensorial comfort descriptors	Silk		Lyocell		Polyester		Cotton		Linen		Viscose	
	\bar{x}		\bar{x}		\bar{x}		\bar{x}		\bar{x}		\bar{x}	
	T	W	T	W	T	W	T	W	T	W	T	W
1. Heavy/Light	4.57	4.60	2.00	2.43	4.50	4.80	2.53	2.67	1.67	2.13	4.27	4.13
2. Thick/Thin	4.47	4.90	1.83	2.23	4.47	4.73	2.27	2.03	1.57	1.53	3.77	3.73
3. Loose/Tight	4.60	4.53	3.93	4.03	4.27	3.97	4.90	4.63	2.23	2.20	3.97	4.07
4. Non-durable/Durable	4.07	3.40	4.57	4.60	4.10	4.20	4.27	4.43	3.67	4.00	4.00	4.27
5. Non-air permeable/Air permeable	-	2.73	-	3.37	-	2.97	-	2.13	-	2.93	-	4.13
6. Rigid/Soft	3.50	4.00	2.70	2.70	4.40	4.40	1.73	1.70	1.37	1.30	4.60	4.27
7. Non-flowy/Flowy	4.37	4.30	2.50	2.93	4.93	4.50	1.20	1.37	1.40	1.40	4.30	4.40
8. Wet/Dry	2.93	2.80	3.43	3.33	3.30	2.67	4.30	4.03	4.20	3.83	2.70	3.27
9. Wrinkled/Non-wrinkled	2.87	2.47	3.07	3.00	4.60	4.63	1.43	1.70	1.17	1.43	2.70	2.33
10. Stretched/Non-stretched	1.50	1.57	1.50	1.33	3.00	3.53	1.40	1.40	1.47	1.47	2.63	2.70
11. Rough/Smooth	4.47	4.70	2.97	3.60	4.00	4.53	3.37	3.80	1.97	1.90	3.93	4.37
12. Non-slippery/Slippery	4.60	4.80	2.10	2.37	4.33	4.53	2.03	2.00	1.60	1.50	3.63	3.27
13. Cold/Hot	2.37	2.27	3.00	2.83	2.80	2.60	2.80	3.17	2.13	2.60	3.23	2.93
14. Prickly/Non-prickly	4.60	4.90	4.13	4.13	4.70	4.90	3.77	3.63	3.57	1.80	5.00	4.97
15. Itchy/ Non-itchy	4.60	4.97	4.37	4.13	4.63	4.67	4.07	3.83	3.77	2.20	4.70	4.93
General Means	3.82	3.80	3.01	3.13	4.15	4.11	2.86	2.83	2.27	2.15	3.82	3.85

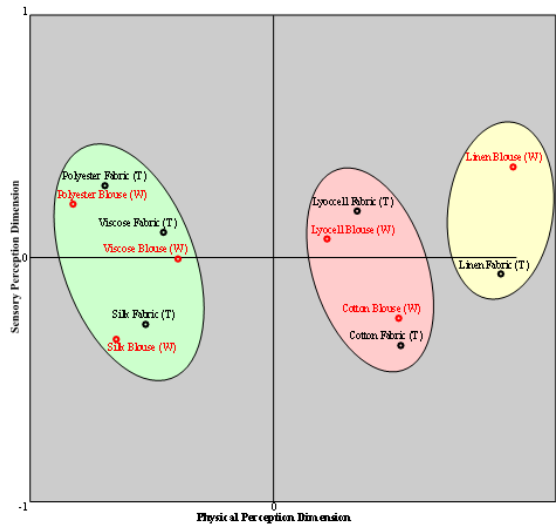


Figure 2. Multidimensional scaling analysis made by touching fabrics and wearing blouses

Analysis of the Figure 2 indicates that the fabrics and the blouses were located in three different groups according to their similarities as silk-polyester-viscose, cotton-lyocell and linen. Furthermore, the positions of all the fabrics except the linen fabric were closer to each other by touching and wearing. Thus, when the perceptions emerging by touching and wearing in the linen fabric were evaluated, there was no difference in the dimension of physical perception and that it was perceived differently in the dimension of sensory perception. The sensory perception about the linen fabric was felt much stronger when the blouse touches the body.

3.3. Relationship between Objective and Subjective Test Results

In the research, *the objective measurement results* showed that the silk fabric was the lightest and thinnest fabric, the polyester fabric was the tightest, softest, draped, driest and wrinkle resistant fabric, and the viscose fabric was the most moist/wet fabric. In the mean time, the lyocell fabric was

the heaviest fabric with the lowest air permeability. The cotton fabric, on the other hand, had more average values. Finally, the objective measurements indicates that the linen fabric was the thickest, loosest, rigidest, driest and easily wrinkled fabric (Table 4).

The subjective evaluation results indicated that the subjective evaluations made by touching the fabrics and wearing the blouses were close to each other. This result showed that the sensorial comfort of the blouse can be felt by touching the fabric (Table 5).

The Multi-Dimensional Scaling Analysis (MDSA) made on the subjective evaluation results proved that the fabrics were divided into three groups as silk-polyester-viscose, cotton-lyocell and linen (Figure 2).

As seen above, the results of the research were obtained in two different methods as the objective measurements and the subjective evaluations. On the other hand, in order to make more meaningful inferences about the results, Table 6 and Table 7 were created and presented below.

Table 6. Objective measurement and subjective evaluation results

Sensorial comfort descriptors	Objective measurements fabric tests	Ordering subjective evaluations by touching the fabrics	Subjective evaluations by wearing the blouses
1. Heavy/Light	CLY-LI-VI-CO-PL-SE	LI-CLY-CO-VI-PL-SE	LI-CLY-CO-VI-SE-PL
2. Thick/Thin	LI-CLY-VI-CO-PL-SE	LI-CLY-CO-VI-PL-SE	LI-CO-CLY-VI-PL-SE
3. Loose/Tight	LI-VI-CLY-CO-SE-PL	LI-CLY-VI-PL-SE-CO	LI-PL-CLY-VI-SE-CO
4. Non-durable/Durable	SE-CO-VI-PL-CLY-LI	LI-VI-SE-PL-CO-CLY	SE-LI-PL-VI-CO-CLY
5. Non-air permeable/Air permeable	CLY-CO-PL-VI-SE-LI	-	CO-SE-LI-PL-CLY-VI
6. Rigid/Soft	LI-CLY-CO-VI-SE-PL	LI-CO-CLY-SE-PL-VI	LI-CO-CLY-SE-VI-PL
7. Non-flowy/Flowy	LI-CLY-CO-VI-SE-PL	CO-LI-CLY-VI-SE-PL	CO-LI-CLY-SE-VI-PL
8. Wet/Dry	VI-CLY-SE-CO-LI-PL	VI-SE-PL-CLY-LI-CO	PL-SE-VI-CLY-LI-CO
9. Wrinkled/Non-wrinkled	LI-CO-CLY-VI-SE-PL	LI-CO-VI-SE-CLY-PL	LI-CO-VI-SE-CLY-PL
10. Stretched/Non-stretched	-	CO-LI-CLY-SE-VI-PL	CLY-CO-LI-SE-VI-PL
11. Rough/Smooth	-	LI-CLY-CO-VI-PL-SE	LI-CLY-CO-VI-PL-SE
12. Non-slippery/Slippery	-	LI-CO-CLY-VI-PL-SE	LI-CO-CLY-VI-PL-SE
13. Cold/Hot	-	LI-SE-PL-CO-CLY-VI	SE-LI-PL-CLY-VI-CO
14. Prickly/Non-prickly	-	LI-CO-CLY-SE-PL-VI	LI-CO-CLY-SE-PL-VI
15. Itchy/ Non-itchy	-	LI-CO-CLY-SE-PL-VI	LI-CO-CLY-PL-VI-SE

In order to compare these results, the similarity coefficients were calculated based on the rankings in Table 6. Additionally, the similarity coefficients of the objective measurement results of the fabrics with the subjective evaluation results by touching the fabrics (OM with SE-T) and the subjective evaluation results made by touching the fabrics with wearing the blouses (SE-T and SE-W) were given in Table 7.

Table 7. Similarities of objective measurement results (OM) and subjective evaluation results (SE-T with SE-W)

Sensorial comfort descriptors	Similarity Coefficients	
	OM with SE-T	SE-T with SE-W
1. Heavy/Light	0.33	0.67
2. Thick/Thin	0.67	0.67
3. Loose/Tight	0.33	0.50
4. Non-durable/Durable	0.17	0.33
5. Non-air permeable/Air permeable	-	-
6. Rigid/Soft	0.17	0.67
7. Non-flowy/Flowy	0.50	0.67
8. Wet/Dry	0.33	0.67
9. Wrinkled/Non-wrinkled	0.50	1.00
10. Stretched/Non-stretched	-	0.50
11. Rough/Smooth	-	1.00
12. Non-slippery/Slippery	-	1.00
13. Cold/Hot	-	0.17
14. Prickly/Non-prickly	-	1.00
15. Itchy/ Non-itchy	-	0.50

When an examination of the results showed that both the objective and the subjective results were similar in sensorial descriptors of 67% thickness/thinness, 50% non-flowy/ flowy, and 50% easily wrinkled/non-wrinkled. In other sensorial comfort descriptors, similarity coefficients were lower.

The similarity coefficients in Table 7 regarding the subjective evaluations made by touching the fabrics and wearing the blouses; sensorial comfort descriptors wrinkled/ non-wrinkled, rough/smooth, non-slippery/ slippery and prickly/non-prickly were 100% and felt completely similar. In addition, the sensorial comfort descriptors of heavy/light, thick/thin, rigid/soft, non-flowy/flowy and wet/dry were in the range of 67% and perceived moderately similar.

Findings the similar results between touching the fabrics and wearing the blouses in this study were acquired information that the feeling of touching of the clothing product with the feeling of using of the clothing was similar. Briefly, the research showed that touching the clothing product was given an idea about the sensorial comfort of the clothing.

The research conducted by Ayçiçek (2019) was related to woven fabrics for shirting in order to meet the expectations of cabin crews. Besides, 3% elastane and woven with plain weave might be added to 100% cotton, 100% bamboo and 100% tencel fabrics in order to gain mobility [19]. In this research, the blouse woven fabrics were in a plain structure as suggested by Ayçiçek (2019) and were considered more widely as silk, lyocell, polyester, cotton, linen and viscose

fabrics. In this research, elastane was not preferred especially, since the use of elastane in fabrics would affect sensory perceptions.

The research of Sülar and Okur (2005) reported that the fabric attitude was evaluated as worse as the thickness of the fabrics increased [14]. In Table 6, it was observed that the thickest fabric in the objective measurements was linen, and the linen fabric was perceived negatively in the subjective evaluations. In accordance with the results obtained regarding the thickness of the fabric were similar to the research results of Sülar and Okur (2005).

The research of Gürcüm (2010) revealed that both the weft density of fabrics and the softness perception of fabrics increased [15]. In the objective measurements of this research, polyester and silk fabrics were the highest weft and warp density and the softest. The objective measurement results of this research were similar to Gürcüm's (2010) research.

According to Özdil (2003), the attitude of the fabric is a perceived property and depends on the sense of touch. It is difficult to express characteristics such as softness, hardness and drape numerically, which are often felt by touching the fabric [10]. At the same time, the handle properties of the fabrics are significantly affected by the finishing processes applied to the fabrics. In this research, the fabrics were washed so that the finishing processes did not affect the results of the research, and then the investigations were made.

In a research conducted by Can (2016), the researcher stated that easily wrinkled clothes are not preferred by users much. High wrinkling resistance is generally a feature preferred in all fabrics [20]. In this research, it was determined that the fabric with the highest wrinkle resistance was the polyester, while the lowest and easily wrinkled fabric was the linen. The easy wrinkling property of the linen fabric may cause it to be perceived negatively and not to be preferred by users.

Regarding women's blouses, TS 10698 numbered "Textile - Dress and Blouse Fabric (2011)" and TS 11436 numbered "Textile Products- Blouse (1994)" standards were prepared by the Turkish Standards Institute [21, 22]. These standards were clearly revealed the importance of fabric and blouse.

When the researches given above are examined, it is seen that there are points to investigate, develop and increase the sensorial comfort of the clothes. It is hoped that this research, which includes woven women's blouses, will serve as an example for examining other types of clothing in terms of sensorial comfort.

4. CONCLUSIONS

The results obtained in the research conducted specifically for woven women's blouses in order to examine the sensorial comfort were the objective measurement results and the subjective evaluation results in terms of similarities. Shortly, the results have revealed that the similarities

between the objective measurement results and the subjective evaluation results by touching the fabrics (OM and SE-T) were lower; however, the similarities between the subjective evaluation results made by touching the fabrics and wearing the blouses (SE-T and SE-W) were at a higher level.

Based on the results obtained in this research, which was conducted to examine women's blouses in terms of sensorial comfort, suggestions for possible future researches are developed and are given as below:

- Stretched/non-stretched, rough/smooth, non-slippery /slippery, cold/hot, prickly/non-prickly and itchy/non-itchy can be added to be extended the objective measurements.
- Innovative raw materials, auxiliary materials and materials that increase sensorial comfort in clothes can be developed.
- Statistical methods can be developed to compare objective and subjective results regarding sensorial comfort in clothing.
- Users' opinions can be obtained and their expectations can be determined for different clothing groups in order to improve sensorial comfort in clothes.

REFERENCES

1. Öner E, Okur A. 2010. Effects of material, production technology and fabric structure on thermal comfort. *Tekstil ve Mühendis*, 17(80), 20-29.
2. Yüksel HG, Okur A. 2011. Relationships between subjective comfort evaluations and laboratory tests. *Tekstil ve Mühendis*, 18(84), 38-47.
3. Akgün Girgin E. 2019. Examining of the woven fabrics used in women's blouses in terms of sensorial comfort. Gazi Üniversitesi Güzel Sanatlar Enstitüsü, Ankara.
4. Karaman C, Kaplan S. 2017. Consumer expectations about socks comfort and performance characteristics. *Pamukkale University Journal of Engineering Sciences*, 23(7), 818-825.
5. Wu HY, Zhang WY, Li J. 2009. Study on improving the thermal-wet comfort of clothing during exercise with an assembly of fabrics. *Fibres & Textiles in Eastern Europe*, 17(4), 46-51.
6. Kilinc Balci FS. 2011. *Testing, analysing and predicting the comfort properties of textiles*. Improving Comfort in Clothing, Woodhead Publishing Series in Textiles, 138-162.
7. Asanovic KA, Cerovic DD, Mihailovic TV, Kostic MM, Reljic M. 2015. Quality of clothing fabrics in terms of their comfort properties. *Indian Journal of Fibre & Textile Research*, 40(December), 363-372.
8. Broega AC, Nogueira C, Cabeço-Silva ME, Lima M. 2010, June. Sensory comfort evaluation of wool fabrics by objective assessment of surface mechanical properties. Proceedings of Autex World Textile Conference (1-4). Vilnius, Lithuania.
9. Yoo S, Barker RL. 2005. Comfort properties of heat-resistant protective workwear in varying conditions of physical activity and environment. Part I: Thermophysical and sensorial properties of fabrics. *Textile Research Journal*, 75(7), 523-530.
10. Özdil N. 2003. *Kumaşlarda fiziksel kalite kontrol yöntemleri*. Ege Üniversitesi Tekstil ve Konfeksiyon Araştırma- Uygulama Merkezi Yayını, Yayın No: 21, İzmir.
11. Utkun E. 2013. The development of comfortable clothes for infants. Ege Üniversitesi Fen Bilimleri Enstitüsü, İzmir.
12. Özçelik Kayseri G, Özdil N, Süpüren Mengüç G. 2012. *Sensorial comfort of textile materials*. INTECH Open Access Publisher, 235-267.
13. Bernard AB. 2009. Factors affecting human comfort response to garments (Master's thesis). North Carolina State University, Textile Engineering, North Carolina.
14. Sular V, Okur A. 2005. The role of subjective evaluation in the determination of tactile properties of fabrics. *Tekstil ve Mühendis*, 12(59-60), 14-21.
15. Gürcüm BH. 2010. Dokuma kumaşların öznel algısı ile bazı fiziksel özellikleri arasındaki ilişkinin belirlenmesi. *Tekstil ve Konfeksiyon*, 20(2), 101-108.
16. Çoruh E. 2018. Preparation of technical specifications regarding garment purchase. *Tekstil ve Mühendis*, 25(109), 53-61.
17. Masteikaitė V, Sacevičienė V, Audzevičiūtė-Liutkienė I. 2013. Influence of structural changes in cotton blend fabrics on their mobility. *Fibres & Textiles in Eastern Europe*, 21, 1(97), 55-60.
18. Kalaycı Ş. 2005. *SPSS uygulamalı çok değişkenli istatistik teknikleri*. Dinamik Akademi Yayın Dağıtım. 8. Baskı, Ankara.
19. Ayçiçek B. 2019. Uçaklarda kabin ekiplerinin gömleklik dokuma kumaşlarının inovatif tasarımı (Yayınlanmamış yüksek lisans tezi). Bursa Uludağ Üniversitesi, Fen Bilimleri Enstitüsü, Bursa.
20. Can Y. 2016. Estimation of the wrinkle resistance of cotton woven fabric by yarn characteristics. *Kahramanmaraş Sütçü İmam Üniversitesi Mühendislik Bilimleri Dergisi*, 19(3), 62-67.
21. Türk Standartları Enstitüsü. 2011. Tekstil- elbise ve bluz kumaşı (TS 10698). Ankara: TSE.
22. Türk Standartları Enstitüsü. 1994. Tekstil mamulleri- bluz (TS 11436). Ankara: TSE.

In summary, this research, which was conducted to examine women's blouses in terms of sensorial comfort, will provide an idea for new researches in the field of sensorial comfort. The limited number of studies in the literature on the sensorial comfort in the fashion industry shows that this topic has many points that can be evaluated and investigated by researchers, designers, suppliers, manufacturers, marketers, retailers and consumers.

Performance Investigation of Textile Triboelectric Generators

Aristeidis Repoulias¹  0000-0003-1254-0955

Sotiria F Galata¹  0000-0003-3007-2235

Argyro Kallivretaki¹  0000-0002-8280-2159

Arzu Marmarali²  0000-0001-6251-0645

Savvas Vassiliadis¹  0000-0002-8360-4728

¹University of West Attica, Department of Electrical and Electronics Engineering, P. Ralli & Thivon 250, 12244 Athens, Greece

²Ege University, Textile Engineering Department, Bornova, Izmir, 35100, Türkiye

Corresponding Author: Aristeidis Repoulias, arepoulias@uniwa.gr

ABSTRACT

With respect to the theory of the four Triboelectric Generators (TEGs) operational modes, a testing method is proposed. It describes and imitates more precisely the real conditions of the motion of the materials in a wearable clothing-based TEG. The phenomenon of triboelectricity is investigated from a clearly textile approach, using typical textile fabrics made by ordinary textile production methods and environmentally friendly materials. The performance investigation is based on the comparison of their triboelectric outcomes. It is of special interest that cotton fabrics showed an adequate electrical response, and among them, the twill 2/2 weave pattern offered the highest voltage outputs.

1. INTRODUCTION

During the last decade, more and more research is applied in the area of Triboelectric Generators (TEGs). The potential energy sustainability which they can offer to wearable electronic devices has been of high importance [1]. Triboelectricity can be briefly defined as the natural phenomenon in which electric charges of opposite signs are induced by the frictional contact and separation of the surfaces of two materials [2,3]. It remains a complicated physical phenomenon, very difficult to investigate without approaching it from a multidisciplinary aspect. But in the meanwhile, beyond the questions about the phenomenon itself, a lot of interest is applied in developing new TEGs which might be used in new application areas and which can provide considerable electrical power outputs [4].

Following the principle of triboelectricity, TEGs are miniaturised devices which exploit the triboelectricity phenomenon in order to collect energy from our daily life movements or our ambient environment which would be otherwise wasted [5]. Until today, TEGs have gained a

significant interest to combine them with human daily motion (e.g walking or running). TEGs constitute by definition a sustainable form of energy, contrary to batteries which are bulkier, stiffer, heavier, need often replacement and cause environmental pollution [6–9]. This advantage and eco-friendly character drive a lot of effort to develop TEGs and apply them in low-consumption wearable electronics, or even to further applications areas independent of the need of a wearer.

The two main functions of TEGs lay between two areas: the one of providing sustainable electrical power by harvesting all kinds of mechanical energy, and that of providing sensing which would be self-powered without the need for an external power supply or batteries [10]. Many studies and trials have been applied over the last decade in order to attach TEGs onto human wearable garments, shoes or accessories (e.g. bags), bringing to the surface a wide range of medical, sportive and other daily life human applications. The power supply of low-consumption wearable devices like a wearable watch, the use as a self-

To cite this article: Repoulias A, Galata SF, Kallivretaki A, Marmarali A, Vassiliadis S. 2022. Performance investigation of textile triboelectric generators. *Tekstil ve Konfeksiyon*, 32(3), 252-257.

powered breathing or heart rate sensor, the use as a garment-embedded keyboard or button, and the use for self-powered wearable temperature or humidity sensors are only a few examples to mention [11].

The intensity of the triboelectric process of a TEG depends on various parameters like the contact force between the two surfaces, the ambient humidity and temperature, the surface structure, the area size of the contact surfaces, the thickness of the contacting materials etc [11,12]. Among these parameters, the pairs of the contacting surfaces play a major role in the produced energy [2, 13–16]. This means that the materials' chemical or mechanical properties also affect the resulting electrical outputs. So for example, many polymer materials like fluorinated ethylene propylene (FEP), polyvinylidene fluoride (PVDF), polydimethylsiloxane (PDMS), polytetrafluoroethylene (PTFE), and polyvinyl chloride (PVC) have been proved to be good for building efficient TEGs, keeping also the cost low [17]. Additionally, the surface structure is important, as it directly relates to the increase of the contacting area. Considering this, significant improvements have been done to develop the surface structures by using nanoparticles, chemical treatments, block copolymer patterning, nature patterns replication and another forms of nanoprocessing. For example, state-of-the-art technologies for particular material structures like aerogels have been introduced in TEGs building in order to achieve high efficiency. Indeed aerogels are particularly interesting in TEGs applications area because of their high porosity, flexibility, light weight and large surface areas, while they can also be combined with another energy harvesting family, called Piezoelectric Generators to build improved hybrid generators [17,18].

The fundamental mechanism of triboelectricity has not been fully and exhaustively clear yet and this is out of the scope of this current work. The fact that triboelectricity can appear between different or identical materials, between conductive or insulative ones, between solid and liquid, solid and solid, gas and solid etc, makes it very complicated to study it under various external conditions and to build an overall mechanism theory which would cover all the cases happening. Among them, the dominant mechanism is the electron transfer (others are ion transfer, material transfer, H^+ and OH^- transfer) which happens when the interatomic distances between the surfaces of two contacting materials become shorter upon contact, driving consequently to electron clouds overlap, a lowering of the energy barrier between the participating atoms of the two surfaces, and the final result of allowing electrons to move from one atom to another [10]. At this point, we must mention that the application of force and rubbing enlarges the participating area of this pre-described mechanism.

In the case of textile-based TEGs, the chosen contacting surfaces are textile structures, so they may have the form of woven, knitted, non-woven or yarns. These textile structures donate to the TEG their mechanical or physical advantages of flexibility, elasticity, breathability, skin-

friendliness, eco-friendliness, tailorability etc. This means for example that the textile-based TEGs may be friendlier to the wearer and the human skin. Additionally, they offer the possibility of getting directly embedded as part of the clothing or textile-based wearable device.

Four operational modes of TEGs exist to step on, develop and construct test mechanisms to harvest electrical energy [1,19]. The most simple and common operational mode used is the vertical contact-separation mode (also known as contact-separation mode). In that, the contacting materials face each other and execute a motion which is perpendicular to their contacting surfaces, resulting in a tapping action. Similar is the single electrode mode, which differs in the fact that one of the two surfaces is simultaneously also the electrode. In the rest two modes, the in-plane (also known as linear sliding) and the free-standing, the contacting materials execute a motion which is longwise to their contacting surfaces, resulting in a sliding action.

In this research work, with respect to the theory of the four operational modes, a testing device has been designed, analysed and constructed. It executes a realistic motion of the contacting surfaces approaching the motions of the human body in real life. It applies on the samples' surfaces a combination of a perpendicular (tapping) and a longwise (sliding) motion. Thus it combines the vertical contact-separation mode and the linear sliding mode. This may imitate more realistically the motion of the materials in a wearable TEG of clothing, as it might take into consideration both the contact-separation state plus the intermediate friction under regular force loads.

2. MATERIAL AND METHOD

2.1 Material

In this study, the phenomenon of triboelectricity was examined from a clearly textile point of view. Thus the tested textile fabrics were made by ordinary textile production methods and without applying any additional chemical or mechanical treatments to affect the properties of their surface. As can be seen in Figure 1, the testing samples were made of three different weaving patterns: plain, twill 2/2 2/2 and honeycomb [20]. Warp and weft density was equal to 20.4 yarns/cm, and they were kept constant during the production of all samples.

All of the patterns were produced using the same two-ply yarn. It came from a 100% cotton carded blend, it had a linear density of 20x2 Tex (30/2Ne) and 620 twists per meter (15.75 twists per inch). Its mass evenness and surface quality characteristics were also measured: Uster evenness value was 8.1U% ($CV_m=10.1$) and hairiness value 6.0. Moreover, the single-ply yarns which were used for the production of the two-ply yarn, had 917 twists per meter (23.3 twists per inch), 12.5U% ($CV_m=15.6$) and 5.1 hairiness.

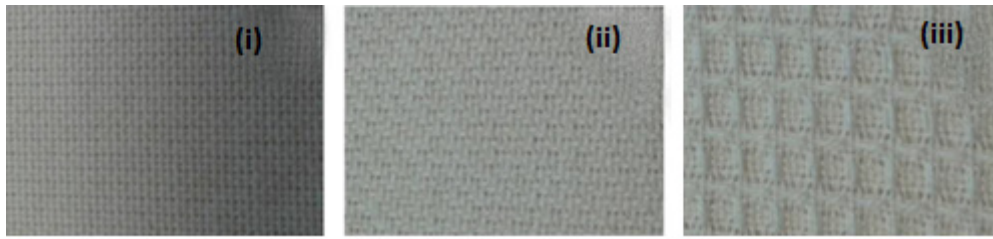


Figure 1. Images showing the used (i) plain, (ii) twill 2/2 and (iii) honeycomb textile patterns [20]

The cotton material was selected because of the high interest it has as it is an environmentally friendly material and also very friendly to human skin. Additionally, it was selected in a frame of investigating the possibilities that natural textile materials may provide to us as contacting parts of a TEG. Each testing specimen had a dimension of 5x5cm. In each measurement series, newly cut specimens were used to compare, avoiding any previous possible wear on the surfaces.

To compare the triboelectric outputs of the three different cotton samples, a second material was selected to combine and pair with each of the samples. For this need, in the currently presented experiments, a 5x5cm PE film was chosen which would provide a clear and flat surface. This was used as the reference material sample. Keeping it constant in all the measurements, we preserved the same conditions for the comparison of the before-mentioned various textile samples.

2.2 Method

This research focused on approaching the triboelectricity phenomenon in a more realistic way from a textile clothing point of view, applying normal weight loads of a few grams (e.g. 10grams) as if the load was caused by the slight motion of a clothing part. The application of significantly high forces usually met in the literature (several Newtons like the ones applied by big linear motors) between the TEGs' contacting surfaces has been avoided, as such conditions might not be met in wearable clothing except for shoes which gather the body's weight during running or walking.

Moreover, friction was taken into account to simulate the TEG's performance under more realistic conditions. As already mentioned, most of the contact-separation testing devices can describe the performance of a TEG taking into account only the movement of the triboelectric surfaces on a perpendicular axis (tapping). Hereby, to keep it more realistic, the appearing friction from the horizontal displacement of the surfaces on the horizontal axis has been considered too.

The proposed method combines the contact, friction and separation of two contacting surfaces, to simulate accurately the real operating conditions on a human body, especially if the two triboelectric surfaces are placed on the

inner side of the sleeve and aside from the body as shown in Figure 2 (black and yellow strips).

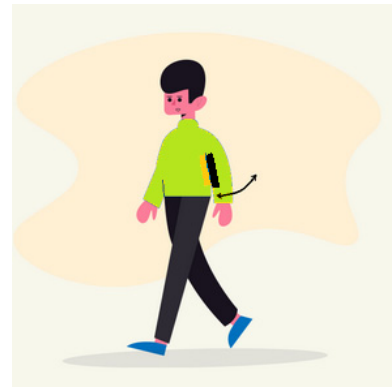


Figure 2. Example of the contact, friction and separation motion executed by two triboelectric surfaces on the inner side of the sleeve (black strip) and aside from the body (yellow strip) while walking

This motion of one sample over the other is thoroughly presented in Figure 3C. Starting from the initial position of phase (i), the upper sample (black color) moves toward the lower sample (yellow color) during phase (ii). At some point it contacts the lower sample at phase (iii) and keeps moving over the surface of the lower sample. During phase (iv) the two samples are positioned and stopped exactly one over the other and they are under a certain weight load. The inverse motion is applied afterwards, moving away the upper sample at phase (v), separating it at phase (vi) and finally stopping it at its initial position in phase (vii).

We may consider that the hereby proposed TEG testing device combines both the two motions which are used individually by more traditional TEGs, as presented in Figure 3 A and B. Firstly, in Figure 3A is represented the vertical motion of the two participating triboelectric surfaces of a vertical contact-separation TEG. In that, the surfaces are coming in contact and separate on a straight vertical axis of motion. During the contact, a load is applied between the two surfaces. Secondly, in Figure 3B, is represented the horizontal motion of the two participating triboelectric surfaces of a in-plane mode TEG. In that, the surfaces are sliding until they cover each other, and then they separate again. During their overlap, a load is applied between the two surfaces resulting in appearance of friction phenomena between them. In this way, friction is introduced into our measurements.

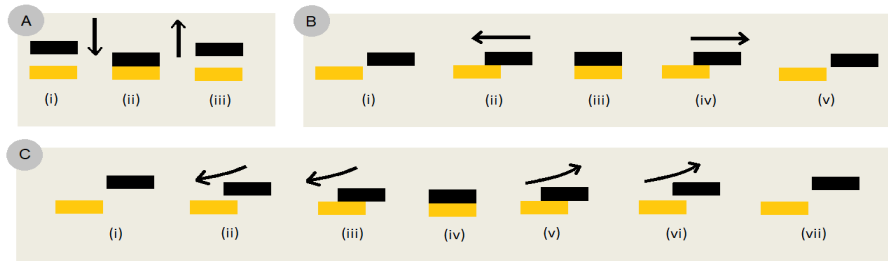


Figure 3. Representation of the relative motion executed by the upper sample over the lower sample

The proposed testing device might be used to test woven, knitted or more complicated textile structures of various densities, thicknesses, materials etc. The compression load applied during phase (iv) can be respectively adjusted. It achieves the desired motion between the two tested samples thanks to the use of a mechanical actuator and a connected pair of arms building a cradle, whose swinging motion brings in contact, rubs and separates the two samples, at the back side of which are attached the electrodes (Figure 4).

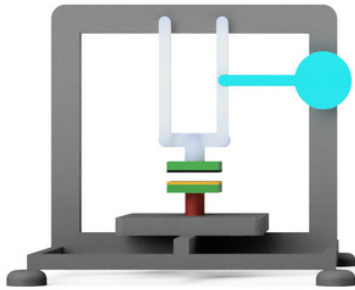


Figure 4. Sketch of the testing device which was designed and constructed, presenting the mechanical actuator (turquoise), the pair of arms (white), the two samples (black and yellow) and the two electrodes (green)

The proposed testing device contains two specially designed specimen holders, with a conductive surface on their exposed side. Each specimen is attached to the conductive surface of the holder, which serves as the output electrode of the TEG. A load sensor is attached to one of the specimen holders to measure the applied load upon sliding. The motion of one sample over the other is executed with high accuracy in what concerns their position and timing (e.g. operating frequency).

Additionally, an oscilloscope was connected with the device's electrodes to measure the electric outcomes. During the test measurements, the peak-to-peak voltage (V_{pp}) was measured.

3. RESULTS AND DISCUSSION

The proposed method is a tool for precise measurements allowing the study of the triboelectric properties of many textile materials, with the cotton included. This is due to the intervention of the friction between the contact and separation phases which increases the electrical outcomes. An example of the electrical response is presented in Figure 5, as it can be seen on the oscilloscope's display screen.

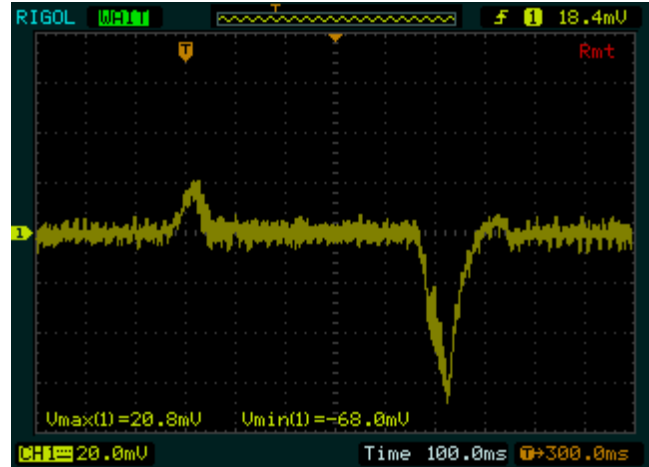


Figure 5. Generated voltage waveform.

Two peaks were appearing upon each test cycle which included one contact, sliding and separation of the two TEG's surfaces. The first peak appears at the moment of the contact phase, which is represented in stage (iii) of Figure 3C. The second peak corresponds to the moment of the separation phase which is represented in stage (v) of Figure 3C. Finally as seen on the oscilloscope, there is no electric output between stages (iii) and (v) of Figure 3C, where friction contact occurs between the two surfaces.

Concerning the comparison of the samples of different weaving patterns, it was found that the twill 2/2 patterned fabric gave the highest peak-to-peak voltage output, followed by the plain, and finally the honeycomb (Figure 6). This result agrees with previous studies which have set the twill 2/2 patterns as more effective than others [13,15,21].

More precisely, when the cotton plain sample was combined with the PE film sample as the two contacting surfaces of the TEG, they gave V_{pp} ranging from 112 to 120mV, with a mean V_{pp} value of 116mV. On the other hand, the cotton twill 2/2 sample combined with the PE film sample as the two contacting surfaces, gave much higher voltage outputs. The V_{pp} was ranging from 142 to 149mV, with a mean V_{pp} value of 145mV. Finally, the cotton honeycomb pattern sample combined with the PE film sample gave the lowest voltage outputs. The V_{pp} was ranging from 100 to 108mV, with a mean V_{pp} value of 104mV.

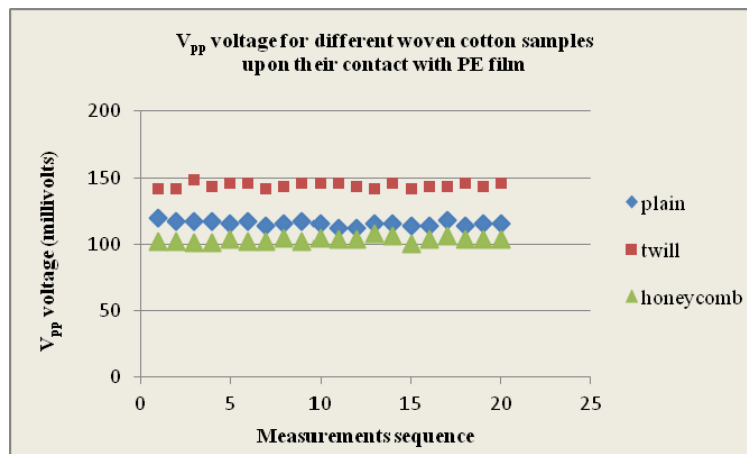


Figure 6. Repeated peak to peak voltage measurements during the contact and separation of the two contacting surfaces.

Traditionally, it has been known that a weaving pattern plays a major role in the regular textile properties like for example the surface roughness [22], the shear behaviour [20] etc. Hereby, it is also proved that as a weaving pattern primarily affects the surfaces of textile-based TEGs, it also secondarily affects its triboelectric outcomes.

It is worth mentioning the high repeatability level of the measurements as it comes from the above graph. The stability and repeatability properties are mainly because of the precise design and construction of the testing device.

In the majority of the related sources, research refers to the development of TEGs whose contacting materials are polymer-based, in the form of film or complicated multi-layered structures [11]. However, this research work has focused on the possibilities of a broadly used natural material like cotton, staying close to traditional and widely used textile structures.

Moreover, each of the four TEGs operational modes is limited to offering only a perpendicular or longwise motion, and cannot provide simultaneously both tapping and sliding action. This can be practical from a laboratory reference point, but not representative of the real usage conditions. Herein a more representative simulation of the motion of the contacting surfaces in a textile-based TEG has been achieved.

4. CONCLUSION

Providing the necessary precision and flexibility, the proposed method will allow a better study of the textile-based TEGs. We have hereby seen a comparison of the electric outputs of three well-known weaving patterns (plain, twill 2/2 and honeycomb), of which the samples

were made out of the same material (carded cotton) and production settings (yarn density, weaving density etc).

During the tests, the executed contact, rubbing and separation of each sample with a PE film under a low load of 10 grams, showed that the twill 2/2 pattern provided a mean V_{pp} value of 145mV. That was the highest in comparison with the plain pattern which gave 116mV and the honeycomb pattern with 104mV.

The patterns of the contacting surfaces of the materials participating in the triboelectric effect of a TEG are of major importance, as from a textile point of view, they correlate to the various textile properties of surface roughness, density, porosity, breathability etc, from which in turn the triboelectric performance depends.

For future study, interest has risen to extend the tests by substituting the hereby used reference sample (PE film) with a reference sample of a textile fabric. In this way, the triboelectric effect of two textile surfaces would be tested, exactly as they might be used under real conditions in a garment.

This proposed method permits a realistic testing motion of the contacting surfaces which approaches the kinetics of the human body in real life. Thus, the use of the specific device it is expected to serve a more realistic loading simulation. Consequently, a precise performance examination is expected, supporting the comparison of the countless textile patterns and materials, which might be used for the design and development of textile-based TEGs. In this way, the optimum weaving, knitting or nonwoven pattern and material might be chosen according to the needs of the desired textile-based TEG and the clothing item or accessory to get attached on.

REFERENCES

1. Lin Z, Chen J, Yang J. 2016. Recent progress in triboelectric nanogenerators as a renewable and sustainable power source. *Journal of Nanomaterials* 2016, 01–24.
2. Zou H, Zhang Y, Guo L, Wang P, He X, Dai G, Zheng H, Chen C, Chi Wang A, Xu C, Wang Z L. 2019. Quantifying the triboelectric series. *Nature Communications* 10(1), 1427.
3. Zhu G, Peng B, Chen J, Jing Q, Lin Wang Z. 2015. Triboelectric nanogenerators as a new energy technology: From fundamentals, devices, to applications. *Nano Energy* 14, 126–138.
4. Luo J, Wang Z L. 2020. Recent progress of triboelectric nanogenerators: From fundamental theory to practical applications. *EcoMat* 2(4).
5. Wang Z L. 2013. Triboelectric Nanogenerators as New Energy Technology for Self-Powered Systems and as Active Mechanical and Chemical Sensors. *ACS Nano* 7(11), 9533–9557.
6. Chacko P, Kapildas K S, Jarin T. 2017. Nano generator intended for energy harvesting. *Asian Journal of Applied Science and Technology* 1(9), 88–91.
7. Paosangthong W, Torah R, Beeby S. 2019. Recent progress on textile-based triboelectric nanogenerators. *Nano Energy* 55, 401–423.
8. Zhong J, Zhang Y, Zhong Q, Hu Q, Hu B, Wang Z L, Zhou J. 2014. Fiber-based generator for wearable electronics and mobile medication. *ACS Nano* 8(6), 6273–6280.
9. Li C, Cao R, Zhang X. 2018. Breathable materials for triboelectric effect-based wearable electronics. *Applied Sciences* 8(12), 2485.
10. Wang Z L, Wang A C. 2019. On the origin of contact-electrification. *Materials Today* 30, 34–51.
11. Korkmaz S, Kariper İ A. 2021. Production and applications of flexible/wearable triboelectric nanogenerator (TENGS). *Synthetic Metals* 273, 116692.
12. Pan S, Zhang Z. 2019. Fundamental theories and basic principles of triboelectric effect: A review. *Friction* 7(1), 2-17.
13. Somkuwar V U, Pragya A, Kumar B. 2020. Structurally engineered textile-based triboelectric nanogenerator for energy harvesting application. *Journal of Materials Science* 55(12), 5177–5189.
14. Muthu M, Pandey R, Wang X, Chandrasekhar A, Palani I A, Singh V. 2020. Enhancement of triboelectric nanogenerator output performance by laser 3D-Surface pattern method for energy harvesting application. *Nano Energy* 78, 105205.
15. Jeong J, Kwon J-H, Lim K, Biswas S, Tibaldi A, Lee S, Ju Oh H, Kim J-H, Ko J, Lee D-W, Cho H, Lang P, Jang J, Lee S, Bae J-H, Kim H. 2019. Comparative study of triboelectric nanogenerators with differently woven cotton textiles for wearable electronics. *Polymers* 11(9), 1443.
16. Liu W, Wang Z, Hu C. 2021. Advanced designs for output improvement of triboelectric nanogenerator system. *Materials Today* 45, 93-119.
17. Korkmaz S, Kariper İ A. 2020. Aerogel based nanogenerators: Production methods, characterizations and applications. *International Journal of Energy Research* 44(14), 11088–11110.
18. Korkmaz S, Kariper İ A. 2022. BaTiO₃-based nanogenerators: fundamentals and current status. *Journal of Electroceramics* 48(1), 8-34.
19. Niu S, Wang Z L. 2015. Theoretical systems of triboelectric nanogenerators. *Nano Energy* 14, 161–192.
20. Inogamdjano D, Matsouka D, Vassiliadis S, Kizlaridis I, Daminov A. 2020. Low stress shear behaviour of cotton fabrics. *Fibers and Polymers* 21(6), 1355–61.
21. Ma L, Wu R, Liu S, Patil A, Gong H, Yi J, Sheng F, Zhang Y, Wang J, Wang J, Guo W, Wang Z L. 2020. A machine-fabricated 3D honeycomb-structured flame-retardant triboelectric fabric for fire escape and rescue. *Advanced Materials* 32(38), 2003897.
22. Jaouani H, Matsouka D, Vassiliadis S, Nikas K S. 2019. Effect of weaving pattern and yarn density on the surface roughness of woven fabrics. *Tekstil ve Mühendis* 26(116), 320–323.



Application of Indigenous Plant-Based Vegetable Tanning Agent Extracted from *Xylocarpus granatum* in Semi-Chrome and Chrome Retanned Leather Production

Raju Kumar Das¹  0000-0002-3071-1925

Al Mizan^{2,3}  0000-0001-8577-9356

Fatema-Tuj-Zohra¹  0000-0002-2298-9978

Bahri Basaran³  0000-0002-0893-6300

Sobur Ahmed¹  0000-0001-9331-038X

¹Institute of Leather Engineering and Technology (ILET), University of Dhaka, Dhaka-1000, Bangladesh

²Department of Leather Engineering, Khulna University of Engineering & Technology (KUET), Khulna-9203, Bangladesh

³Department of Leather Engineering, Faculty of Engineering, Ege University, Bornova, Izmir 35100, Türkiye

Corresponding Author: Sobur Ahmed, soburahmed@du.ac.bd

ABSTRACT

Environmental issues are nowadays the prime concern worldwide for leather industries due to chrome containing solid and liquid wastes generated from the tannery. Therefore, experts are being encouraged in exploring alternative tanning agents. This study aimed at applying a novel vegetable tanning agent extracted from *Xylocarpus granatum* barks for the production of semi-chrome (SC) and chrome retanned (CR) leathers to reduce chromium use. Characterization of the SC and CR leathers was performed by Fourier Transform Infrared (FTIR) spectroscopy which revealed prominent tanning activity of the extracted tannins. The tanned leathers exhibited shrinkage temperatures of 112°C for SC and 103°C for CR leathers. The physico-mechanical properties were found as tensile strength >230 kg/cm², tear strength >30 kg/cm, grain cracking load >20 kg, distention at grain crack >7 mm, ball bursting load >38 kg, and distention at ball bursting >12mm that was comparatively acceptable according to UNIDO standard for shoe upper leathers.

1. INTRODUCTION

The leather industry is under pressure due to worldwide concerns environmentally as it releases huge amounts of effluents to the environment, particularly during the tanning process. Putrescible raw hides and skins, a by-product of the meat industry, are turned to be imputrescible through the tanning process. The transformation of raw hides and skins into leather involves several steps, i.e. pre-tanning, tanning, and post-tanning [1]. In tanning processes, tanning materials with various substances having crosslinking ability react with the moieties being isolated and activated of fibrous protein in which a series of complex preliminary attempts are executed to enhance the tanning reactions. Hence, leather making is a lengthy process and involves the use of many different

mechanical and chemical processes viz., soaking, liming, de-liming, pickling, tanning, post tanning, and finishing operations using several chemicals e.g., sodium hydroxide, lime, chlorides, sulfuric acid, formic acid, chromium, ammonium salts, metallic salt, different organic chemicals, enzyme etc. [2]. Among the processes, tanning is considered one of the important and unavoidable processes that protect the leather against microbial degradation. It influences the properties of the end product by stabilizing the raw skin collagen proteins with different tanning agents, e.g. mineral, vegetable, aldehyde, syntan, resin, and oil tannage [3]. Among the varieties of tanning agents, basic chromium sulphate accounts for 88-90% of total tannage consumption which provides excellent heat stability and strength properties to the leather [1,4]. However, environmental pollution is the only key concern for the use of chromium in

ARTICLE HISTORY

Received: 01.02.2022

Accepted: 07.07.2022

KEYWORDS

Vegetable tanning, FTIR, shrinkage temperature, physico-mechanical properties, strength properties

To cite this article: Das RK, Mizan A, Zohra FT, Basaran B, Ahmed S. 2022. Application of indigenous plant-based vegetable tanning agent extracted from *xylocarpus granatum* in semi-chrome and chrome retanned leather production. *Tekstil ve Konfeksiyon* 32(3), 258-264.

leather tanning, because only about 54-57% of chromium is consumed by pelt in the tanning and retanning process [3], and the remaining must be treated before being released into the environment. Alteration of Cr(III) to Cr(VI) by various environmental influences could be harmful and carcinogenic for human health and possibly is of a detrimental effect on the ecosystem. During the manufacturing and finishing process of the leather and leather products, the application of heat and UV radiation to the chrome tanned leather could convert chromium (III) to chromium (VI) [5, 6]. Furthermore, the human health risks associated with chromium-rich solid waste could impact respiratory, skin, and bone damage, renal problems, liver damage, kidney failure, infertility, cancer, and even birth defects [6-8]. Although chrome tanning has gained importance in leather manufacture, its advantage is overshadowed by its negative impact on the environment. Chromium wastes are released from tannery effluent to the environment due to low uptake by pelt; thereby, accumulating in the soil where it was discharged. However, vegetable tanning is an eco-friendly method as compared to the chemical tanning process like chrome tanning and also discharges minimum amounts of pollutants to the environment. Therefore, the total or partial substitution of chromium in leather production is an environmental demand that can outperform the advantages of chromium in leather manufacture.

Semi-chrome tanning and chrome re-tanning processes are the methods where the properties of leather could be approached to that of chromium leather by supplementation for lackings. Mimosa, quebracho, sumac, tara, valonea, divi-divi, oak, and chestnut etc. are the most widely used tannins in re-tanning and pre-tanning processes for semi-chrome and chrome re-tanned leather at present [9, 10]. Several researchers have previously investigated novel vegetable tanning systems based on tannins derived from alternative plant sources such as acacia seyal bark [1], acacia nilotica fruit [11, 12], acacia xanthoploea bark [12], hogenia abyssinica bark [12], acacia senegal bark [13, 14], henna extract [3], longan bark [15]. These vegetable tanning materials exhibited promising results; however, they are not practiced commercially.

Xylocarpus granatum (Family: Meliaceae) known as "Dhundul" in Bangladesh is generally found in low-lying, salt-tolerant forest and muddy areas of the Sundarban mangrove forest [16]. It's also found in East Africa, Polynesia, Thailand, Indonesia, Myanmar, Malaysia, India, China, and Australia's tropical regions [17, 18]. The bark of *X. granatum* has never been used as a new source of vegetable tanning material in pre-tanning and re-tanning. According to research published for dye extraction from this plant's bark, *Xylocarpus granatum* barks from mature plants may include tannin content and reddish-brown dye on a dry matter basis [18]. Also, this is a mangrove plant that has yet to be evaluated and classified as a tanning material. Several studies have indicated that the bark of several mangrove plants contains 16-48% tannin [19].

The objectives of this study were i) to evaluate *X. granatum* bark extract as a vegetable tanning substitute in the manufacture of semi-chrome and chrome retanned leather, ii) to examine and analyze the tanning properties of the semi-chrome and chrome-retanned leather processed by *X. granatum* bark whether it meets the tanning requirements, and iii) to analyze the strength properties, e.g. tensile strength, tear strength, grain cracking load, shrinkage temperature, and distention at grain crack of leather tanned with the combination of extracted tanning materials and chromium, and to verify them with the concerned recommended values of United Nations Industrial Development Organization (UNIDO).

2. MATERIAL AND METHOD

2.1 Material

Xylocarpus granatum, also known as "Dhundul," was collected from the Sundarban, the world's largest mangrove forest, along the Malancha River, situated 16 kilometers south of Shyamnagar, Satkhira, Khulna, Bangladesh. The Sundarban covers 6017 square kilometers in Bangladesh's southern region [20, 21]. The bark of *X. granatum* was collected from three different matured plants and mixed thoroughly for identical sample preparation. Wet salted 06 pcs mature goat skins with approximately 6-7 square feet each were taken for the leather processing. These wet salted goat skins were collected from the Posta hides/skins market, Dhaka, Bangladesh. Leather processing chemicals were collected from the local market of Bangladesh other than standards.

2.2 Methods

2.2.1 Application of extracted tanning materials (*X. granatum* bark) in semi-chrome and chrome retanning processes

Extract of *X. granatum* bark (vegetable tanning agent) was prepared using 100% methanol by rotary evaporator in a previous study of the same author and found 31.22% extraction efficiency of tannin [22]. The extracted tannin was found to be a condensed type of tannin whereas the *Xylocarpus granatum* bark tannin contained 48% of condensed tannin [22]. It was applied in leather to produce semi-chrome and chrome retanned leather for evaluating their necessary properties.

The soaking to pickling process (a common series of steps) of leather processing was carried out in this study maintaining the conventional process. The pre-tanning process was done for both conventional with chrome tanning and experimental with developed tannin respectively following the recipe depicted in Table 1.

After aging (pile-up for 8 days) of the leather, re-tanning and post-tanning processes were carried out for both chrome re-tanned and semi-chrome leather respectively by following the recipe shown in table 2 and table 3. The

wetback and fatliquoring processes were done according to the conventional procedure, thus not mentioned in the table.

Table 1. Pre-tanning with chrome and vegetable tannin agent (developed) of goat skin

Wet blue process			
Percentage	Chemicals	Duration (min)	Observation
In the pickle liquor at pH 2.8			
4	Basic chromium sulfate (33%)	30	
1	Chrome stable fat (Remsol OCS)	30	
0.20	Fungicide		
4	Basic chromium sulfate (33%)	60	Penetration 100%
1.50	Sodium formate	30	
0.40	Sodium bicarbonate	3 steps after 20 min with 2 hours additional run	pH 4.0
0.10	Fungicide	45	pH 4.0
Drained and piled up			
Vegetable pre-tanning (Developed Tannin)			
Percentage	Chemicals	Duration (min)	Observation
Pelt in pickle bath at pH 2.8			
1.50	Sodium formate	30	pH 3.5-4.0
0.10	Fungicides (Busan 30L)		
0.10	Polyphosphate (RW)	30	
0.20	Sequestering agent (Trilon B)		
1	Hypo	30	
3	Developed tannin	2 steps 60 min and 30 min	
0.5-0.8	Sodium bicarbonate (1:20)	3 steps 20 min and 120 min	
0.10	Fungicide (Busan 30L)	35	pH 3.8-3.9
Drained and piled up			

Table 2. Tanning, and post tanning process of goat skin for chrome retanned leather

Neutralization and retanning			
Percentage	Chemicals	Duration (min)	Observation
Wet blue leathers were taken and prepared for neutralization			
150	Water at 45°C		
3	Neutralizing syntan (Naphthalene syntan)	50	pH 5
2	Sodium formate		
4	Acrylic resin	20	
1	Sequestering agent (Trilon B)		
6	Developed tanning agent		
4	Replacement syntan (Dihydroxydiphenyl sulphonic acid)	60	
3	Phenolic replacement (Phenol sulphonic acid) syntan		
0.50	Synthetic fat (Lanoline based)		
6	Developed tanning agent		
3	Replacement syntan (Dihydroxydiphenyl sulphonic acid)	60	
3	Phenolic replacement syntan (Phenol sulphonic acid) syntan		
1	Dispersing agent		
6	Developed tanning agent		
3	Replacement syntan (Dihydroxydiphenyl sulphonic acid)	60	
3	Phenolic replacement syntan (Phenol sulphonic acid)		
1	Fatliquor (Lanoline based)		
Left overnight			
0.50	Formic acid	2 steps after 15 min interval	
Drained and washed well			

Table 3. Tanning and post tanning process of goat skins for semi-chrome leather

Acid wash and rechroming			
Percentage	Chemicals	Duration (min)	Observation
150	Water	25	pH 3
0.40	Formic acid		
6	Basic chromium sulfate (33%) Chrome syntan Sodium formate Chrome stable fat (Remsol OCS)	60	
2			
1			
1			
1	Sodium formate	40	
1.50	Neutralizing syntan (Naphthalene syntan)		
2	<i>X. granatum</i> bark tannin (Developed tannin)		
Left overnight, run 20 min next day, drained and washed well			
Neutralization			
150	Water at 45°C	45	pH 5
2	Neutralization syntan (Naphthalene syntan)		
0.50	Sodium formate		
0.50	Synthetic fat (Lanoline based)		
Drained and washed well			
Re-tanning			
150	Water at 45°C	20	
3	Acrylic resin		
0.50	Sequestering agent (Trilon B)	65	
6	Develop tanning agent		
3	Replacement syntan (Dihydroxy diphenyl sulphonic acid)		
3	Phenolic replacement (Phenol sulphonic acid) syntan		
1	Dispersing agent		
1	Synthetic fat (Lanoline based)		
100	Water at 45°C	Left overnight	
The next day run 20 min, drained, and washed well			

2.2.2 Determination of hydrothermal stability

The shrinkage temperature (T_s) of pre-tanned and re-tanned leather was measured to determine its hydrothermal stability. The leather samples were cut (50mm×12mm) across the backbone and carried out the test following the standard method IUP-16 [23]. For this analysis, three replicates were examined, and the mean with standard deviation was reported in this study.

2.2.3 Determination of the phenolic compound in tanned leather using FT-IR

The functional groups and other polyphenolic compounds were identified using Fourier Transform Infrared (FT-IR) spectroscopy such as -OH group, aromatic C-H stretch, -CO group, C-H bending, and carbon-carbon double bond stretch present in the tanned leather. The FT-IR spectra were examined using IRPrestige 21, Shimadzu (Japan) in the range of 4000–400 cm^{-1} .

2.2.4 Determination of physico-mechanical properties of tanned leather

The tanned leather (semi-chrome and chrome re-tanned) was cut for sampling into specific measurements for a specific test done in this study and conditioned the cut sample maintaining temperature $25\pm 2^\circ\text{C}$, relative humidity $65\pm 2\%$, and 48 hours by following the ISO-2419 standard method

[24]. Tensile strength, percentage of elongation, tear strength, resistance to grain cracking, and distension at grain crack, ball bursting strength, and distension at ball burst were carried out to assess the mechanical and physical characteristics of semi-chrome and chrome re-tanned leather [25-27]. In this study, all experiments were checked three times for both parallel and perpendicular to the backbone and represented as the mean with standard deviation.

3. RESULTS AND DISCUSSION

3.1 Hydrothermal stability

The shrinkage temperature (T_s) of the leather sample represents the hydrothermal stability of the leather and table 4 describes the T_s values of pickle pelt, wet blue, pre-tanned (developed tannin), semi chrome, and chrome retanned crust leather for both semi-chrome and chrome re-tanned leather. The T_s for wet blue and experimental wet-tanned leather were found at 100.67°C and 78.67°C respectively shown in table 4. The statistics reported previously for shrinkage temperature on pre-tanning with chromium sulfate ranges up to 120°C [9, 28]. The shrinkage temperature of the pickled pelt was around 58°C and increased to 79°C after tanning (tanned with *X. granatum* extract) which might be due to the cross-linking between reactive moieties of collagen and polyphenolic compounds of *X. granatum*. The T_s of semi-chrome leather was 103.34°C and chrome re-tanned leather

was found at 112.34°C which suggests that the extracted tanning material from *X. granatum* could substitute conventional mimosa and quebracho vegetable tannins with chrome in terms of increasing hydrothermal stability. The size of polyphenol molecules and the number of -OH groups determine the rise in shrinkage temperature. The kinetic stability of linkages between the tanning agent molecules and the protein's side-chain determines the shrinkage temperature [29]. In semi-chrome leather, pre-tanning with developed tannin and the addition of chromium to the re-tanning process could increase the cross-linking between polyphenol and collagen, resulting in a stable complex matrix where chromium acts as a ligand [29]. As a result, the hydrothermal stability of the tanned leather showed an elevated level.

Table 4. Shrinkage temperature (T_s) of pickle, wet blue, and leather tanned by developed tannin (mean \pm standard deviation)

Samples	Shrinkage Temperature °C
Pickle pelt	58.67 \pm 1.15
Wet blue	100.67 \pm 1.52
Experimental wet-tanned leather (Extracted <i>X. granatum</i> tannin)	78.67 \pm 1.15
Chrome re-tanned leather	112.34 \pm 1.53
Semi-chrome leather	103.34 \pm 2.05

3.2 Analysis of the phenolic compound in tanned leather using FT-IR

FTIR Spectra of the pickle pelt, semi-chrome, and chrome re-tanned leather are shown in figure 1. The tanned leather sample showed the presence of O-H stretching, C=O stretching, aromatic C-H stretching, C=C ring stretching, C-H bending, C-O stretching, Out-of-plane C-H bending compared with pickle pelt. FTIR spectrum of chrome re-tanned and semi-chrome leather showed respectively a relatively broadband at 3325 cm^{-1} , and 3425 cm^{-1} representing the presence of -OH groups of polyphenols such as tannin and flavonoids which is in congruence with the other studies [30-33]. On the other hand, the pickle pelt showed a relatively spike-type band at 3383 cm^{-1} representing the presence of the amino group of the protein collagen. Besides, a medium band was found at 2935 cm^{-1} for both semi-chrome and chrome re-tanned leather that

indicates the presence of aromatic C-H stretching in these leather samples whereas pickle pelt showed no band at this region. Again for both leather samples strong peak at 1716 cm^{-1} and 1612 cm^{-1} was noticed while the pelt showed peaks at 1643 cm^{-1} that indicate the presence of C=O stretching and C=C ring stretching with a substituted benzene ring. In this study, peak(s) at 1519 cm^{-1} and 1516 cm^{-1} was found for both leather samples which stipulate the presence of catechin and its near derivatives (e.g., epicatechin) in the sample. Therefore, the leather tanned with the extracted *Xylocarpus granatum* bark tannins showed vegetable tanning material-rich compounds in it because it confirmed the presence of several polyphenolic groups in its chain.

3.3 Physico-mechanical properties of tanned leather

Table 5 shows the physico-mechanical characteristics of leathers investigated in this study. The tensile strength of experimental chrome re-tanned and semi-chrome leather was 243 kg/cm^2 and 364 kg/cm^2 respectively, which is much greater than the acceptable quality levels declared by United Nations Industrial Development Organization's (UNIDO). Similar investigations on indigenous crossbred sheepskin done in Ethiopia and Turkey revealed average tensile strengths of combination tanned leather of 249 kg/cm^2 and 218 kg/cm^2 respectively [3, 34]. Further, the experimental semi-chrome leather had a very high percentage of elongation (41.12%), which is considerably above the chrome re-tanned leather (35.47%) and is a well-accepted value suggested by UNIDO (Table 5). Therefore, the experimental leather could stretch and may hold more loads without breaking. As a mangrove plant, *X. granatum* bark tannin contains flavonoid chemicals (e.g., catechin hydrate, epicatechin, etc.) and phenolic hydroxyl groups, which may react with collagen via numerous hydrogen bonding and quinoid processes, which potentially increase leather strength. The variation of tensile strength varies on the composition of the tanning agents, type of tannin, quantity of tannin, the control of beam-house operations, pre-tanning, tanning, post-tanning and /or methods of tanning [12]. The higher strength properties of the experimental leather could be due to the high content of condensed tannin (48%).

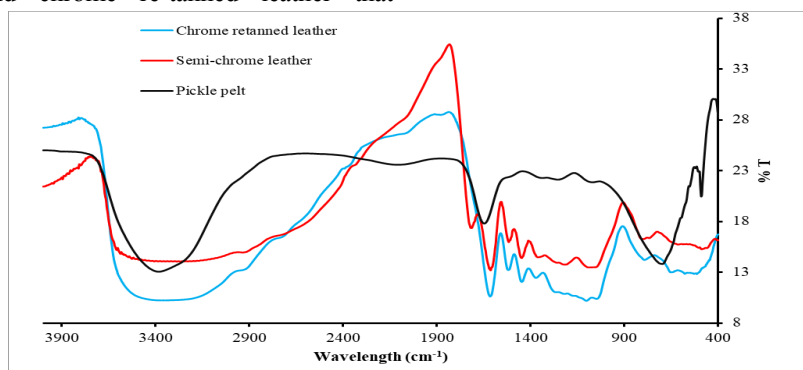


Figure 1. FTIR spectra of pickle pelt, semi-chrome, and chrome re-tanned leather

Table 5. Physico-mechanical properties of semi-chrome and chrome re-tanned leathers (mean \pm standard deviation)

Parameters	Chrome re-tanned leather	Semi-chrome leather	Acceptable values [35]
Tensile strength (kg/cm ²)	243.46 ± 12.76	364.71 ± 19.52	≥ 230
Elongation (%)	35.47 ± 4.15	41.12 ± 1.28	30 – 45
Tear strength (kg/cm)	31.34 ± 3.01	46.92 ± 4.06	≥ 30
Grain crack load (kg)	28 ± 1.00	35 ± 3.60	≥ 20
Distension at grain crack (mm)	12.71 ± 0.46	13.57 ± 0.98	≥ 7
Ball burst load (kg)	38.67 ± 1.15	44.67 ± 2.31	-
Distension at ball burst (mm)	14.89 ± 0.98	15.98 ± 1.94	-

In this study, for tearing strength, the chrome re-tanned leather showed 31.34 kg/cm and 46.92 kg/cm for semi-chrome leather. Other research has shown tear strength of 39.79 kg/cm when using 20% nilotica L. pods tannin [34] which is similar to this study. Also, the type of the tannin and the regulation of beam-house activities seem to be highly influencing parameters for leather tearing strength [12, 36].

The lastometer test which measures the real cracking and bursting load with distension is another essential physical test for evaluating the overall quality and strength of the leather. Grain cracking and ball bursting loads were found to be 28 kg and 38.67 kg for chrome re-tanned leather and 35 kg and 44.67 kg for semi-chrome leather respectively. Also, the distention at grain crack and ball burst for chrome re-tanned leather were 12.71 mm and 14.89 mm respectively whereas semi-chrome leather showed 13.57 mm and 15.98 mm respectively (Table 5) which are far beyond the minimum recommended value set by UNIDO for distention at grain crack (6.5 mm) and distention at ball burst (7.0 mm) respectively for all types of leather. For various sheep leathers, several researchers reported distention at grain fracture 6.74 mm/9.9 mm and distention at ball burst 7.72 mm/ 10 mm [37]. The types of tannin ingredients, pre-tanning procedures, tanning, and post-tanning processes are considered to be the influencing factors of the grain cracking load and ball-bursting load of leather [12].

4. CONCLUSION

The experimental semi-chrome and chrome retanned leathers exhibited excellent strength properties,

hydrothermal stability, and smoothness. The high shrinkage temperature obtained in this study which is greater than 102 °C made the leathers usable parallel to conventional leather and provided an opportunity to be utilized as well alternative to the conventional SC and CR leathers. In addition, tensile strengths over 243 kg/cm² with 35-41% elongation provided the produced leathers better strength with proper flexibility for shoe uppers. Further, the main fact is that *Xylocarpus granatum* naturally grown in the southern part of Bangladesh (Sundarban region) could be regarded as a renewable material because it regenerates bark (after a few months of being peeled off). Hence, its utilization in tanning could pave the way for sustainable leather processing. Apart from our findings, as an indigenous source, cheaper sale price than that of commercial mimosa and quebracho, with greater extraction efficiency, and environmentally safe characteristics could make this material a potential tanning agent for future use. It is possible to conclude that *Xylocarpus granatum* bark extracts can be utilized as pre-tanning and retanning agents in leather tanning.

ACKNOWLEDGMENT

The authors wish to express their gratitude to Prof. Dr. Mohammed Mizanur Rahman, Director, Institute of Leather Engineering and Technology, University of Dhaka, Prof. Dr. Md. Zahangir Alam and Prof. Dr. Mohammad Nurnabi, Department of Applied Chemistry and Chemical Engineering, University of Dhaka, for their laboratory support. This work was partially funded by the Ministry of Science and Technology, Bangladesh under the National Science and Technology (NST) fellowship (Group: Physical Science, Reg. No: 317).

REFERENCES

- Hussein SA. 2017. Utilization of tannins extracts of acacia seyal bark (taleh) in tannage of leather. *Journal of Chemical Engineering and Process Technology* 8, 334-342.
- Ahmed S, Fatema-Tuj-Zohra, Mahdi MM, Nurnabi M, Alam MZ, Choudhury TR. 2022. Health risk assessment for heavy metal accumulation in leafy vegetables grown on tannery effluent contaminated soil. *Toxicology Reports* 9, 346-355.
- Adiguzel-Zengin AC, Zengin G, Kilicarislan-Ozkan C, Dandar U, Kilic E. 2017. Characterization and application of acacia nilotica l. as an alternative vegetable tanning agent for leather processing. *Fresenius Environmental Bulletin* 26(12), 7319-7326.
- Mahdi H, Palmina K, Gurashi AG, Covington D. 2009. Potential of vegetable tanning materials and basic aluminum sulphate in sudanese leather industry. *Journal of Engineering Science and Technology* 4, 20-31.
- Basaran B, Ulas M, Bitlisli BO, Aslan A. 2008. Distribution of Cr (III) and Cr (VI) in chrome tanned leather. *Indian Journal of Chemical Technology* 15, 511-514.

6. Hedberg YS, Liden C, Odnevall Wallinder I. 2015. Chromium released from leather-I: exposure conditions that govern the release of chromium (III) and chromium (VI). *Contact Dermatitis* 72(4), 206-215.
7. Al-Mizan, Juel MAI, Alam MS, Pichtel J, Ahmed T. 2020. Environmental and health risks of metal-contaminated soil in the former tannery area of Hazaribagh, Dhaka. *SN Applied Science*. <https://doi.org/10.1007/s42452-020-03680-4>
8. Ahmed S, Fatema-Tuj-Zohra, Khan MSH, Hashem MA. 2017. Chromium from tannery waste in poultry feed: A potential cradle to transport human food chain. *Cogent Environmental Science* 3, 1312767.
9. Kilicariskan C, Ozgunay H. 2012. Ultrasound extraction of valonea tannin and its effects on extraction yield. *JALCA* 107, 394-403.
10. Galvez JMG, Riedl B, Conner AH. 1997. Analytical studies on Tara tannins. *Holzforchung* 51, 235-243.
11. Mahdi H, Palmira K, Glavtch I. 2006. Characterization of *Acacia nilotica* as an indigenous tanning material of Sudan. *Journal of Tropical Forest Science* 18, 181-187.
12. Kuria A, Ombui J, Onyuka A, Sasia A, Kipyegon C, Kaimenyi P, Ngugi A. 2016. Quality evaluation of leathers produced by selected vegetable tanning materials from laikipia county, Kenya. *IOSR Journal of Agriculture and Veterinary Science* 9(4), 13-17.
13. Elgailani IEH, Ishak CY. 2014. Determination of tannins of three common acacia species of Sudan. *Advances in Chemistry* Article ID 192708.
14. Elgailani IEH, Ishak CY. 2016. Methods for extraction and characterization of tannins from some acacia species of Sudan. *Pakistan Journal of Analytical and Environmental Chemistry* 17(1), 43-49.
15. Chai WM, Huang Q, Lin MZ, Ou-Yang C, Huang WY, Wang YX, Xu KL, Feng HL. 2018. Condensed tannins from longan bark as inhibitor of tyrosinase: structure, activity, and mechanism. *Journal of Agriculture and Food Chemistry* 66, 908-917.
16. Shahid-ud-daula AFM, Basher MA. 2009. Phytochemical screening, plant growth inhibition, and antimicrobial activity studies of *Xylocarpus granatum*. *Malaysian Journal Pharmaceutical Sciences* 7(1), 9-21.
17. Baba S, Chan HT, Kainuma M, Kezuka M, Chan EWC, Tangah J. 2016. Botany, uses, chemistry and bioactivities of mangrove plants-III: *Xylocarpus granatum*. *ISME/GLOMIS Electronic Journal* 14(1), 1-4.
18. Pisitsak P, Hutakamol J, Jeenapak S, Wanmanee P, Nuammaiphum J, Thongcharoen R. 2016. Natural dyeing of cotton with *Xylocarpus granatum* bark extract: dyeing, fastness, and ultraviolet protection properties. *Fibers and Polymers* 17(4), 560-568.
19. Covington T. 2009. *Tanning Chemistry: The Science of Leather*. UK: The Royal Society of Chemistry.
20. Brown BE. 1997. *Integrated coastal management-South Asia*. Department of International Development, University of Newcastle, UK.
21. Zafar TB, Khan GM. 2018. A geographical overview of sundarban: the largest mangrove forest of Bangladesh. *International Journal of Geology, Agriculture and Environmental Sciences* 6, 9-10.
22. Das RK, Mizan A, Zohra FT, Ahmed S, Ahmed KS, Hossain H. 2022. Extraction of a novel tanning agent from indigenous plant bark and its application in leather processing. *Journal of Leather Science and Engineering* 4, 18.
23. International Union of Leather Technologist and Chemist Societies. IUP-16. 2001. Measurements of shrinkage temperature up to 100°C. *Society of Leather Technologist and Chemist*.
24. ISO-2419. 2012. Leather-physical and mechanical tests. Sample preparation and conditioning.
25. International Union of Leather Technologist and Chemist Societies. IUP-06. 2001. Measurement of tensile strength and percentage of elongation. *Society of Leather Technologist and Chemist*.
26. International Union of Leather Technologist and Chemist Societies. IUP-08. 2001. Measurement of tearing strength. *Society of Leather Technologist and Chemist*.
27. ISO-3378/IUP-12. 2002. Leather-physical and mechanical tests. Determination of resistance to grain cracking and grain crack index.
28. Zengin AC, Crudu M, Maier S, Deselnicu V, Albu L, Gulumser G, Bitlisli BO, Basaran B, Mutlu MM. 2012. Eco-leather: chromium-free leather production using titanium, oligomeric melamine formaldehyde resin, and resorcinol tanning agents and the properties of the resulting leathers. *Ekoloji* 21, 17-25.
29. Kasmudjiastuti E, Pidhatika B, Griyanitasari G, Pahlawan IF. 2018. November. The effect of alum addition on shrinkage temperature, chemical properties, and morphology in the manufacture of vegetable-tanned leather. IOP Conference Series: Materials Science and Engineering. 602(012044), Conference on Innovation in Technology and Engineering Science, Padang, Indonesia.
30. Yallappa S, Manjanna J, Sindhe MA, Satyanarayan ND, Pramod SN, Nagaraja K. 2013. Microwave assisted rapid synthesis and biological evaluation of stable copper nanoparticles using T. arjuna bark extract. *Spectrochimica Acta Part A: Molecular and Biomolecular Spectroscopy*. 110, 108-115.
31. Ricci A, Olejar KJ, Parpinello GP, Kilmartin PA, Versari A. 2015. Application of Fourier transform infrared (FTIR) spectroscopy in the characterization of tannins. *Applied Spectroscopy Reviews* 50, 407-442.
32. Foo LY. 1981. Proanthocyanidins: gross chemical structures by infrared spectra. *Phytochemistry* 20, 1397-1402.
33. Silva PMS, Fiaschitello TR, Queiroz RS, Freeman HS, Costa SA, Leo P, Montemor AF, Costa SM. 2020. Natural dye from croton urucuranabail bark: extraction, physicochemical characterization, textile dyeing and color fastness properties. *Dyes and Pigments* 173, 1-14.
34. Musa AE, Gasmelseed GA. 2013. Development of eco-friendly combination tanning system for the manufacture of upper leathers. *International Journal of Advance Industrial Engineering* 1(1), 9-15.
35. United Nations Industrial Development Organization. 1996. Acceptable quality standards in the leather and footwear industry. Vienna, Austria. United Nations Industrial Development Organization (UNIDO).
36. Basaran B, Iscam M, Bitlisli B, Asian A. 2006. Heavy metal content of various finished leathers. *Journal of Society of Leather Technologists and Chemists* 90, 229-234.
37. Lawal AS, Odums CP. 2015. Tanning of different animal skin/hides and study of their properties for textile applications. *British Journal of Applied Science and Technology* 6, 588-594.

Characterization of High-Pressure Fuel Hose with Braided Reinforcement

Mustafa Ertekin¹  0000-0002-5492-7982

Gözde Ertekin¹  0000-0003-2150-9255

Gökçe Bakiler²  0000-0002-0422-5050

İrem Seçkin İşcan²  0000-0002-3960-2506

Seçkin Erden³  0000-0002-8560-3585

¹Ege University, Faculty of Engineering, Department of Textile Engineering, 35100, Bornova, İzmir, Türkiye

²Erenli Kauçuk ve Plastik Sanayi, 35170, Kemalpaşa, İzmir, Türkiye

³Ege University, Faculty of Engineering, Department of Mechanical Engineering, 35100, Bornova, İzmir, Türkiye

Corresponding Author: Gözde Ertekin, gozde.damci@ege.edu.tr

ABSTRACT

This study aims to investigate the effect of material type and braiding angle on the performance characteristics of the reinforced multi-layered hose, to manufacture a high-pressure fuel hose. For this purpose, NBR (Acrylo-Nitrile Butadiene rubber)/CPE (chlorinated polyethylene) fuel hose was manufactured using a single-screw extruder and for the production of the reinforcement layer, braiding technology was used. With an attempt to discuss the effect of braiding angle on the performance characteristics of the reinforced multi-layered hose, the take-up speed of the radial braiding machine was altered. E-glass, aramid, carbon, polyester, and basalt yarns were used for the production of the braided layer. Then CPE (chlorinated polyethylene) rubber was extruded for the cover application. Performance properties of the fuel hose such as hardness, ply adhesion, vacuum collapse bursting pressure, and diametric expansion were measured and evaluated according to the requirements of the related standards. The results revealed that, with increased braiding take-up speed, ply adhesion, vacuum collapse, and diametric expansion properties of hoses increase, while hardness, permanent deformation, and bursting pressure of hoses decrease. It has been determined that NBR/Basalt/CPE fuel hose produced in 4m/min braiding take-up speed provided optimum functional and adhesion properties, because of its hardness, permanent deformation, bursting, and vacuum test values at 25°C are within the limit. Additionally, the results were verified by running finite element analysis (FEA) using the ANSYS simulation program.

1. INTRODUCTION

Hoses are manufactured using a range of materials and configurations depending on their function. There are several types of hoses such as air intake, radiator, fuel-oil, vacuum, breather, power steering, and brake hoses. They can be used in a wide range of application areas like automotive, construction equipment, railways, defense, farm track equipment, etc. These hoses can be produced using a single material, or multi-layered structure and reinforcement layers can also be used to increase durability, resistance against coolant, fuel oil, chemicals, high

pressure, vacuum, etc. Formed hoses that are normally with reinforcement are mandrel built. First, the tube is extruded with a specific ID, and then the reinforcement (braiding or knitting) is applied to it followed by crosshead extrusion for cover applications with specific wall thickness [1]. There are several studies carried out on the deformation analysis and fatigue damage of the braided composite hoses used in automotive industry [2-17]. This study differs from the previous researches by using braiding technique with technical yarns during the production of the fuel hoses.

In the automotive industry, the transportation of fuel and air

ARTICLE HISTORY

Received: 06.10.2021

Accepted: 23.05.2022

KEYWORDS

High pressure, rubber composites with technical textile reinforcement, high-performance yarns, braiding, fuel hose.

To cite this article: Ertekin M, Ertekin G, Bakiler G, İşcan İS, Erden S. 2022. Characterization of high-pressure fuel hose with braided reinforcement. *Tekstil ve Konfeksiyon*, 32(3), 265-276.

are critical factors for the operation. Fuel hoses are designed for the transportation of fuel oils in engines and fluids in hydraulic systems. Hoses made from rubber have been the primary means of carrying fuel or air although metal tubes have also been used in some instances. A fuel line hose consists of an inner tube, a textile reinforcement, and an outer layer. An inner tube has to be resistant to variable fluids and heat acc. to the user requirements. These rubber types would be NBR (acrylonitrile butadiene rubber), ECO (epichlorohydrin rubber), ACM (acrylic rubber), or FKM (fluorocarbon rubber). A textile reinforcement is used to increase the functionality of the hose. Moreover, an outer layer should be resistant to ozone gas, fuel, and heat again acc. to the user requirements. These rubber types would be CPE (chlorinated polyethylene rubber), CR (chloroprene rubber), ECO (epichlorohydrin rubber), ACM (acrylic rubber), or FKM (fluorocarbon rubber) (Fig.1). The recent trend has been led to develop multilayer hoses using hybrid materials with special functionalities and specific requirements [1, 18].

Nitrile rubber is used in oil and fuel seals and hoses in the automotive industry due to its high abrasion resistance and chemical resistance. This polymer has good oil and fuel resistance and heat resistance, but it has low permeability, poor electrical isolation, weak stretching feature, and ozone resistance Nitrile is a Butadiene-Acrylo Nitrile (ACN) polymer. ACN ratio varies between 18-50% in nitrile rubber mixes. Nitrile rubber has a polar structure thanks to

the acrylonitrile monomer in it and thus has high fuel and oil resistance features [19].

The CPE (Chlorinated Polyethylene) polymer is classified according to the Cl content. These ratios are between 25% and 42%. It has good thermal stability, oil resistance, ozone, and water resistance, and also its resistance to burning is good. It can be used in the cable industry and in the production of all kinds of extrusion and molded parts where resistance to air, oil, and chemicals is required [19].

There are several methods such as braiding, spiraling, helical wrapping, knitting, and circular weaving for the manufacture of hoses [21]. Braiding, which is also used in this study, is defined as a textile process of intertwining at least three parallel strands (or yarns) of fiber to manufacture narrow fabrics like cords and ropes with non-orthogonal fibre orientation or to cover (overbraid) some profile [22-24]. The braiding technique is mainly used for the production of smaller bore hoses, up to around 50 mm internal diameter, particularly for medium to high-pressure applications, such as automotive brake hoses [21].

Fuel hoses provide the fuel in vehicles to reach the engine from the tank. Fuel systems can vary from several interconnected circuits, depending on the operating pressures, functions, and engine capacity of these circuits. Fuel hoses used in fuel systems are designed according to high operating pressure, temperature, and chemicals to be exposed (Fig. 2).



Figure 1. Layer configuration of a fuel hose [20]

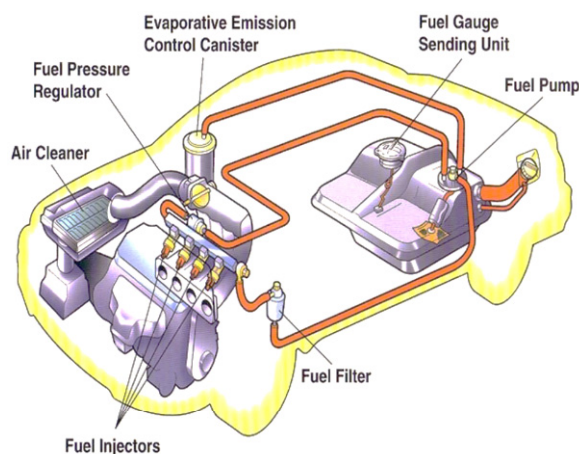


Figure 2. Example of fuel system [25]

Especially in recent years, the significant decrease in petroleum reserves and the economic concerns have accelerated the alternative fuel production activities of fuel oil producers. While the search for alternative fuel use in the sector continues rapidly, the use of existing fuel (diesel, gasoline) resources in an efficient manner and with the least harm to the environment has come to the fore and the issue has now become supported by laws. Under the main heading that the automobile engine works with less fuel, with more efficiency, and with less damage to the environment, fuel permeability has been brought to the agenda for all products used in fuel systems and studies have been initiated in this regard. Achieving the permeability limit in fuel hoses can be possible with the improvement studies to be carried out on the following matter [26]:

- Using high-performance elastomers,
- To produce two-component rubber hoses,
- Using different materials together with rubber,
- Improving the chemical properties of the hose,
- To install a material with low permeability between the two layers.

Two-component hose production is a preferred method because it means to implement new technology, the result to be achieved serves the targeted purpose with all parameters and it allows competing globally. Because markets now demand products that are cheaper, lighter, more robust, and more aesthetically appealing [26]. Additionally, commercial fuel hoses used in industry are manufactured by using two-component hose production method by combining the rubber hoses with circular knitting technique, which has disadvantages such as needle breakages and consequently productivity and labour losses.

This study aims to investigate the effect of material type and braiding angle on the performance characteristics of the reinforced multi-layered hose, to manufacture high-pressure fuel hoses. For this purpose, NBR (Acrylo-Nitrile Butadiene rubber)/CPE (chlorinated polyethylene) fuel hose was manufactured and for the production of the reinforcement layer, braiding technology was used. With an attempt to discuss the effect of braiding angle on the performance characteristics of the reinforced multi-layered hose, the take-up speed of the radial braiding machine was altered. E-glass, aramid, carbon, and basalt yarns were used for the production of biaxial braided fabrics. Then CPE (chlorinated polyethylene) rubber was again used for the cover application. Some performance properties of the fuel

hose such as hardness, ply adhesion, vacuum collapse bursting pressure and diametric expansion were measured and evaluated according to the requirements of the related standards.

2. MATERIAL – METHOD

2.1. Material

This paper investigates the performance properties of a NBR (Acrylo-Nitrile Butadiene rubber)/CPE (chlorinated polyethylene) fuel hose reinforced with braided structures. For this purpose, NBR and CPE were used as inner and outer layers of the fuel hoses, respectively. Additionally, E-glass, aramid, carbon, and basalt yarns were used as textile reinforcement in the multi-layered fuel hose.

NBR rubber mixture was used in the inner layer of the hose construction with its high fuel resistance feature. The recipe consists of NBR polymer, filler, plasticizer, additional chemicals, and curing agents. In rubber mixture recipes, the amount of ingredients is given proportional to 100 parts of rubber (PHR; “Part per Hundred Rubber”) by weight in the recipe. Total weight is related to banbury mixer volume. In this study, NBR polymer containing a 33 % ACN ratio. A peroxide vulcanization system was used as a vulcanization system to strengthen the adhesion of the NBR rubber mixture with the second layer rubber mixture and to improve the physicomechanical properties. The recipe of NBR rubber mixture following the MS263-20 International Automotive material test standard was used in the study.

The CPE rubber mixture was coated on the braided layer and formed the outer layer of the hose. The recipe consists of NBR polymer, filler, plasticizer, additional chemicals, and curing agents. In the recipe, CPE polymer containing above 33% Cl value, which is the optimal % Cl value of CPE rubber to increase oil and fuel resistance. A peroxide curing system was used as a curing system. The recipe of CPE rubber mixture following the MS263-20 International Automotive material test standard was used in the study.

The specifications of the yarns used as textile reinforcement are listed in Table 1.

Table 1. The specifications of the yarns [27]

Type of yarn	Yarn count (tex)	Number of filaments	Tensile strength (GPa)	Elongation (%)
Carbon	-	3K	230-600	1.5-2
Basalt	132	-	93-110	3.1-6
E-glass	300	-	72.5-75.5	4.7
Para-aramid	110	-	71-140	2.8-3.6
Polyester HT	167	-	1.1	14.5

2.2. Production of NBR and CPE rubber mixtures of the fuel hoses

The raw materials specified in the NBR and CPE rubber mixture recipes were weighed in an automatic formulation-weighing machine. Rubber mixture production's first step has been done with the help of intermesh rotor type Banbury, which has a capacity of 50 lt (Fig. 3a). Rotor cycle, pressure and temperature values, time, and cooling water system temperature can set on the system of banbury. In this study, different set parameters were used for the production of NBR and CPE rubber mixtures. Production parameters of the mixtures are listed in Table 2.

The second step of rubber mixture production was done with open mill mixing (Fig. 3b). Mixtures were transferred separately to the open mill to get the final shape. In open mill thickness and width of can set. The final shape values

of NBR and CPE values were 10 mm of thickness, 80 mm of width.

The cooling step was done with the help of a batch-off system as a final step of rubber mixture production (Fig. 3c). According to the open mill, mixtures were transferred separately to the batch-off system to cool down the mixture. Mixtures were passed inside of the cooling pool and left to cool.

2.3. Production of the inner layer of the fuel hoses

The inner layer of the fuel hose was produced by using NBR rubber mixture in a single-screw extruder (Fig. 4a). The setting parameters of the extruder according to the type of NBR rubber mixture are given in Table 3.

Table 2. Production parameters of the NBR and CPE mixtures

Type of mixture	Process no	Definition of process	Time(s)/ Temperature (°C)	Rotor cycle (rpm)	Pressure (bar)
NBR rubber mixture Banbury	1	NBR rubber mixing	5s	49	50
	2	Adding filler+plasticizer+chemicals+curing agents	65°C	49	50
CPE rubber mixture Banbury	1	CPE rubber mixing	30s	49	50
	2	Adding filler+plasticizer+chemicals+curing agents	75°C	49	50

*Cooling water temperature: 30 °C



(a)



(b)



(c)

Figure 3. (a) Intermesh banbury with the capacity of 50 lt, (b) Open mill, (c) Batch-off system



(a)



(b)

Figure 4. (a) Rubicon extruder, (b) T head extruder

Table 3. The setting parameters of extruders used in the production of inner and outer layers of hoses

Parameter	Rubicon	
	single-screw extruder	T head extruder
Head temperature (°C)	75	75
1 st area temperature (°C)	70	70
2 nd area temperature (°C)	65	65
Feed temperature (°C)	60	60
Screw cycle (rpm)	8	9
Pulling speed (m/min)	7	8
Vacuum pressure (mmHg)	650	670
Head pressure (bar)	130	135
Cooling water temperature (°C)	23-24	23-24
Dimensional stability of the product (%)	2	2

2.4. Production of the braided hoses

After the production of the inner tube of the hoses, five different yarns, whose specifications were listed in Table 1, were used for the production of 2D biaxial braided reinforced hoses. The braiding process was performed on a radial braiding machine built up in laboratory with 48 carriers (Fig. 5) in three different take-up speeds (4, 6, and 8 m/min) which resulted in different braid angles (65° , 55° , 45° , respectively) and braid cover factors. A low carrier speed with a higher take-up speed results in loose braided structures with low braiding angles, which have a low cover factor [28]. Fig.6 shows the obtained braiding angle values at three different hose take-up speeds.

2.5 Production of the outer layer of the fuel hoses

To increase the adhesion between the textile reinforcement and the cover layer, a special solution mixture that is a combination of NBR rubber and solvent is applied to the reinforcement (Fig 7a). Then, CPE rubber was used for covering the braided hose. The covering process was

performed on a T head extruder (Fig. 4b). The setting parameters of the extruder according to the type of CPE rubber are given in Table 3.

2.6. Vulcanization process

The final product of the extrusion process is NBR/braided fabric/CPE construction hose. As the hoses are raw, the shape of the hoses can be changeable. To keep the constant shape of the hoses, a vulcanization process was carried out (Fig.7b). The hoses were placed in autoclaves and cured at 9 bar pressure for 15 minutes.

2.7. Testing Methods

To determine the performance characteristics of the hoses, quality tests were performed according to their main usage where high pressure is required.

2.7.1. Hardness measurement from the hose

The hardness values of the braided hoses were measured by shoremeter (DIN 53505).

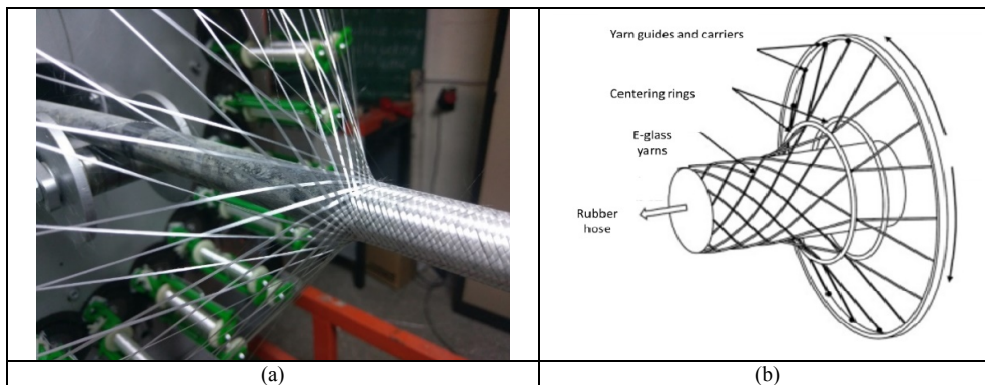


Figure 5. (a) Braiding process, (b) Schematic view of the radial braiding machine

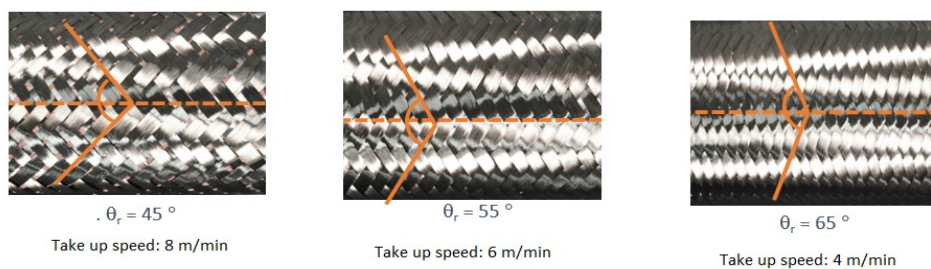


Figure 6. Braiding angle values depending on the take-up speeds



(a)



(b)

Figure 7. (a) Solution applying process, (b) Vulcanisation process

2.7.2. Ply adhesion test

Zwick universal testing equipment was used for the measurement of ply adhesion of the hoses. The test was carried out according to DIN 53530 to find adhesion force (N/mm) between the inner and outer layers. According to the standard samples should be at least 150 mm long, 200 mm wide and the test speed 100 mm/min respectively.

2.7.3. Permanent deformation test

Permanent deformation test was applied to determine how much the hoses undergo deformation under certain heat and load. The test has been carried out according to PV 3307 test standard. Suitable apparatus was used for the test with four samples. Test temperature and duration shall be 160°C and 22 hours with 50% compression. All thickness of samples were measured before the test (h_0), under 50% compression (h_1), and after (h_2) the test to determine the change of the thickness. Permanent deformation percentage calculated according to Equation (1).

$$PD \% = \frac{h_0 - h_2}{h_0 - h_1} * 100 \quad (1)$$

2.7.4. Burst test

Burst test was conducted at both room temperature and 110°C, according to standard TL 52624. One end of the hose was assembled to the bursting test machine and the other end was plugged with a fitting. Fluid that consists of 50/50 % volume distilled water and volume cooling liquid, was pumped inside the hose at a rate of 20 bar/sec. The pressure, where the hose bursted, was detected. At 100°C test, fluid inside the test machine was heated up and fed inside the hose.

2.7.5. Vacuum test

A vacuum test according to standard MS200-43 is applied to measure the vacuum strength of the hoses. One end of the hose was connected to the vacuum machine, the other end was closed with a gauge. The width of the hose is measured with a caliper from the middle of the hose. The

manometer connected to the vacuum device was operated until it shows the desired vacuum value. After waiting for the specified time at the desired vacuum value, the width is measured from the middle part. The percentage change between the initial and final width values gives the slump value. In this study, the test was applied by keeping it in a 100 mmHg vacuum for 15 seconds.

2.7.6. Diametric expansion test

Diameter expansion test was conducted at both room temperature and 110°C in accordance with DIN 73411. In order to investigate the expansion behavior of the hose with hot fluid that is a mixture of water and coolant liquid, the degree of 110 C was selected. The test was applied to measure the swelling percentage of the hoses under 3 bar pressure. The width of the hose was measured with a caliper at the middle region. After the hose was connected to the device, the pressure was fixed at 3 bars and the second width measurement value was taken. The percentage change between the initial and final width value gives the swelling value.

Limit values were taken from the requirements of a high-pressure fuel hose. Tests, where do not mention any limits, can help evaluation of all limited results. All test limits are given in Table 4.

2.7.7. Finite Element Analysis

The studied fuel hose constructions were modeled as three dimensional (3D) and analyzed as static structural by using the finite element (FE) software ANSYS. The model consisted of the inner NBR layer which was braided over by textile reinforcements, and finally the outer CPE layer. The mechanical properties of the materials used in the FE model are given in Table 5. Element types used in meshing of the geometric model, which were given in Table 6, were chosen as program controlled. Loading conditions were defined as fixed supports at both ends of the hose and a linear pressure ramp of 0.8 MPa to be achieved in 1 s of inflation period.

Table 4. The requirements of a high-pressure fuel hose

Test	Unit	Limit values	
		Minimum	Maximum
Hardness measurement from hose	Shore A	65	75
Ply adhesion	N/mm	2	-
Permenant deformation	%	-	65
Diametric expansion at 25°C	%	-	-
Burst test at 25°C	bar	70	-
Diametric expansion with coolant at 110°C	%	-	-
Burst test with coolant at 110°C	bar	-	-
Vacuum	bar	-	15

Table 5. Mechanical properties of the materials used in the FE model [27, 29, 30]

Material	Young's modulus (GPa)	Poison's ratio (-)	Shear modulus (GPa)	Tensile strength (MPa)	Elongation (%)
NBR (Inner layer)	3.4	0.49	-	12.4	1.4
CPE (Outer layer)	4.1	0.49	-	14.8	3.1
Carbon fabric	3.4	0.1	1.55	-	1.4
Basalt fabric	4.1	0.3	1.58	-	3.1
E-glass fabric	3.5	0.2	1.46	-	4.8
Para-aramid fabric	2.9	0.3	1.12	-	3.6
Polyester (HT) fabric	0.8	0.495	0.27	-	15

Table 6. Element types used in the meshes

Geometry	Type of element	Element shape	Element name
Reinforcement	Tetrahedral	TET10	SOLID187
Inner layer	Hexagonal	HEX20	SOLID186
Outer layer	Hexagonal	HEX20	SOLID186
Contact surfaces	Quadrilateral	QUAD8	CONTAC174
Contact surfaces	Quadrilateral	QUAD4	TARGE170
Contact surfaces	Quadrilateral	QUAD8	SURF154

3. RESULTS AND DISCUSSION

According to MS 263-20 Type-A standard, the hardness values of the hoses should be between 65–75 ShoreA (Table 4). Fig. 8 illustrated that hardness values of all types of hoses are within the limit values. As braiding take-up speed decreases, the hardness values of the hoses increases. This situation can be explained by the tight structure of the braided materials produced with lower braiding take-up speed. The denser structure can lead to an increase in hardness independently from the type of rubber.

The ply adhesion characteristic of the hoses should be higher than 2 N/mm (Table 4). The ply adhesion results revealed that, NBR/carbon/CPE and NBR/polyester/CPE hoses produced with the braiding take-up speed of 8 m/min exhibit acceptable values (Fig. 9). Hoses produced with a braiding take-up speed of 8 m/min provide higher ply adhesion characteristics than those produced with lower braiding take-up speed. This is due to the looser braided construction and lower yarn consumption in the production with the braiding take-up speed of 8 m/min. The more the contact areas between the rubber materials used for the production of the inner and outer layers of the hoses, the higher the ply adhesion characteristic of the structures.

For high-pressure fuel hoses, the permanent deformation value should not exceed 65% (Table 4). As is expected, NBR/braided fabric/CPE hoses with denser knitted structures exhibit higher strength properties. A hybrid composite material with a higher strength value will be more resistant to deformation under pressure in a hot environment. Fig.10 showed that the permanent deformation values increase with higher braiding take-up speed hence lower consumption. A hybrid hose construction in which less fiber is used is expected to give worse permanent set values because of its low strength properties. Also, the permanent deformation values of the NBR/basalt/CPE and NBR/polyester/CPE hoses produced with the braiding take-up speed of 4 m/min are within the acceptable limit. Hoses produced with a braiding take-up speed of 4 m/min have denser character than the others. It is thought that braiding take-up speed and type of material have a synergic effect on permanent deformation parameters since the permanent elongation values of the carbon, e-glass, and aramid braided hoses produced with the braiding take-up speed of 4 m/min are not within the limits.

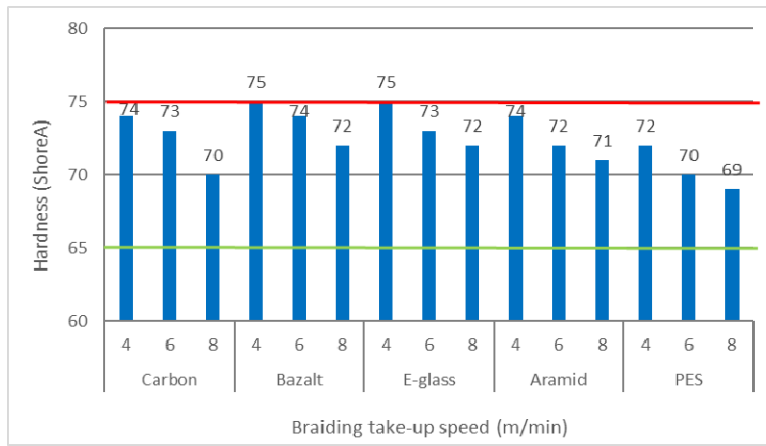


Figure 8. Hardness values of the braided hoses

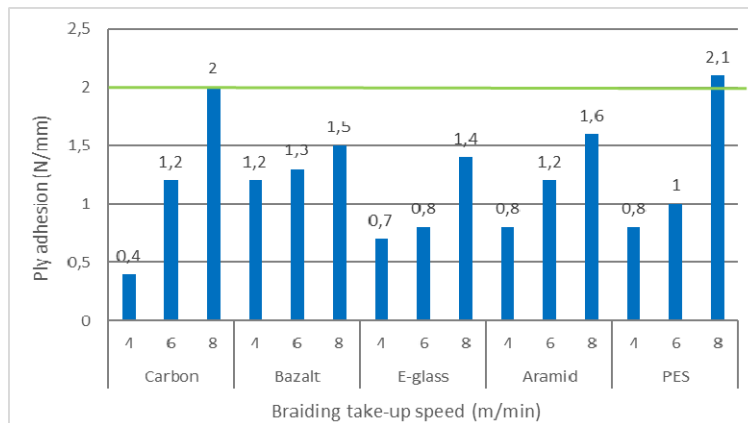


Figure 9. Ply adhesion results of the braided hoses

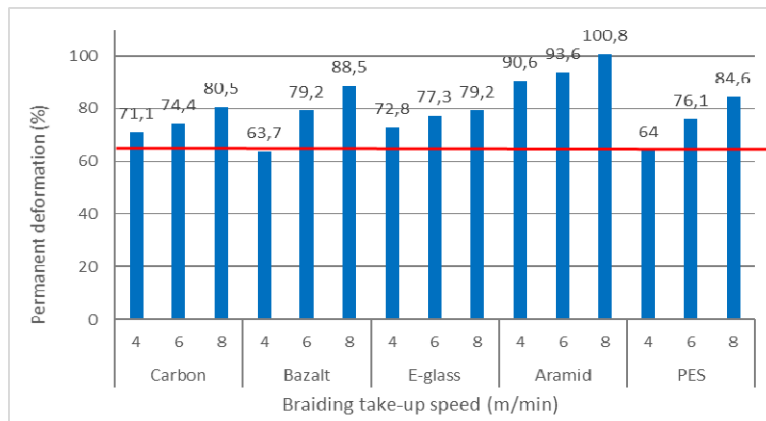


Figure 10. Permanent deformation results of the braided hoses

There is no limit specified for the diametric expansion test at 25 °C in the ASTM D380, MS 263-20 TypeA standard. According to the results, it is observed that the diametric expansion rates of the hoses varied between 0.2 and 3.6 %. For all braided hoses, as the braiding take-up speed increased, diametric expansion rates have been increased, as well. It is thought that the most effective parameter influencing this parameter is the density of the braided structures. The diametric expansion rate of the looser braided structure is higher because the looser structure leads to an increase in the gap between the loops which reduces the cover factor of the fabric. When the effect of

material types is examined, it is found that the lowest diametric expansion rates at 25°C were obtained from NBR/carbon/CPE hoses for all braiding take-up speeds. Since these fuel hoses will run in hot circumstances on the engine block, this test was additionally performed at 110 °C, to predict the diametric expansion behavior of the hoses in hot conditions. The diametric expansion rate values at 110 °C exhibited the same inclinations. As the braiding take-up speed increased, the diametric expansion rates have been increased (Fig. 11).

One of the most important criteria for high-pressure fuel hoses is the bursting pressure at 25°C. According to Table 4, the bursting pressure characteristic of the hoses at 25°C should be higher than 70 bar. As seen in Fig. 14, NBR/carbon/CPE and NBR/aramid/CPE hoses produced with the braiding take-up speeds of 4 and 6 m/min have acceptable bursting pressure values. Also, the bursting pressure values of NBR/basalt/CPE and NBR/E-glass/CPE hoses with the braiding take-up speed of 4 m/min are higher than 70 bar. Additionally, for all braiding take-up speeds, the bursting pressure results of the NBR/polyester/CPE hoses are out of the limit values. This may be due to the chemical and physical properties of the polyester yarn. It is a conventional yarn used in the polyester sector where less functionality is required. It can be explained by the low tensile strength of the polyester fiber. Its low tensile strength leads the hose not to resist pressure loaded to the structure. Regardless of the material type, the bursting pressure values of the hoses have been decreased as the braiding take-up speed increased. This situation can also be explained by the loose structure of the braided materials produced with higher braiding take-up speed. A loose structure will cause the hose to deform and burst more easily under high pressure. Rubber hoses expand more in hot conditions resulted in decrease of pressure resistance

and large deformation. Since these fuel hoses will run in hot circumstances on the engine block, this test was additionally performed at 110 °C, to predict the bursting pressure of the hoses in hot conditions. The bursting pressure values at 110 °C exhibited the same inclinations. As the braiding take-up speed increased, the bursting pressure values have been decreased (Fig. 12).

The vacuum collapse test values of the fuel hoses should be lower than 15 bar concerning ASTM D380 standard. The results revealed that the vacuum collapse values of all hose types were within the limits (Fig. 13).

The FE model prepared and run in ANSYS software contained 11.515 elements and 27.542 nodes. The solutions took 8 s, required a memory size range of 835-865 MB, and had a result file size range of 16.063-18.125 MB. The total deformation values of the hoses with defined constructions were obtained via FEA by including 5% standard deviation rate (Fig. 14 (a-e) and Table 7).

The results revealed that NBR/basalt/CPE hoses provided the lowest total deformation value. By using finite element analysis, it was predicted that NBR/basalt/CPE constructed hoses can be preferable for high-pressure fuel hoses.

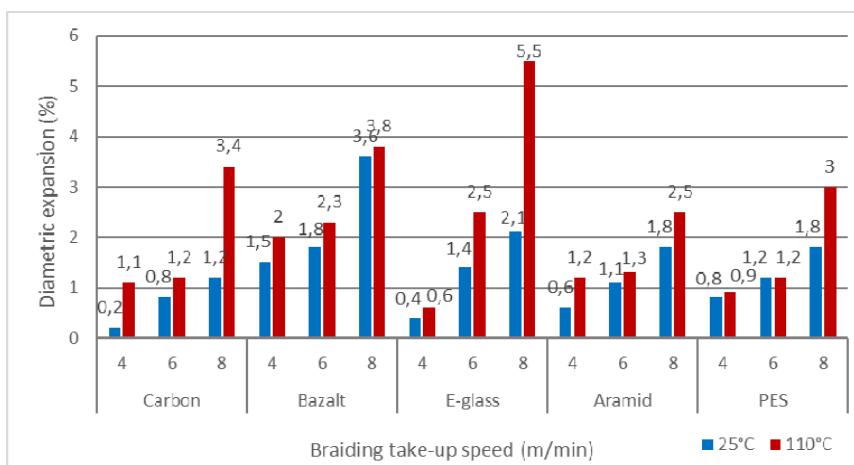


Figure 11. Diametric expansion results at 25 °C and 110 °C of the braided hoses

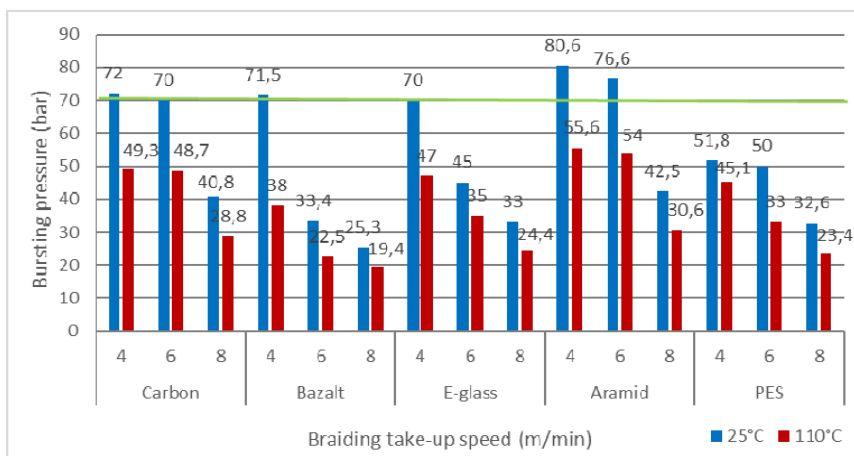


Figure 12. Bursting pressure results at 25 °C and 110 °C of the braided hoses

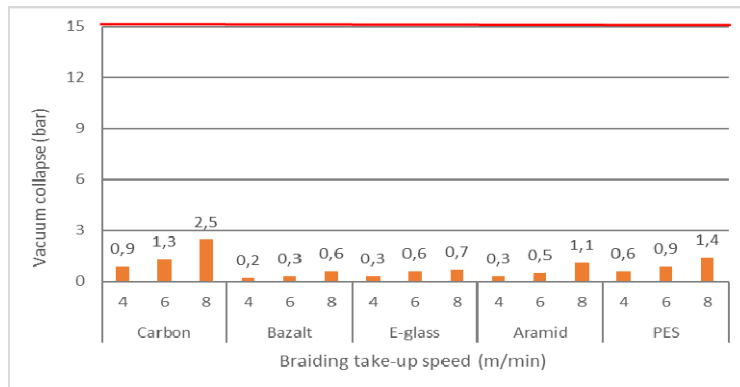


Figure 13. Vacuum collapse test results of the braided hoses

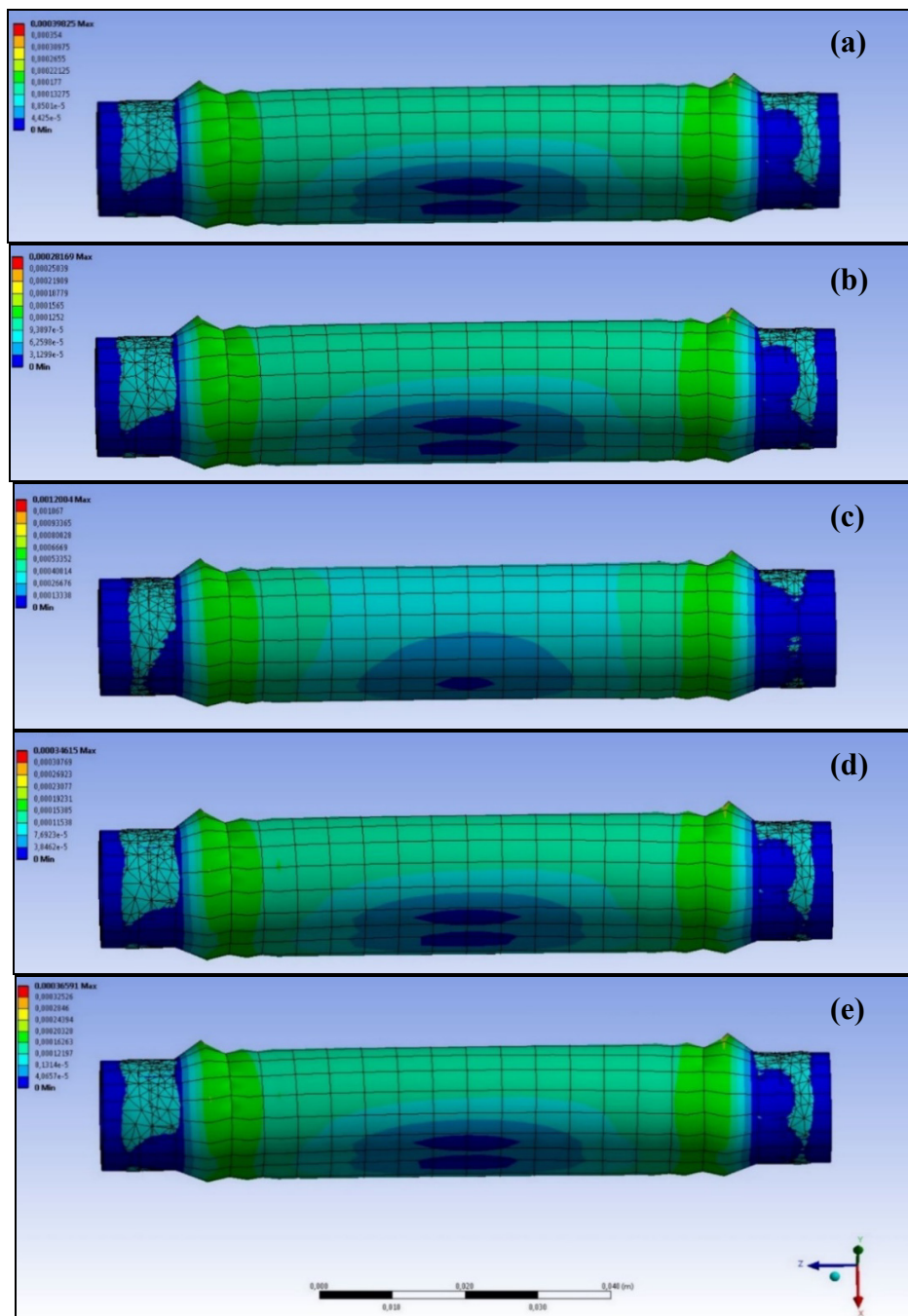


Figure 14. FE results of (a) NBR/Carbon/CPE, (b) NBR/Basalt/CPE, (c) NBR/Polyester/CPE, (d) NBR/Aramid/CPE, (e) NBR/E-glass/CPE hoses

Table 7. Total deformation values of the fuel hoses

Material	Total deformation (mm)
NBR/Carbon/CPE	0.398
NBR/Basalt/CPE	0.282
NBR/Polyester/CPE	1.200
NBR/Aramid/CPE	0.346
NBR/E-glass/CPE	0.366

4. CONCLUSION

This study aims to investigate the effect of material type and braiding angle on the performance characteristics of the reinforced multi-layered hose, to manufacture a high-pressure fuel hose. For this purpose, NBR (Acrylo-Nitrile Butadiene rubber)/CPE (chlorinated polyethylene) fuel hose was manufactured using a single-screw extruder and for the production of the reinforcement layer, braiding technology was used. With an attempt to discuss the effect of braiding angle on the performance characteristics of the reinforced multi-layered hose, the take-up speed of the radial braiding machine was altered. E-glass, aramid, carbon, polyester, and basalt yarns were used for the production of biaxial braided fabrics. Then CPE (chlorinated polyethylene) rubber was extruded for the cover application. Performance properties of the fuel hose such as hardness, ply adhesion, permanent deformation, vacuum collapse, bursting pressure, and diametric expansion were measured and evaluated according to the requirements of the related standards.

The results are summarized below:

- By using finite element analysis, it was predicted that NBR/basalt/CPE constructed hoses can be preferable for high-pressure fuel hoses.

- With increased braiding take-up speed, ply adhesion, vacuum collapse, permanent deformation and diametric expansion properties of hoses increase, while hardness and bursting pressure of hoses decrease.
- As a result of the vacuum test, it was observed that all hose types had a collapse percentage within the limit.
- It has been determined that NBR/Basalt/CPE fuel hose produced at 4 m/min braiding take-up speed provides optimum functional and adhesion properties, except ply adhesion property of basalt hose with 4m/min, because of its hardness, permanent deformation, bursting and vacuum test values at 25°C are within the limit. Additionally, the results were verified with the results of the Ansys simulation program.

In future studies, it is planned to develop an adhesive solution and improve process parameters to enhance the ply adhesion force of the NBR/basalt/CPE hoses whose ply adhesion values were out of the limits.

Acknowledgements

This work is supported by The Scientific and Technological Research Council of Turkey (TUBITAK) with grant numbers 217M004 and 217M005.

REFERENCES

1. Molded hose, formed hose and reinforced rubber hose. 2021,10.27, Retrieved from <https://www.unitedrubber.net/pdf/product-sheets/rubber-hoses.pdf>.
2. Hua G, Changgeng S, Jianguo M, Guomin X. 2021. Study on theoretical model of burst pressure of fiber reinforced arc-shaped rubber hose with good balance performance. *Polymers and Polymer Composites*, 29(7), 919-930.
3. Huang D, Zhang J. 2021. Research on the tensile mechanical properties of a braided corrugated hose and its axial stiffness model. *Journal of Marine Science and Engineering*, 9(9), 1029.
4. Huang D, Zhang J. 2021. Numerical simulation and experimental study on axial stiffness and stress deformation of the braided corrugated hose. *Applied Sciences*, 11(10), 4709.
5. Huang D, Lin Y, Zhang J. 2021, July. 12th International Conference on Mechanical and Aerospace Engineering (ICMAE) (280-284). Athens, Greece.
6. Karpenko M, Prentkovskis O, Šukevičius Š. 2021, September. Comparing Analysis of standard and compact versions of two metal braid high-pressure hoses basing on experimental research. In International Conference TRANSBALTICA: Transportation Science and Technology (pp. 253-262). Springer, Cham.
7. Ruhland P, Berger M, Coutandin S, Fleischer J. 2019. Production of hybrid tubular metal-fiber-preforms: material characterization of braided hoses with a binder. *Procedia CIRP*, 85, 121-126.
8. Cho JR. 2017. Anisotropic large deformation and fatigue damage of rubber-fabric braid layered composite hose. *Procedia Engineering*, 173, 1169-1176.
9. Cho JR, Kim YH. 2017. Multi-objective durability and layout design of fabric braided braking hose in cyclic motion. *Steel and Composite Structures*, 25(4), 403-413.
10. Cho JR, Kim YH. 2017. Numerical investigation of deformed layout and fatigue life of automotive braking hose to the helix angle of fabric braided layers. *Journal of Mechanical Science and Technology*, 31(6), 2893-2900.
11. Cho JR, Kim YH. 2016. Analysis of large deformation and fatigue life of fabric braided composite hose subjected to cyclic loading. *Steel and Composite Structures*, 21(4), 949-962.
12. Cho JR, Yoon YH. 2016. Large deformation analysis of anisotropic rubber hose along cyclic path by homogenization and path interpolation methods. *Journal of Mechanical Science and Technology*, 30(2): 789-795.
13. Cho JR, Yoon YH, Seo CW, Kim YG. 2015. Fatigue life assessment of fabric braided composite rubber hose in complicated large deformation cyclic motion. *Finite Elements in Analysis and Design*, 100, 65-76.
14. Cho JR, Jee YB, Kim WJ, Han SR, Lee SB. 2013. Homogenization of braided fabric composite for reliable large deformation analysis of reinforced rubber hose. *Composites Part B: Engineering*, 53, 112-120.

-
15. Hachemi H, Kebir H, Roelandt JM, Wintrebert E. 2011. A study of the braided corrugated hoses: Behavior and life estimation. *Materials & Design*, 32(4), 1957-1966.
 16. Ren JS, Zhou JW. 2008. Mechanical performances and destruction analysis for fiber braided high pressure rubber hoses. *Advances in Heterogeneous Material Mechanics*, 1292-1295.
 17. Cho JR, Song JI, Noh KT, Jeon DH. 2005. Nonlinear finite element analysis of swaging process for automobile power steering hose. *Journal of Materials Processing Technology*, 170(1-2), 50-57.
 18. Kim JK, Thomas S, Saha P. 2016. *Multicomponent polymeric materials*, Dordrecht: Springer.
 19. Savran HÖ. 2001. *Elastomer teknolojisi-I*, İstanbul: Acar Matbaacılık.
 20. Stahlbus. 2021, 10.27. Fuel hose. Retrieved from <https://www.stahlbus.com/info/en/products/fuel-hoses>.
 21. Wooton DB. 2001. *The Application of Textiles in Rubber*, UK: Rapra Technology Limited.
 22. Bogdanovich AE. 2016. An overview of three-dimensional braiding technologies. In Y. Kyosev (Ed.), *Advances in braiding technology: Specialized techniques and applications*. UK: Elsevier, 5.
 23. Kyosev Y. 2015. *Braiding technology for textiles*. UK: Elsevier.
 24. Mecit D, Ilgaz S, Duran D, Başal G, Gülümser T, Tarakçıoğlu I. 2007. Technical textiles and applications (Part 2). *Tekstil ve Konfeksiyon*, 17(3), 154-161.
 25. Ingenieria Y Mecanica Automotriz. 2021, 10.27. Fuel System: Components, Working Principles, Symptoms and Emission Controls. Retrieved from <https://www.ingenieriamecanicaautomotriz.com/fuel-system-components-working-principles-symptoms-and-emission-controls/>.
 26. Kısacık F. 2006. İki komponentli kauçuk hortum (Unpublished master's thesis), Kocaeli Üniversitesi Fen Bilimleri Enstitüsü, Kocaeli.
 27. Bunsell AR. 2018. *Handbook of properties of textile and technical fibres*. UK: Woodhead Publishing
 28. Alagirusamy R, Padaki NV. 2016. Introduction to braiding. In S. Rana and R. Figueiro (Eds.), *Braided structures and composites*. Boca Raton: CRC Press.
 29. Horrocks AR, Anand SC. 2000. *Handbook of technical textiles*. UK: Elsevier.
 30. Basalt fibers. 2019,02.26. Lance Brown import and export data sheet. Retrieved from: <http://www.lbie.com/PDF/n3011.pdf>.



Effects of Needle Size and Sewing Thread on Seam Quality of Traditional Fabrics

Derya Tama Birkocak  0000-0002-2720-2484

Ege University / Textile Engineering Department / 35100, Bornova, Izmir, Türkiye

Corresponding Author: Derya Tama Birkocak, derya.tama@ege.edu.tr

ABSTRACT

The role of fabric properties in sewing performance and seam quality is essential, therefore, it is crucial to understand the effect of different parameters on traditional fabrics' sewability properties. This study aimed to evaluate the seam quality of traditional fabrics produced from silk, cotton and linen fibres and their blends in terms of seam strength, seam slippage, seam efficiency and fabric sewability and determine the optimum sewing thread and sewing needle size for the sewing process of these fabrics. The samples were sewn using two different sewing needle size (75 Nm and 90 Nm) and sewing thread (100% mercerised cotton and 100% polyester corespun). Based on the obtained results, it can be concluded that sewing thread and fabric type had significant effect on seam strength, seam slippage and seam efficiency. The samples sewn with polyester corespun sewing thread had higher seam strength than other. The sewing needle significantly affected the needle penetration force values and the silk fabric had lowest sewability values both in warp and weft direction.

1. INTRODUCTION

Textile and fashion industry has quite inconvenient features from an ecological point of view, with parameters such as the raw material, energy and water consumption, the intense chemical process content in the production process, mass production capacity, and the potential for waste after production [1, 2]. For this reason, the effects of the concept of sustainability in industrial production are also observed in textile and fashion industry. The solutions such as adopting the slow fashion trend, using cyclical production methods, and turning to recycling raw materials are applied to the textile industry [2, 3]. In addition, local fabrics produced traditionally and ecologically attract the attention of the fashion industry and their use creates a new dimension in terms of sustainability in textile [4, 5].

The traditional shirts made of natural fibres, which are also the subject of this study, are preferred also in daily life. The materials used in these shirts generally depend on the characteristics of the region such as the climate of the region, the availability of raw materials, the production techniques, etc. [6]. The traditional fabrics made of natural fibres, namely silk, linen, cotton and their blends were

evaluated in this research. Especially silk is one of the most important natural fibres due to its unique properties such as specific gravity of 1.25-1.3 g/cm and diameter of 12 µm [7]; whereas cotton has 1,54 g/cm specific gravity and 10-27 µm diameter, flax has 1,4 g/cm specific gravity and 15-20 µm diameter [8].

It is crucial to know the quality of the end product before commercializing. Seam quality is one of the outstanding parameter that effects the overall quality of a garment. The seam quality could be characterized as functional (strength, elasticity, durability, stability) and aesthetic (the proper appearance) [9-11]. Many researchers were studied on seam characterization both in functional and aesthetic aspect [9-25]. Data et al. (2017) evaluated the effect of stitch density and the linear density of sewing thread on seam efficiency of a woven linen men shirt's production. It was found out that, the most suitable stitch density is 13-13,5 stitch per inch and the sewing thread is 40 Tkt number spun polyester [10]. Malek et al. (2018) developed a regression model to predict the seam quality through studying sewing performance by measuring the seam efficiency, slippage and puckering of 18 denim fabrics [11]. Abou Nassif (2013), investigated the effect of needle size, stitch density,

ARTICLE HISTORY

Received: 18.03.2022

Accepted: 13.09.2022

KEYWORDS

Traditional fabrics, seam strength, seam efficiency, fabric sewability, needle penetration force

To cite this article: Tama Birkocak D. 2022. Effects of needle size and sewing thread on seam quality of traditional fabrics. *Tekstil ve Konfeksiyon*, 32(3), 277-287.

sewing thread tension and sewing direction on the seam tensile strength, seam elongation and seam efficiency of cotton woven fabric. It was obtained that the sewing machine parameters have a certain influence on the seam quality [12]. Choudhary and Goel (2013) analysed the effect of blend composition (3 varying in the blend composition of polyester and cotton components), sewing thread size, and sewing needle parameters on seam strength, seam efficiency, seam puckering, seam stiffness, and drape coefficient and stated that seam efficiency is higher and the seam puckering is lower in the 100% cotton structure of fabric. The low seam strength efficiency was observed for the polyester fabric due to polyester's high extensibility and tenacity [13]. Gribaa et al. (2006) investigated the influence of the sewing thread, the stitch type, the stitch density, the needle size and the edge of the seam on tensile behaviour of a plain weave cotton/polyester fabric. It was demonstrated that the sewing thread, the stitch density, the edge of the seam as well as the sewing direction have a significant effect on seam strength [14]. Rogina-Car and Kovacevic (2021) analysed the damage caused by the needle piercing the cotton fabric during sewing. The specimens were prepared using three types of needle point shapes and four needles. It was obtained that the samples sewn with SUK-designated needles creates larger holes, whereas SES-designated needles give the best results [15]. In the research performed by Gurarda and Meric (2005), the effect of elastane feeding ratio, pre-setting temperature and finishing process on needle penetration force was examined. 12 cotton/elastane woven fabrics were produced and tested using L&M sewability tester, same as used in the present research; the obtained results showed that treating the elastic fabric with silicone during the finishing process helps to prevent the fabric damage [18]. In the study conducted by Carvalho et al. (2020), the sewability of towels were determined by quantifying the needle penetration force. Different sewing needles were used with different sizes, points, and coatings. The effect of needle size on needle penetration force was significant, however the effect of needle point is not clearly demonstrated [20]. Karypidis (2018) as well tested the sewability properties of rigid structures in their natural, washed and softened states, which are higher mass per square metre fabrics known to be problematic in the sewing stage. It was found out that washing and softening fabric treatments decreases the needle penetration force [23]. Pamuk et al. (2011) investigated the sewability properties of six lining fabrics using L&M sewability tester and found out that yarn count and density have a significant effect on the sewability values of lining fabrics [25].

In this study, the seam quality of traditional shirt fabrics was evaluated in terms of seam strength, seam slippage, seam efficiency and fabric sewability. Seam strength is the strength of a sewn seam by applying a force perpendicular when seam finally ruptures [26]. Seam efficiency is another parameter that demonstrates seam performance defined as the seam carrying capacity of a fabric itself [17] and is measured by the ratio of sewn and unsewn fabric strengths

[27]. Furthermore, seam slippage (opening) is a mode of failure evidenced by yarn movement at either side of the seam creating a gap or opening [8]. Seam slippage is affected by fabric characteristics such as weave, type of weaving yarn, coefficient of friction between yarns, fabric density, and so on [28, 29].

There are many factors affecting the seam strength, seam slippage and seam efficiency; the properties and the construction of fabric, sewing thread, sewing needle size, sewing needle point type, stitch density, seam type and sewing machine parameters. The seam strength and so the seam efficiency increases with the sewing thread linear density. Islam et al. (2018) evaluated the effect of sewing thread's effect of seam strength and seam efficiency using 14 tex, 18 tex and 60 tex polyester corespun sewing thread and obtained better efficiency in 60 tex sewing thread samples [26]. A similar observation was done by Choudhary and Goel (2013); where the percentage contribution of sewing thread on seam efficiency was found out as 5% [13]. Unal and Baykal (2018) also investigated the effect of PES/CO as well as PES/PES corespun sewing threads on seam quality and come up with similar results as the higher the yarn strength, the higher the seam strength [21]. Another important factor affecting seam quality is the sewing needle, which is one of the elements used in forming the seam. To determine the proper sewing needle, the needle size and the needle point type should be chosen properly considering the fabric type. During a seam formation, the sewing needle passes between the weft and warp yarns through the fabric. The thicker needle has more possibility to coincide the conjunctions of yarns, where it has to pierce. As Rogina-Car and Kovačević (2021) stated, the greater needle size creates higher contact with the material, which creates holes with larger surface area and lowers the seam quality [15]. Abou Nassif (2013) found out a 5% decrease in seam strength when the samples prepared using 80 Nm to 100 Nm needles [12]. The approach to explain this situation is the possibility of breaking the fabric yarn when using a needle with a greater diameter [31].

A good fabric sewability is related with a proper seam forming without fabric damage and a desired seam appearance. It is mainly evaluated by measuring needle penetration force (NPF). NPF is the quantitative measure of the friction between the fabric and the sewing needle and the damage which appears in the garment due to sewing process [18, 23]. Several authors studied the subject of measuring the NPF since decades, in 1976, Hurt and Tyler measured NPF in a lockstitch sewing machine by placing a tensiometer [22]. In 1973, Leeming and Munden were developed the L&M sewability tester and they obtained the patent in 1976 [31]. In the recent studies conducted by Carvalho (2004) and Carvalho et al. (2009), new technique was developed including a piezoelectric force sensor inserted into the needle bar of an industrial sewing machine [32, 33]. Measuring the NPF is essential to evaluate the fabric sewability; the lower NPF indicates the higher fabric sewability [23].

The objective of the study was to identify the optimum sewing thread and sewing needle size for the sewing process of traditional shirting fabrics produced from silk, linen and cotton, and their blends. Some existing researches in the literature focused on evaluating the seam performance of silk fabrics [34, 35], linen fabrics [10], cotton fabrics [18, 19, 22, 24, 36] and comparing silk and cotton fabrics' seam quality [37]; however, there was no systematic study focusing on silk, linen and cotton fabrics and their blends systematically. Therefore, the focus of this research was to examine the effects of determined parameters on the seam strength, seam slippage, seam efficiency and fabric sewability. As the literature review reveals, there are limited researches on evaluating the seam quality of traditional shirting fabrics, especially produced from silk, linen and cotton, and their blends. Findings of this research contributes to fill this gap in the literature. Moreover, this study could help apparel manufacturers to understand the seam quality of traditionally woven fabrics from silk, linen and cotton materials, to determine the optimum sewing thread and sewing needle size, and therefore to manufacture the products with higher overall quality.

2. MATERIAL AND METHOD

2.1 Material

2.1.1. Fabric properties

The traditional fabrics produced from silk, linen and cotton raw materials and their blends, to be used in shirt manufacturing in the Izmir region were procured. The construction of the all fabrics was plain weave structure and they have not been subjected to any dyeing or softening process. In Table 1, the yarn counts and fabric parameters are given.

Table 1. Fabric properties

Fabric composition	Weft yarn count (Ne)	Warp yarn count (Ne)	Weft yarn density (threads/cm)	Warp yarn density (threads/cm)	Fabric weight (g/m ²)	Fabric thickness (mm)
100% Silk	100/2	100/1	38	34	58.4	0.13
100% Linen	12/1	12/1	20	18	165.9	0.47
100% Cotton	30/1	30/1	22	34	119.9	0.37
25% Silk /75% Linen	40/1 (linen)	100/1 (silk)	26	36	98.6	0.22
30% Silk / 70% Cotton	18/1 (cotton)	100/1 (silk)	38	36	66.5	0.21
25% Cotton / 75% Linen	22/1 (linen)	100/1 (cotton)	26	36	101.5	0.24

Table 2. Sewing thread specifications

Sewing thread	Linear density (tex)	Average strength (cN/tex)	Elongation % (min – max)
100% polyester corespun	24	1190	17-22
100% mercerised cotton	30	830	4-9

Table 3. The sewing specifications

Sewing type	Stitch length (mm)	Needle size (Nm)	Needle point type	Needle point shape [15]
Lockstitch (Type 301)	3	75	SES	
		90	Light Ball Point	

2.1.2. Sewing thread

To assess the effect of sewing thread on seam quality, 100% polyester corespun and 100% mercerised cotton sewing threads were selected. The main reason for choosing them was that the sewing threads used in the garment industry are generally produced from cotton and polyester fibres [30]. Especially polyester corespun sewing threads dominate the market due to their very high yarn strength property [21] and are suitable for the production of normal clothing products thanks to their versatile structure [10]. Table 2 presents the properties of commercial sewing threads (Coats Group plc, Uxbridge, UK) used in the study.

2.1.2. Sewing parameters

All samples were sewn using a Juki DDL-9000B high speed single needle lockstitch machine. The sewing conditions are presented in Table 3. The settings of the sewing machine were done before the sewing process and the other parameters such as lower and upper thread tensions kept constant.

The sewing needle, one of the seam forming elements, is essential to ensure good seam quality. Especially choosing the right needle size and needle point is one of the most important parameters in the production of garments' joints [11, 14, 30, 38]. As the existing literature proves the significant effect of needle size on seam quality, the thicker needles decrease the seam strength, seam efficiency and seam elongation, whereas increase the force required to pierce the needle through the fabric [12, 15]. Two needle sizes were used in this study, namely 75 Nm and 90 Nm considering the fabric characteristics as well as the recommendations of the sewing thread company.

Moreover, the light ball point (SES) needle type, which is most commonly used needle point type for sewing general knit fabrics and lightweight woven fabrics [39], was chosen. These needles easily penetrate through the weft and warp yarns of the fabric, produce less yarn breakages than medium ball point needle (SUK) [15]. The range of the stitch length is between 0 and 5 mm on most sewing machines [17]. In this study, the stitch length was determined as 3 mm, which is an average stitch length in apparel industry.

In a cut and sew garment, cut pieces of fabric can be sewn in both the weft and warp directions. Therefore, the examination of the sewing direction comes to the forefront in the evaluation of the sewing quality. Many researchers studied the effects of sewing direction on the seam quality and found out it has a significant effect on the seam strength [9, 12, 40, 41]. For this reason, the sewn samples were prepared for both warp and weft directions in the present study.

2.2. Experimental Design

To determine the seam quality, all seams were formed both in warp and weft directions for all specimens. Before the tests, all specimens were conditioned under standard atmosphere conditions for 24 hours maintaining the temperature at $20 \pm 2^\circ\text{C}$ and the relative humidity at $65 \pm 4\%$.

2.2.1. Seam strength

Seam strength is the strength of a sewn seam by applying a force perpendicular when seam finally ruptures. In this paper, it is followed ISO 13935-1 (2014) standard for sample preparation and testing to measure the seam strength and to evaluate the seam efficiency [42]. The tests were conducted using Zwick Z010 (Roell) tensile strength testing machine. Five tests were conducted consecutively in warp and weft direction for each specimen. The maximum forces only resulting with seam break that occurs by breaking seam thread were evaluated due to the fact that, the breakage may occur for different causes. Furthermore, to determine the tear strength of fabrics, ISO 13937-2 standard was used to prepare the trouser-shaped test specimens and to perform the tear tests [43]. The warp tear strength was measured on weft direction, whereas the weft tear strength was measured on warp direction.

2.2.2. Seam efficiency

Seam efficiency is defined as the seam carrying capacity of a fabric itself [17]. Seam efficiency is the ratio between the original and the seamed fabric strength, which is calculated as the ratio of seam strength by fabric tensile strength as presented in Equation (1) [10, 11, 17, 27, 36]. The fabric tensile strength was determined using the Strip Method according to ISO 13934-1 standard [42].

$$\text{Seam Efficiency (\%)} = \frac{\text{Seam strength}}{\text{Fabric tensile strength}} \times 100 \quad (1)$$

2.2.3. Seam slippage

Seam slippage defines the ability of the warp yarns slip over the weft yarns, or weft yarns slip over the warp yarns near the seam. To measure the warp yarn slipping, the specimen is subjected to a given load in weft direction and the extension is observed in the warp direction. The reverse is done to measure the weft yarn slippage [44, 45]. Seam slippage values were tested using Zwick Z010 (Roell) tensile strength testing machine and five tests were performed in warp and weft direction for each specimen. ISO 13936-1:2004 standard was followed.

2.2.4. Fabric sewability

Sewability can be defined as the ability of the fabric components to be seamed effectively without fabric damage and to provide a desired quality for the end-use performance [47-49]. Sewability is mainly related with needle penetration force (NPF), which is the friction between the fabric and the sewing needle. The NPF was measured using L&M Sewability Tester (John Godrich) (Figure 1) by monitoring the force required for a sewing needle to penetrate the fabric [50]. A total of 100 needle penetrations were performed for each test and the average force applied to the fabric in grams was recorded. The threshold value was determined as 50 gf for silk and silk blended fabrics and as 100 gf for other fabrics according to the recommended values of the L&M sewability tester catalogue considering the fabric mass area.



Figure 1. L&M sewability tester [46]

2.2.5. Statistical analyses

Statistical analyses were carried out by using SPSS software. The Univariate and Independent-samples t-tests were applied to examine the interaction as well as individual effects of each parameter on the seam strength, seam efficiency and needle penetration force. Post-hoc analysis were also performed by using Duncan test in order to determine which means of groups differ significantly. All test results were assessed at significant levels of 0.05.

3. RESULTS AND DISCUSSION

3.1. Seam strength

The fabrics were seamed with two different sewing needles using two different sewing threads in both warp and weft directions. Table 4 presents the seam strength, fabric tensile strength and fabric tear strength mean values.

In Figure 2, examples obtained during seam strength tests were given. In the image on the left, a clear seam break can be seen, however, fabric tear was occurred before the seam break in the image on the right side. This situation was only happened for silk/cotton fabric's warp samples however; the tensile strength of the silk fabric was similar with silk/cotton fabric. The yarn count of the warp yarns of silk fabric and silk/cotton fabric was the same, and the weft and warp densities were very similar. However, although the slippery were occurred between the warp and weft yarns. Since the fabrics procured were produced traditionally, it was thought that the desizing process was also done traditionally. This may have affected the properties of the cotton yarn and caused the slippery. Therefore, these results were eliminated from the data used in statistical tests. The relevant data was written in bold in Table 4.

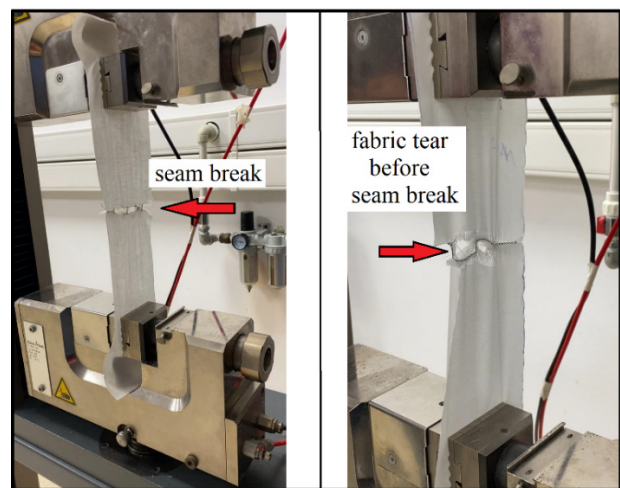


Figure 2. Some examples of images obtained during testing

Table 4. Seam strength, fabric tensile strength and fabric tear strength values

Fabric type	Sewing needle*	Sewing thread*	Seam strength (N)		Fabric tensile strength (N)		Fabric tear strength (N)	
			Weft	Warp	Weft	Warp	Weft**	Warp***
Silk	SN1	ST1	189.69	239.31	272.48	244.19	22	14.3
		ST2	169.78	205.42				
	SN2	ST1	162.40	238.53				
		ST2	201.96	225.87				
Linen	SN1	ST1	237.58	210.34	665.98	477.92	28.2	24
		ST2	234.94	246.24				
	SN2	ST1	220.62	207.00				
		ST2	263.19	263.12				
Cotton	SN1	ST1	255.45	246.59	278.86	445.91	5.27	7.9
		ST2	271.07	300.87				
	SN2	ST1	232.00	215.57				
		ST2	246.97	250.79				
Silk / Linen	SN1	ST1	180.97	208.37	707.97	245.96	35.6	16
		ST2	243.98	200.31				
	SN2	ST1	198.10	197.32				
		ST2	251.76	163.11				
Silk / Cotton	SN1	ST1	219.02	35.96	401.13	256.56	39.7	16.4
		ST2	291.40	35.31				
	SN2	ST1	214.33	44.18				
		ST2	216.87	26.97				
Cotton / Linen	SN1	ST1	183.82	148.61	810.19	248.23	40.1	17.1
		ST2	212.47	208.45				
	SN2	ST1	148.89	141.18				
		ST2	262.69	149.56				

*SN1 = 75 Nm sewing needle, SN2 = 90 Nm sewing needle, ST1 = 100% mercerised cotton sewing thread, ST2 = 100% polyester corespun sewing thread

** Tear strength values of weft yarns on warp direction *** Tear strength values of warp yarns on weft direction

The Independent Samples t-Test was performed to define the effect of individual factors on seam strength. Regarding the results, the sewing thread had statistically significant effect on seam strength values of all fabric types ($p=0.00$); whereas, it was not statistically significant for the sewing needle ($p=0.17$).

Afterwards, in order to have a better comprehending of the effects of fabric type and sewing thread values and their interactions on seam strength, the univariate analysis was applied, which is used to understand the distribution of values for a single variable. The statistical analysis of the

results (Table 5) showed that the fabric type and the sewing thread had a statistically significant effect on the seam strength for both warp and weft samples ($p<0.05$). When the sewing threads used in the study were compared, the general trend was the polyester corespun sewing thread used samples had higher seam strength values than mercerised cotton sewing thread used samples both in warp and weft direction. Similar observations were reported in the literature [10, 21, 26, 34, 51] due to polyester corespun's high yarn strength property. However, this was the opposite for the silk (warp and weft direction) and

silk/linen (warp direction) fabrics. It is thought that, this may be due to the multifilament structure of silk yarns and also the fact that more silk yarns coincide within one stitch length, considering the fabric density. The cotton fabric samples sewn by polyester corespun sewing thread in warp direction showed the highest seam strength. Moreover, the interaction of parameters, namely fabric type and sewing thread, did not have statistically significant effect on weft samples ($p=0.085$) as it had a high observed power very close to “1” (Table 5). However, the interaction effects were statistically significant on warp samples ($p=0.005$). The reason for this situation could be interpreted as the interaction was moved to a significant level with fabric type’s dominant effect (obs. power = 1).

Although the silk fabric was the thinnest among all fabrics and had prominently lower fabric tensile strength than cotton as well as linen fabrics (Table 4), the seam strength

values were close to each other especially in warp direction (Figure 3). Furthermore, the general trend in seam strength values was, the values of the weft samples were higher than those the values of the warp samples.

In both warp and weft samples, the seam strengths among fabric types were statistically significant, therefore four subsets were formed for each direction (Table 6). As it was mentioned before, silk/cotton fabric results in warp direction were eliminated due to fabric tearing occurred prior to the seam break. As seen from the mean values, some results overlapped, still it was clear that cotton had the highest seam strength in both directions. Unlike the cotton and linen fabrics, cotton/linen fabric was in the first subset group in both weft and warp direction, which were the groups had the lowest seam strength values. The fabric thickness nearly doubled that of cotton/linen fabric, with cotton fabric also having the highest fabric weight.

Table 5. The univariate analysis results

Sewing direction	Source	F	Sig.	Observed power
Weft samples	Fabric type	9.029	0.00	1
	Sewing thread	24.687	0.00	1
	Fabric type * Sewing thread	2.048	0.085	0.998
Warp samples	Fabric type	17.597	0.00	1
	Sewing thread	4.360	0.042	1
	Fabric type * Sewing thread	4.19	0.005	0.535

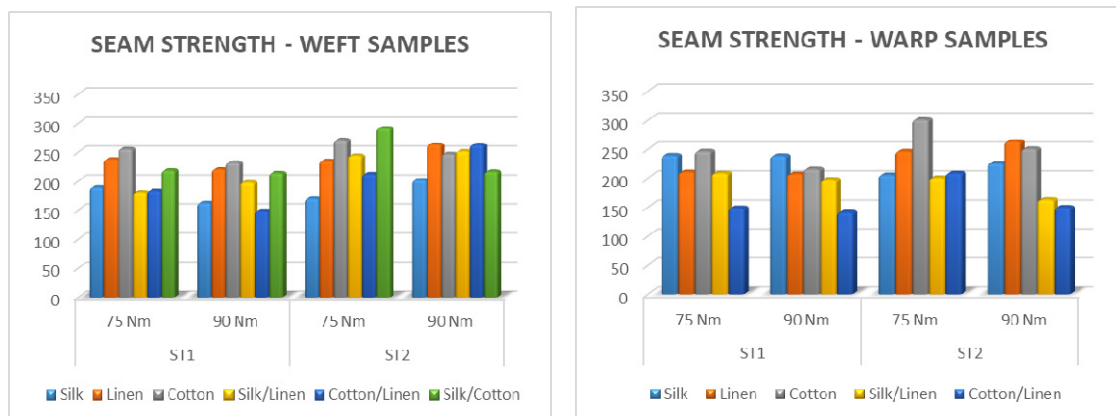


Figure 3. The seam strength values of samples in warp and weft direction

Table 6. Multiple comparisons of seam strength values

Sewing direction	Fabric type	N	Seam strength			
			Subsets 1	2	3	4
Weft samples	Silk	12	180.96	-	-	-
	Cotton / Linen	12	201.97	201.97	-	-
	Silk / Linen	12	-	218.71	218.71	-
	Silk / Cotton	12	-	-	235.41	-
	Linen	12	-	-	239.08	239.08
	Cotton	12	-	-	-	251.37
Sewing direction	Fabric type	N	Seam strength			
			Subsets 1	2	3	4
Warp samples	Cotton / Linen	12	161.95	-	-	-
	Silk / Linen	12	-	192.28	-	-
	Silk	12	-	-	227.28	-
	Linen	12	-	-	231.68	231.68
	Cotton	12	-	-	-	253.46

3.2. Seam efficiency

The seam efficiency was calculated using Equation (1), which is used to measure the loss in fabric strength caused by needle damage [27]. It is inversely proportional to fabric tensile strength; the high fabric strength lowers the seam efficiency. The highest seam efficiency both in weft direction was observed at silk fabric (Figure 4), which had lowest fabric weight (Table 1), as supporting the Cheng and Poon's (2002) [9] and Datta et al. (2017) research [10], which were indicated that the high fabric weight increased the fabric strength, which reduced the seam efficiency. In order to determine the effects of sewing thread, sewing needle and sewing direction parameters on seam efficiency, the Independent Samples t-Tests were performed. The sewing thread ($p=0.451$) and the sewing needle ($p=0.495$) did not have statistically significant effect on seam efficiency values.

In several researches, it was stated that, the high strength of sewing thread as well as the high needle size increase the seam efficiency [10, 12, 14, 19, 24]. This trend could be seen in Figure 4 as well. The corespun polyester sewing thread had higher sewing efficiency values, the exceptions

were observed for silk and silk/linen fabrics similar with seam strength values. Moreover, seam efficiency values of silk, silk/linen and cotton/linen fabrics in warp direction were higher than those obtained in weft direction. It is thought that this may be caused by the warp yarns of these fabrics being thicker than the weft yarns. Vice versa, the seam efficiency of silk/cotton fabric was higher in weft direction where the yarn thickness of weft yarns was greater than warp yarns.

3.3. Seam slippage

When a seam is stretched, separation of the interface line between two sewn fabrics occurred, however if the slippage is notable, it is considered as a sewing defect [8, 28]. Table 7 presents the seam slippage results of samples in both warp and weft direction. According to the experimental results, it can be said that the lightweight fabrics were tend to cause seam slippage than others due to finer yarns used in the fabric. The silk, silk/linen and silk/cotton fabrics had similar seam slippage results on warp direction; the silk yarns used were same 100/1 Ne in warp direction and also the fabrics had similar warp yarn density.

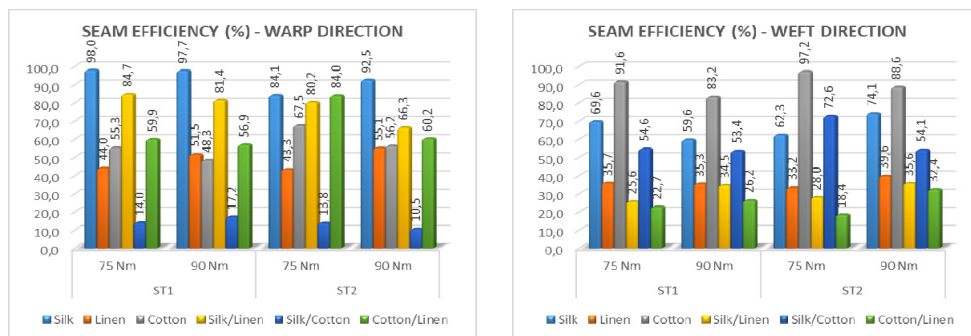


Figure 4. Seam efficiency values for both warp and weft samples

Table 7. Seam slippage values

Fabric type	Sewing needle*	Sewing thread*	Seam slippage	
			Weft	Warp
Silk	SN1	ST1	36	34.7
		ST2	39	28
	SN2	ST1	26	22
		ST2	24.5	20.2
Linen	SN1	ST1	68	54.5
		ST2	57	55
	SN2	ST1	70.5	69
		ST2	71	63
Cotton	SN1	ST1	47.5	57.8
		ST2	52.7	59
	SN2	ST1	51.5	64
		ST2	63	69
Silk / Linen	SN1	ST1	46	32
		ST2	53	36
	SN2	ST1	52	46
		ST2	45.5	36
Silk / Cotton	SN1	ST1	27	21
		ST2	25	20.4
	SN2	ST1	28.2	23
		ST2	24.9	22
Cotton / Linen	SN1	ST1	45	39
		ST2	39	30
	SN2	ST1	51.3	38.5
		ST2	34	31

Similar observations were obtained with Seif (2014) that sewing needle size and sewing direction had significant influence on seam slippage (Figure 5) [29]. Pasayev et al. (2012) stated that the seam slippage values in the weft direction were higher than the values in warp direction [52]. The general trend of the obtained results confirmed this statement, however the cotton fabric had results in the opposite way it is thought to be due to the warp and weft density of the fabric.

3.4. Fabric sewability

The NPF was measured both in warp and weft direction to determine the fabric sewability. The average values of NPF and also the sewability values were presented at Table 8. There is a defined range of sewability values as 0 to 10% considered good, 10% to 20% considered fair (no great difficulties arise during sewing) and more than 20% considered poor [18, 48, 50, 53]. Regarding obtained data, the sewability values of all fabrics were considered good, only cotton fabric had highest values both warp and weft directions as 3% (Table 8).

A good sewability requires low NPF values; a high NPF may alert sewability problems [23]. As observed in the Figure 6, the test results conducted with 90 Nm sewing

needle had higher NPF values than those conducted with 75 Nm sewing needle and regarding the statistical analysis, sewing needle had statistically significant effects on NPF values ($p=0.002$). This has been found in other studies as well, carried out by Grancaric et al. (2005), Haghghat et al. (2014) and Carvalho et al., (2020) [20, 48, 54].

Afterwards, the univariate analysis was applied to define the effects of fabric type and sewing needle values and their interactions on NPF. In Table 9, it can be seen that, the fabric type ($p=0.00$) and sewing needle ($p=0.00$) had a statistically significant effect for both warp and weft samples. As stated by Bakıcı and Kadem (2015) and Haghghat et al. (2014), the NPF of the fabrics increases with the increase in fabric weight [48, 53]. In Table 8, the lowest NPF values both in warp and weft direction were observed for silk fabric, the lightest fabric (Table 1), which means the needle passed through the silk yarns easily. Additionally, the effect of the interaction of needle size and fabric type also had a statistically significant effect for both warp and weft samples ($p=0.00$). It is thought that, this situation may be due to the fact that both fabric type and sewing needle parameters were very dominant (obs. power = 1).

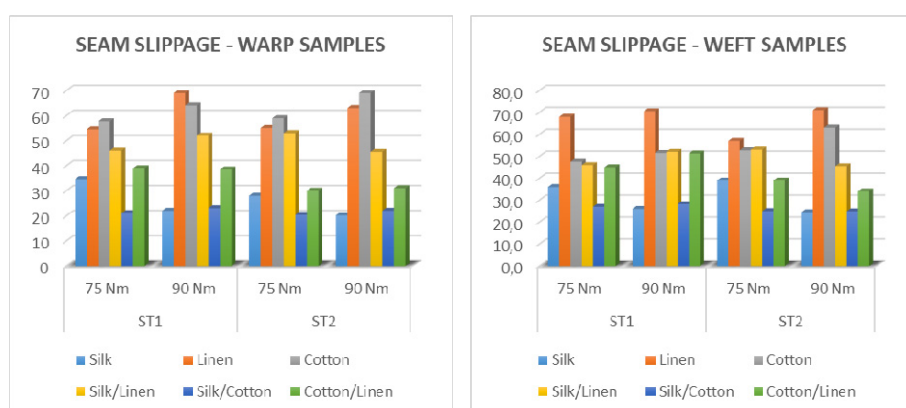


Figure 5. The seam slippage values of weft and warp samples

Table 8. The NPF and the sewability values

Fabric type	Sewing needle	NPF		Sewability value (%)	
		Weft	Warp	Weft	Warp
Silk	75 Nm	4.67	5.00	0	0
	90 Nm	15.00	12.33	0	0
Linen	75 Nm	15.67	12.67	0	0
	90 Nm	27.00	20.67	1	0
Cotton	75 Nm	17.67	25.00	0	0
	90 Nm	48.33	63.33	3	3
Silk / Linen	75 Nm	15.00	9.67	0	0
	90 Nm	22.33	15.00	1	0
Silk / Cotton	75 Nm	17.33	15.33	1	0
	90 Nm	15.00	6.67	0	0
Cotton / Linen	75 Nm	21.33	17.00	0	0
	90 Nm	23.00	19.00	0	0

The threshold values:

Silk, Silk/Cotton and Silk/Linen = 50 gf

Linen, Cotton and Cotton/Linen=100gf

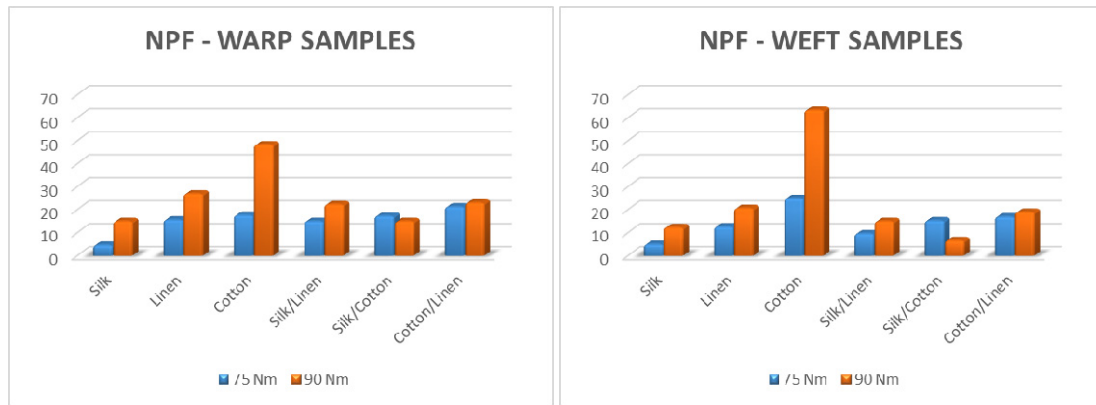


Figure 6. NPF values for both warp (left) and weft (right) samples

Table 9. The univariate analysis results

Sample direction	Source	F	Sig.	Observed power
Weft samples	Fabric type	12.485	0.00	1
	Sewing needle	30.685	0.00	1
	Fabric type * Sewing needle	6.955	0.00	0.992
Warp samples	Fabric type	71.722	0.00	1
	Sewing needle	47.955	0.00	1
	Fabric type * Sewing needle	26.019	0.00	1

Regarding the Duncan test results, three subsets were formed for weft samples; whereas, four subsets were formed for warp samples (Table 10). Similar with seam strength values, some results overlapped here as well. Only cotton fabric created a clear subset, the mean values of cotton were obviously greater than the other fabrics. In both warp and weft samples, the mean NPF values of fabrics were in same order, from smallest to greatest silk, silk/cotton, silk/linen, linen, cotton/linen and cotton.

4. CONCLUSION

Especially in last decades, the consumption cycle has become very fast in the textile and fashion industry, which is one of the oldest and largest industries in the world. The increase in the awareness of consumers has led to an increase in the importance given to sustainability. As a result of this, the manufacturers has been directed to make

more sustainable production. In this context, the use of traditionally produced fabrics from natural raw materials attracts the attention of the textile and fashion industry. Considering the increasing interest, the analysis of sewing properties of Izmir region's traditional fabrics produced from natural fibres were carried out within the scope of this study.

Based on this research the following conclusions can be drawn out;

- The seam strength of 100% cotton and 100% linen fabrics was higher than the others, it was relatively lower in silk and silk-containing fabrics. Similar results were obtained by Courtney LaPere (2006) and was found out that the seam strength values of cotton fabric were higher than silk fabric [37].

Table 10. Multiple comparisons of seam NPF values

Sample direction	Fabric type	N	NPF			
			Subsets 1	2	3	
Weft samples	Silk	6	9.83	-	-	
	Silk / Cotton	6	16.17	16.17	-	
	Silk / Linen	6	-	18.67	-	
	Linen	6	-	21.33	-	
	Cotton / Linen	6	-	22.17	-	
	Cotton	6	-	-	33.00	
Sample direction	Fabric type	N	NPF			
			Subsets 1	2	3	4
Warp samples	Silk	6	8.97	-	-	-
	Silk / Cotton	6	11.00	-	-	-
	Silk / Linen	6	12.33	12.33	-	-
	Linen	6	-	16.67	16.67	-
	Cotton / Linen	6	-	-	18.00	-
	Cotton	6	-	-	-	44.17

- As supporting the literature [10, 21, 26, 34, 51], the polyester corespun sewing thread used samples mostly had higher seam strength values than mercerised cotton sewing thread, and it is thought this was due to polyester corespun's high yarn strength property.
- The yarn count, the fabric thickness and mass per unit area properties of the fabrics were also found as important parameters for sewing strength.
- The seam efficiency of silk fabric was higher than cotton and linen fabrics and their blends in warp direction and was similar with cotton in the weft direction. Beside other parameters, this research proves the statement that, the lower the fabric weight, the higher the seam efficiency [9, 10].
- The higher seam efficiency results of the corespun polyester sewing thread used samples support the existing literature [10, 12, 14, 19, 24] that is, the high strength of sewing thread as well as the high needle size increase the seam efficiency.
- The use of different fabric types and sewing needles in different sizes had significant effects on fabric

sewability. The NPF values of silk fabrics were the lowest in both warp and weft directions, which also had the lowest fabric weight; supporting the fact that the increase in fabric weight increases the NPF [39, 44].

- Fabric properties, needle size and sewing direction had a particular effect on seam slippage of a garment, supporting the literature [29, 44].
- The results in the warp direction proved that there are some differences with the weft direction, which can be inferred as the fabric structure affects the behaviour of the sewn fabrics.

In summary, in addition to the sewing needle size, sewing thread and sewing direction parameters that important to form a seam, it was obtained that the material and physical properties of the fabrics are also effective on the sewing properties, and this study contributed to the literature in this direction. Based on the results given, the fabric properties and the joining processes can be optimised for the products to be produced from traditional fabrics. Future studies will focus on conducting wide spectrum researches involving other types of traditional fabrics and sewing parameters.

REFERENCES

1. Fletcher, K. & Grose, L. (2012). *Fashion & Sustainability*. Laurence King Publishing Ltd.
2. Sarı, B., Tama Birkocak D. & Isler M. (2021). *Sports clothing production techniques*. IKSAD Publishing.
3. Öz, C., & Çileroğlu, B. (2021). Differentiation of basic sewing techniques with an interdisciplinary approach: sample applications in textile surface design. *Journal of Textiles & Engineers*, 28(122).
4. Qian, T., & Ying, C. (2015). Ecologically sustainable implementations in contemporary fashion design. *International Journal of Literature and Arts*, 3(6), 158-161.
5. Guan, Z. (2017). Fabric reconstruction based on sustainable development: Take the type of fabric recycling as an example. *Journal of Arts and Humanities*, 6(7), 13-18.
6. Isler, M., Tama Birkocak, D., & Abreu, M. J. (2021). The Influence of Starch Desizing on Thermal Properties of Traditional Fabrics in Anatolia. In *Handloom Sustainability and Culture* (pp. 197-219). Springer, Singapore.
7. Uzumcu, M. B., Sari, B., Oglakcioglu, N., & Kadoglu, H. (2019). An Investigation on comfort properties of dyed mulberry silk/cotton blended fabrics. *Fibers and Polymers*, 20(11), 2342-2347.
8. Bunsell, A. R. (Ed.). (2009). Introduction, In *Handbook of tensile properties of textile and technical fibres* (pp. 1-17). Elsevier.
9. Cheng, K. P. S., & Poon, K. P. W. (2002). Studies on the seam properties of some selected woven fabrics. In *Conference Proceedings, Institute of Textiles and Clothing*.
10. Datta, M., Nath, D., Javed, A., & Hossain, N. (2017). Seam efficiency of woven linen shirting fabric: process parameter optimisation. *Research Journal of Textile and Apparel*, 21(4), 293-306.
11. Malek, S., Khedher, F., Jaouachi, B., & Cheikrouhou, M. (2018). Determination of a sewing quality index of denim fabrics. *The Journal of the Textile Institute*, 109(7), 920-932.
12. Abou Nassif, N. A. (2013). Investigation of the effects of sewing machine parameters on the seam quality. *Life Science Journal*, 10(2), 1427-1435.
13. Choudhary, A. K., & Goel, A. (2013). Effect of some fabric and sewing conditions on apparel seam characteristics. *Journal of Textiles*, Article ID 157034.
14. Gribaa, S., Amar, S. B., & Dogui, A. (2006). Influence of sewing parameters upon the tensile behavior of textile assembly. *International Journal of Clothing Science and Technology*, 18(4), 235-246.
15. Rogina-Car, B., & Kovačević, S. (2021). The study of needle type influence on woven fabric surface area during the sewing process. *Textile Research Journal*, 00405175211019133.
16. Amirbayat, J. (1993). Seams of Different Ply Properties. Part II: Seam Strength. *The Journal of the Textile Institute*. 84:1, 31-38, DOI: 10.1080/00405009308631244
17. Gurarda, A. (2019). Seam performance of garments. In *Textile Manufacturing Processes*. IntechOpen.
18. Gurarda, A., & Meric, B. (2005). Sewing needle penetration forces and elastane fibre damage during the sewing of cotton/elastane woven fabrics. *Textile Research Journal*, 75(8), 628-633.
19. Jebali, N., Babay Dhouib, A., & Ben Hassen, M. (2016). Modeling the overall seam quality of woven cotton fabric. *International journal of applied research on textile*, 4(1), 47-61.
20. Carvalho, M., Rocha, A. M., & Carvalho, H. (2020). Comparative study of needle penetration forces in sewing hems on toweling terry fabrics: influence of needle type and size. *Autex Research Journal*, 20(2), 194-202.
21. Ünal, B. Z., & Baykal, P. D. (2018). Determining the effects of different sewing threads and different washing types on fabric tensile and sewing strength properties. *Tekstil ve Konfeksiyon*, 28(1), 34-42.
22. Vidrigo, C., Abreu, M. J. A. M., Soares, G., & Carvalho, H. (2015). Cost and efficiency analysis of commercial softeners in the sewability behavior of cotton fabrics. *Journal of engineered fibers and fabrics*, 10(2), 155892501501000203.
23. Karypidis, M. (2018, December). Sewability interdependence on rigid structures. In *IOP Conference Series: Materials Science and Engineering* (Vol. 459, No. 1, p. 012048). IOP Publishing.

24. Sular, V., Meşegül, C., Kefsiz, H., & Seki, Y. (2015). A comparative study on seam performance of cotton and polyester woven fabrics. *The Journal of the Textile Institute*, 106(1), 19-30.
25. Pamuk, O., Kurtoğlu, Ö., Tama, D., & Öndoğan, Z. (2011). Sewability properties of lining fabrics. *Tekstil ve Konfeksiyon*, 21(3).
26. Islam, T., Khan, S., Mia, M., Hossen, M. & Rahman, M. (2018). Effect of seam strength on different types of fabrics and sewing threads. *Research Journal of Engineering and Technology*. 7. 1-8.
27. İllez, A. A., Dalbaşı, E. S., & Özçelik Kayseri, G. (2017). Seam Properties and Sewability of Crease Resistant Shirt Fabrics. *AATCC Journal of Research*, 4(1), 28-34.
28. Gürarda, A., & Meric, B. (2010). Slippage and grinning behaviour of lockstitch seams in elastic fabrics under cyclic loading conditions. *Tekstil ve Konfeksiyon*, 20(1), 65-69.
29. Seif, M. A. (2014). Investigating the seam slippage of satin fabrics. *International Journal of Textile and Fashion Technology*, 4(5), 1-10.
30. Yıldız, E. Z., & Pamuk, O. (2021). The parameters affecting seam quality: a comprehensive review. *Research Journal of Textile and Apparel*, 25(4), 309-329.
31. Leeming, C. A., & Munden, D. L. (1978). Investigations into the factors affecting the penetration force of a sewing needle in a knitted fabric and its relationship with fabric sewability. *Clothing Research Journal*, 6(3), 91-118.
32. Carvalho, H. (2004). Optimisation and Control of processes in Apparel Manufacturing. PhD diss., School of Engineering, University of Minho, Portugal, available at <http://hdl.handle.net/1822/59>
33. Carvalho, H., Rocha, A. M., & Monteiro, J. L. (2009). Measurement and analysis of needle penetration forces in industrial high-speed sewing machine. *The Journal of the Textile Institute*, 100(4), 319-329.
34. Sharma, N., Jain M. & Kashyap R. (2019). Assessment of sewability parameters of ahimsa and conventional silk union fabrics. *Indian Journal of Applied Research*. 9(3), 60-62.
35. Sharma, N., Jain, M., & Kashyap, R. (2019). Assessment of Seam Properties of Ahimsa Silk Union Fabrics. *International Journal of Recent Technology and Engineering*, 8(4), 3059-3062.
36. Islam, M. R., Asif, A. A. H., Razzaque, A., Al Mamun, A., & Maniruzzaman, M. (2020). Analysis of seam strength and efficiency for 100% cotton plain woven fabric. *International Journal of Textile Science*, 9(1), 21-24.
37. Courtney LaPere (2006). The Effects of Different Fabric Types and Seam Designs on the Seams Efficiency. From <https://commons.emich.edu/cgi/viewcontent.cgi?article=1052&context=honors>
38. Stjepanovic, Z., & Strah, H. (1998). Selection of suitable sewing needle using machine learning techniques. *International Journal of Clothing Science and Technology*, 10(3/4), 209-218.
39. Erdoğan M.Ç., Boz S. & Küçük M., (2020). Machines used in sewing rooms in apparel industry, Ege University Press, Izmir. (In Turkish)
40. Namiranian, R., Najar, S. S., Etrati, S. M., & Manich, A. M. (2014). Seam slippage and seam strength behavior of elastic woven fabrics under static loading. *Indian Journal of Fibre & Textile Research*, 39, 221-229.
41. Islam, M. M., Saha, P. K., Islam, M. N., Rana, M. M., & Hasan, M. A. (2019). Impact of different seam types on seam strength. *Global Journal of Research in Engineering*, 19(4), 23-25.
42. ISO 13934-1 Textiles- Tensile properties of fabrics- Part 1: Determination of maximum force and elongation at maximum force using the strip method
43. ISO 13937-2- Textiles-Tearproperties of fabrics -- Part 2: Determination of tearforce of trouser-shaped test specimens (Singletearmethod)
44. Chen, D., & Cheng, P. (2019). Investigation of factors affecting the seam slippage of garments. *Textile Research Journal*, 89(21-22), 4756-4765.
45. Miguel, R. A. L., Lucas, J. M., de Lurdes Carvalho, M., & Manich, A. M. (2005). Fabric design considering the optimisation of seam slippage. *International Journal of Clothing Science and Technology*, 17(3/4), 225-231.
46. ISO 13936-1:2004 Textiles — Determination of the slippage resistance of yarns at a seam in woven fabrics — Part 1: Fixed seam opening method
47. Behera, B. K., Chand, S., Singh, T. G., & Rathee, P. (1997). Sewability of denim. *International Journal of Clothing Science and Technology*.
48. Haghghat, E., Etrati, S. M., & Najar, S. S. (2014). Evaluation of woven denim fabric sewability based on needle penetration force. *Journal of Engineered Fibers and Fabrics*, 9(2), 155892501400900206.
49. Ala, D. M., & Bakıcı, G. G. (2019). Sewability (Based on Needle Penetration Force) of 1×1 Rib Knitted Fabrics Produced with Separate Ends of Yarns. *Autex Research Journal*, 19(4), 340-346.
50. L&M Sewability Tester Manual (John Godrich), (2010).
51. Mukhopadhyay, A., Sikka, M., & Karmakar, A. K. (2004). Impact of laundering on the seam tensile properties of suiting fabric. *International Journal of Clothing Science and Technology*.
52. Pasayev, N., Korkmaz, M., & Baspinar, D. (2012). Investigation of the techniques decreasing the seam slippage in chenille fabrics (Part I). *Textile Research Journal*, 82(9), 855-863.
53. Bakıcı, G. G., & Kadem, F. D. (2015). An experimental study about sewability and bending strenght properties of cotton fabrics. *Tekstil ve Konfeksiyon*, 30(2), 177-182.
54. Grancaric, A.M., Lima, M., Vasconcelos, R., Tarbuk, A. (2005). Handle of cotton knitted fabrics: influence of pretreatments. AUTEX World Textile Conference 2005, University of Maribor, Portoroz, Slovenia.



Maximization of Sewing Strength and Minimization of Seam Pucker for Denim Fabrics Using Taguchi Method

Gulsah Pamuk  0000-0002-9358-2331

Ege University / Emel Akin Vocation School / Izmir / Türkiye

Corresponding Author: Gulsah Pamuk, gulsah.pamuk@ege.edu.tr

ABSTRACT

Seams provide the shape of the garments and support the fabric pieces together. The seam quality is important for the serviceability of any garment. In general, the seam quality depends on various factors such as fabric weight, sewing thread type, and stitches per unit area. In this research, three different levels of fabric types with the same construction and different weights, which are mostly used in the production of denim products, were examined. For this purpose, each fabric was sewn in the warp direction with three different levels of sewing threads and three different levels of stitch densities. Then, the values of seam strength, and the seam pucker values were obtained with three replications for each combination of levels. In this study, it is aimed to obtain the optimum levels of fabric weight, sewing thread type, and stitch density of denim fabrics by using the Taguchi method. Custom Taguchi Design is employed to observe the efficiency of factor levels on seam strength and seam pucker, and existence of interactions among fabric weight, sewing thread type, and stitch density.

ARTICLE HISTORY

Received: 29.05.2022

Accepted: 13.09.2022

KEYWORDS

Seam quality, seam strength, seam efficiency, denim fabric, Taguchi method

1. INTRODUCTION

Denim is considered indispensable for clothing industry worldwide because, regardless of their area, age, sex and status, most of the population owns a pair of jeans [1]. Among woven fabrics, the denim usage, as a main part of garment fashion, greatly increases year on year [2]. Denim fabrics are mostly produced using cotton fiber in twill weave with colored warp and white weft yarns that are mainly used for the production of jeans, work clothes and casual wear [3].

Fabric quality alone does not fulfil all the criteria for production of high quality garments. The conversion of a two-dimensional fabric into a three-dimensional garment involves many other interactions such as selection of a suitable sewing thread, optimization of sewing parameters, ease of conversion of fabric to garment and actual performance of a sewn fabric during wear of the garment [4]. The specifications of fabrics for apparel manufacturing can be considered in terms of primary and secondary quality characteristics. The primary quality characteristics

are static physical dimensions and the secondary characteristics are the reactions of the fabric to an applied dynamic force. The apparel manufacturer is usually interested in the secondary characteristics of the fabric and focuses on the seam quality during the fabrication and production of apparel [5].

Seam quality is determined by the correlation between types of fabric, structures of fabric, sewing threads and selection of stitches and seams. The performance of seam also depends on the sewing conditions like size of needle, sewing thread tension, stitches per inch and lastly on the proper working and maintenance of the stitching machine [6]. Seam quality problems such as skipped stitches, thread breakage, fabric damage, faulty seam appearance, needle damage and etc., can be time-consuming and frustrating. They may spoil the appearance of a garment and be the cause of ultimate failure and rejection reduce productivity and seam quality [7, 8]. Good overall seam quality is essential for the longevity of the apparel product, which together with consumer satisfaction affects its saleability [9]. Seam quality is also an important factor to determine

To cite this article: Pamuk G. 2022. Maximization of sewing strength and minimization of seam pucker for denim fabrics using taguchi method. *Tekstil ve Konfeksiyon*, 32(3), 288-295.

the garment quality which is a big deal in today's competitive world market as quality can be seen as the synonym of excellence and as a means to make differentiation of different products having perceived value [10]. Since numerous factors such as seam type, sewing thread, fabric and sewing parameters, technological adjustments have influence on seam's quality, making research on about this subject may be difficult [11, 12].

It is necessary to determine the most appropriate seam for each type of fabric structure to achieve a desired product quality. The quality reflects the performance of the apparel product. Certain stitches are suitable for particular fabrics because each fabric has its own unique properties [13]. All the factors required for the production of high quality ready-made garments in standard sizes and specifications must be determined in advance and adjusted for each model to be the same for all machines in the assembly line. Today, in the apparel industry, while the number of models has increased, production amounts have decreased. Since each different model, fabric and thread feature require different sewing types, the settings of all machines in the assembly line need to be changed. It is very important to optimize the sewing performance, that is, to adjust all these variables that will give the best sewing performance during the sewing process [14].

Seam quality affects two factors; appearance and strength [15]. The sewing performance and sewing strength properties of denim fabrics have been considered by many researchers. Tiber and Yilmaz studied the comparison of seam performance properties of elastic and regular polyester sewing threads on stretch denim fabrics [16]. Ates et al. analyzed the seam performance of the chain stitch and lockstitch used in denim trouser. They examined fabric strength, seam strength and seam efficiency of cotton denim woven fabrics with elastane and without elastane [17]. Sarkar et al. aimed to predict and develop a model for forecasting the seam strength of denim garments with respect to the thread linear density (tex) and stitches per inch by using a Fuzzy Logic Expert System. That model showed good performance in prediction of the seam strength of denim garments [18]. Tuteja and Sen investigated the impact of commercial sewing thread counts and stitch densities on seam strength, seam elongation and seam efficiency on medium-heavy and heavy weight cotton denim fabrics. The effects of different sewing thread sizes and different levels of stitch densities were assessed on the selected seam parameters. It was found that statistically there was a significant interaction between stitch density, sewing thread count and fabric weight on strength, elongation and efficiency of lapped seam [13]. Nayak and Padhye, analyzed the sewability of denim fabrics stitched with air-jet textured sewing thread. The authors found that the fabric formability is dependent on the fabric weight [19]. Seam appearance which is the second side of seam quality concerns the situation known as seam pucker. Seam pucker is an unacceptable waviness in appearance along the seam length [15]. Also the seam performance by means of

durability is based on the strength and efficiency of seam as well as seam appearance along the seam line attributed by the seam puckering [20]. Sular et al., compared the seam performance of 12 woven fabrics by means of seam pucker and other seam properties. They observed that twill fabrics which are also used in denim garments showed lower seam pucker values for all types of the test fabrics [21]. Mak and Li emphasized the importance of seam pucker evaluation in quality control of garments manufacturing [22]. The authors presented an objective method which using image analysis and pattern recognition technologies in their paper.

Process variability causes quality problems in product. Therefore, methods used to reduce variability increase product quality and reduce product cost [23]. The origins of the idea of reducing variability were revealed in 1920 by Dr. Walter Shewhart. This idea, later, has been expanded by the work of W. Edwards Deming, J. A. Juran, Armand Feigenbaum, and Genichi Taguchi [23]. Taguchi method is an experimental design method that tries to minimize the variability in the product and process by choosing the most appropriate combination of the levels of the controllable factors against the uncontrollable factors which create the variability in the product and the process [24]. This method, besides being effective in product quality improvement, gives better results with much less experimentation. In addition, as a philosophy, it envisages ensuring quality in design and process [25].

Taguchi methods have extensive applications in manufacturing enterprises and are applied in various manufacturing fields such as plastics, automotive, metal fabrication, process, electronics, and in service [26]. This methodology has been also employed in textile engineering [27]. Onal et al. evaluated the effect of factors such as fabric width, folding length of joint, seam design and seam type on seam strength. They studied using both Taguchi's design of experiment and artificial neural network [28]. Almetwally analyzed multi-response optimization based on Taguchi-grey relational analysis to maximize tensile strength, breaking extension and air permeability of cotton woven fabrics. Cotton woven fabric parameters such as weft yarn count, weave structure, weft yarn density with three levels, and twist factor of the weft yarn with two levels were used as control factors [29]. Ustuntag and Turksoy aimed to optimize the various coating process parameters for the air permeability properties of denim fabrics by using Taguchi method. They found that weft density and viscosity have significant influence on the air permeability properties of coated denim fabrics [27]. Hossain et al. found the optimal dyeing conditions and predicted the colour strength of viscose/lycra blended knitted fabrics using Taguchi method. The controllable factors such as dye concentration, temperature, time, alkali concentration, salt concentration and liquor ratio have been used as input variables and colour strength of the fabric as response variable. The authors pointed out that Taguchi method is efficient on the optimisation and prediction of fabric colour strength in non-linear complex dyeing [30].

Ghosh et al. investigated the effect of yarn count, loop length, knitting speed, and yarn input tension in the presence of two uncontrollable noise factors on selected comfort properties of single jersey and 1×1 rib knitted fabrics using the Taguchi experimental design. It is observed that yarn count and loop length have significant influence on the thermo-physiological comfort properties of knitted fabrics [31].

The main purpose of this study was to observe the sewing performance properties of denim fabrics by using Taguchi's Custom Design technique and obtain the optimum levels of fabric weight, sewing thread type, and stitch density of denim fabrics by using the Taguchi method.

2. MATERIALS AND METHOD

2.1. Materials

Twill woven denim fabrics, commercially used for the manufacture of men's and women's wear, were used for this study. Three types of commonly used denim fabric weights were chosen. All fabrics had 1% elastane content in the weft direction. The properties of the denim fabrics used in this study is shown in Table 1.

Three different compositions of sewing threads commonly used for stitching denim fabrics were selected for this research. The details of the selected threads with their codes are given in Table 2. The ticket number indicates the thickness of the thread; the higher the value, the finer the thread. In order to observe the effect of the sewing thread type, same ticket number were used.

An industrial Juki DDL 9000A lockstitch machine was used for sewing the denim samples. The sewing was performed with Type-301 (Figure 1) stitch in three different stitch densities (3/4/5 stitches/cm). 90 size needle with rounded end was selected, and machine speed was kept constant during sewing as 3000 cycle/minute.

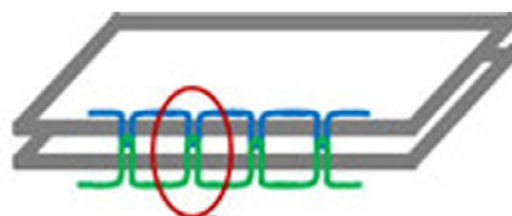


Figure 1. Lockstitch type 301 [5]

2.2. Method

The produced samples were conditioned on a flat surface for 24 hours under standard atmospheric conditions at relative humidity before testing. The seam strength test was carried out using a Zwick Roell ZO10 tensile tester, in accordance with the standard TS EN ISO 13935-1. Specimens with a length of 350 mm and a width of 100 mm were prepared for the test. The device setting was kept constant for all tests. The set distance between the jaws was 200 mm, and the gauge speed was 50 mm/min. In order to prepare samples for seam strength test, the fabrics were sewn in the warp direction because the warp density is usually greater than weft density. Hence the effect of inserting a thread during sewing in the warp direction should have a more pronounced effect on the seam performance. Furthermore, in apparel manufacturing, the fabrics are usually cut and sewn in the warp direction due to the texture and design of the fabric [15].

Seam pucker was determined by measuring the difference in fabric and seam thickness under a constant compressive load. Therefore, fabric thickness values of unsewn and sewn fabric samples were utilized. The seam thickness strain (%) as an indicative of seam pucker of the sewn fabrics is calculated by using the following formula (1) where seam thickness and fabric thickness are in mm [21, 32]. The seam area of about 30 cm was examined and measurements were taken from ten different locations on the sample using a Wira digital thickness gauge.

Table 1. The properties of denim fabrics

Fabric code	Fiber composition	Weight (gr/m ²)	Fabric thickness (mm)	Warp yarn density (ends/cm)	Weft yarn density (picks/cm)
1	99% Cotton - 1% Elastane	342	0,78	30	22
2	99% Cotton - 1% Elastane	424	0,92	28	20
3	99% Cotton - 1% Elastane	298	0,70	23	19

Table 2. Properties of sewing threads

Sewing thread code	Composition	Number of plies	Ticket number
1	Polyester-Polyester Corespun	2	50
2	Polyester-Cotton Corespun	2	50
3	Staple Polyester	2	50

$$\text{Seam pucker (\%)} = \frac{\text{Seam thickness} - 2 \times \text{Fabric thickness}}{2 \times \text{Fabric thickness}} \times 100 \quad (1)$$

2.3. The Taguchi Approach to Analysis of Test Data

In this study, the Taguchi Method is used to analyze test data obtained by the method described in Section 2.2. This method emphasises on variance reduction. The variables under consideration may be quantitative or qualitative, and the performance criterion is the signal-to-noise ratio (SNR). There are four types of SNRs suggested by Taguchi [33]. Depending on the goal of the experiment, different signal-to-noise ratio can be chosen. There are three specific goals and therefore signal to noise ratios:

In this work two goals are considered i)to maximize the mean seam strength(the larger the better) ii) to minimize the mean seam pucker(the smaller the better). Therefore, the larger the better and the smaller the better are the goals aimed to achieve.

In the larger the better case, the SNR is given by Myers et al., as follows [33]:

$$SNR_l = -10 \log \sum_{i=1}^n \left[\frac{1}{y_i^2} \right] / n \quad (2)$$

where y_i $i=1,2,...,n$ are observed values of the response, seam strength. In this study factors; fabric weight, sewing thread type, and stitch density, that maximize SNR_l are sought.

In the smaller the better case, the SNR is given by Myers and Montgomery as follows [33]:

$$SNR_s = -10 \log \sum_{i=1}^n \left[\frac{y_i^2}{n} \right] \quad (3)$$

where y_i $i=1,2,...,n$ are observed values of the response, seam pucker, and values of the variables, fabric weight,

type of sewing thread, and stitch density, that minimize SNR_s are sought.

Table 4 shows the factors; fabric weight, sewing thread type and stitch density, and their levels. Each factor has three levels and Taguchi analysis was carried out using Minitab Statistical Software version 16.0, in order to find the factor levels giving the maximum seam strength and minimum seam pucker. During the usage of software, "Define Custom Taguchi Design" was selected, so that the factor-interactions could be investigated.

For collecting data on factors and responses, three replicates were performed at each combination of factors' levels. Thus totally 81 measurements were made. For the sake of simplicity, average value of three replicates are computed and given in Table 5.

3. RESULTS AND DISCUSSION

3.1. Maximizing the Mean Seam Strength

In this part of the study the aim was to determine the conditions, optimum factor levels, which give the highest mean seam strength. Calculated S/N ratios (larger-the-better) for seam strength were given in Table 6. Delta statistics were given in Table 6 compare the relative magnitude of effects. This statistic value is calculated by subtracting the highest value from the lowest value among the values in each column. Rank 1 is assigned to the highest Delta value where Rank 2 is assigned to the highest Delta value. The delta values in Table 6 indicates that among three factors (fabric weight/sewing thread type/stitch density) stitch density has the greatest influence on SNR where fabric weight has the lowest influence on SNR.

Table 3. Types of SNRs

Signal to noise ratio (SNR)	Goal of the experiment
Larger is better	Maximize the response
Nominal is best	Target the response and the signal-to-noise ratio is based on standard deviations only
Smaller is best	Minimize the response

Table 4. Factors and their levels

Levels	Factors		
	Fabric weight (gr/m ²) (A)	Sewing thread type (B)	Stitch density (stitch/cm) (C)
1	342	Polyester/Polyester Corespun	3
2	424	Polyester/Cotton Corespun	4
3	298	Staple Polyester	5

Table 5. Design matrix and mean response values

FACTORS			RESPONSES	
Fabric weight (gr) (A)	Sewing thread type (B)	Stitch density (stitch/cm) (C)	Seam strength (N)	Seam pucker (%)
1	1	1	531,19	21,87
1	1	2	540,22	8,49
1	1	3	563,41	7,48
2	1	1	484,43	16,72
2	1	2	842,03	15,19
2	1	3	892,27	14,97
3	1	1	773,04	14,58
3	1	2	802,79	8,47
3	1	3	829,69	4,31
1	2	1	629,17	15,97
1	2	2	765,98	7,05
1	2	3	782,43	3,31
2	2	1	567,56	15,74
2	2	2	732,60	14,75
2	2	3	990,98	14,75
3	2	1	782,65	11,81
3	2	2	892,30	7,50
3	2	3	931,02	4,03
1	3	1	667,64	25,18
1	3	2	649,34	11,94
1	3	3	669,50	10,94
2	3	1	629,17	21,75
2	3	2	801,56	18,69
2	3	3	839,98	18,58
3	3	1	679,26	18,33
3	3	2	781,95	12,78
3	3	3	878,11	10,14

Table 6. Response table for signal to noise ratio for seam strength

Level	Fabric weight (A)	Sewing thread type (B)	Stitch density (C)
1	56,04	55,58	55,32
2	56,92*	56,96*	56,46
3	56,12	56,54	57,30*
Delta	0,88	1,38	1,98
Rank	3	2	1

As a result, the following can be suggested as the optimal levels of A₂, B₂, and C₃ if factor interactions are not considered. In other words 424 gr/m² fabric weight, Polyester/Cotton Corespun sewing thread and 5 stitch/cm gave the maximum seam strength value.

In Table 7, Analysis of Variance results for seam strength are displayed. It includes components of the total variability in the response variable, seam strength. From the analysis

of Table 7, it is concluded that factors A(fabric weight), B (sewing thread type), and C (stitch density), and interactions A-B, A-C, B-C and A-B-C have significant effects on seam strength at an α level of 0,10 since their p-values are less than 0,10. The value of coefficient of multiple determination, R-Sq, is 0,7438. That is, the factors and their interactions explain about 74,38% of the variability observed in seam strength.

Table 7. Analysis of variance results for seam strength

Source	DF	SS	MS	F	p-value
A	2	89349	44674	8,83	0,000
B	2	138606	69303	13,70	0,000
C	2	297270	148635	29,38	0,000
A*B	4	46802	11701	2,31	0,069
A*C	4	72721	18180	3,59	0,011
B*C	4	63914	15979	3,16	0,021
A*B*C	8	84362	10545	2,08	0,053
Error	54	273145	5058		
Total	80	1066169			

S = 71,1213 R-Sq = 74,38% R-Sq(adj) = 62,05%

In addition to the ANOVA results in Table 7, the two factor interaction plots are depicted in Figure 2 which also explores that the effect of each factor is influenced by the level of another factor [34]. It is clear that the second levels of fabric weight and sewing thread are more effected by the third level of stitch density. As can be seen, the highest mean seam strength is produced with stitch density (5 stitch/cm) when fabric weight is second level. This result is consistent with the optimal levels of factor levels mentioned above.

3.2. Minimizing the Mean Seam Pucker

Seam pucker is a distortion in the surface of a sewn fabric and appears as a swollen effect along the line of the seam. It is determined by measuring the percentage increase in the thickness of the seamed fabric over the original fabric under a constant load [4]. Therefore, main aim is minimizing the mean seam pucker. For each experimental run, design matrix and response values were given in Table 5.

In the smaller the better case, the factor levels that maximize SNRs, as in the larger the better case, but minimize the mean seam pucker are sought. Means for SNRs and response against levels of factors were given in Table 8.

As a result, the following can be suggested as the optimal levels of A_3 , B_2 , and C_3 if factor interactions are not considered. In other words 298 gr/m² fabric weight, Polyester/Cotton Corespun sewing thread and 5 stitch/cm gave the minimum seam pucker value. Seam pucker takes place mainly due to the contractive forces introduced in the seam during sewing. When the contractive force exceeds the buckling resistance of fabric inside a stitch, the fabric starts puckering along the seam line. If the sewing thread penetrates into a heavy weight fabric, it introduces very high contractive force and so high puckering has been seen in heavy weight fabrics [4]. The result given in Table 8 also supports this situation.

From Table 9, it can be concluded that A (fabric weight), B (sewing thread type), C (stitch density), two factor interactions; A – C, and three factor interaction; A – B – C have significant effects on mean seam pucker at an α level of 0,10 since their p-values are less than 0,10. It must be noted that although A-B, and B-C interactions appear as insignificant, the A–C and three-factor interactions are significant. The value of coefficient of multiple determination, R-Sq, is 0,8948. That is, the factors and their interactions explain about 84,41% of the variability observed in seam pucker.

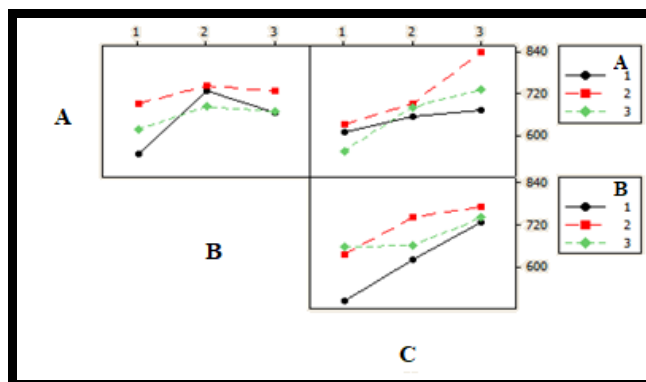


Figure 2. Interaction plot (data means) for seam strength

Table 8. Response table for signal to noise ratio for seam pucker

Level	Fabric weight (A)	Sewing thread type (B)	Stitch density (C)
1	-20,46	-21,04	-25,01
2	-24,42	-19,27*	-20,87
3	-19,51*	-24,08	-18,50*
Delta	4,91	4,80	6,51
Rank	2	3	1

Table 9. Analysis of variance results for seam pucker

Source	DF	SS	MS	F	p-value
A	2	564,67	282,33	47,34	0,000
B	2	530,15	265,08	44,45	0,000
C	2	1091,24	545,62	91,49	0,000
A*B	4	35,25	8,81	1,48	0,222
A*C	4	388,88	97,22	16,30	0,000
B*C	4	31,26	7,82	1,31	0,278
A*B*C	8	97,69	12,21	2,05	0,058
Error	54	322,05	5,96		
Total	80	3061,20			

S = 2,44211 R-Sq = 89,48% R-Sq(adj) = 84,41%

When the plots displaying the factor interactions in Figure 3 are considered, third levels of A (fabric weight) and C (stitch density), produce smaller response with the second level of B (sewing thread type). A*C interaction plot implies that the smallest seam pucker is produced with the third level of stitch density (5 stitch/cm) when the second level of sewing thread type is used. This result is consistent with the suggested operating conditions mentioned in Table 8.

4. CONCLUSION

In experimental design, Taguchi Method has great importance in optimization of input factors. In the current study, according to the results obtained by Taguchi Custom

Design *i*) maximum seam strength was obtained by 5 stitch/cm, Polyester/Cotton Corespun thread and 424 gr/m² fabric weight, and *ii*) the seam pucker was minimized when process is settled to 5 stitch/cm, 298 gr/ m² fabric weight and Polyester/Cotton Corespun thread. Furthermore, three-way ANOVA results showed that *i*) fabric weight, sewing thread type, stitch density, and their two-way, and also three-way interactions have significant effects on the seam strength, *ii*) for seam pucker; effects of three factors, and fabric weight-stitch density interaction are significant. Since three-way interaction is also significant, it can be concluded that fabric weight-stitch density interaction may differ for one level of sewing thread type compared to another level of sewing thread type.

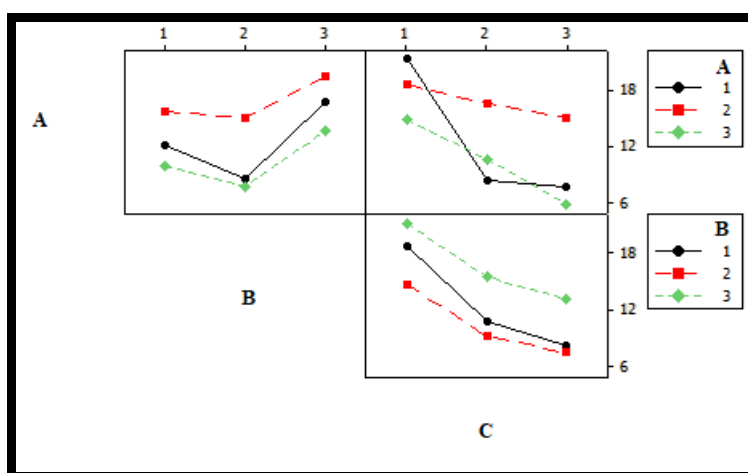


Figure 3. Interaction plot (data means) for seam pucker

REFERENCES

1. Annapoorani, S.G., 2017. Introduction to Denim, In S.S. Muthu (Ed.), *Sustainability in Denim*, Woodhead Publishing, 1-26.
2. Haghghat, E., Etrati, S.M., Najar, S.S., 2014. Evaluation of Woven Denim Fabric Sewability based on Needle Penetration Force. *Journal of Engineered Fibers and Fabrics*, 9(2), 47-60.
3. Eryuruk, H. S. 2019. The effects of elastane and finishing processes on the performance properties of denim fabrics, *International Journal of Clothing Science and Technology*, 31(2), 243-258.
4. Behera, B.K., Chand, S., Singh, T.G. and Rathee, P. 1997. Sewability of denim", *International Journal of Clothing Science and Technology*, 9 (2), 128-140.
5. Malek, S., Jaouachi, B., Khedher, F., Said, S.B. and Cheikhrouhou, M. 2017. Influence of some sewing parameters upon the sewing efficiency of denim fabrics, *The Journal of the Textile Institute*, 108 (12), 2073-2085.
6. Rajpu, B. et. al., 2018. Effect of sewing parameters on seam strength and seam efficiency", *Trends in Textile Engineering & Fashion Technology*, 4 (1), 1-5.
7. Hayes, S. and McLoughlin, J. 2013. The sewing of textiles", in Jones, I. and Stylios, G.K. (Eds), *Joining Textiles Principles and Applications*, Woodhead Publishing Series in Textiles, No. 110.
8. Mandal, S. and Abraham, N. 2010. An overview of sewing threads mechanical properties on seam quality, *Pakistan Textile Journal*, Vol. 59(1), 40-43.
9. Bharani, M. and Mahendra Gowda, R.V. 2012. Characterization of seam strength and seam slippage on pc blend fabric with plain woven structure and finish", *Research Journal of Recent Sciences*, 1(12), 7-14.
10. Hossain, A. et. al, 2020., Effect of Different Sewing Parameters on Lockstitch Seam Strength for Denim Fabric, *Journal of Engineering Advancements*, 1 (4), 139-143.
11. Germanova-Krasteva, D. and Petrov H. 2008. Investigation on the seam's quality by sewing of light fabrics. *International Journal of Clothing Science and Technology*, 20 (1), 57-64.
12. Malek, S., Khedher, F., Jaouachi, B. and Cheikhrouhou, M. 2019. Influence of denim fabric properties and sewing parameters upon the seam slippage and seam quality prediction, *Journal of Textile and Apparel, Technology and Management*, 11(1), 1-17.
13. Tuteja, S. and Sen, P. 2019. Influence of stitch density and sewing thread count on the seam performance of denim fabric, *Journal of The Textile Association*, 9 (2), 442-448.
14. Yildiz, E.Z. 2018. Modeling of Seam Quality by Using Different Seam Parameters, Ege University, Turkey, PhD Thesis.
15. Ghani, S.A. and Gong, H. 2010. "Seam quality: experimental and modelling works using the structural equation methodology", *Scientific Research Journal*, 7(1), 13-36.
16. Tiber, B. and Yilmaz, N. 2022, Investigation of the effects of elastic sewing thread on seam performance properties of stretch denim fabrics. *Tekstil ve Konfeksiyon*, 32 (1), 47-56.

-
17. Ateş, M., Gurarda, A. and Ceven, K. 2019. Investigation of seam performance of chain stitch and lockstitch used in denim trousers, *Tekstil ve Mühendis*, 26 (115), 263-270.
 18. Sarkar, J., Al Faruque, A. and Mondal, M.S.. 2021. Modeling the seam strength of denim garments by using fuzzy expert system. *Journal of Engineered Fibers and Fabrics*, 16, 1-10.
 19. Nayak, R. and Padhye, R. 2013. Sewability of Air-Textured Sewing Threads in Denim. *Journal of Textile and Apparel, Technology and Management*, 8(1), 1-11.
 20. Kakde, M.V. and Gulhane, S.S. 2018. Effect of sewing parameters on seam strength and seam efficiency, *Trends in Textile Engineering and Fashion Technology*, 4(1), 1-5.
 21. Sular V., et al., 2015. A Comparative Study on Seam Performance of Cotton and Polyester Woven Fabrics, *The Journal of Textile Institute*, 106 (1), 19-30.
 22. Mak, K.L. and Li, W. 2008. Objective Evaluation of Seam Pucker on Textiles by Using Self-Organizing Map, *International Journal of Computer Science*, 35 (1), 1-8.
 23. Ross, J. E. 1999. Total Quality Management (3rd edition). ABD: St. Lucie Press
 24. Canyılmaz, E. ve Kutay, F. 2003. Taguchi Metodunda Varyans Analizine Alternatif Bir Yaklaşım, *Gazi Üniversitesi Mühendislik Mimarlık Dergisi*, 18 (3), 51-63
 25. Taguchi, G. ve Clausing, D. 1990. Robust Quality, *Harvard Business Review*, pp. 65-76.
 26. Rowlands, H., Antony, J. ve Knoles, G. 2000. An Application of Experimental Design for Process Optimization. *The TQM Magazine*, 12 (2), 78-83.
 27. Ustuntag, S. and Turksöy, H.G., 2019. Optimization of coating parameters for air permeability of denim fabrics through Taguchi method", *Industria Textila*, 70 (3), 259-264.
 28. Onal, L., Zeydan, M., Korkmaz, M. and Meeran, S. 2009. Predicting the seam strength of notched webbings for parachute assemblies using the Taguchi's design of experiment and artificial neural networks, *Textile Research Journal*, 79 (5), 468-478.
 29. Almetwally, A.A. 2020, Multi-objective Optimization of Woven Fabric Parameters Using Taguchi-Grey Relational Analysis, *Journal of Natural Fibers*, 17 (10), 1468-1478.
 30. Hossain, I., Hossain A., and Choudhury, I.A., 2016. Dyeing process parameters optimisation and colour strength prediction for viscose/lycra blended knitted fabrics using Taguchi method, *The Journal of The Textile Institute*, 107 (2). 154-164.
 31. Ghosh, A., Mal, P., Majumdar, A. and Banerjee, D. 2017. An investigation on air and thermal transmission through knitted fabric structures using the Taguchi method, *AUTEX Research Journal*, 17 (2). 152-163.
 32. Hati, S. and Das, B.R. 2011. Seam Pucker in Apparels: A Critical Review of Evaluation Methods, *Asian Journal of Textile*, 1, 60-73.
 33. Myers, R.H., Montgomery, D.C., Anderson, C.M., (2009), *Response Surface Methodology: Process and Product Optimization Using Designed Experiments*, John Wiley&Sons, Inc., New Jersey.
 34. Hines W.W. and Montgomery, D.C., 1990. *Probability and Statistics in Engineering and Management Science*, third edition, John Wiley and Sons, New York.

